

Incorporation of Carbon-based Nanoparticles in Ultrafiltration Membranes to Remove Steroid Hormone Micropollutants

Zur Erlangung des akademischen Grades eines

Doktors des Ingenieurwissenschaften (Dr.-Ing.)

von der KIT-Fakultät für Chemieingenieurwesen und Verfahrenstechnik des
Karlsruher Instituts für Technologie (KIT)

genehmigte

DISSERTATION

von

Minh Nhat Nguyen, M.Sc.

aus Hanoi, Vietnam

Tag der mündlichen Prüfung: 19.09.2022

Erstgutachterin: Prof. Dr.-Ing. Andrea Iris Schäfer

Zweitgutachter: Prof. Dr. Jürgen Hubbuch

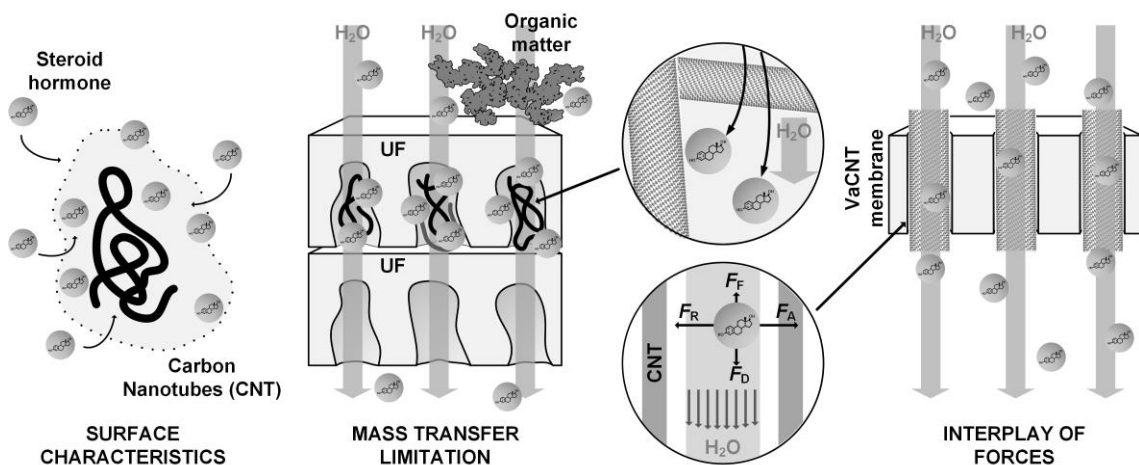
Executive Summary

Steroid hormone micropollutants are compounds of emerging concern in surface water and wastewater that result in elevated risks of reproductive system disorders, cardiovascular disease, and malignancies in humans. Membrane technology is a suitable solution to remove these compounds, but the effective treatments (nanofiltration and reverse osmosis) are costly because much energy is required to elevate the pressure to 5–60 bar. Ultrafiltration (UF) is a lower-cost solution, and when coupled with adsorptive materials, can provide good removal of steroid hormone micropollutants. The possibility of removing these micropollutants with adsorptive composite (UF) membranes is the primary target of this dissertation.

In such adsorptive composite membranes, the residence times of water and solutes are short (below one minute), as opposed to the residence (contact) times in activated carbon adsorbers or contactors. In addition, there is a limit of loading (which is the amount of adsorbent per amount of membrane) in such compact membranes. Therefore, the incorporated adsorbents must have a sufficiently large external surface compared with activated carbon to minimise the mass transfer limitation. Carbon-based nanoparticles (CNPs), such as multi-/single-walled carbon nanotubes (MW-/SWCNTs), graphene, graphene oxide, and fullerene, are promising materials for incorporation into the UF membrane.

However, high accessible surface area and good mass transfer do not guarantee good adsorption by the composite membranes. In vertically aligned carbon nanotube (VaCNT) membranes, the hormone immediately reaches the wall of the pores with an almost ideal cylindrical shape and low tortuosity. This membrane adsorbs very little hormone, which can be explained by the interplay of forces acting on the hormone molecule at the VaCNT membrane surface.

The aims of this dissertation are to characterise the three main aspects of (adsorptive) composite membranes that influence steroid hormone adsorption, which are the i) *surface characteristics* of the incorporated adsorbents (Chapter 4), ii) *mass transfer limitation* within short residence times and in the presence of organic matter in water (Chapters 5 and 6), and iii) *interplay of forces* (Chapter 7).



Static adsorption experiments (without any membrane) were performed in an incubator shaker to determine the adsorption performance without the limitation of residence time. Most filtration experiments were performed with a micro-crossflow filtration system with a filtration area of 2 cm². The flow of the feed was induced by an HPLC pump, and the flow of permeate was controlled with a needle valve placed on the retentate side. The permeate was separated into different vials based on time or permeate volume by a switching valve and weighted on a balance.

Steroid hormone micropollutants (estrone, 17 β -estradiol, testosterone, and progesterone) were radiolabelled and analysed *via* liquid scintillation counting. The scintillation counter measures hormone concentrations between 100 and 0.1–0.2 ng/L. Organic matter concentrations were determined with a TOC analyser, UV–Vis spectroscopy, and liquid chromatography – organic carbon detection techniques.

Several key findings are drawn from this dissertation.

- The good adsorption performance of several types of CNPs, namely SWCNTs, comes from the good access of steroid hormone micropollutant to the adsorbent surface.
- The composite of SWCNT and UF (SWCNT–UF) allows partial removal of steroid hormones. Only the most accessible surface of SWCNT adsorbs hormones, where the residence time (in seconds or sub-seconds) does not limit the adsorption.
- Aromatic and small organic matter can reduce the accessibility of hormone to the surface or the affinity of hormones for the surface, which prevents hormone adsorption. The shielding effect of UF membrane was demonstrated with humic acid interferants.
- The VaCNT membranes (with hydrophobic and smooth pores) adsorb very little hormone. The contact and ‘friction’ between the membrane and hormones are not strong enough to resist the hydrodynamic drag force to allow adsorption.

CNPs are currently not applicable in water treatment because of toxicity concerns. The following insights and considerations are gained from this dissertation for the future development of adsorptive composite membranes.

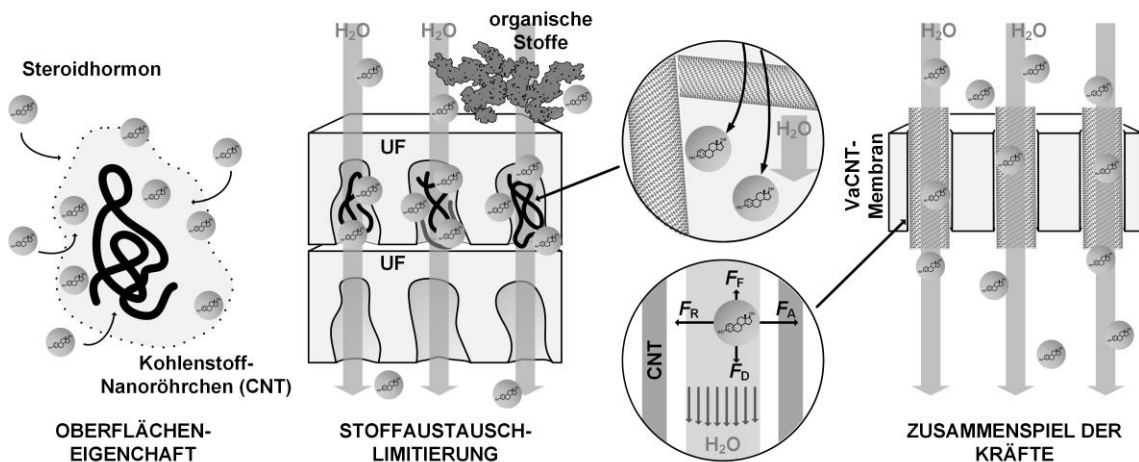
- Using materials with predominantly external surface in the adsorptive composite membrane is a good direction. The adsorbent loading needs to increase to improve hormone removal. Unfortunately, this may require an alternative membrane design.
- Permeate side incorporation of adsorbents is a good idea when the UF membrane can shield the adsorbents from the interfering organic matter. A dense membrane with low molecular weight cut-off (≤ 10 kDa) is needed.
- Good adsorptive membranes need to provide good contact and ‘friction’ with the adsorbates. This can be achieved by increasing the pore tortuosity and pore surface roughness.

Kurzfassung

Mikroverunreinigungen (insbesondere Steroidhormone) sind besorgniserregende Verbindungen in Oberflächengewässern und Abwässern, die zu einem erhöhten Risiko für Probleme mit dem Fortpflanzungssystem, Herz-Kreislauf-Erkrankungen und Krebs beim Menschen führen. Die Membrantechnologie ist eine gute Lösung, um diese Verbindungen zu entfernen, aber die effektiven Behandlungen (Nanofiltration und Umkehrosmose) sind kostspielig, da viel Energie erforderlich ist, um den Druck auf 5 bis 60 bar zu erhöhen. Ultrafiltration (UF) ist eine kostengünstigere Lösung und kann in Verbindung mit adsorptiven Materialien eine gute Entfernung von Steroidhormonen ermöglichen. Die Möglichkeit, diese Mikroverunreinigungen mit adsorptiven Komposit-Membranen zu entfernen, ist das Hauptziel dieser Doktorarbeit.

In solchen adsorptiven Komposit-Membranen ist die hydraulische Verweilzeit von Wasser und gelösten Stoffen kurz (unter einer Minute), im Gegensatz zu den Verweilzeiten (oder Kontaktzeiten) in Adsorbern oder Kontaktoren mit Aktivkohle. Außerdem gibt es bei solchen kompakten Membranen eine Kapazitätsgrenze (das ist die maximale Menge an Adsorptionsmittel pro Membranmenge). Daher müssen die Adsorptionsmittel im Vergleich zu Aktivkohle eine ausreichend große äußere Oberfläche haben, um die Stoffaustauschlimitierung zu minimieren. Kohlenstoffbasierte Nanopartikel (CNPs), wie mehr-/einwandige Kohlenstoff-Nanoröhren (MW-/SWCNTs), Graphen, Graphenoxid und Fulleren, sind vielversprechende Materialien für den Einbau in die UF-Membran. Eine hohe Oberfläche und ein guter Stoffaustausch garantieren jedoch keine gute Adsorption. Bei vertikal ausgerichteten Kohlenstoff-Nanoröhren (VaCNT)-Membranen erreicht das Hormon sofort die Wand der Poren mit nahezu idealer zylindrischer Form und weniger Tortuosität. Diese Membran adsorbiert sehr wenig Hormon, was durch die Kräfte erklärt werden kann, die auf das Hormonmolekül an der Oberfläche einwirken.

Die Ziele sind es, die drei Hauptaspekte mit Komposit-Membranen zu untersuchen, die die Hormonadsorption bestimmen, nämlich i) *Oberflächeneigenschaft* des Adsorptionsmittels (Kapitel 4), ii) *Stoffaustauschlimitierung* bei kurzen Verweilzeiten (Kapitel 5) und iii) *Zusammenspiel der Kräfte* (Kapitel 7). Kapitel 6 untersucht weiter die Behinderung des Stoffaustausches, die durch organische Stoffe verursacht werden.



Adsorptionsexperimente ohne Membranen wurden in einem Inkubationsschüttler durchgeführt, um die Adsorptionsleistung ohne Begrenzung der Verweilzeit zu bestimmen. Die meisten Filtrationsexperimente wurden mit einem Mikro-Crossflow-Filtrationssystem mit einer Filtrationsfläche von 2 cm² durchgeführt. Der Speisewasserfluss wurde durch eine HPLC-Pumpe induziert. Der Permeatfluss wurde mit einem auf der Retentatseite platzierten Nadelventil gesteuert. Das Permeat wurde über einen Ventilantrieb nach Zeit oder Permeatvolumen in Fläschchen getrennt und auf einer Waage gewogen.

Steroidhormon-Mikroverunreinigungen (Östron, 17 β -Östradiol, Testosteron und Progesteron) wurden radioaktiv markiert und mit einem Flüssigszintillationszähler analysiert. Die analysierten Konzentrationen liegen zwischen 100 und 0,1–0,2 ng/L. Die Konzentrationen organischer Stoffe wurden mit einem TOC-Analysator, UV-Vis-Spektroskopie und Flüssigkeitschromatographie-System – Kohlenstoffdetektor (LC-OCD) bestimmt.

Aus dieser Arbeit lassen sich mehrere Schlüsselerkenntnisse ableiten.

- Die gute Adsorptionsleistung mehrerer CNPs, nämlich SWCNTs, beruht auf dem guten Zugang von Steroidhormonen zur Oberfläche des Adsorptionsmittels.
- Die Kombination aus SWCNT und UF (SWCNT-UF) ermöglicht eine teilweise Entfernung. Es wurde nur die am besten zugängliche Oberfläche verwendet, bei der die Verweilzeit (in Sekunden oder weniger als Sekunden) die Adsorption nicht begrenzt.
- Aromatische und kleine organische Stoffe können die Oberfläche blockieren oder die Affinität von Hormonen zur Oberfläche verringern, wodurch die Hormonadsorption verringert wird.
- Die VaCNT-Membranen (mit hydrophoben und glatten Poren) adsorbieren sehr wenig Hormon. Der Kontakt und die „Reibung“ zwischen der Membran und den Hormonen sind nicht stark genug, um der hydrodynamischen Widerstandskraft zu widerstehen und eine Adsorption zu ermöglichen.

Derzeit sind CNPs aufgrund von Toxizitätsbedenken nicht in der Wasseraufbereitung anwendbar. Aus dieser Arbeit ergeben sich folgende Erkenntnisse und Überlegungen für die zukünftige Entwicklung adsorptiver Komposit-Membranen.

- Die Verwendung von Materialien mit hauptsächlich äußerer Oberfläche in adsorptiven Komposit-Membranen ist eine gute Richtung. Die Kapazitätsgrenze dieser Adsorptionsmittel muss erhöht werden, um die Hormonentfernung zu verbessern. Leider kann dies ein alternatives Membrandesign erfordern.
- Der Einbau von Adsorptionsmittel auf der Permeatseite ist sinnvoll, wenn die UF-Membran die Adsorptionsmittel von störenden organischen Stoffen abschirmen kann.
- Gute adsorptive Membranen müssen guten Kontakt und Reibung mit den Adsorbaten bieten. Dies kann durch Erhöhen der Tortuosität und der Oberflächenrauigkeit der Membranporen erreicht werden.

Table of Contents

1	Introduction.....	1
1.1	Challenges of sustainable water management	1
1.2	Micropollutants in the water environment.....	3
1.3	Steroid hormone micropollutants	4
1.4	Drinking water guidelines for steroid hormones	6
1.5	Technologies for steroid hormone removal.....	8
1.6	Objectives of the dissertation.....	12
1.7	Structure of the dissertation	13
2	Adsorptive Composite Membranes for Steroid Hormone Micropollutant Removal	16
2.1	Prospective of adsorptive composite membranes	17
2.2	Hybrid membrane processes vs. adsorptive composite membranes.....	18
2.3	Carbon-based nanoparticles (CNPs) for membrane incorporation.....	21
2.4	Adsorption and mass transfer mechanisms in CNPs	24
2.5	Technical considerations for adsorptive composite membranes (ACMs).....	29
2.6	ACM designs	37
2.7	Summary of the key interests in ACM research.....	42
3	Study Approach – Materials and Methods.....	44
3.1	Membrane systems	45
3.2	Incubator shaker for static adsorption.....	46
3.3	Materials and reagents	47
3.4	Analytical techniques.....	53
3.5	Calculations	57
3.6	Error analysis	61
3.7	Membrane and nanoparticle characterisation	67
4	Influence of Adsorbent Surface on Hormone Adsorption.....	70
4.1	Literature summary of the surface characteristics of CNPs.....	71
4.2	Experimental methods to characterise CNP surface and hormone adsorption	72
4.3	Steroid hormone adsorption performance.....	78
4.4	Relationship between surface accessibility and adsorption	85
4.5	Relationship between surface chemistry and adsorption	91
4.6	Examination of the adsorption mechanisms and limiting factors.....	93
4.7	Concluding remarks on the adsorption at the CNP surface	95
5	Influence of Mass Transfer Limitation on Steroid Hormone Adsorption	97
5.1	Mass transfer limitation in ACMs	98
5.2	Experimental methods to determine hormone adsorption	99
5.3	Filtration property of the single-walled carbon nanotube – ultrafiltration membrane (SWCNT–UF)	101

5.4	Influence of SWCNT loading on hormone adsorption	104
5.5	Influence of residence time on hormone adsorption	107
5.6	Influence of water chemistry on hormone adsorption.....	110
5.7	Concluding remarks on the mass transfer limitation.....	112
6	Mass Transfer Limitation Caused by Organic Matter	113
6.1	Interference of organic matter (OM) with steroid hormone adsorption.....	114
6.2	Experimental methods to examine OM interference	115
6.3	Interference of various OM types with hormone adsorption	118
6.4	Relationship between OM characteristics and interference	121
6.5	Determination of the OM interference mechanisms	124
6.6	Shielding of the UF membrane against OM interference	127
6.7	Concluding remarks on the mass transfer limitation caused by OM	129
7	Influence of the Forces on Steroid Hormone Adsorption.....	130
7.1	Utilisation of vertically aligned carbon nanotube (VaCNT) membranes to investigate the forces.....	131
7.2	Experimental methods to quantify adsorption and the forces.....	133
7.3	Adsorption performance of VaCNT membranes	137
7.4	Influence of the drag force on adsorption	139
7.5	Influence of adhesive force on adsorption	141
7.6	Influence of membrane pore diameter on adsorption	142
7.7	Concluding remarks on the interplay of forces	142
8	Conclusions and Outlook.....	144
8.1	Summary and conclusions	144
8.2	Outlook	150
	Bibliography	152
	Appendices	i
A.	Preparation of calibration solutions	i
B.	Error analysis calculations	ii
C.	Static adsorption protocol	iii
D.	Fitting parameters of the adsorption models.....	v
E.	Surface area and adsorption capacity based on the ideal shapes of CNPs.....	vi
F.	‘Pore’ characterisation of CNPs.....	viii
G.	Filtration protocols.....	ix
H.	Determination of the SWCNT–UF area in contact with water and solution	xi
I.	Maximum loading of SWCNTs in SWCNT–UF	xii
J.	Maximum E2 adsorbed mass with SWCNT–UF	xiii
K.	Characterisation of organic matter with LC-OCD	xiv
L.	Reproducibility of OM analysis with LC-OCD	xv
M.	UV–Vis absorbance of nine OM types	xvi
N.	Flow enhancement in VaCNT membranes	xvii
O.	Pressure issues in VaCNT membranes	xviii
	Abbreviations.....	xx

List of Symbols	XXV
List of Figures.....	xxviii
List of Tables	XXXV

Acknowledgements

Foremost, I would like to thank my supervisor, Prof. Andrea Iris Schäfer, who has gifted me with the scientific knowledge of membrane technology and rich experiences in various aspects of life. I learnt very much from you on conceptualising and presenting interesting research concepts, managing my schedule, organising Team Days, teaching courses, a lab opening and a conference, and dealing with stress, difficult peoples and when things do not go my way. Thank you so much for always giving me timely and critical feedback so I would not diverge from my career choice.

I would like to acknowledge my Scholarship providers, DAAD and BMBF, for providing me the funds for my research under the Sustainable Water Management concept. Thank you very much, Dr. Holger Finken, Ms. Ingrid Kasperek and Ms. Monika Osman and everyone else at ST43, for granting me the scholarship and several extensions. Thank you again Dr. Finken and ST43 for selecting me for the DAAD Travel Grant to Ho Chi Minh City, Vietnam, to attend an international conference (GTSW 2019). This was proven to be a delightful and worthwhile career opportunity. I am also thankful that they provided me another Grant to Tahoe, USA for the Lake Tahoe Nanofluidics 2022 conference, but I unfortunately could not attend. I am also thankful for IET, VAST, Vietnam, for allowing me to do my PhD abroad with full support.

I would like to thank my colleagues at IAMT. None of you can be excluded from this acknowledgement for various discussions and a lot of fun we have through the many years of my arduous PhD study. Thank you all very much for making my PhD an incredible and memorable journey. Special thanks are given to Isaac Owusu-Agyeman, Tobias Berger, Matteo Tagliavini, Roman “Luby” Lyubimenko, and Yang-Hui Cai, who assisted me very much in filtration system building, protocol development, and sample analysis, beside a lot of scientific discussions.

The students that I worked with as a junior supervisor deserve many thanks, for having taught me back so much on being a better supervisor: Master students Jinju Zhang, Phuong B. Trinh (who has been both my student and colleague) and Rubén Hervás-Martínez; and Luiza von Sperling, who worked with me as a Hiwi student. I hope you find to your passions and perform wonderfully.

I would like to acknowledge all the collaborators with whom I have had the opportunity to discuss about my research and learnt very much from their insight and experiences. Thank you very much, Prof. Jiansheng Li, Dr. Francesco Fornasiero, Dr. Pia Lipp, and Dr. Stefan Huber for the rich experiences from our collaborations. Special thanks to Prof. Ruth Schwaiger, Dr. Peter Weidler, Dr. Claus Burkhardt, Dr. Johannes Lützenkirchen, Dr. Florian Vollnhals and Prof. Silke Christiansen for helping me with characterising the carbon-based nanoparticles and membranes. Dr. Matthias Hettler and Hartmut Speck helped me a lot with logistics.

Finally, I would like to thank my parents, who are always supportive and caring; and my grandmother, who has always been waiting for me. Thank you, Ha Vi, my then girlfriend and now my wife, for always caring me and being by my side through many ups and downs. I would not be able to get this work done without you.

Karlsruhe, 23th September 2022, Minh Nhat Nguyen

“...There is an ecstasy that marks the summit of life, and beyond which life cannot rise. And such is the paradox of living, this ecstasy comes when one is most alive, and it comes as a complete forgetfulness that one is alive.

This ecstasy, this forgetfulness of living, comes to the artist, caught up and out of himself in a sheet of flame; it comes to the soldier, war-mad in a stricken field and refusing quarter; and it came to Buck, leading the pack, sounding the old wolf-cry, straining after the food that was alive and that fled swiftly before him through the moonlight...”

The Call of the Wild, Jack London

Note: for the sake of the environment, this PhD dissertation contains only greyscale images, and shall be printed in black and white.

Publications

The following publications were produced from this study (the four core papers are in bold). The contribution of co-authors in the core papers are indicated in the opening of each corresponding chapter.

Accepted:

J. Zhang, M.N. Nguyen, Y. Li, C. Yang, A.I. Schäfer, Steroid hormone micropollutant removal from water with activated carbon fiber–ultrafiltration composite membranes, *J. Hazard. Mater.*, 391 (2020) 122020.

Z. Liao, M.N. Nguyen, G. Wan, J. Xie, L. Ni, J. Qi, J. Li, A.I. Schäfer, Low pressure operated ultrafiltration membrane with integration of hollow mesoporous carbon nanospheres for effective removal of micropollutants, *J. Hazard. Mater.*, 397 (2020) 122779.

M.N. Nguyen, P.G. Weidler, R. Schwaiger, A.I. Schäfer, Interactions between carbon-based nanoparticles and steroid hormone micropollutants in water, *J. Hazard. Mater.*, 402 (2020) 122929.

M.N. Nguyen, P.B. Trinh, C.J. Burkhardt, A.I. Schäfer, Incorporation of single-walled carbon nanotubes in ultrafiltration support structure for the removal of steroid hormone micropollutants, *Sep. Purif. Technol.*, (2021) 118405.

M.N. Nguyen, R. Hervas-Martínez, A.I. Schäfer, Organic matter interference with steroid hormone removal by single-walled carbon nanotubes – ultrafiltration composite membrane, *Water Res.*, 199 (2021) 117148.

In preparation:

M.N. Nguyen, M.L. Jue, S.F. Buchsbaum, S.J. Park, F. Vollnhals, S. Christiansen, F. Fornasiero, A.I. Schäfer, Steroid hormone micropollutant adsorption by vertically aligned single-walled carbon nanotube membranes (submitted to *ACS Nano* in 2022).

A. Imbrogno, M.N. Nguyen, A.I. Schäfer, Error estimation in experimental water research: Application to membrane technology.

1 Introduction

This chapter first provides a broad context of the research project and guides the readers through the major challenges of sustainable water management.

The next part emphasises water contamination with micropollutants and underlines the need to remove these compounds (steroid hormones in particular) from wastewater and surface water. The production of micropollutant-free water for human consumption is an important quest of sustainable water management.

Subsequently, the main treatment technologies for micropollutants are discussed. This section also highlights the prospect of membrane technology and adsorption composite membranes (the focus of this dissertation) in removing and controlling steroid hormone micropollutants.

The last part of this chapter outlines the research objectives and questions and describes the overall structure of the dissertation.

1.1 Challenges of sustainable water management

In 2015, the United Nations established seventeen Sustainable Development Goals by 2030, among which Goal 6 determines to “ensure availability and sustainable management of water and sanitation for all”¹. Sustainable water management is a means to balance water demand and availability, as such the needs of water services (domestic use, ecology, agriculture, industry, and other services) can be met without impairing the future supply of water². Achieving this sustainability requires the world to acknowledge and address many water-related challenges that can get worse in the future generations, including: i) water scarcity and low water quality for human consumption in third-world countries, ii) increasing water demand driven by the population growth and urbanisation, iii) vulnerability to natural disasters (floods and droughts), and iv) water pollution leading to the destruction of ecosystems^{3,4}.

The water scarcity and quality issues are challenging to address. Figure 1.1 provides a geographical overview of the population share in every country without access to an improved water source in 2020. Severe water stress is observed in the Middle East, Southeast Asia, and especially Africa. In most African countries where poverty is prevalent, up to 40% of the population is not guaranteed safe water for consumption. The lack of improved water sources is linked to increased risks of serious water-borne diseases, such as diarrhoea, cholera, malaria, and hepatitis⁵. For example, diarrhoea causes the death of more than half a million children (under the age of 5) annually⁶.

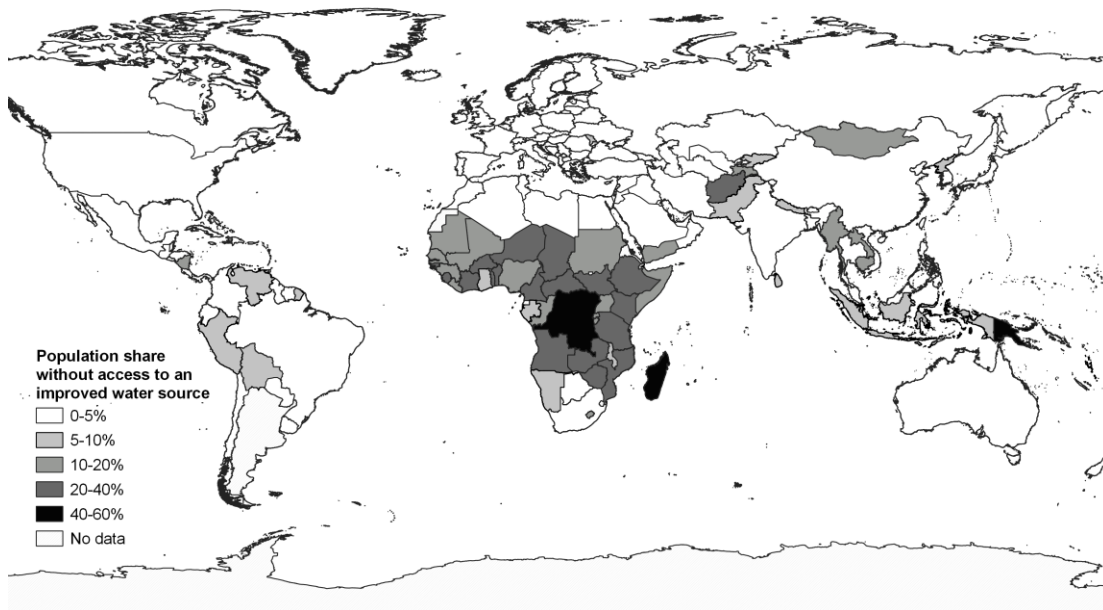


Figure 1.1: Population share without access to an improved water source in 2020. The database was published by WHO/UNICEF (JMP_2021_WLD) in 2022⁷⁾. The map was created by M.N.

The above challenge in maintaining water security and sanitation in parts of the world will require changes in the way water, food, energy, and services are provided and consumed. Seeking alternative safe and clean water resources is a priority⁸⁻¹¹. Scientific and technological advancement is crucial in providing new solutions to address the challenges directly, offering policy makers the benchmarks to mitigate and adapt to water issues, and allowing less-developed countries to achieve sustainability *via* ‘technological leaps’^{12,13}.

For example, reverse osmosis (RO) is the core technology in the desalination scheme, which converts seawater in vast quantity on Earth into drinking water¹⁴. Today, thousands of desalination plants have been operated around the globe¹⁵; many of those are coupled with energy recovery devices to compensate the high costs of desalination¹⁶. Desalination resolves the water stress in several water-scarce countries, such as Saudi Arabia, Israel, United Arab Emirates, and Singapore¹⁷. RO is also applied in wastewater reclamation, in which (grey) wastewater is recycled into high-quality water for domestic and industrial purposes. For instance, the NEWater project in Singapore utilises RO and a sequence of disinfection steps to convert wastewater into potable water¹⁸, and now provides 30% of the country’s water demand¹⁹. The success of NEWater is an example of how advanced water technologies can be pioneered. Other examples of technological advances include: direct integration of solar panels to power water treatment technology (nanofiltration, NF) in off-grid regions²⁰ and water harvesting from air with highly porous materials²¹.

Advanced technologies are particularly needed to tackle the emerging challenge of micropollutant occurrence in water sources²². The details of this course will be discussed in the next parts of the Introduction.

1.2 Micropollutants in the water environment

Micropollutants are contaminants that occur at very low concentrations in waters (nanograms or picograms per litre), but they can cause adverse effects on the environment and human health²³. Some of these, such as dichlorodiphenyltrichloroethane and perfluorinated compounds, persist in the water environment^{24, 25}. Other micropollutants, such as steroid hormones, are less persistent but continuously discharged from various sources²⁶.

Because of the low concentrations in waters, persistence and/or ubiquity of micropollutants, difficulties arise in all parts of the treatment process, from detection, monitoring, impact assessment, to mitigation and prevention²². In a comical way, Figure 1.2 highlights that some micropollutants originating from household discharge can penetrate through all the water treatment steps, and finally occur in drinking water to (re)enter the body. These micropollutants include 17β -ethinylestradiol in contraceptive pills, carbamazepine and ibuprofen in drugs, sulfamethoxazole in antibiotics, and so forth²⁷⁻²⁹.

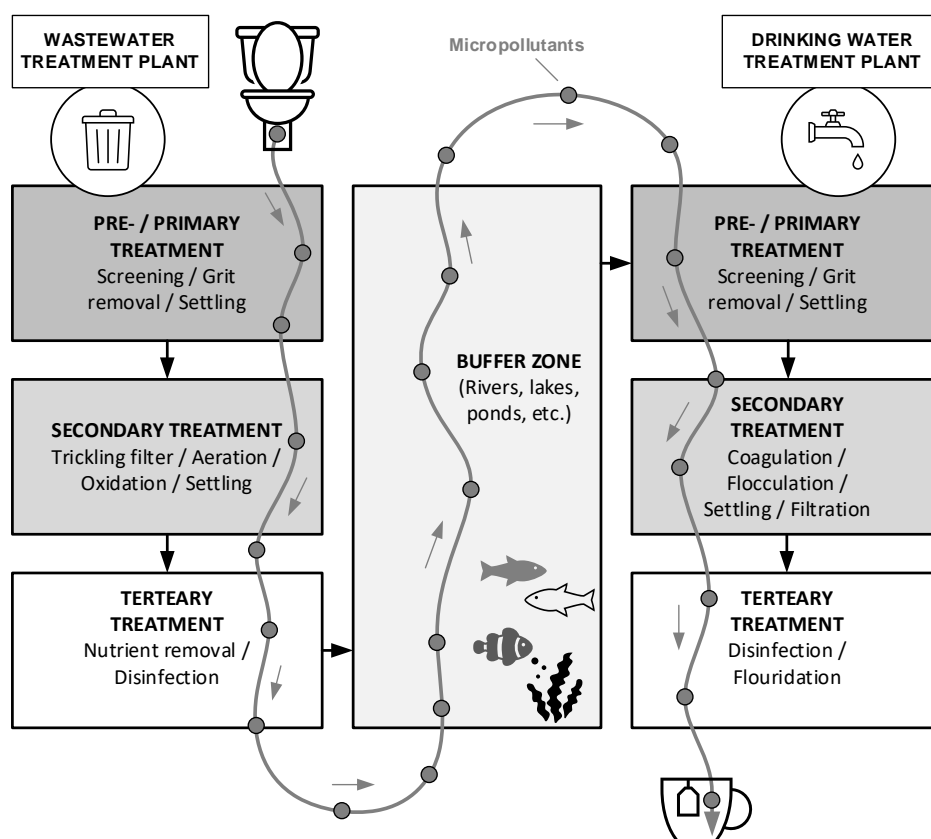


Figure 1.2: Summary of steps in conventional wastewater and drinking water treatment facilities. Micropollutants can penetrate through all these steps and occur in the drinking water. The investigation in this dissertation fits in the tertiary treatment step of wastewater treatment.

In the next parts of the Introduction, the focus will shift to steroid hormones, a potent class of micropollutants. The toxicology, occurrence, and legislative and technological measures that surround these compounds will be examined.

1.3 Steroid hormone micropollutants

The term “endocrine disrupting chemicals” (EDCs), or “endocrine disruptors”, refers to a class of micropollutants that can interfere with the functions of the endocrine system in the body³⁰. The damages caused by EDCs lead to huge economic burdens annually, of over 200 million dollars in Europe³¹ and 350 million dollars in the USA³². These calculated costs only considered several types of EDCs and their likely health outcomes (such as neuro-behavioural diseases, obesity, diabetes and reproductive disorders); therefore, the actual burdens can be much more severe³³.

Steroid hormones are a sub-class of EDCs that have both natural and synthetic origins and are potent *via* the binding with the hormonal receptors in the body. Natural and endogenous steroid hormones, such as estrone (E1), 17 α -estradiol (17 α -E2), 17 β -estradiol (E2), estriol (E3), testosterone (T) and progesterone (P) are secreted by respective steroid glands and can biotransform in the body (Figure 1.3)³⁴.

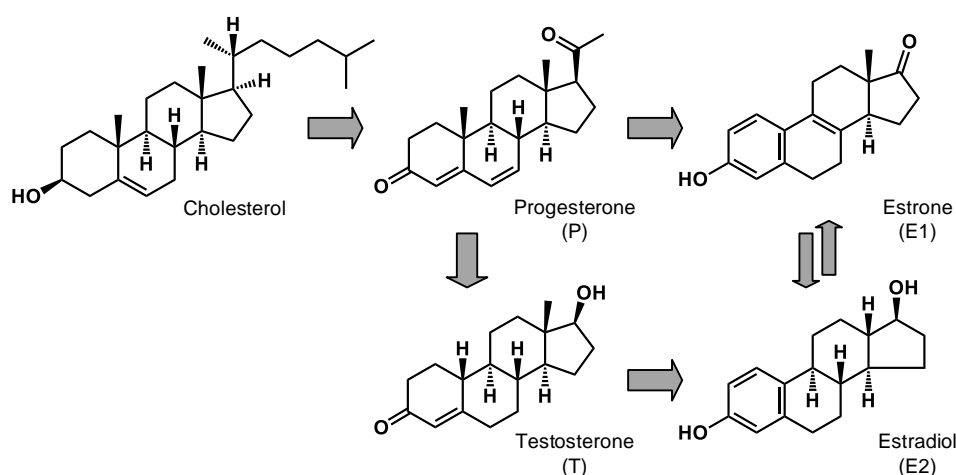


Figure 1.3: Simplistic view of the biotransformation of steroid hormones in the body; each arrow represents a biotransformation pathway. The four hormones E1, E2, T and P are the removal targets of this research project. Adapted from Chatuphonprasert *et al.*³⁴.

These hormones carry out a range of physiological functions, including the reproductive ones, at low (usually in ng/L or sub- μ g/L) concentrations³⁵⁻³⁷. Several synthetic hormones mimic the physiologic function of estrogens; a notable example is 17 α -ethinylestradiol (EE2), which is a common ingredient in contraceptive pills³⁸. Other synthetic compounds are produced for completely different purposes, for example Bisphenol A (BPA) in the plastic industry; but when entering the body, they bind with the steroid receptors and affect the hormonal functions³⁹. Both synthetic and natural steroid hormones can cause reproductive system failures, cardiovascular diseases, and cancer when exceeding the functional concentrations in the body⁴⁰⁻⁴². Drinking water that contains even sub-ng/L concentrations of steroid hormones can lead to various potential health risks.

Steroid hormone micropollutants have been found in wastewater treatment plant (WWTP) influents and effluents, surface water and even groundwater⁴³ at concentrations varying from sub-

ng/L to several $\mu\text{g/L}$. Hormone concentrations vary depending upon the water type, location, season, and economic status of the region.

Table 1.1 gives a summary of the maximum concentrations of several hormones in WWTP effluents and surface water from 1998 to 2019. These concentrations are benchmarked against the predicted no-effect concentrations (PNECs) proposed by Caldwell *et al.*, of 6, 2, 60 and 0.1 ng/L for E1, E2, E3 and EE2, respectively ⁴⁴; other reported PNEC values are similar and varying in the range between sub-ng/L and several ng/L ^{45, 46}.

Table 1.1: Maximum concentrations of steroid hormone micropollutants (E1, E2, E3 and EE2) in wastewater effluents and surface water ^{43, 44, 47-58}. Abbreviations: WE: wastewater effluent, SW: surface water, N.A.: not available, N.D.: not detected (below detection limit).

No.	Reference	Reviewed period	Water type (location)	Maximum conc. in ng/L			
				E1	E2	E3	EE2
1	Ying <i>et al.</i> 2002 ⁴⁷	1998–2002	WE	82	64	18	42
			SW	4.1	27	0.3	5.1
2	Pal <i>et al.</i> 2010 ⁴⁸	2006–2010	WE	200	43	25	5.6
			SW	38	4.5	12	4.5
3	Gardner <i>et al.</i> 2012 ⁴⁹	2012	WE (UK)	100	13	N.A.	1.6
4	Zhou <i>et al.</i> 2012 ⁵⁰	2012	WE (Beijing, China)	70	19	320	7
5	Aris <i>et al.</i> 2014 ⁵¹	2003–2012	SW	180	175	94	24
6	Barbosa <i>et al.</i> 2016 ⁴³	2009–2015	WE	220	88	N.A.	8
			SW	69	10	N.A.	1.9
7	Tran <i>et al.</i> 2018 ⁵²	2003–2017	WE	95	N.A.	275	106
8	Sacdal <i>et al.</i> 2020 ⁵³	2013–2019	SW (Asia)	84	33	57	44
9	Madikizela <i>et al.</i> 2020 ⁵⁴	2017–2019	WE (Africa)	41	165	540	4600*
			SW (Africa)	46	16	N.A.	0.9
12	Tang <i>et al.</i> ⁵⁵	2020	WE (China)	15	N.D.	7.2	N.A.
			SW (China)	11	7.6	4.3	N.A.
13	Sta. Ana & Espino ⁵⁶	2020	SW (Philippines)	0.3	0.4	N.A.	N.D.
14	Ng <i>et al.</i> 2021 ⁵⁷	2021	SW (USA)	38	< 25	80	6.7
15	Lu <i>et al.</i> 2021 ⁵⁸	2021	SW (China)	1.5	3.2	18	21
Predicted no-effect concentration (PNEC) ⁴⁴				6	2	60	0.1

* Data for hospital wastewater effluents are included.

The summary of data from 1998 to present indicates that E1, E2, E3 and EE2 concentrations ranged from sub-ng/L (*i.e.* not detectable) to several hundred ng/L in both WWTP effluents and

surface water. The environmental impacts of E1, E2 and EE2 at elevated concentrations have been universally reported. In 1994, Purdom *et al.* observed the feminisation of fish when the fish were exposed to EE2 from wastewater effluents; the ensuing lab tests indicated that the same response can be triggered at EE2 concentrations as low as 0.1–0.5 ng/L⁵⁹. Since then, many research groups have determined the impact of estrogens on various communities of fish^{60, 61}, mussels^{62, 63} and amphibians^{64, 65}. It is summarised from these works that the toxicological effects of estrogens can be observed at concentrations as low as 0.3 ng/L, and hence it is necessary to completely eliminate these micropollutants from water.

Steroid hormone concentrations in wastewater influents are one or two orders of magnitude higher than those in WWTP effluents^{28, 66} (data are not included in Table 1.1). Because conventional WWTPs are not capable of complete removal of micropollutants, they are carriers of micropollutants into the water environment^{67, 68}. In the more developed countries (USA, UK, Germany, and China), drinking water is safe from natural steroid hormones because these compounds are either not found or at lower concentrations than the PNECs⁶⁹⁻⁷⁴; the same statement cannot be confirmed for less developed countries where data are not available.

In addition, the sensitivity of analytical instrument is a challenge for EE2 determination. The detection limit needs to reach the PNEC of EE2 (0.1 ng/L) for a meaningful assessment, which is very hard to attain. Relevant laws and their associated guidelines will play an important role to address the increasing concerns over EDCs and steroid hormones in waters *via* stringent monitoring and control.

1.4 Drinking water guidelines for steroid hormones

In response to the increasing public concern over specific types of micropollutants, several regulations related to EDC and steroid hormones monitoring and control have been promulgated. Table 1.2 gives a list of main regulations and guidelines / recommendations in USA, Europe, Japan, Australia, and Switzerland, and guidelines from international organisations.

In the USA, several laws (namely the *Food Quality Protection Act* and *Amendments to Safe Drinking Water Act*) and accompanying guidelines / rules are in effect, but all these documents propose no health-based standards. Similarly, the Japanese *Strategic Programs on Environmental Endocrine Disruptors* and accompanying *Extended Tasks* do not contain the health-based standards⁷⁵. The Swiss *Water Protection Ordinance* requires all WWTPs to remove at least 80% of a several micropollutants in a priority list, but this list include no steroid hormones⁷⁶. The Swiss regulation sparks controversy, because i) the 80% removal is not a health-based but an ‘one-size-fits-all’ indicator, and ii) all WWTPs are required to upgrade regardless of the capacity and dilution factors of receiving waters^{77, 78}. As such, difficulties arise for a proportion of WWTPs in adopting this regulation.

The *Guidelines for Drinking Water and Water Recycling* in Australia^{79, 80} in 2008 and 2011 recommend the health-based standards of E1, E2, 17 α -E2, E3, EE2 in drinking water to be 110, 175, 175, 50, 1.5 ng/L, respectively, although these standards were calculated or extrapolated from limited toxicological data, and are 1–2 orders of magnitude higher than the PNECs⁴⁴.

Table 1.2: Notable laws (in italics) and guidelines / recommendations on the monitoring and treatment of EDCs and steroid hormones.

Country / region	Main documents	Comments	Health-based standards (if any)
United States	<i>Clean Water Act 1972, Food Quality Protection Act 1996, EDSP 1998</i> UMCR 1, 2, 3 and 4 (2011–2021), EDSP EDC Tiers 1 (2009) and 2 (2013), CCL3 (2009) and CLL4 (2016)	No health-based standards	N.A.
European Union	<i>Water Framework Directive 2000, REACH 2006, Directive 2008/105/EC, Decision 2013/39/EU, Decision 2015/495/EU, Decision 2018/840, Directive 2020/2184</i> SCHER Opinions E2 (2011)	Proposed health-based standards for steroid hormones are not approved in regulations and only serve as guideline values	In discharged water: 0.4 ng/L of E1 and E2 and 0.035 ng/L of EE2 (<i>Decision 2015</i>), In drinking water: 1 ng/L E2 (<i>Directive 2020</i>)
Japan	<i>SPEED 98, Extended Tasks on Endocrine Disruption 2005 & 2010</i>	No health-based standards	N.A.
Australia	Australian Drinking Water Guidelines 2011 Australian Guidelines for Water Recycling – Phases 1 (2006) and 2 (2008)	Health-based standards are much higher than PNECs because of predictions from limited toxicological data	In drinking water: 110 ng/L E1, 175 ng/L E2, 175 ng/L 17 α -E2, 50 ng/L E3, and 1.5 ng/L EE2
Switzerland	<i>Water Protection Ordinance, latest ed. 2016</i>	One-size-fits-all approach (80% removal demanded), requires all WWTPs to upgrade regardless of capacity	N.A.
International	WHO Guidelines for Drinking-water Quality (latest ed. 2017), OECD EDTA Guidelines (2012, 2018), WHO–EU Drinking Water Parameter Cooperation – Recommendations (2017)	Health-based standards are given in the WHO–EU Recommendations document	In drinking water: 1 ng/L of E2

Abbreviations: EDC – Endocrine Disrupting Chemicals, EDSP – Endocrine Disruptor Screening Program, UMCR – Unregulated Contaminant Monitoring Rule, CCL – Contaminant Candidate List, REACH – Registration, Evaluation, Authorisation and Restriction of Chemicals, SCHER – European Scientific Committee on Health and Environmental Risks, SPEED – Strategic Programs on Environmental Endocrine Disruptors. OECD – Organisation for Economic Cooperation and Development, EDTA – Endocrine Disruptors Testing and Assessment.

Europe has the most adequate framework for regulating EDCs, with a list of priority contaminants in water that is updated once in several years ⁸¹, although many problematic compounds do not appear in the priority list ⁷⁷. E2 and EE2 had been proposed for inclusion in this priority list with respective environmental quality standards of 0.4 and 0.035 ng/L ⁸², but only appeared in the ‘watch list’ of the official *Decision 2015/495/EU* regulating WWTP discharge water ⁸³. In the 2015 Decision, the concentrations 0.4 ng/L for E1 and E2 and 0.035 ng/L for EE2 are instead

proposed as the maximum detection limits of analytical tools. Related to drinking water, the official *Directive 2020/2184* rejected a proposal for regulating E2 at 1 ng/L; instead, E2 was only added to the watch list for future consideration⁸⁴. It is implied that water treatment and analytical technologies are not advanced enough to accomplish the satisfactory health-based standards. The value of 1 ng/L only serve as a guideline value to evaluate the performance of water treatment technologies.

It is also challenging to utilise treatment technologies that are competent enough to remove micropollutants to such very low concentrations (1 ng/L), and easily integrated into existing plants. In the next section, a number of appropriate technologies will be evaluated for steroid hormone removal.

1.5 Technologies for steroid hormone removal

This sub-chapter gives a review on three treatment technologies, which are ozonation, adsorption and filtration. Ozonation and adsorption with powdered / granular activated carbon (PAC / GAC) are the applicable technologies for large-scale WWTPs, as both are effective in micropollutant removal and competitive in terms of treatment costs^{85, 86}.

In the state of Baden–Württemberg, Germany, 21 WWTPs with micropollutant removal are active, 8 WWTPs are under construction, and 15 WWTPs are planned as of May 2021; the adopted technologies to remove micropollutants are either adsorption or ozonation⁸⁷. The locations these plants are shown in Figure 1.4 (the WWTP information and administrative boundaries were provided by KOMS-BW⁸⁷ and LDL-BW⁸⁸, respectively).

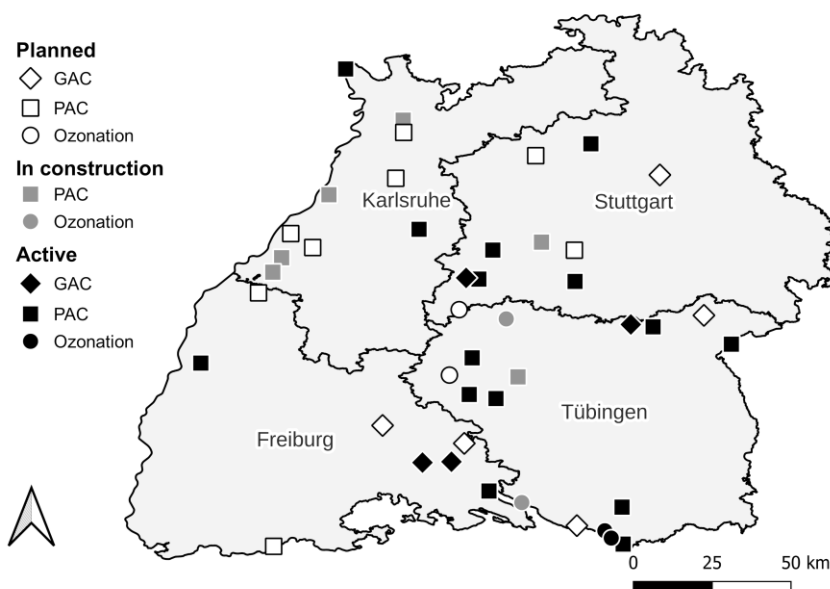


Figure 1.4: Map of WWTPs with micropollutant removal technologies (granular / powdered activated carbon (GAC/PAC) adsorption, and ozonation) in Baden–Württemberg (BW), including those in construction or planned. Data were taken from the BW websites^{87, 88} in March 2022. The map was created by M.N.

Filtration processes such as NF and RO are more energy-demanding than adsorption and ozonation^{89,90} although RO is an essential component in wastewater reclamation facilities where wastewater is directly transformed into potable water. RO is accepted because it offers very high removals of all types of organic contaminants, along with added benefits such as salt removal⁹¹.

1.5.1 Ozonation technology

Ozonation is a treatment process in which highly reactive oxygen species are produced, which then attack and break down a wide range of organic compounds and microorganisms⁹². A simplistic view of this process is given in Figure 1.5. Ozonation is effective at eliminating steroid hormones^{85,93-96}.

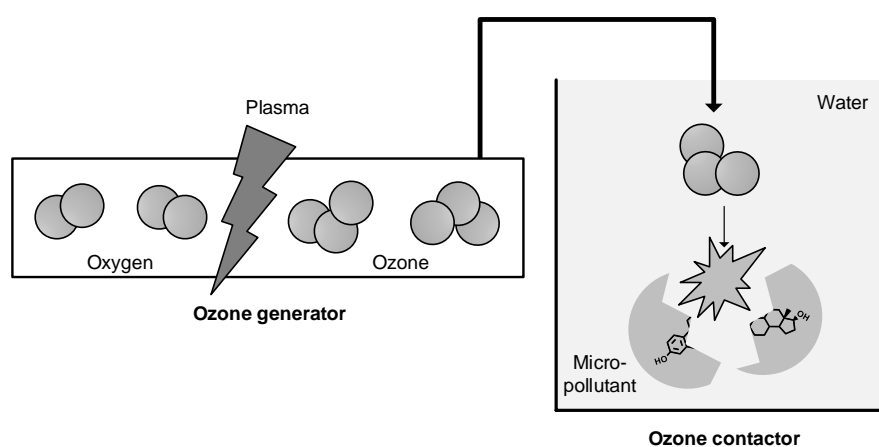


Figure 1.5: Schematic view of the ozonation process.

However, a drawback of ozonation is the formation of toxic by-products, namely ketones, aldehydes, nitrogen-containing species, and bromate^{92,97,98}. Bromate⁹⁹ and nitrogen-containing by-products, such as N-nitroso-dimethylamine (NDMA)¹⁰⁰, are carcinogenic by-products of oxidation. Some of these by-products can be retained in a subsequent sand filtration step^{101,102}. However, it appears that, while sand filtration is practical, it does not guarantee complete elimination of known toxic compounds, while the list of potentially toxic by-products of ozonation (especially brominated organic compounds) is continuously growing¹⁰³⁻¹⁰⁶.

Because of the toxicity of the ozonation by-products, adsorption and membrane filtration are considered as ‘safer’ alternative technologies to remove steroid hormone micropollutants.

1.5.2 Adsorption technology

Adsorption processes allow good micropollutant removal based on the high affinity of the micropollutants (*adsorbates*) for the surface of the adsorbing materials (*adsorbents*)¹⁰⁷. In this dissertation, three types of carbonaceous adsorbents are mentioned, which are GAC, PAC, and carbon-based nanoparticles (CNPs). While GAC and PAC have been largely applied in industrial scale, CNPs have only been examined in lab scale. Only the application of GAC and PAC for

steroid hormone removal are discussed in this section, whereas the evaluation of CNPs will be provided in Sub-chapter 2.3.

Both GAC and PAC are effective at steroid hormone removal from relevant concentrations in waters (sub- $\mu\text{g/L}$ to several $\mu\text{g/L}$) in a *static adsorption* process¹⁰⁸⁻¹¹². It appears that for various activated carbon types, both moderately high doses (sub-g/L to several g/L) or long residence times (at least 1 h) are required to remove steroid hormones with high effectiveness. Industrial applications require that water continuously flows through the adsorbents while giving sufficient residence time for the adsorbents to remove the pollutants^{113, 114}. The shorter required residence time, the more efficient this *dynamic adsorption* process. The main designs of adsorbents illustrated in Figure 1.6. GAC with sizes of several millimetres are typically arranged in fixed-bed adsorbers where the adsorber heights and diameters are up to several metres¹¹⁵⁻¹¹⁷. In contrast, the sizes of PAC are too small to allow good water permeation in fixed-bed configuration; instead, PAC are dosed in powder or slurry form into the contactor¹¹⁸. Spent particles are retrieved *via* coagulation / flocculation for replacement¹¹⁸, and loose particles are retained in the subsequent filtration step (such as UF)¹¹⁹. In pilot and industrial scale plants, adsorption by PAC offers similar effectiveness as ozonation in removing micropollutants from wastewater^{85, 86}.

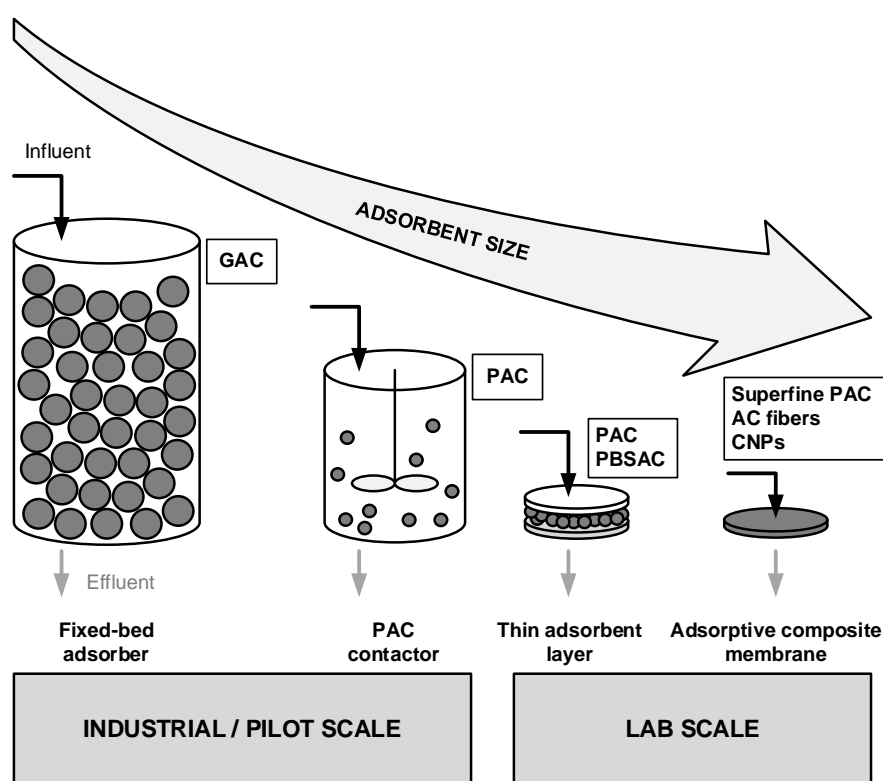


Figure 1.6: Schematic of different adsorption system designs based on the adsorbent size: large (GAC, several millimetres), medium (PAC and PBSAC, several to a few hundred micrometres), and small (*e.g.* CNPs, a few nanometres to sub-micrometres). The adsorptive composite membranes are the research targets of this dissertation.

Adsorption technology have several drawbacks. The most important one is the trade-off between the dose of activated carbons and residence time: the lower the dose, the longer residence time

required to achieve a good steroid hormone removal, and *vice versa*^{109, 112}. For example, with a relatively long residence time of 24 h, many micropollutants in hospital wastewater were removed by >80% in a PAC adsorption process with a PAC dose of 23 mg/L¹²⁰. However, in another study, when the residence time was much lower (less than 1 min) by directly dosing the feed stream with PAC at 15–30 mg/L, only 20–70% removal of similar compounds was attained¹²¹.

Another drawback of adsorption is the recurrent retrieval of adsorbents, because the adsorbents lose the adsorption capability over time¹²². Regeneration methods, such as thermal regeneration¹²³, are resource-consuming. In addition, some water components may interact with either the micropollutants or the adsorbents and lower the micropollutant–adsorbent, and the adsorption performance declines as a result¹²⁴⁻¹²⁶.

1.5.3 Membrane technology

Membrane technology has been increasingly applied in water treatment because of several advantages: i) good separation capability that is adjustable *via* tuning the membrane pore size and surface properties, ii) low to moderate energy consumption, iii) small footprint, iv) good integrability in existing water treatment plants, v) long lifetime of several years, and v) easy operation and maintenance^{127, 128}. The characteristics and removal targets of four types of membranes (microfiltration MF, ultrafiltration UF, NF and RO) are given in Table 1.3.

Table 1.3: Characteristics of different types of membranes (MF, UF, NF and RO)¹²⁹⁻¹³⁶. N.D.: Not determined.

	MF	UF	NF	RO
Pore size (nm) ¹²⁹	100–10,000	2–100	0.5–2	<0.5
Targets of retention ¹²⁹	Particles	Particles and macro-molecules	Small organic compounds and multivalent ions	Small organic compounds, mono- and multivalent ions
Pressure (bar) ¹²⁹	0.1–2	0.1–5	3–20	5–120
Permeability (L/m².h.bar) ¹²⁹	>1,000	10–10,000	1.5–30	0.05–1.5
Specific energy consumption* (kW.h/m³)	0.05–0.1 ¹³⁶	0.03–0.3 ^{130, 131}	0.2–0.4 ^{132, 133}	Sea water: 2.3–5.2 ¹³⁴ Brackish water: 0.4–1.7 ¹³⁵
Cost per m³ of treated water with membrane** (Euro)	0.01–0.02	0.007–0.07	0.05–0.09	Sea water: 0.5–1.2 Brackish water: 0.09–0.4
Ability to remove steroid hormones (0.8 nm in size)	No	No	Yes	Yes

* For moderate- and large-scale water treatment plants with at least several hundred m³ of treated water per day.

** Estimated from European electricity price in the first half of 2022, at 0.23 Euro per kW h¹³⁷.

Membranes with pore sizes in sub-nanometre range (such as NF) or no distinctive pores (RO) are applicable to retain steroid hormone micropollutants (which are around 0.8 nm in size)¹³⁸⁻¹⁴⁶. Some RO membranes for brackish water remove 90–95% of steroid hormones^{138, 140}, although a major disadvantage with RO is that the energy barrier is very high due to the elevated pressures (5–120 bar) required to push water across the semi-permeable but non-porous membranes¹⁴. NF may excel over RO in terms of energy consumption while still offering good but incomplete steroid hormone removals of 80–95%^{138, 140, 146, 147}. The energy requirements for pressures of 5–20 bar is still high (see Table 1.3). Size exclusion is a dominant removal mechanism, as such RO removes hormones more effectively than NF, although some hormone adsorption by both membrane types was observed^{139, 140, 142}. The adsorbed molecules (*i.e.* those partitioned to the membrane materials) gradually permeate (break) through the membrane and reach the clean filtrated water. As a result, hormone removal is lower than expectations from pore models¹⁴⁸.

Beside the high energies required for NF and RO (see Table 1.3), the membranes have several other drawbacks, namely the challenge in disposing highly contaminated waste (concentrate)¹⁴⁹, risk of exposure to contaminants upon membrane failure¹⁵⁰, and decrease in filtration performance over time caused by membrane fouling¹⁵¹. These combined drawbacks have stalled the industrial scale application of membrane technology for micropollutant removal.

High-permeability membranes such as MF and UF cannot retain steroid hormones because the pore sizes of these membranes are larger than those of the hormones^{122, 143}. However, hormone removal may be possible if the adsorptive functionality is incorporated into these membranes¹²². Several adsorbing materials (which are called adsorbents), such as granular and powdered activated carbons (GAC/PAC), and carbon-based nanoparticles (CNPs), such as carbon nanotubes (CNTs) and graphenes, have been applied or evaluated for micropollutant and steroid hormone removal^{85, 122, 152-155}. The CNPs are small enough in size (nanometres to micrometres) to be incorporated into the UF or MF membrane¹⁵⁶⁻¹⁵⁸ to form an adsorptive composite membrane (ACM). This ACM combines the retention of macromolecules, colloids, bacteria and viruses, and adsorption of small compounds such as micropollutants.

Although GAC and PAC have been investigated for decades, CNPs have just recently been considered for environmental applications¹⁵², and ACMs that incorporate CNPs are still in their infancy.

1.6 Objectives of the dissertation

The main research objective is to investigate the possibilities of **removing micropollutants (steroid hormones) from waters with ultrafiltration membranes**, with specific focus on incorporating carbon-based nanoparticles (CNPs) in these membranes to allow removal *via* adsorption. Currently, CNPs are not applied in water treatment because of the toxicity concerns. However, the characteristics of adsorbents and membranes are examined in this work to attain the key considerations for improving the ACMs. The primary research problems are as follows.

- Surface characteristics affect the micropollutant access and adsorption to the adsorbent surface. Examination of the adsorbent surface is necessary to determine the suitable adsorbents for membrane incorporation.
- Short residence times (in which the hormones are in contact with the adsorbent layer) limit the adsorption performance of the ACMs; the choice of membranes and process configurations is important to achieve good removal against the mass transfer limitation.
- When the surface and mass transfer no longer limit adsorption, the hormone molecules are still under the influence of an interplay of forces. These forces need to be quantified to evaluate hormone adsorption in ACMs and polymeric membranes.

(It is worth clarifying that the mass transfer described throughout this dissertation refers to the “mass transfer of steroid hormone micropollutants from the bulk to the sorbed phase”.)

To attain the research objective and address the research problems associated with ACMs, the following research questions will be answered in the dissertation.

1. Which CNPs provide fast adsorption kinetics and high adsorption capacity (which reflects good amounts of accessible surface) and hence are suitable for the incorporation in ACMs?
2. How are mass transfer limitation and hormone adsorption influenced by varying operational conditions and water quality in the filtration with ACMs?
3. How does the interplay of forces dictate hormone adsorption in the nanopores of VaCNT membranes (which can then explain adsorption in ACMs and UF/NF membranes)?

The long-term goal is to **design a micropollutant treatment process that requires little or no chemicals, consumes low energy, and is easy to maintain and operate**. This process should be appropriate for water treatment plants to improve natural and drinking water quality, although several next steps toward industrial applications must be considered beyond this research project, namely: regeneration strategies, nanoparticle leakage prevention, cost analysis, and public acceptance of the treatment. The adoption of ACMs will take a long way, although the conclusions drawn from this study will certainly contribute to the future development of effective composite membranes.

1.7 Structure of the dissertation

The structure of this dissertation is illustrated in Figure 1.7 and described as follows.

Chapters 2 is structured like a literature review paper. Chapter 3 summarises the materials and methods. Each of Chapters 4–7 is structured in a similar to an original research paper:

- The first sub-chapter introduces the main research problem to be addressed,
- The next sub-chapter gives a brief summary of the experiments,
- The several following sub-chapters present and discuss the experimental results,
- The last sub-chapter states the three key main findings and remarks on the significance of the results.

The last chapter, Chapter 8, summarises the major results of this dissertation and suggests ideas for future investigations. The Appendices A–O add background information. All the references are combined and presented at the end of the dissertation.

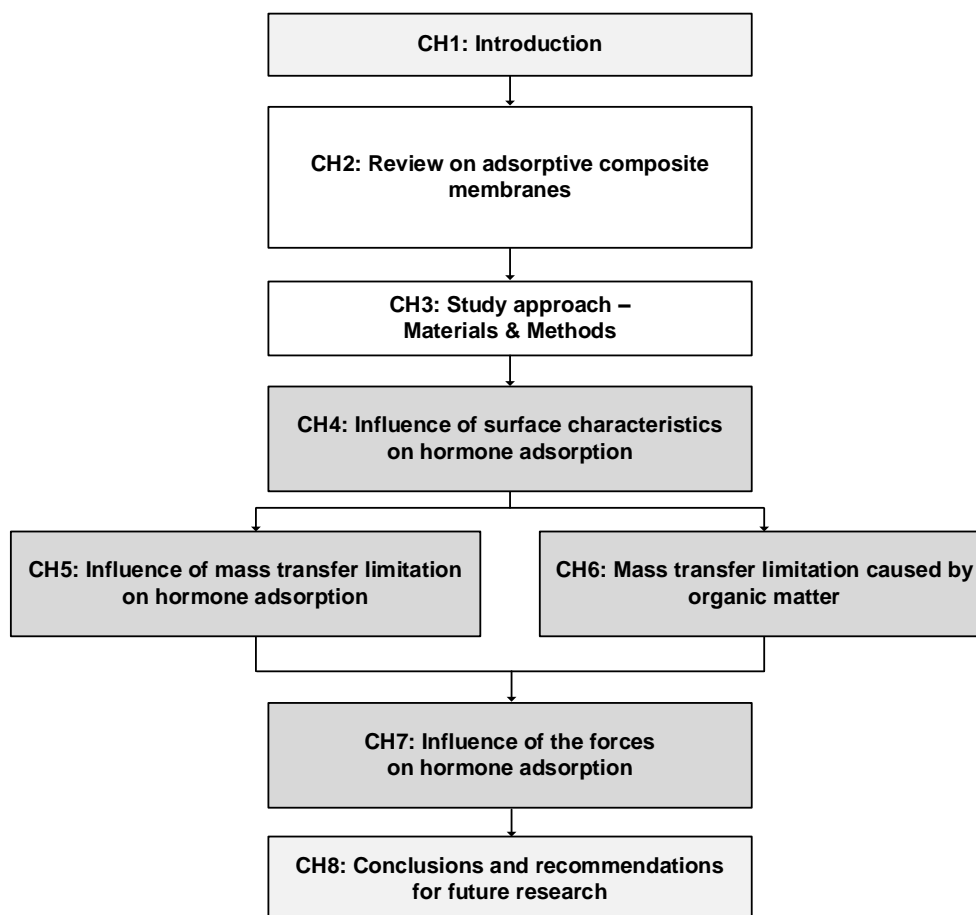


Figure 1.7: Schematic of the dissertation structure.

Chapter 2 is a review on the ACMs, which compare these membranes with hybrid filtration processes (where the filtration and adsorption modules are separate), the five technical considerations associated with ACM development, and evaluation of several composite membrane designs.

Chapter 4 presents the experimental results of steroid hormone adsorption by six nanoparticles with varied surface properties (area, morphology, and chemistry), discusses the influence of surface characteristics for hormone adsorption, and justifies which nanoparticles are suitable for incorporation in the UF membrane.

Related publication: “M.N. Nguyen, P.G. Weidler, R. Schwaiger, A.I. Schäfer, *Interactions between carbon-based nanoparticles and steroid hormone micropollutants in water*, J. Hazard. Mater., 402 (2020) 122929.”

Chapter 5 presents the experimental results of steroid hormone removal by CNP–UF composite membranes with varying CNP loading, residence time, and solution pH, and discusses the

influence on adsorption of mass transfer limitation due to the low loading and short residence time. The CNP in focus is single-walled carbon nanotube (SWCNT), which has the best performance according to Chapter 5 results.

Related publication: “M.N. Nguyen, P.B. Trinh, C.J. Burkhardt, A.I. Schäfer, *Incorporation of single-walled carbon nanotubes in ultrafiltration support structure for the removal of steroid hormone micropollutants*, Sep. Purif. Technol., (2021) 118405.”

Chapter 6 presents the experimental results of the interference of nine types of organic matter (OM) with steroid hormone adsorption by the SWCNT–UF membranes, and discusses the mass transfer limitation caused by some specific OM types. The OM interference mechanisms and shielding effect of the UF MWCO against OM are examined.

Related publication: “M.N. Nguyen, R. Hervás-Martínez, A.I. Schäfer, Organic matter interference with steroid hormone removal by single-walled carbon nanotubes - ultrafiltration composite membrane, Water Res., 199 (2021) 117148.”

Chapter 7 presents the experimental results of steroid hormone removal with vertically aligned carbon nanotube (VaCNT) membranes, where adsorption takes place inside the 1.7–3.3 nm hydrophobic and atomically smooth pores. This chapter discusses the interplay of forces that dictates hormone adsorption where mass transfer limitation is non-existent.

Related submitted manuscript: “M.N. Nguyen, M.L. Jue, S.F. Buchsbaum, S.J. Park, F. Fornasiero, F. Vollnhals, S. Christiansen, A.I. Schäfer, *Adsorption of steroid hormone micropollutants in the nanoconfinement of vertically aligned single-walled carbon nanotube membranes*, submitted to ACS Nano (2022).”

2 Adsorptive Composite Membranes for Steroid Hormone Micropollutant Removal

In addressing the water sustainability challenges, in particular the emergence of endocrine disrupting micropollutants, a detailed discussion on adsorptive composite membranes (ACMs) is provided in this chapter, with steroid hormone micropollutant removal as the focus of application.

After a short introduction on the prospective of ACMs, the chapter presents a brief comparison between an ACM and a hybrid membrane process that comprises separate (activated carbon) adsorption and filtration modules.

Subsequently, based on the current state of knowledge, five technical considerations in developing ACMs are discussed. These are: i) adsorbed mass at saturation, ii) adsorption kinetics, iii) interference of water components with adsorption, iv) adsorbent replacement or regeneration, and v) leakage possibility and toxicological concerns.

According to these technical considerations, the next part assesses several designs of ACMs for steroid hormone micropollutant removal.

The last part of this chapter highlights the key research interests related to micropollutant removal with ACMs.

2.1 Prospective of adsorptive composite membranes

In recent decades, the occurrence of micropollutants has led to serious concerns over their toxicity to water organisms and human ²². Several technologies have been developed to remove micropollutants from waters, including biological treatment ¹⁵⁹, nanofiltration (NF) / reverse osmosis (RO) ^{138, 160}, ozonation ^{92, 96}, adsorption ¹⁰⁷, photodegradation ^{161, 162}, and so forth.

As discussed in the Introduction, NF and RO are effective in removing micropollutants but with high energy costs to achieve pressures of 5–120 bar (see Table 1.3). Adsorption technology with granular and powdered activated carbons (GAC/PAC) has several drawbacks. The most prominent drawback is the requirement of high doses and/or long residence times to achieve good removal (see Section 1.5.2), which leads to an increasing research interest in carbon-based nanoparticles (CNPs) as alternative adsorbents ¹⁵². CNPs such as carbon nanotubes, graphene, and graphene oxide have shown good adsorption of various types of organic compounds, such as dyes ^{163, 164}, pesticides ^{165, 166}, pharmaceutical and personal care products ^{167, 168}, and steroid hormones ¹⁶⁹⁻¹⁷⁵. CNPs can overcome some mass transfer limitations of GAC/PAC since most of the surface of CNPs is external, which means adsorption can take place within short residence times and at low adsorbent quantity.

However, compared to PAC, it will be more difficult to prevent the CNPs from entering the treated water because of the small sizes of CNPs (sub-micrometres to several micrometres) ¹⁵². In addition, the toxicity of these nanoparticles in the water environment is not adequately addressed ¹⁷⁶⁻¹⁷⁸. As a result, CNPs have not been considered for water treatment due to the toxicity concerns.

Because of the small sizes, CNPs can be incorporated in the micro- (MF) and ultrafiltration (UF) membranes to form an adsorptive composite membrane (ACM). The low mass transfer limitation displayed by CNPs may allow good adsorption in very short residence times of several seconds to a minute in the membranes ¹⁷⁹. The MF/UF membranes can be effective for immobilising the adsorbing nanoparticles, while sieving other water components such as natural organic matter (OM), bacteria, and viruses ¹²⁹. Depending on the design of the ACMs, the membrane layer can act as a physical barrier to prevent CNPs from leaking into the filtrated water.

Based on the concepts described above, this review chapter aims to assess the technical considerations and several design strategies for ACMs. Although the toxicity of CNPs presently hinders the application of ACMs, the messages derived from this chapter can be key to developing more effective (and risk-free) ACMs in the future. The research questions are: i) What are the advantages and disadvantages of ACMs compared with hybrid membrane processes? ii) What are the technical considerations for developing ACMs? and iii) How can the ACM and system be designed for removing steroid hormone micropollutants?

2.2 Hybrid membrane processes vs. adsorptive composite membranes

2.2.1 Definition of hybrid membrane processes

To elucidate the advantages and disadvantages of ACMs compared with hybrid membrane processes, it is necessary to first understand how the hybrid membrane process is defined, and its associated technical considerations.

Hybrid membrane process refers to a design where the membrane process is coupled with another unit process, namely adsorption, ion exchange, coagulation bioconversion or catalysis, to perform multiple functions¹⁸⁰. Unlike ACMs that have only been research in lab scale, hybrid membrane processes that integrate adsorption are mature and have been applied in the industry and pilot scale plants, with three main design concepts indicated by Stoquart *et al.*¹¹⁹ and schematically shown in Figure 2.1.

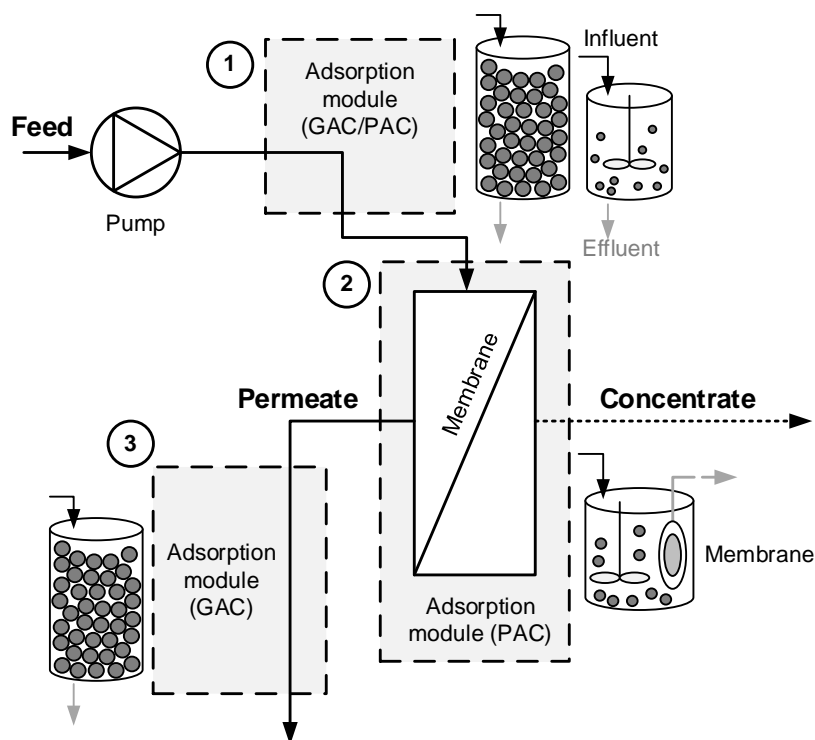


Figure 2.1: Schematic of three hybrid system designs: feed-side adsorption (Design 1), integrated adsorption-filtration (Design 2) and permeate-side adsorption (Design 3). Concentrate flow is not available in Design 2 and optional in Designs 1 and 3. In Design 2, PAC is injected into the filtration module. Adapted from Stoquart *et al.*¹¹⁹.

In Design 1, the fixed-bed GAC adsorber or PAC contactor is placed on the feed side of the membrane module to remove the micropollutants in the feed. In Design 2, the adsorbents (PAC) are directly injected into the membrane module, so membrane filtration and adsorption occur at the same location. Design 2 differs from an ACM as in the ACM, adsorbents are fully deposited on or incorporated inside the membrane material. In Design 3, the adsorbents (usually GAC

arranged in fixed beds) are located in the permeate side of the filtration membrane to remove micropollutants from the polished water. Stoquart *et al.* explained that Design 3 was not commonly adopted because of the need to retain fine activated carbons with an additional physical barrier in the post-treatment step; Design 1 has been prioritised for industrial scale applications, although Design 2 has a lower footprint and construction costs than both Designs 1 and 3 ¹¹⁹.

2.2.2 Comparison of hybrid membrane process designs

In Designs 1 and 2, the UF or MF membrane retain not only OM, bacteria, and viruses from the feed water but also the loose adsorbents ¹¹⁹. Many pilot and lab scale systems use Designs 1 and 2 to obtain satisfactory removals of micropollutants, including steroid hormones ^{85, 120, 121, 181}. Margot *et al.* reported good E1 and E2 removals of 90% and 60%, with a feed-side PAC contactor (Design 1) and residence time of 0.5–3 h; the removal of other micropollutants was also high ⁸⁵. Kovalova *et al.* reported that, with a longer residence time of 24 h, many micropollutants in hospital wastewater were removed by >80% in a (Design 1) PAC/UF process ¹²⁰. Löwenberg *et al.* compared the adsorption performance of Design 1 and 2; a main difference is the residence time, which is 2 h in Design 1 with pressure-driven UF, and 30 h in Design 2 with directly-dosed submerged UF ¹⁸¹. Removal of several micropollutants (except sulfamethoxazole) with both systems are similarly high (70–95%), implying that the system design does not affect micropollutant removal if the residence times are sufficiently long. Schwaller *et al.* directly dosed the feed stream with PAC, and the UF retained PAC after less than a minute of residence time (in Design 2), and only obtained 20–70% removals of the selected micropollutants ¹²¹.

A main drawback of Designs 1 and 2 is that adsorbents are exposed to the feed water components (such as OM) that may interfere with micropollutant adsorption ¹⁸²⁻¹⁸⁴ (see Figure 2.2).

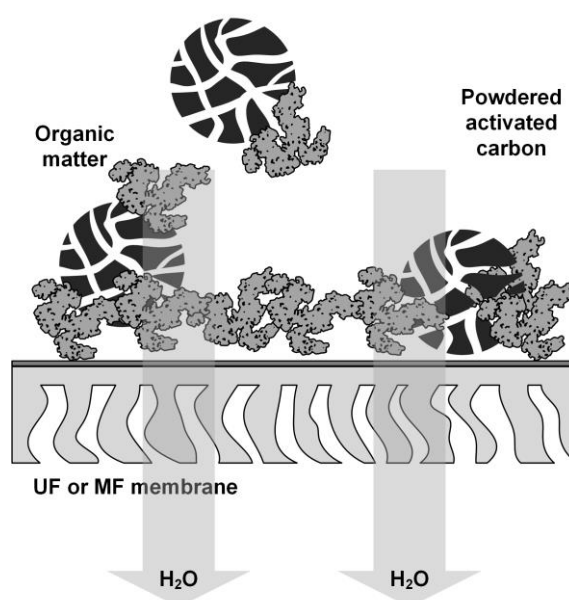


Figure 2.2: Schematic of the deposition of PAC on the UF or MF membrane in the presence of OM.

There are two consequences, both of which are more severe in Design 2 compared with Design 1. Firstly, PAC is more likely to deposit on the membrane surface in the presence of OM, reducing the membrane filtration performance¹⁸⁵⁻¹⁸⁷, and increase the effective chemical dose for membrane cleaning¹⁸⁷.

Secondly, because of the lower exposed surface area to micropollutants, deposited PAC on the membrane surface may adsorb less amounts of micropollutants than free PAC. For example, Lee *et al.* injected PAC into the submerged MF system and allowed a residence time of 2 h, as such the PAC are both suspended and deposited on the MF membrane¹⁸⁸. They observed that suspended PAC adsorbs hormone (E2) better than deposited PAC.

Design 3 is not common with PAC because an additional physical barrier in post-treatment means higher costs¹¹⁹. Nevertheless, it is interesting to explore the concept of using MF/UF in Design 3 to avoid interferants and mass transfer limitations encountered in Designs 1 and 2. Knopp *et al.* compared the Design 1 with PAC and MF and Design 3 with MF and GAC in a pilot study¹⁸⁹. The authors pointed out that, while micropollutant removal from wastewater was similar, Design 3 allows a lower backwash frequency (10.3 days) compared with Design 1 (1.4 days), because the MF membrane was not clogged by PAC in Design 3. Paredes *et al.* reported good removal of several pharmaceutical micropollutants in the UF permeate from a WWTP with GAC fixed-bed¹⁹⁰. Without the GAC, these micropollutants would reach the receiving water. Another pilot-scale study confirms that the upstream MF/UF removes dissolved OM that would otherwise affect the removal of micropollutants by the PAC¹⁹¹.

Design 3 was applied by Tagliavini *et al.* in lab scale to remove steroid hormones from 100 ng/L feed in very short residence times (6–36 s) with a 2 mm polymer-based spherical activated carbon (PBSAC) layer underneath the UF membrane^{192, 193} (see Figure 2.3). The hormone removal was 50–98% with the adsorbents immobilised either in polymeric mats¹⁹², or placed on a stainless-steel support that completely retained the PBSAC¹⁹³.

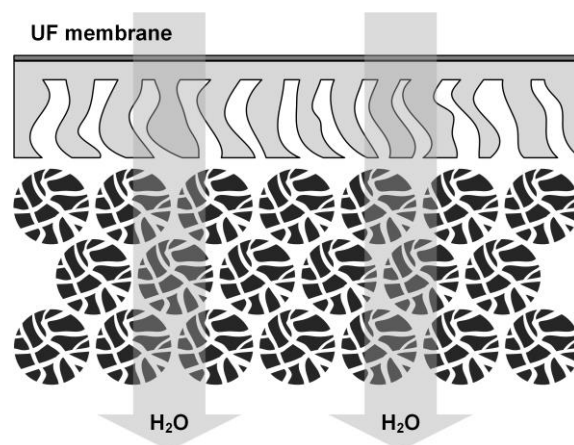


Figure 2.3: The concept of permeate side deposition of adsorbents (polymer-based spherical activated carbon) described by Tagliavini *et al.*^{192, 193}.

2.2.3 Comparison between the ACM and hybrid membrane process

A comparison between the ACM and the hybrid membrane process is then provided in Table 2.1. The effectiveness of the hybrid membrane process is decided by the long residence times and abundant amounts of adsorbents, which in turn depend on the adsorber dimension for GAC or dosage for PAC. The residence time is particularly important for the interactions between the micropollutants (or hormones) and adsorbents *via* kinetic processes.

Table 2.1: Comparison between ACMs and hybrid membrane processes (that combine adsorption and filtration).

	Adsorptive membranes	Hybrid membrane processes
Readiness	Low (lab-scale only)	High (full-scale and pilot plants)
Footprint	Low, because membrane	High, with separate filtration and adsorption modules
Energy consumption	Potentially lower than a hybrid system as a result of low footprint	Higher than adsorptive membranes
Integrability in existing treatment plants	Probably not integrable, because the conventional membranes need to be replaced	Integrable
Adsorbent size	Sub-micrometres or even nanometres (<i>i.e.</i> nanoparticles or superfine PAC), so they can be incorporated into the membrane material	Micrometres (PAC) to millimetres (GAC) are possible
Adsorbent dosage or loading*	Limited, depends on the dimension of the membrane and incorporation method	Not as limited as adsorptive membranes, depends on the dosing or adsorber dimension
Adsorption longevity	Currently short because the adsorbent loading is limited	Can be long because of the potentially high loadings or doses

* In an ACM, the loading (in mg per g of adsorbent or g per m² of filtration area) is defined as the quantity of adsorbents that can be incorporated with respect to a specific mass or filtration area of membrane.

The ACM does not allow long residence times or abundant adsorbent amounts, although it allows the use of smaller adsorbents, such as CNPs, which may promise effective adsorption despite the very thin adsorbent layer and short residence times. This adsorptive membrane approach with CNPs may also enable the design of even smaller scale systems, facilitate operation control, and reduce energy consumption. The examination of CNPs is provided in the next sub-chapter.

2.3 Carbon-based nanoparticles (CNPs) for membrane incorporation

2.3.1 Types of carbon-based nanoparticles

Carbon-based nanoparticles (CNPs) are a class of adsorbents that can be promising for environmental applications¹⁵². The main types of CNPs include multi- and single-walled carbon

nanotubes (MW-/SWCNTs), graphene, graphene oxide, and fullerenes (Figure 2.4). A specific SWCNT fabrication technique¹⁹⁴⁻¹⁹⁶ allows the SWCNTs to align in one direction instead of orienting randomly, which results in vertically aligned carbon nanotube (VaCNT) membranes (Figure 2.4). In SWCNT, micropollutants can adsorb to both the convex external and concave internal surfaces; in a VaCNT membrane, only the internal surface is available for adsorption.

Graphene, discovered in 2004, is a single layer of carbon atoms arranged in a honeycomb lattice¹⁹⁷. It is noted that graphene products in the market are not single-layered sheets, but flakes consisting of several monolayers or multilayers¹⁹⁸. Graphene oxide (GO) has the same 2D structure as graphene but with oxygen-containing groups, such as hydroxyl, carboxylate, and epoxy groups, attached to the carbon plane or edges¹⁹⁹.

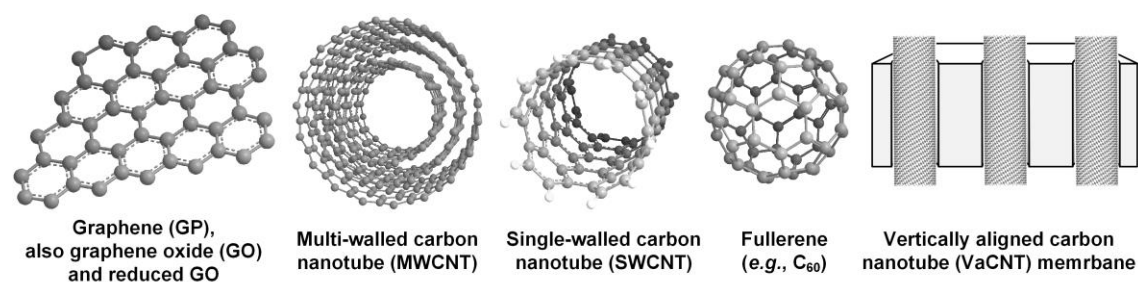


Figure 2.4: Main types of carbon-based nanoparticles (MW-/SWCNTs, graphenes, and C₆₀)^{197, 200, 201} and the VaCNT membrane¹⁹⁴.

MWCNTs discovered in 1991²⁰⁰ nest several SWCNTs (which are idealised one-dimensional products when rolling a graphene sheet in a certain direction) with different diameters that are bound together by van der Waals forces. The interlayer spacing of MWCNTs is around 0.34 nm²⁰², which is similar to the interlayer spacing between two monolayers in graphite²⁰³.

Fullerenes, first reported in 1985²⁰¹, are spheres made of carbon atoms connected to one another *via* single and double bonds²⁰⁴. Each individual fullerene molecule (C₆₀ or C₇₀, among other types) is very small in size (sub-nanometres) and has very high surface area per volume ratio. However, they aggregate at room temperature; the intermolecular bonds are relatively strong and can reassemble covalent bonds in strength²⁰⁵. The sizes of fullerene aggregates in water can range between several nanometres to sub-micrometres^{206, 207}.

Graphene, MW-/SWCNTs and fullerene contain predominantly carbon; oxygen only occurs at the edges of graphene sheets, tips of MW-/SWCNTs, or the defects^{208, 209}. In contrast, GO surface contains a significant proportion of oxygen (for instance, 10–34% of the total surface elemental composition²¹⁰). Because of the different geometries and surface compositions, the CNPs may display distinct electronic, chemical, and hence adsorptive properties. However, the properties of CNPs can be modulated *via* functionalisation. For instance, oxygen-containing groups can be introduced in MW-/SWCNTs to improve the adsorption of certain organic compounds¹⁵².

The SSA varies between different CNPs. MWCNT, SWCNT and graphene have relatively high SSA, of 150–800 m²/g^{168, 172, 211-213}. These values are similar or lower than the SSA of PAC and GAC (500–1200 m²/g)^{111, 187, 214-216}. In contrast, the surface areas of graphene oxide can be as low as <50 m²/g due to aggregation or monolayer stacking^{217, 218}. The SSA of fullerene is very low

(for example, $1.1 \text{ m}^2/\text{g}$ ²¹⁹) because the strong intermolecular bonds in C_{60} aggregates²⁰⁵ makes it impossible for the probe atoms / molecules to access the surface. For graphene, the number of monolayers in the adsorbent sample (purchased from the market) dictates the SSA. For a graphene monolayer, the SSA is very high at $2300 \text{ m}^2/\text{g}$ ²²⁰, which is beneficial for adsorption.

In contrast to ACs, CNPs have an interesting feature related to adsorption: the dominance of external surface. The majority of AC surface is inside the pores, and the percentages of the external surface to the total surface is only 1–2%^{193, 216, 221} even when the ACs are milled to sub-micrometre sizes²¹⁶. CNPs have predominantly external surface. SWCNT has in theory a percentage of external surface of 50%²²², while that of MWCNT can reach 88%²²³. According to the idealised structures, graphenes and fullerenes may contain only external surface. The carbon surface in VaCNT membranes can be considered as internal surface because barrier materials (such as parylene-N¹⁹⁵) completely block the outer walls of the aligned CNTs²²⁴.

The abundant external surface in CNPs and accessible internal surface of VaCNT membrane may indicate low mass transfer limitation that is associated with pore diffusion and imply a faster adsorption kinetics (which means more adsorbed amounts of micropollutants within short residence times) compared with GAC and PAC. The assessments on the mass transfer mechanisms are provided in the next sub-chapter.

2.3.2 Steroid hormone adsorption by carbon-based nanoparticles

Certain CNP types, such as carbon nanotubes and graphenes, are efficient at removing steroid hormones from waters¹⁶⁹⁻¹⁷⁵. Hormone adsorption by CNPs is characterised by the domination of physical adsorption, fast adsorption kinetics, and high adsorption capacity. Prior to this work, all adsorption experiments with CNPs were conducted at several $\mu\text{g}/\text{L}$ concentrations, which are several orders of magnitude higher than the hormone concentrations in waters (see Table 1.1). This hinders comparison with ACs that had been investigated with more realistic hormone concentrations (such as $100 \text{ ng}/\text{L}$)^{108, 109, 111, 112, 225}. Prior to this study, adsorption by VaCNT membranes has never been investigated.

Some comparative results are given as follows. Pan *et al.* studied the adsorption of EE2 ($0.1\text{--}3 \text{ mg}/\text{L}$) and BPA ($0.1\text{--}40 \text{ mg}/\text{L}$) by several CNPs; up to $70 \text{ mg}/\text{L}$ methanol was present in the solution to increase the hormone solubility¹⁶⁹. The EE2 and BPA adsorption capacities of SWCNT were estimated to be 300 and $600 \text{ mg}/\text{g}$, respectively, while those of MWCNTs were lower (both $100 \text{ mg}/\text{g}$) and those of C_{60} were very low (0.23 and $2.36 \text{ mg}/\text{g}$, respectively). The poorer hormone adsorption by MWCNTs and C_{60} were attributed to the surface inaccessibility caused by aggregation¹⁶⁹. Jiang *et al.* later determined the E2 and EE2 adsorption capacities of various carbon-based materials with initial hormone concentrations between $50 \mu\text{g}/\text{L}$ and $2.5 \text{ mg}/\text{L}$ ¹⁷². Reported adsorption performances for both steroid hormones follow the order $\text{PAC} > \text{SWCNT} > \text{reduced GO} > \text{MWCNT} > \text{GAC}$ ¹⁷². The adsorption isotherm is the main focus of the above studies, which explains why the authors selected elevated hormone concentrations. However, adsorption results may not be the same if steroid hormones are in much lower but realistic concentrations in water (of sub- $\mu\text{g}/\text{L}$). At low adsorbate concentrations, the surface area of adsorbents is not a limiting factor, and adsorption may be controlled by the adsorption kinetics and adsorption–adsorbate affinity.

Some CNPs (MW-/SWCNTs and graphenes) have been deposited on the membranes for the dynamic adsorption of contaminants (pesticides and pharmaceuticals)²²⁶⁻²²⁸, but prior to this work, investigations with steroid hormones had not been carried out. In the next sub-chapter, five technical considerations for developing adsorption composite membranes will be discussed, with steroid hormone removal being the main focus of application.

2.4 Adsorption and mass transfer mechanisms in CNPs

To achieve good adsorption performance in ACMs, the adsorbents must have appropriate characteristics to overcome the limitation of residence time and surface area / loading. The adsorption and transfer mechanisms are summarised below, and for each mechanism, the differences between CNPs and ACs (GAC and PAC) are highlighted.

The differences in transfer mechanisms may determine the differences in steroid hormone adsorption between CNPs and ACs. The adsorption progress of any adsorbate, including steroid hormone micropollutant, by CNPs or ACs can be characterised *via* four consecutive steps^{229, 230}, which are described below and schematically illustrated for the case of ACs in Figure 2.5.

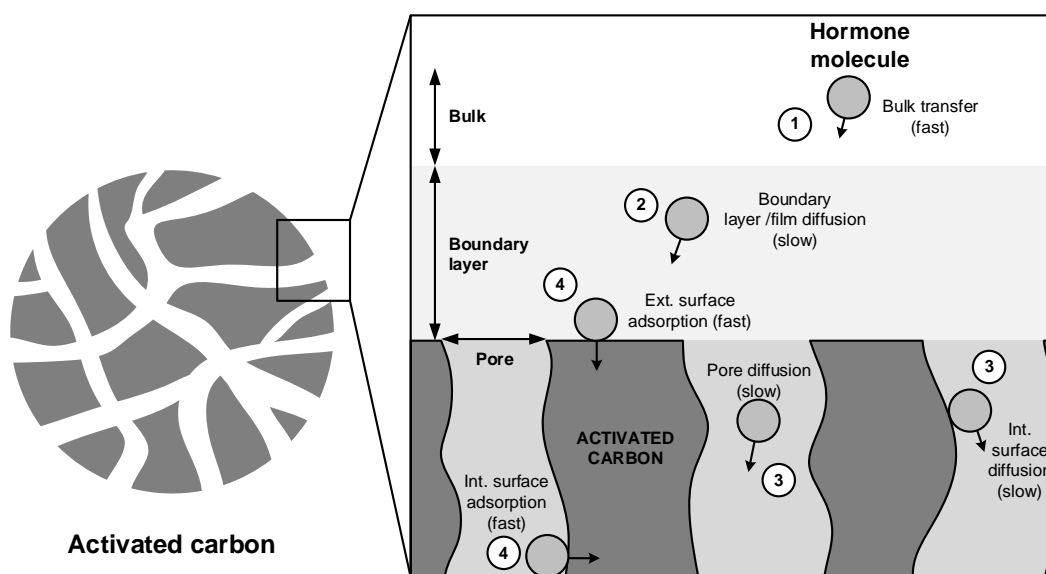


Figure 2.5: Schematic of adsorbate mass transfer mechanisms (in activated carbons as an example). Ext.: external, Int.: internal.

1. Transfer of the adsorbates from the bulk to the hydrodynamic boundary (film) layer,
2. Transfer of the adsorbates through the boundary layer to the adsorbent surface (film diffusion),
3. Transfer of the adsorbates into the interior of the adsorbent (intra-particle diffusion, IPD), which consists of the transfer of the adsorbate in the liquid phase (pore diffusion) and the sorbed phase (surface diffusion), and
4. Energetic interaction between the adsorbates and the adsorption sites of both the external and internal surfaces.

2.4.1 Bulk transfer

Bulk transfer (step 1) is considered a very fast process and assisted by mechanical shaking in static adsorption and water flow in dynamic membrane adsorption^{223, 224}. Bulk transfer does not control the speed of adsorption (*i.e.* the *adsorption kinetics*).

2.4.2 Film (boundary layer) diffusion

In ACs, film (boundary layer) diffusion is slow, and either this process (step 2) or intra-particle diffusion (IPD, step 3) controls the rate of adsorption, depending on which process is slower²²⁹.

Several kinetic models have been developed to characterise the film diffusion process, such as the Boyd model²³¹, Frusawa–Smith model²³², Mathews–Weber model²³³, and phenomenological external mass transfer model²³⁴. The simplified version the Boyd model takes the form of the first-order kinetics equation as shown below.

$$q_{ads,S(t)} = q_E (1 - e^{-k_{FD} t}) \quad (2.1)$$

where q_E is the specific adsorbed mass at equilibrium, and k_{FD} is the film diffusion constant, which is essentially a first-order kinetic rate constant. For example, the simplified Boyd model fitted the adsorption of sulfamethoxazole and E2 by carbon nanotube composites, which indicates that film diffusion could be a rate controlling factor²³⁵. In contrast, Al-Khateeb *et al.* pointed out that the Boyd model did not fit the adsorption of pharmaceutical compounds by graphene²³⁶. From the presented data, it appears that the adsorption was ultrafast and adsorption equilibrium was established within a few minutes, after which the limitation of film diffusion was no longer evident.

It is noteworthy that the film / boundary layer thickness can be reduced *via* increasing the stirring speed of the adsorbent suspension in static adsorption or increasing the flux in dynamic adsorption.

2.4.3 Intra-particle diffusion

IPD (step 3) is considered as a slow process and may control the rate of adsorption in ACs²²⁹. Several kinetic models have been developed to characterise IPD, such as the Boyd model²³¹, Weber–Morris model²³⁷, and phenomenological internal mass transfer model²³⁸. The Weber–Morris model is the simplest and most convenient one, hence it has been frequently applied in adsorption studies. The Weber–Morris model²³⁷ is presented as follows.

$$q_{ads,S(t)} = K_d \cdot t^{0.5} + C \quad (2.2)$$

where $q_{ads,S(t)}$ is the specific adsorbed mass of the adsorbate at time t , K_d is the intra-particle diffusion coefficient, and C is a correction factor. If $C = 0$ and the plot of $q_{ads,S(t)}$ against $t^{0.5}$ yields a straight line that passes through the origin, IPD is the only process that controls

adsorption. Otherwise, if a straight line is not yielded or does not pass through the origin ($C \neq 0$), the adsorption is controlled by multiple processes ²³⁹.

The Weber–Morris model has been applied to characterise the initial phase of adsorption of various organic compounds by ACs ²⁴⁰⁻²⁴⁵. Tagliavini *et al.* successfully fitted this model to characterise the steroid hormone adsorption kinetics of PBSAC (particle diameters of 200 and 450 μm) at low particle concentrations of 2 and 10 mg/L ¹¹². In another work with AC fibres (around 30 μm in size), the model fits for the first 30 min of the E2 adsorption with the same particle concentrations (2 and 10 mg/L), indicating that IPD controlled the adsorption rate only for a short time ²⁴⁶. Because CNPs contain mostly external surface, IPD may not be a relevant adsorbate transfer mechanism for CNPs, which implies that film diffusion controls adsorption.

According to several studies, the Weber–Morris model still fits the adsorption of organic compounds (for instance, dyes) by MW-/SWCNTs ²⁴⁷⁻²⁴⁹ and graphenes ^{250, 251}. The authors cautiously concluded that IPD might have certain involvement in the adsorption. While the intrinsic pores of MW-/SWCNTs are not accessible and graphenes and fullerenes have no intrinsic pores, some pores can be induced by the aggregation of CNPs in solution, which form surfaces of CNP that are less accessible to adsorbates ^{168, 252, 253}. In addition, some pores may be found at the graphene defects ²⁵⁴. The relatively slow diffusion of adsorbates into these regions may be described under IPD.

2.4.4 Energetic adsorbent–adsorbate interactions

The energetic interactions between the adsorption sites and adsorbates (step 4) occur in the order of nanoseconds ²⁵⁵ and are much faster than the diffusional steps ²²⁹. Hence, step 4 may not determine the adsorption rate, but instead affects the adsorbed mass at equilibrium and hence the adsorption capacity. In general, adsorption of organic molecules by carbon-based materials is the result of various intermolecular interactions that are both directional and non-directional ²⁵⁶⁻²⁵⁹. Directional interactions include π / π stacking, XH / π interaction ($X = \text{C}$ or O) – also named $\pi \cdots \text{H}$ hydrogen bonding – and $\text{O} \cdots \text{H}$ hydrogen bonding. Non-directional interactions include London dispersion force, electrostatic attraction / repulsion, and hydrophobic effect. The interactions between two atoms or molecules can fall into the category of van der Waals force, which indicates the attraction between the multipoles of the interacting species (atom or molecule) ²⁶⁰. The directional interactions may be explained as the stronger van der Waals interactions between certain parts of the molecules, for instance, the π -rings ²⁶¹.

π / π stacking (see Figure 2.6) results from the strong affinity between the π - (aromatic) rings of the adsorbate and adsorbent. π / π stacking has been confirmed by experimental data ²⁶²⁻²⁶⁴, *ab initio* simulations ²⁶⁵, quantitative structure–property relationship models ²⁶⁶, X-ray diffraction ²⁶⁷, X-ray photoelectron (XPS) and Raman spectroscopies ^{268, 269}, and nuclear magnetic resonance (NMR) ²⁷⁰. The maximum bond length of π / π stacking is approximately 0.5 nm ²⁶⁵.

XH / π interaction ($X = \text{C}$ or O) (Figure 2.6) should be considered alongside π / π stacking to describe interactions between an aromatic and a non-aromatic molecules ²⁷¹. XH / π interaction can explain the adsorption of non-aromatic compounds by CNPs, both computationally from *ab*

initio simulations²⁷² and experimentally^{273, 274}. XH / π interaction has also been observed by NMR²⁷⁵. The XH / π bond length is approximately 0.3 nm²⁷².

O \cdots H hydrogen bonding (Figure 2.6) is not as important as aromatic interactions for pure graphene and CNTs that contain very small quantities of oxygen-containing groups at the edges and defects. In contrast, oxygen containing groups in GO can form hydrogen bonds with both micropollutants²⁷⁶ and water^{277, 278}. According to simulation results the introduction of –OH groups to the graphene basal plane enhance the binding affinity of graphene for micropollutants²⁷⁹. The bond length of the O \cdots H hydrogen bond is <0.5 nm²⁷⁹⁻²⁸².

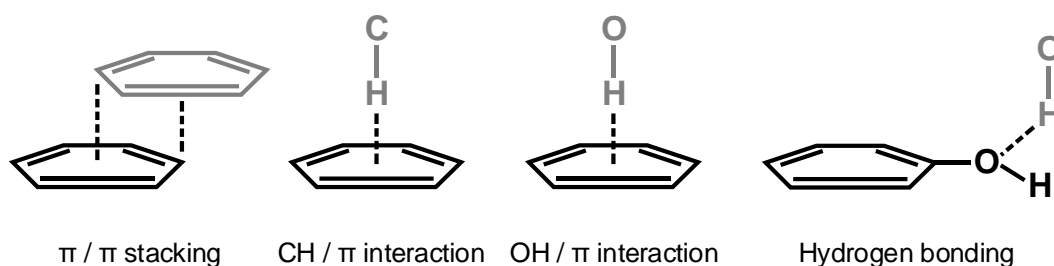


Figure 2.6: Directional interactions between parts of the CNP (black) and hormone E2 (grey), including π - π stacking, X-H / π interaction (X = C, O), and O \cdots H hydrogen bonding.

London dispersion (van der Waals) force (Figure 2.7) is a particular case of the van der Waals force when both atoms that interact with each other are ‘electrically symmetric’²⁸³. Hence, London dispersion between a pair of atoms (or molecules) is relatively weak compared to hydrogen bonding or π / π interactions, and decays sharply with the interatomic or intermolecular distance. London dispersion is only significant at 0.3–0.5 nm distances^{284, 285}.

Electrostatic interaction (Figure 2.7) can be considered as a part of van der Waals force. Electrostatic interaction is distinguished from London dispersion because of the permanent charges. Some CNPs can have negative surface charges at high pH²⁸⁶⁻²⁸⁸ so the adsorption performance of CNPs can be affected by solution pH¹⁶⁸. Because some steroid hormones are deprotonated at high solution pH (*e.g.* E1 and E2 have pK_a values of 10.2–10.7²⁸⁹⁻²⁹¹), the charged CNP or AC surface can repel the charged hormone molecules. Electrostatic interaction can be stronger than London dispersion and could act at longer distances of several nanometres^{292, 293}.

Hydrophobic effect (Figure 2.7) refers to the difference in affinity (*i.e.* strength of the van der Waals force) between the water–molecule and molecule–molecule interactions²⁹⁴. If both molecules in water are hydrophobic (namely, graphene and E2), they tend arrange themselves to minimise the contact area with the surrounding water. Hydrophobicity can be characterised by the K_{OW} value (octane–water partition coefficient), but hydrophobic effect is often not an exclusive mechanism resulting in poor relationship between K_{OW} and adsorption²⁶³. Hydrophobic effect is stronger and can act at longer distances than London dispersion²⁹⁵, even up to 10 nm²⁹⁶.

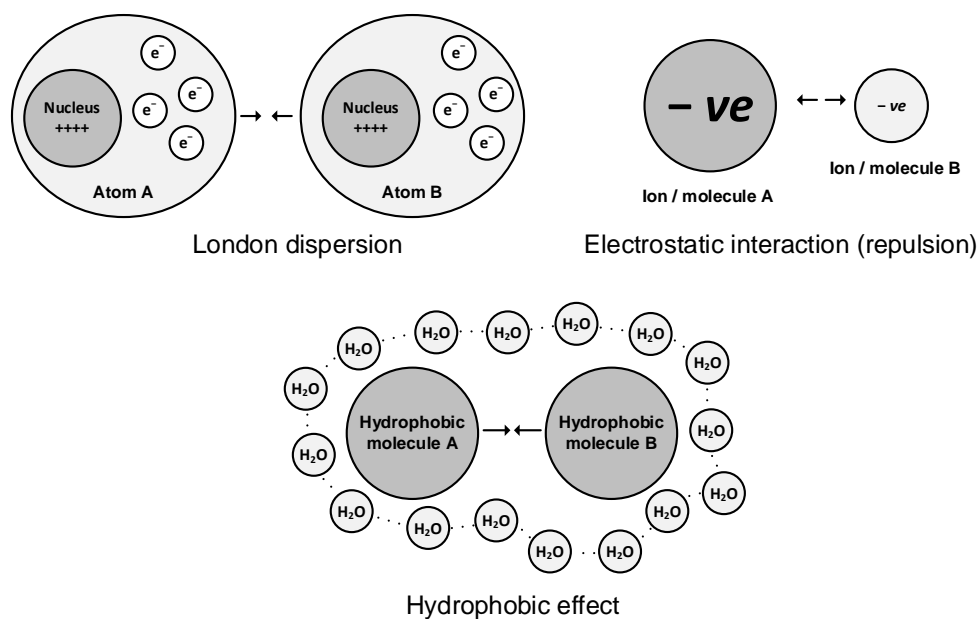


Figure 2.7: Non-directional interactions at atomic level (London dispersion), and ionic / molecular level (electrostatic interaction and hydrophobic effect). The symbol $-ve$ indicates the local negative charge of the ion or molecule.

2.4.5 Summary of adsorption mechanisms

The CNPs (except graphene oxide) and ACs are both characterised by a strongly hydrophobic surface, high aromaticity and small quantities of oxygen containing groups. As such, both types of adsorbents can adsorb micropollutants steroid hormones *via* π / π stacking, XH / π interaction, and hydrophobic effect, but $O \cdots H$ hydrogen bonding and electrostatic interaction are less important especially when the adsorbates are neutral.

The graphene-like surface of ACs is typically not as integrated as graphene and MW-/SWCNTs, so π / π stacking and XH / π interaction is not as spontaneous as in the case of CNPs. CNPs contain edges, tips, and defects^{208, 209} where $O \cdots H$ hydrogen bonding with the micropollutants is permitted. The adsorption of steroid hormones by graphene oxide may be more complex to characterise, because of the i) disrupted graphene network that inhibits π / π stacking and XH / π interaction, ii) abundant oxygen containing groups that promotes $O \cdots H$ hydrogen bonding, and iii) competition for adsorption sites between hormones and other hydrophilic components, including water^{277, 278}.

In VaCNT membranes, the flow velocity at the wall may be significant as a result of slippage on the hydrophobic and atomically smooth surface²⁹⁷. Hence, the strength of the energetic (van der Waals) interaction resulting in a hormone-wall adhesive force can determine whether steroid hormones adsorb to the CNT inner surface; or slips along with the flow and exits the membrane pores²⁹⁸. A force interplay can be established to dictate hormone adsorption, which will be discussed in more detail in Section 2.6.4.

2.5 Technical considerations for adsorptive composite membranes (ACMs)

The following considerations are needed when developing an adsorptive membrane for micropollutant or steroid hormone removal: i) adsorbed mass at equilibrium or saturation, ii) adsorption kinetics, iii) interference from other water components, iv) replacement or regeneration measures, and v) risk of adsorbent leakage and toxicological concerns (Figure 2.8).

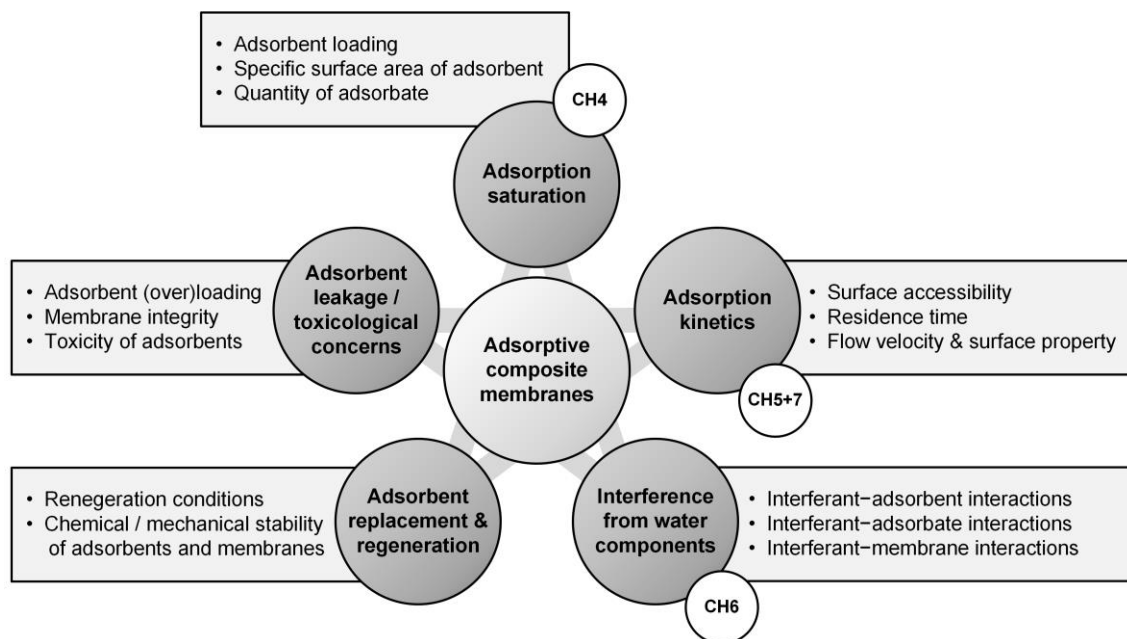


Figure 2.8: Five technical considerations (in grey spheres) with ACMs. The chapters (CH) in this dissertation are indicated where the relevant determining factors (in the rectangular boxes) are evaluated.

2.5.1 Adsorbed mass at the saturation point

Physical adsorption, or physisorption, which is characteristic for the adsorption of various organic compounds by CNPs^{152, 258, 299}, indicates that a thermodynamic equilibrium may be established between the adsorbates in the aqueous phase and in sorbed phase. For the sorption of steroid hormones, the equilibrium equation is as shown below.



where SH(aq) and SH \cdots CNP indicate the quantity of steroid hormone in the aqueous and sorbed phases, respectively, and CNP indicates the quantity of adsorption sites. The forward reaction is adsorption and the backward reaction is desorption. Three main points can be drawn based on principles on equilibrium dynamics³⁰⁰.

- If the number of adsorption sites is in excess, adsorption is driven by the quantity of adsorbed hormones, until the *adsorption equilibrium* is reached (where the adsorption rate is equal to the desorption rate).

- If there is more hormone in the system (*i.e.* higher initial concentration) and the number of adsorption sites is still in excess, the quantity of adsorbed hormones at equilibrium increases.
- If the number of adsorption sites becomes limited, the quantity of adsorbed hormones stays constant even when the initial hormone concentration increases. The maximum adsorbed mass of hormone attained is called the *adsorption capacity*.

For ACMs, the *adsorbed mass at the saturation point* (equivalent to the adsorption equilibrium in static adsorption) is important because it indicates the maximum quantity of adsorbed hormones at a specific feed hormone concentration. This adsorbed mass depends on the amount of surface area and hence the quantity or loading of adsorbents.

In a filtration experiment, given that there is no retention by the membrane, the permeate concentration increases with time until it reaches the concentration in the feed. At this point, the material is fully saturated with micropollutants and adsorption is no longer significant, which defines a *complete breakthrough*³⁰¹. An example complete breakthrough is shown in Figure 2.9 for the SWCNT loading of 0.1 g/m² in an SWCNT–UF composite membrane; the corresponding specific adsorbed mass did not increase to above 0.8 ng/cm²³⁰². An early breakthrough means that the adsorbents may need frequent regeneration or replacement.

In certain lab-scale experiments, the adsorption saturation and hence complete breakthrough may not be reached. For example, a complete breakthrough was not obtained for the SWCNT–UF with a loading of 2 g/m² after 3 h, and the specific adsorbed mass still increases³⁰² (see Figure 2.9). Incomplete breakthrough occurs when the duration of experiment was not long enough, especially when the adsorption became effectively slower with time.

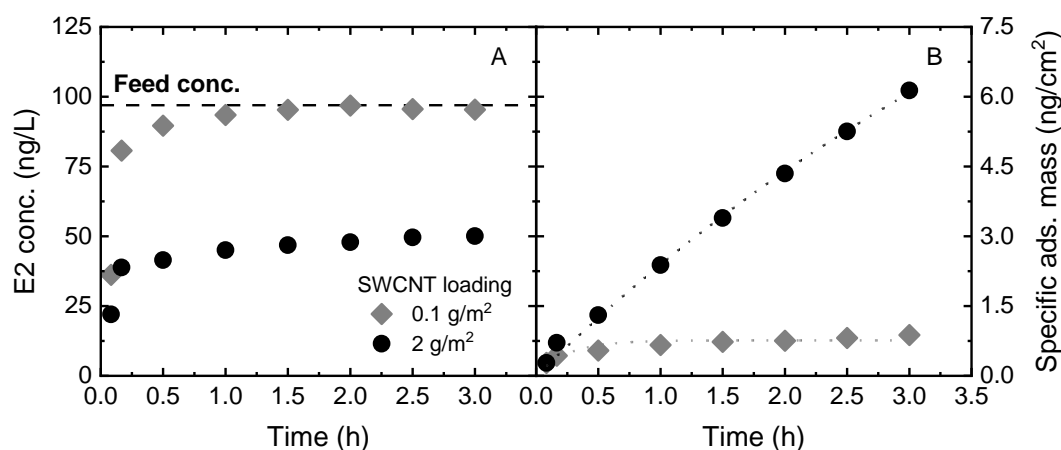


Figure 2.9: Permeate E2 concentration (A) and specific adsorbed mass (B) determined with SWCNT–UF composite membranes at two SWCNT loadings (0.1 and 2 g/m²). 100 ng/L feed E2, 1 mM NaHCO₃, 10 mM NaCl, pH 8.1 ± 0.2, 23.0 ± 1.6 °C. Data taken from Nguyen *et al.*³⁰².

High specific surface areas (SSAs) of the CNPs are important because they influence the adsorbed mass at equilibrium and adsorption capacity. MWCNTs with lower SSAs has lower adsorption capacities for EE2 and BPA (both around 100 mg/g) than SWCNT (EE2: 300 mg/g, BPA: 600

mg/g)¹⁶⁹. Similarly, Jiang *et al.* observed that the trend PAC > SWCNT > reduced GO > MWCNT in E2 adsorption is correlated with the order of SSA¹⁷².

Based on the SSA alone (as summarised in Sub-chapter 2.3), it appears that MW-/SWCNTs and graphenes are good choices of material in an ACM. It is noteworthy that the adsorbent loading is limited given the compactness of the adsorptive membranes. Hence, adsorbents with high SSAs are more desirable than those with low SSAs. However, poor adsorption may be obtained even with materials with high SSAs if the adsorption kinetics is low and residence time is short.

2.5.2 Adsorption kinetics

The adsorption kinetics and residence time may determine adsorption by ACMs. The *hydraulic residence time* (or hydraulic contact time) is the amount of time that the micropollutants are in contact with the membrane and/or the adsorbents in a hypothetical case where the adsorbate flow is not slowed down by their interactions with the adsorbents. In a typical membrane, the residence time ranges from sub-seconds to a minute¹⁷⁹. In contrast, the residence times in GAC adsorbers or PAC contactors can be from 30 minutes to many hours^{115, 118, 184}. Fast adsorption kinetics are desired in adsorptive membranes because adsorption needs to take place within such short residence times. An example is given in Figure 2.10, where the evolution of specific adsorbed mass of E2 with time in static adsorption experiments with MW- and SWCNT³⁰³.

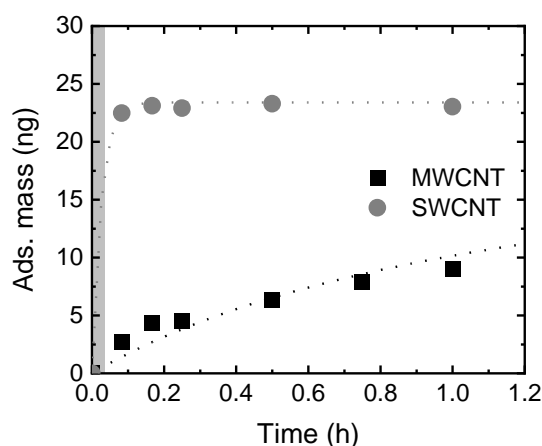


Figure 2.10: Adsorbed mass of steroid hormone (E2) vs. residence time in static adsorption obtained with MW- and SWCNT (0.01 g/L). Grey box indicates the hydraulic residence time range relevant in an ACM (~1 min). Data taken from Nguyen *et al.*³⁰³.

In this example, the adsorbed masses at equilibrium determined at 26 h vary little between the two CNPs (not shown in the figure), while the difference in adsorption kinetics is distinctive. For SWCNT, the adsorption equilibrium was attained within 5 min, while for MWCNT, the adsorption equilibrium was not attained after 1.2 h. The grey box in Figure 2.10 indicates the residence time in an ACM, of around 1 min. Within such a short time, SWCNT appears to adsorb hormone better than MWCNT, and is more favourable to be incorporated in a membrane. The difference in adsorption performance is attributed to mass transfer limitation, because SWCNT may have more surface that is accessible in short residence times than MWCNT.

In ACs, the external surface accounts for only 1–2% of the total surface^{193, 216, 221}, and the domination of internal surface means that micropollutants readily migrate into the AC pores. This IPD process is relatively slow and can limit the adsorption rate^{229, 240}. Even when superfine PAC are small enough to be incorporated in adsorptive membranes, IPD may limit their adsorption performance²¹⁶. In dynamic adsorption studies, Tagliavini *et al.* concluded that the internal surface of PBSAC in a 2 mm thin layer contributed minimally to hormone removal¹⁹². The same authors later pointed out the initial increasing trend of E2 adsorption with the external surface of PBSAC, but E2 adsorption levelled out when the external surface was in excess¹⁹³. It was implied from these findings that a large proportion of the PBSAC (internal) surface had not been used.

To overcome the mass transfer limitation, a high external surface area and good mass transfer are required²¹⁵. Compared with PAC and PBSAC, CNPs have predominantly external surface, which allows fast adsorption kinetics. However, in ACMs where the residence times are very short, the quantity of accessible adsorption sites may still be a limiting factor. Surface access can be hindered when the suspended CNPs in aqueous solutions aggregate, which potentially reduces the adsorption kinetics^{168, 252}. In ACMs, the CNPs can be immobilised in a stable manner, which prevent further aggregation.

2.5.3 Interference from water components such as organic matter

To ascertain the OM interference mechanisms, it is firstly emphasised that the surface inside the MW-/SWCNTs pores appears not accessible while graphenes and C₆₀ do not have intrinsic pores, so pore blocking mechanism is not relevant³⁰⁴. The two relevant mechanisms (Figure 2.11) are i) direct competition between OM and hormones for the adsorption sites, and ii) indirect competition as the OM–hormone complex may have low affinity for binding with the adsorbents or poorer accessibility to the surface. Both interference results in mass transfer limitation of steroid hormones. The extent of each mechanism is influenced by the strengths of respective OM–adsorbent and OM–hormone interactions described below.

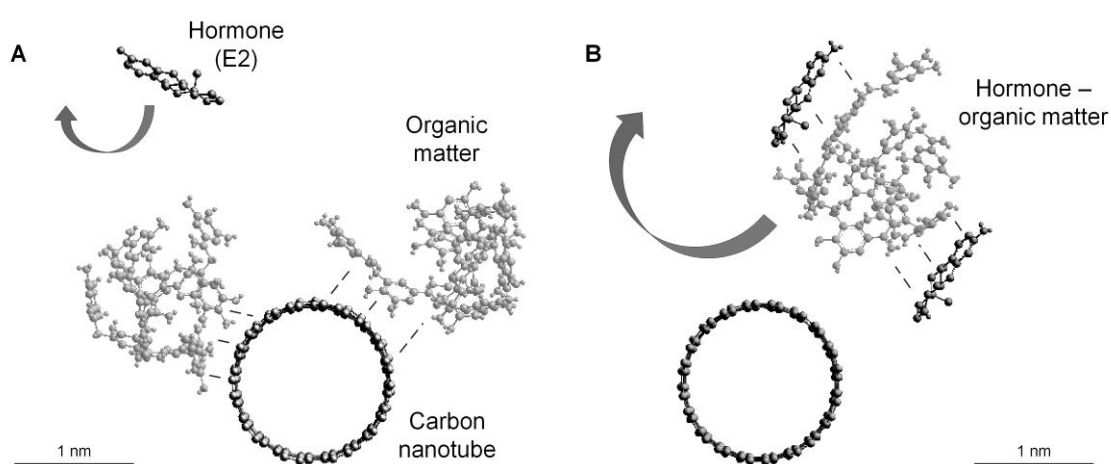


Figure 2.11. OM (TA) interference mechanisms relevant to hormone (E2) adsorption by adsorbents (SWCNTs). Models of idealised molecules were constructed in Chem3D 19.0, PerkinElmer, USA. SWCNTs are viewed from the top. Reprinted from Nguyen *et al.*³⁰⁵.

First, the interactions between OM and the adsorbents are investigated in an OM–adsorbent binary system. MW-/SWCNTs and graphenes can adsorb OM strongly at their accessible surfaces³⁰⁶. The main OM–adsorbent interactions include π / π stacking, hydrogen bonding (both O··H and XH / π), and hydrophobic effect^{307,308}. Electrostatic interaction is also a relevant mechanism with hydrophilic adsorbents such as graphene oxide³⁰⁹. Highly-aromatic and hydrophobic OM types, such as HA and tannic acid (TA), are adsorbed at adsorption capacities of hundreds of mg/g^{307, 310-312}. Solution chemistry affects both the effective charges and conformations of OM and adsorbent, and hence alters hydrophobic effect^{308, 313}. In contrast, OM adsorption is not directly linked with OM size^{304, 314, 315}.

The OM–hormone binary system is subsequently investigated. π / π stacking, hydrogen bonding and hydrophobic effect form the interactions between OM and steroid hormones³¹⁶. Electrostatic repulsion is relevant when both the OM and hormones are negatively charged (for example, E2 at pH > 10)³¹⁷. At neutral pH, highly aromatic OM types, such as TA and HA, interact strongly with steroid hormones, while non-aromatic and hydrophilic OM such as alginate (ALG) provides only weak interactions^{317, 318}. Similar to OM–adsorbent interactions, OM–hormone interactions do not depend on OM size^{319, 320}.

Based on the above findings, OM aromaticity seems to impact both OM–adsorption and OM–hormone interactions, which implies that aromatic OM potentially interferes with hormone adsorption by the CNPs when the three components are present. It is necessary to emphasise that in such tertiary systems, the relative concentrations of OM and micropollutants / hormones are important³²¹. In real water, OM are in mg/L concentration range^{322, 323} while steroid hormone micropollutants may only be found in ng/L or sub- μ g/L concentration range (see Table 1.1). Most prior works were performed with unrealistically high hormone concentrations (*i.e.* in same order of magnitude as OM concentrations (up to 2.5 mg/L)^{172, 174}).

In a batch experiment with more relevant E2 concentrations (100 ng/L), Tagliavini *et al.* observed only a slight decrease in the maximum E2 adsorbed mass by polymer-based spherical activated carbon (PBSAC), from 98 to 80 ng/g, with increasing HA concentration up to 100 mgC/L. The poor competition is caused by the exclusion of HA from the PBSAC pores where hormones can be adsorbed. The same phenomenon can explain the poor HA removal and interference in a dynamic adsorption process with the PBSAC-integrated membrane³²⁴. It appears that HA is not ideal for such interference studies with PBSAC, because this OM type obstructed only some external surface of PBSAC and may not limit hormone mass transfer from the bulk to the available adsorption sites inside the pores. More significant results may be obtained once the interference to micropollutant removal is evaluated for a broad range of synthetic and nature-derived OM types, in both static and dynamic membrane adsorption processes.

Several strategies are proposed to overcome the OM interference. Altering the solution chemistry (pH and ionic strength) has minimal impact on OM interference with the adsorption of micropollutants³²¹. Another strategy that only works with permeate-side incorporation of adsorbents is *via* tailoring the UF MWCO (Figure 2.11). As such, certain OM fractions can be retained based on size, and hence their interference with the permeate-side adsorbents is prevented.

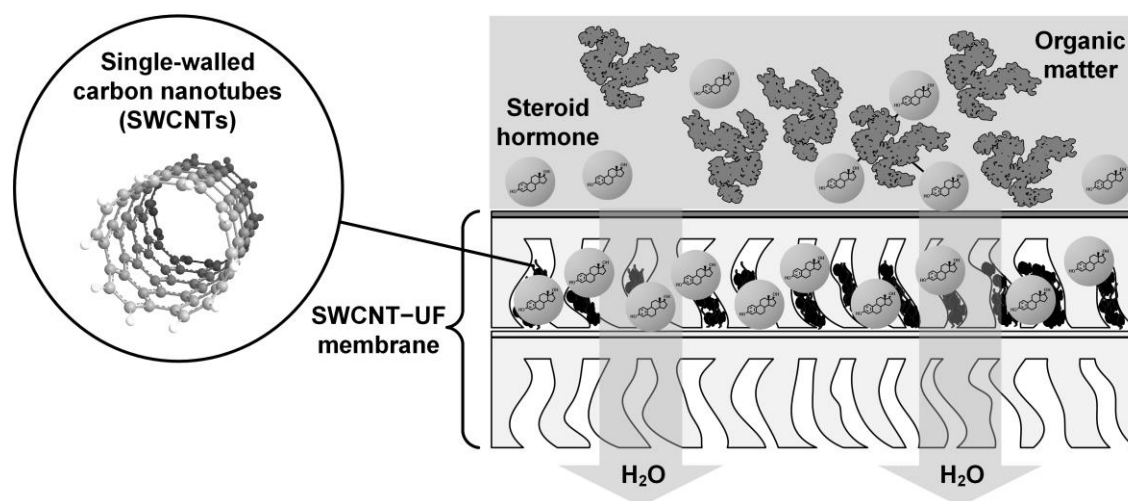


Figure 2.12. Schematic of the shielding of organic matter by UF membrane in an advanced composite membrane set-up. Adapted from the graphical abstract of Nguyen *et al.* 2021³⁰⁵.

Humic substances, which constitute 40–60% of natural OM (NOM)³²⁵, are effectively removed by 5–10 kDa UF membranes *via* size exclusion^{323, 326-328}. Most aromatic components in the water matrix can be found in this fraction³²⁹, so with the above membrane MWCs, a major source of interference can be eliminated. Nevertheless, NOM contains other compounds with diverse properties, such as biopolymer-like (MW >20 kDa) and LMW (MW <350 Da) compounds. Biopolymer-like OM can be excluded with even higher UF MWCs of 30–300 kDa^{330, 331}, whereas LMW compounds effectively permeate through all UF membranes³²⁸.

Prior to this work, the effectiveness of UF shielding has not been examined in detail because the permeate-side deposition of adsorbents is not common. With the UF–PBSAC composite, Wolters *et al.* observed minimal impact on E2 adsorption in the presence of HA and NOM when the UF MWCO decreased from 300 kDa to 1 kDa. These findings were certainly unexpected by the authors, especially when a decreasing trend in HA and NOM removal was established with increasing UF MWCO. The above results highlight the importance of system design: i) HA and NOM were not suitable as they were excluded from the pores of PBSAC (where adsorption of E2 was relevant), ii) these OM types probably have low interference potential, and iii) the quantity of adsorbents needs to be adjusted, as such the adsorption sites are not excessive, which allows the observations of OM / hormone competition. With the use of adsorbents that contain mainly external surface (such as CNPs) in ACMs, the interference of OM is potentially stronger, and control strategies can lead to more significant findings.

2.5.4 Adsorbent regeneration

Several reviews and original researches have been dedicated to evaluate various adsorbent regeneration techniques, which include thermal, chemical, hydrothermal, electrochemical, microbiological, catalytic oxidative, microwave, and ultrasound regeneration techniques³³²⁻³³⁶. Among these, the thermal technique is the most commonly used in WWTPs with AC treatment³³⁷, whereas the applicability of this technique for ACMs is discussed below. Discussions about the chemical and hydrothermal techniques are also given. The other techniques are not evaluated

in this dissertation. If they were, the evaluation would include the compatibility with the composite membrane, whether additional treatment modules are required, and/or whether alteration of the filtration module design is necessary.

Thermal regeneration is an efficient technique for GAC and PAC. GAC particles and PAC slurry can be retrieved from the respective modules and incinerated at very high temperatures (from 200 to 1000 °C) to vaporise the adsorbates^{123, 332, 334, 335, 338}. The required temperature to achieve high removal depends on the decomposition temperature (*i.e.* volatility) of the adsorbed compounds³³⁹, whereas the GAC/PAC loses the adsorption capacity after each adsorption–desorption cycle^{123, 338}. Thermal regeneration does not work with ACMs because membrane materials readily melt at low temperatures³⁴⁰. Therefore, to regenerate CNPs *via* the thermal method, the CNPs need to be detached from the composite membranes, which is not practical.

Chemical regeneration is an alternative technique that is more compatible with ACMs. The chemicals used in regeneration can be acids/bases³⁴¹⁻³⁴³, solvents (namely acetone and alcohols)³⁴⁴⁻³⁴⁶ and surfactants³⁴⁷. These chemicals cause the adsorbates to detach from the adsorbent surface *via* enhancing the affinity between the adsorbates and the surrounding medium (*e.g.* with ethanol/methanol), and/or reducing the affinity between the adsorbates and the adsorbents (*e.g.* with bases).

For example, Machado *et al.* reported good recovery (87%) of MWCNT following dye adsorption with a combination of methanol and 4 M NaOH³⁴⁸. In contrast, the recovery of PAC was very poor at all solvent conditions (<12%), implying that solvents did not affect the adsorbed compounds inside the pores. From another study, methanol and ethanol recovered 50–95% of the maximum adsorbed masses of MWCNT for pharmaceuticals³³⁴. However, in the same study, very good adsorption performances were observed after the MWCNT was regenerated with only 0.1 M NaCl (95% recovery of adsorption) or pure water (80%).

These findings imply that the desorption from the external adsorbent surfaces is facile, as indicated with the adsorption equilibrium law (see Eq. (2.3) in Section 2.5.1). Several other studies also indicate good recovery of CNPs from organic pollutants with only pure water or simple water matrices^{169, 217, 349-351}. Because the regeneration of CNPs appears easier than that of ACs, the use of ACMs is advantageous in this regard.

Hydrothermal regeneration is another practical technique, where desorption is promoted by hot water at elevated temperatures³⁵²⁻³⁵⁴. The concept is demonstrated by Aumeier *et al.*, who pointed out that the combination of a moderately high temperature (120 °C) and backwash resulted in much better amitrole desorption from GAC compared with the scenario where backwash was not applied³⁵⁴. The same group then utilised the temperature of 120 °C and pressure of 1 bar in a hybrid membrane process to regenerate GAC and enhance UF membrane backwash³⁵⁵. The pressure was increased inside a pressure cooker containing both the GAC and membrane modules. Amitrole was desorbed from the GAC with 91–97% recovery.

The hydrothermal technique is promising for ACMs where the energy requirement to heat water to 120 °C is achievable, the filtration system is already pressurised, and the UF membrane may not disintegrate at 120 °C. The single-module design allows less energy dissipation, and molecules adsorbed to the external surface may desorb more easily than those inside the AC pores.

2.5.5 Adsorbent leakage and toxicity concerns

Many recent reviews have provided thorough assessment on the toxicological effects of CNPs on the aquatic environment¹⁷⁶⁻¹⁷⁸. A brief summary is given below, which first illustrates the impacts of CNPs on the cellular and higher-order organisms, then examines whether these toxicological effects can be found at environmentally relevant CNP concentrations, and finally explains the implications to ACMs.

The bacterial cells are a useful model to characterise environmental stress because they are the foundation of all ecosystems. Zou *et al.* highlighted the three main antibacterial mechanisms of CNPs³⁵⁶ as follows.

- Nano-knives: The sharp edges of graphenes or pointy tips of SWCNTs can pierce through the cell membrane, which leads to cell death.
- Oxidative stress: When the CNPs wrap around or stay in proximity of the bacterial cell, 'oxidative stress' because of the imbalanced accumulation of reactive oxygen species and damage the cell membrane and cellular components.
- Cell wrapping: High densities of CNPs immobilise the cells and hinder the cell growth and proliferation.

These three mechanisms may explain several trends in toxicity. For instance, well-dispersed SWCNTs at 5 mg/L can pierce the bacterial cell membrane, hence they are more toxic than SWCNT aggregates or MWCNTs^{357,358}. At very high concentrations of 1 g/L, long (5 µm) strains of SWCNTs wrap around the bacterial cells more effectively than short (< 1 µm) strains of SWCNTs, as such the long strains are more lethal³⁵⁹.

From *in vitro* and *in vivo* tests, CNPs have been found to accumulate in higher-order organisms, such as water fleas^{360,361}, algae^{362,363}, protozoa³⁶⁴, mussels^{365,366}, and fish³⁶⁷. Lethal effects are observed at high concentrations of CNPs of at least several milligrams per litre. Other ecotoxicological assessments reveal that the lethal concentrations of CNPs are in the mg/L range^{176,368}. In contrast, the concentrations of CNPs in surface water and even wastewater effluent are expected to be low. In 2009, from probabilistic material flow analysis, the predicted concentrations of CNTs and fullerene were 0.001–0.04 ng/L in surface water, and 3.8–14.8 ng/L in WWTP effluents³⁶⁹. A later study in 2014 underlines a rise in the predicted concentrations of CNPs in surface water, but these concentrations are still in sub-ng/L range³⁷⁰.

Although the expected CNP concentrations in waters is much lower than the toxic concentrations, concerns still arise because the CNPs (except fullerenes) in water are not quantifiable, because it is difficult to distinguish CNPs from natural particles (colloids) that are present at higher concentrations^{371,372}. C₆₀ and C₇₀ can be quantified *via* mass spectrometry with fixed molecular weights of 720 and 840 g/mol, respectively. Several wastewater samples contain C₆₀ and C₇₀ with concentrations up to 20 ng/L^{373,374}. In surface waters, these nanoparticles were detected in sub-ng/L concentrations³⁷⁵. The concentrations of CNTs and graphenes are expected to fall in the similar ranges as fullerenes.

If the ACMs are widely applied but measures to control CNP leakage, the concentrations of CNPs in polished water may elevate, and the CNPs can become a danger to the aquatic environment.

Another concern is that CNPs indirectly impact the aquatic life by acting as carriers of toxic pollutants. For example, fish survival, metabolism and behaviour are affected when the fish are exposed to pesticides carried by CNPs^{376,377}. Another mechanical or chemical barrier underneath the MF/UF membrane is necessary if the CNPs are physically incorporated inside an MF membrane or in the permeate side of an UF membrane; however, the detection of down-stream CNPs needs to be realised first before the applicability of ACMs can be evaluated. Further discussions on various membrane designs will be provided in the next sub-chapter.

2.6 ACM designs

Several designs of ACMs are evaluated for steroid hormone removal (Figure 2.13). The adsorbents are not exclusive to the CNPs described above (carbon nanotubes, graphenes, and fullerenes), but also include AC fibres²⁴⁶ (10–30 μm in size), superfine PAC²¹⁶ and nanospheres³⁷⁸ (both are sub-micrometres in size).

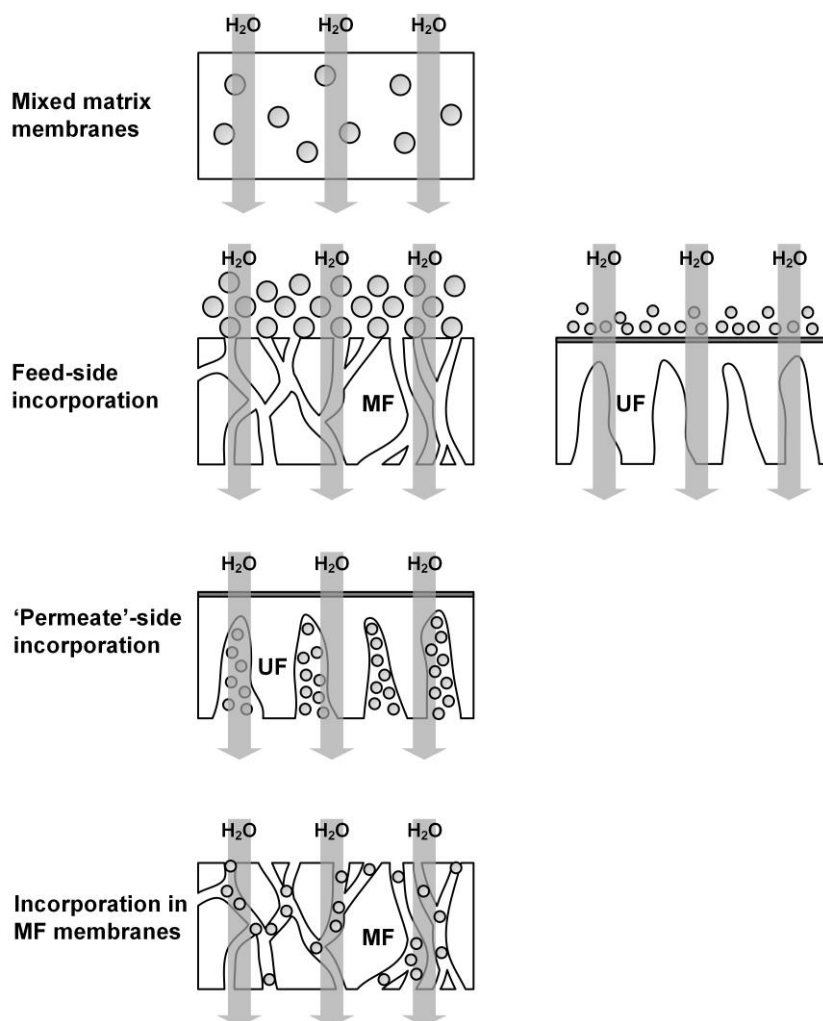


Figure 2.13: Schematic of common composite membrane configurations where particles or nanoparticles (grey spheres) are incorporated.

2.6.1 Mixed-matrix membranes

Nanoparticle-incorporated mixed-matrix membranes (MMMs) are named for membranes where the nanoparticles (fillers) are mixed with the membrane materials in dense liquid form during the fabrication^{379, 380}. There is a narrow window of nanoparticle loading in MMMs: too high nanoparticle quantity may cause the MMM to lose integrity and increase the chance of nanoparticle leakage, while too low nanoparticle quantity may lead to poor (adsorptive) function³⁸¹. The selection of the suitable filler loadings should be handled on the case-by-case basis.

Adsorptive MMMs have the following drawbacks beside the filler loading. First, a significant portion of the adsorbent surface is covered by membrane material^{382, 383}, which limits the contact between the adsorbents and micropollutants, and may result in poor adsorption. Second, the MMMs can leak nanoparticles if these nanoparticles are not compatible with the membrane polymers. The leakage of silver nanoparticles from MMMs at up to 200 µg/L has been detected³⁸⁴⁻³⁸⁶ with either inductively-coupled plasma mass spectrometry, or atomic absorption spectroscopy with detectable concentrations as low as 1 µg/L. It is impossible to detect any small amounts of leaked CNPs that contain mostly carbon. Third, irreproducible membrane permeabilities are usually observed in self-fabricated MMMs³⁸⁷, which complicates the determination of residence time and prevents the comparison between membranes. Therefore, the MMMs produced in the laboratory need to undergo thorough integrity and permeability tests before their adsorption performance can be evaluated.

Several groups have reported the efficiency of CNP–MMMs fillers in removing steroid hormones. Hydrophilised SWCNT fillers at 0.1 wt.% loading (or around 1 mg per gram of membrane) enhanced the removal of nonylphenol and BPA from wastewater by 30% compared with the control polysulfone-based MMMs³⁸⁸. The control MMM (without SWCNT loading) already adsorbed a lot of nonylphenol and BPA (45% and 63% removals, respectively), so the fillers only caused a moderate improvement. Wang *et al.* reported that, with a MWCNT loading of 15 wt.% (or around 150 mg/g), the adsorbed mass of BPA increased from 2.5 mg/g at saturation, to 6 mg/g where the saturation was not reached³⁸⁹. The loading of 15 wt.% was very high and may cause CNP leakage and irreproducible results.

Physical deposition of adsorbents on the membrane surface can be a chemical-free route to produce an ACM. With UF membranes, the adsorbents can be deposited either on the membrane dense layer (feed side), or in the support structure (permeate side).

2.6.2 Feed-side incorporation in MF/UF membranes

Feed-side incorporation is a straight-forward method to produce adsorptive composite MF/UF membranes. The adsorbents / nanoparticles can be incorporated *via* simple filtration^{226, 227, 390, 391}, or spray-coating^{392, 393}. Additional steps may be taken to the mechanical stability of the adsorbent layer, such as the use of crosslink agents³⁹³ or irradiation beams³⁹⁴.

A benefit of feed-side deposition is that a high adsorbent loading can be achieved, and the adsorbent loading may scale with adsorption performance. However, feed-side deposition has a number of drawbacks. First, the small adsorbents / nanoparticles can penetrate the membrane

pores, which causes pore blocking, increases the membrane resistance, and decreases the membrane permeability^{215, 226}. Pore blocking is more severe if the nanoparticles and the membrane pore have similar diameters. For example, a decrease in membrane permeability of around 20% when 0.24 μm superfine PAC are deposited in the 0.45 μm MF membrane²²⁶. Second, micropollutant adsorption by CNPs in the feed side is influenced by other components in the water, such as NOM. This drawback is described in detail in Section 2.5.3. Finally, the adsorbent layer presents an additional boundary layer, and mass transfer from solution to the nanoparticles in this layer will limit the adsorption performance.

Several studies have shown enhanced removal of micropollutants where carbon particles and CNPs are deposited on the feed side. Ellerie *et al.* coated the surface of MF membranes with graphene, MWCNTs and superfine PAC (0.24 μm in size) at a loading of 1.4 g/m^2 , and observed significant enhancement in atrazine adsorption²²⁶. The order of atrazine removal was MWCNT < graphene < superfine PAC up to a specific permeate volume of 600 L/m^2 . In another work, MWCNT and reduced GO was deposited on MF membrane to enhanced pharmaceutical removal²²⁸. Wang *et al.* reported that the composite membranes with 22 g/m^2 MW-/SWCNT loading enhanced the adsorption of pharmaceuticals by 8–35 times compared with the control 0.45 μm MF membrane²²⁷. The concentrations of spiked pharmaceuticals in this work were high (1 mg/L), although adsorption equilibrium was not reached with most composite membranes.

2.6.3 'Permeate'-side incorporation in MF/UF membrane

In an asymmetric UF membrane, the carbon-based adsorbents can be deposited in the support structure, which typically have empty spaces with sizes that reach 100–300 μm in size³⁹⁵. The UF structure can accommodate CNPs with the aggregate sizes in the sub-micrometre or nanometre ranges. Nanoparticles can also penetrate the pores of symmetrical MF membranes, and for convenience, the resulting composite membranes are grouped under this category.

Permeate-side deposition has several benefits over feed-side deposition. First, in the asymmetric UF membranes, the adsorbents are not likely to penetrate the dense layer pores and cause pore blocking. Secondly, this set-up enables very close contact between the micropollutants and surface because the boundary layer that inhibit adsorption does not exist. Thirdly, the UF membrane dense layer exclude certain interferants in the feed water, which prolong the adsorptive function of the CNPs. Unfortunately, strong enhancement in adsorption as a result of this UF shielding had not been indicated prior to this work³²⁴. A better examination of interference is given in Chapter 6.

A major disadvantage of permeate-side incorporation is that a physical or chemical barrier underneath the adsorbent is required so that the adsorbents does not leak into the permeate. These barriers may include another membrane or a chemical sealant layer. Madaeni *et al.* deposited MWCNTs in a hydrophilic MF membrane, and then coated the composite with a layer of superhydrophobic polydimethylsiloxane sealant, which caused a massive permeability drop, from several thousand $\text{L}/\text{m}^2\cdot\text{h}\cdot\text{bar}$ to 7.5 $\text{L}/\text{m}^2\cdot\text{h}\cdot\text{bar}$ (*i.e.* the NF-range)³⁹⁶. Polydopamine outperforms polydimethylsiloxane in this regard, as the flux obtained with the glued membranes is similar to that of the control ones³⁹⁷. This membrane–polydopamine concept has been applied to immobilise different nanoparticle types³⁹⁷⁻⁴⁰⁰. Disintegration of polydopamine when exposed to

water has not been observed over the course of several days⁴⁰¹, although in extended operation periods of months or years, the possibility of adsorbent leakage from polydopamine-sealed membranes cannot be ruled out.

While a chemical sealant layer is more elegant, a strong physical barrier reduces the leakage concerns. An example of such layer is a commercial UF membrane of which pore size is smaller than the size of CNP aggregates (see Figure 2.14). A consequence of this dual UF set-up is that the membrane resistance is essentially doubled^{402, 403}, which increases the energy costs for operation.

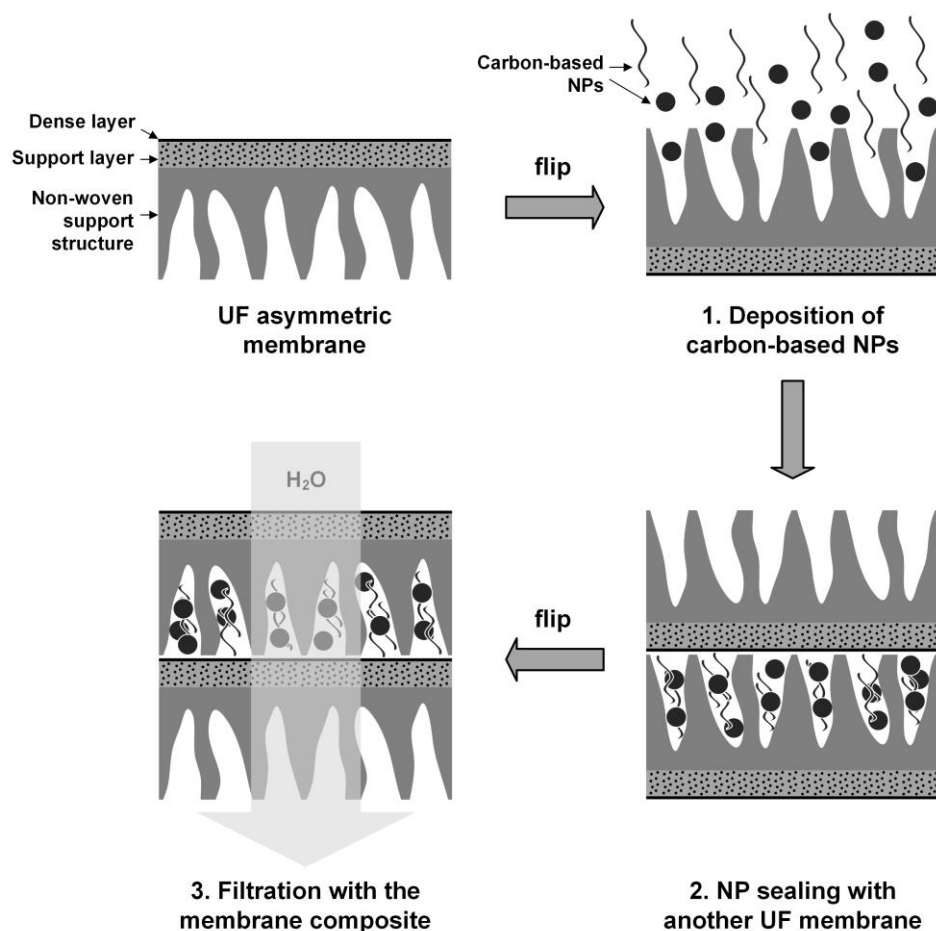


Figure 2.14: Schematic of the dual membrane composite concept. Reprinted from Nguyen *et al.*³⁰².

The proof of concept study of the dual UF membrane set-up involves AC fibres (10–30 μm in size) ‘sandwiched’ between two polyethersulfone (PES) UF membranes²⁴⁶. The permeability of this composite decreased a little (10%) with increasing the loading of AC fibres from 0 to 8 g/m^2 . At an AC fibre loading of 2 g/m^2 , the adsorbed mass of E2 was around 5 ng/cm^2 obtained for a specific permeate volume of 1500 L/m^2 , and adsorption was contributed by both the membrane materials and AC fibres²⁴⁶.

2.6.4 Advanced membranes

Advanced membranes designed from the molecular level are promising for water purification and desalination⁴⁰⁴⁻⁴⁰⁶. Carbon-based advanced membranes include graphene / graphene oxide membranes, where the water and solute channels are the spaces between the graphene layers, and VaCNT membranes, where the channels are the CNT interior. This section specifically discusses VaCNT membranes, which offer anomalous water flow compared with UF/NF membranes in pressure-driven filtration⁴⁰⁷.

VaCNT membranes are built from the self-aligning MW-/SWCNT building blocks *via* a chemical vapour deposition process^{408, 409}. The external surface of CNTs is covered by barrier material (for example parylene-N⁴⁰⁹), which makes the interior of CNTs the only conducting channels. The diameter of the CNTs (*i.e.* of the VaCNT membrane pores) can be modulated⁴¹⁰ between several nanometres^{194, 409} to tens of nanometres⁴¹¹. The integrity of VaCNT membranes with 1–5 nm pore diameters is confirmed *via* stringent filtration (of water or nitrogen gas) and dye retention tests^{196, 224}.

Good water conduction in VaCNT membranes^{194, 196, 412} is quantified *via* the flow enhancement (EF) factor, which is the ratio between the experimental flow rate and the theoretical flow rate described with the Hagen–Poiseuille equation. The Hagen–Poiseuille equation is loosely applied to estimate the flow rate in UF and NF^{129, 413}, so an enhancement in water transport of the VaCNT membrane over UF/NF is indicated. For instance, with a pore diameter of ~2 nm (which is similar to those of tight UF or loose NF membranes¹²⁹), the EF with VaCNT membranes^{194, 196} is at the magnitudes of 10^3 and 10^4 .

VaCNT membranes are an interesting system to understand the adsorption mechanisms according to two reasons. First, the diffusion distance between the adsorbate and surface is very short (several nanometres), which is the range of dense UF and loose NF membranes of 1–3 nm (see in Figure 2.15). When entering the pores of VaCNT membrane (and UF/NF membranes), the adsorbate molecule instantaneously reaches the pore wall, as such the mass transfer limitation is non-existent. Therefore, the pore diffusion processes described in Sub-chapter 2.3.2 are not relevant limiting mechanisms in VaCNT membranes.

Second, hormone adsorption by VaCNT membranes will differ from that by UF/NF and composite membranes (in which the mass transfer limitation also does not exist). A comparison between the pores of UF/NF and those of the VaCNT membranes is schematically shown in Figure 2.15, and adsorption in these pores can be explained by the interplay of forces.

Four forces act on the hormone molecule at the fluid–wall interface, which are: 1) hydrodynamic drag force F_H in the flow direction, 2) adhesive force F_A that is perpendicular to the flow direction and directed at the wall, 3) repulsive force F_R that oppose the F_A as a result of the electrons of the CNT and solute repelling each other, and 4) the hormone–wall friction force F_F that hinders the hormone movement with the flow (Figure 2.15).

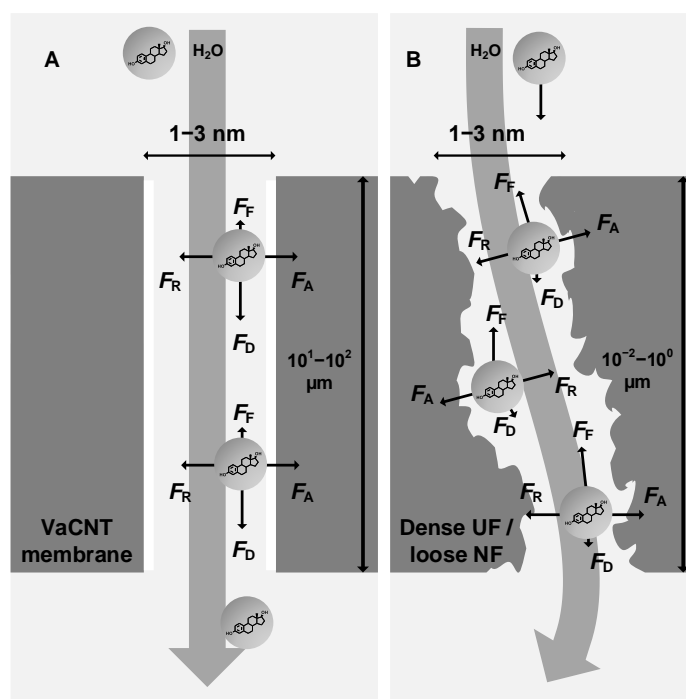


Figure 2.15: Schematic of the transfer of steroid hormone (E2) molecules through a VaCNT membrane (A) and active / dense layer of an UF or NF membrane (B), and the forces acting on the molecules (F_H : hydrodynamic drag, F_F : friction, F_A : adhesive, F_R : repulsive). The pore and hormone diameters are roughly to scale. Adapted from Nguyen *et al.*⁴¹⁴.

The magnitudes of these forces dictate whether hormone adsorption by VaCNT membranes is possible. The low viscous friction of water inside the hydrophobic pores of VaCNT membranes²⁹⁷ provides a non-zero drag force (denoted as F_H in Figure 2.15) that ‘pushes’ the adsorbed hormone towards to pore exit. The absence of pore surface roughness and low pore tortuosity (1.1–1.25^{195, 408}) causes a low hormone–wall friction force (F_F in Figure 2.15) that allows hormone to move along and exit the pores under the action of F_H . The friction force F_F is influenced by the adhesive (van der Waals) force (F_A in in Figure 2.15) that acts perpendicular to the flow direction^{415, 416} and dictates the strength of adsorption (discussed in Section 2.4.4) At a hormone–wall separation distance of ~ 0.3 nm, the repulsive force (F_R) balances F_A ⁴¹⁷ and keep the hormone static in the direction perpendicular to the flow.

Unlike the VaCNT membranes, UF/NF membranes and ACMs have high pore tortuosity (1.5–2.5⁴¹⁸), high pore surface roughness (in UF/NF membranes) due to the interconnected pore network^{419, 420}, and higher surface hydrophilicity⁴²¹. These properties result in a weak or negligible hydrodynamic drag force F_H and strong friction force F_F , which causes the hormone to attach to the membrane wall and adsorbent surface.

2.7 Summary of the key interests in ACM research

In this chapter, the technical considerations and several designs of ACMs have been reviewed. The following points are obtained from this investigation.

- In ACMs, the incorporated CNPs can have low intrinsic mass transfer limitation because of the dominant and excessive external surface.
- However, the low loading, short residence time, and interference of organic matter may restraint adsorption as such it takes place only at the most accessible adsorbent surface.
- Five key technical considerations for ACMs and several ACM designs have been discussed. Because the toxicity concerns of CNPs have not been adequately addressed, ACMs (in the current state of development) cannot be applied in water treatment.

The following research interests are derived and will be explored in the next chapters.

- The evaluation of adsorbents (CNPs) and ACMs needs to be performed at the realistic concentrations of micropollutants in the environment (sub- $\mu\text{g/L}$ for steroid hormones). As such, the surface area of adsorbents may be in excess and will not limit adsorption.
- Many operational and water quality factors (adsorbent loading, residence time, solution pH, organic matter in water) influence the mass transfer limitation in ACMs and need thorough investigation.
- The interplay of forces that determines whether the hormone adheres to or detaches from the adsorbent surface has not been indicated. VaCNT membranes are suitable to quantify these forces as both the surface and mass transfer limitations are non-existent.

3 Study Approach – Materials and Methods

This chapter describes the experimental systems, carbon-based nanoparticles, membranes, solution chemistry, and analytical instrument used in this study.

The methods for sample analysis, model application, sample characterisation, and error determination are described. The static adsorption and filtration protocols are not described in this chapters but in Appendices B and G.

The development of the error analysis method has been an inseparable part of this PhD research. Sub-chapter 3.6 on error analysis is adapted from a manuscript in preparation entitled “Error estimation in experimental water research: Application to membrane technology”, by Alessandra Imbrogno, Minh N. Nguyen, and Andrea I. Schäfer.

Whilst the original manuscript comprehensively describes the mistakes and inconsistencies in error analysis and proposes solutions applicable to membrane technology, the included section only remarks on the errors encountered in filtration experiments with the adsorptive composite membranes.



3.1 Membrane systems

The main membrane system used in this research project is the micro-crossflow filtration system that can also be operated in dead-end mode.

Other filtration systems that assisted nanoparticle deposition (a stainless-steel stirred cell and a vacuum filtration apparatus, both having an effective membrane area of 38.5 cm²) are described in Section 3.3.3. Stainless-steel membrane holders (effective membrane area 1.3 cm²) attached to a plastic syringe were used to separate nanoparticles from solutions in static adsorption experiments and described in Section 3.3.2.

The micro-crossflow filtration system⁴²² (designed by Benjamin Chatillon, Cristina Onorato and Tobias Berger, KIT) is a bench-scale system that operates with relatively small membrane coupons, of which the effective filtration area is 2.0 cm². The stainless-steel cell that holds the membrane was designed and manufactured by Heinz Lambach (IMVT, KIT). Despite the name, the system can be operated in either dead-end or cross-flow mode. In cross-flow mode, the operating conditions (pressure, crossflow velocity, and Reynolds number) can reassemble those in industrial spiral-wound modules⁴²² although the membrane area in this bench-scale system is $\sim 10^4$ times smaller (in spiral wound modules for instance, the membrane area can be several square metres^{423, 424}). The photograph and schematic of this system are given in Figure 3.1.

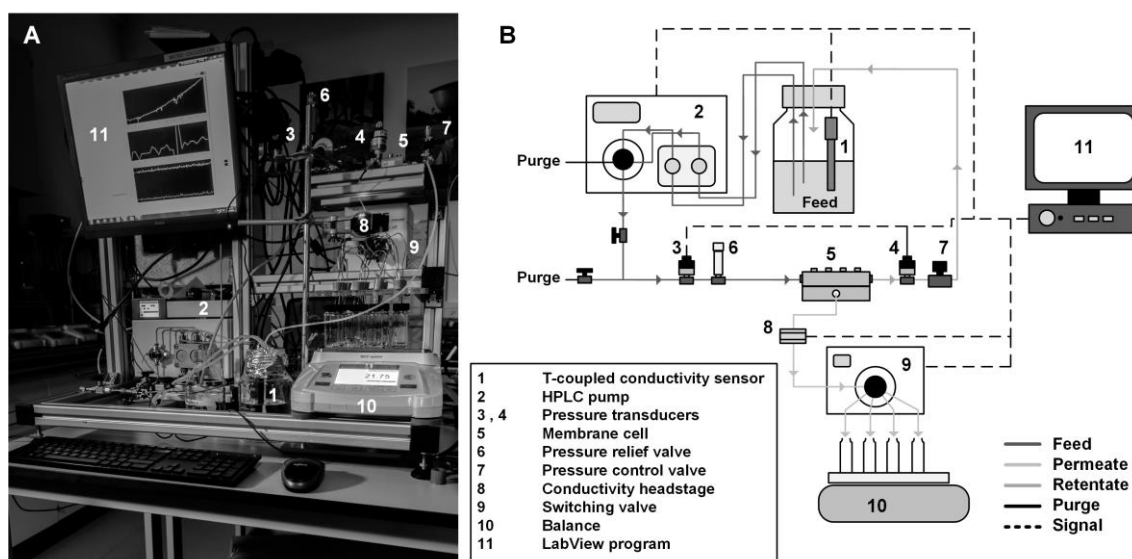


Figure 3.1: Photograph (A) and schematic (B) of the micro-crossflow filtration system.

The components of this filtration system are as follows. Submerged in the feed bottle (500 mL Duran, VWR, Germany), a thermo-coupled electrode (1) (Blackline LF, JUMO, Germany) determines the feed temperature and conductivity in the ranges of 5–80 °C and 0.1–10 mS/cm, respectively. Constant feed flow rates between 0.1 and 500 mL/min are generated with a HPLC pump (2) with a 500 mL pump head (Blue Shadow 80P, Knauer, Germany). Two pressure transducers (3 and 4) (Model A-10, WIKA, Germany) determined the feed and retentate pressures, respectively. The membrane cell (5) is a custom-built cell (IMVT, KIT) that has an effective rectangular filtration area with dimensions 1 · 2 cm². A pressure relief valve (6) set at

22 bar (SS-4R3A, Swagelok, Germany) is placed on the feed side to protect the filtration system from overpressure malfunction. Pressure adjustment is done with a needle valve (7) (SS-RL3S4, Swagelok, Germany, or HF1300SSL, Ham-Let, Germany) placed on the retentate side. The permeate conductivity between 0.02 and 2 mS/cm was determined with a contactless headstage (8) (ET131, eDAQ, USA). A switching valve (9) (model E1379, Knauer, Germany) with 16 outlets separates the permeate in different glass vials (each has a 20–25 mL capacity) and beakers (each has 50–100 mL capacity). A balance (10) (AX2022, Ohaus, USA) recorded the mass of permeate, from which the permeate flow rate can be determined with Eq. (3.8). A LabView 2014 program (11) (National Instruments, USA) allows the control of pump and switching valve, and acquires the data of pressures, temperature, conductivities, and permeate mass every second.

In the experiments with vertically aligned carbon nanotube (VaCNT) membranes in Chapter 7, the needle valve (7) was closed, which allowed the filtration system to operate in dead-end mode. The feed bottle was connected to a water chiller (Minichiller 300 OLÉ, Huber Kältemaschinenbau, Germany), so that the feed temperature is controlled at 23.0 ± 0.5 °C.

3.2 Incubator shaker for static adsorption

Static adsorption experiments were done in an incubator shaker (Innova 43R, New Brunswick Scientific, USA) that house up to 40 conical flasks (250 mL capacity, Duran, VWR). The photograph of this shaker is given in Figure 3.2. The temperature inside the shaker is controlled between 5 and 80 °C. Unless indicated otherwise, this temperature is kept at 20.0 ± 0.5 °C. The shaking speed can vary between 25 and 500 rpm, and in all static adsorption experiments this parameter is kept constant at 260 rpm following the experimental protocol established by Tagliavini *et al.*¹¹².



Figure 3.2: Photographs of the incubator shaker.

3.3 Materials and reagents

The materials and reagents used in this project are divided into four categories: 1) carbon-based nanoparticles, 2) commercial membranes, 3) carbonaceous composite membranes, and 4) solution chemistry (including organic matter types, steroid hormones micropollutants, and other reagents).

3.3.1 Carbon-based nanoparticles

Six types of carbon-based nanoparticles were evaluated for the incorporation in an adsorptive composite UF membrane. The focus of the whole research project however was on the particular single-walled carbon nanotubes (SWCNTs), which was justified based on the evaluation of adsorption performance of all these six nanoparticles as described in Chapter 4. The list of these nanoparticles is given in Table 3.1.

Table 3.1: List of carbon-based nanoparticles. N.A.: not available.

No.	Nanoparticle type	Abbr.	Brand (product code, company, country)	Batch ID(s)
1	Multi-walled carbon nanotube	MWCNT	BU-201, BuckyUSA, USA	GFR8875
2	Single-walled carbon nanotube	SWCNT	Elicarb Low Residue, Thomas Swan, UK	117476/29 121217/36
3	Graphene, Grade 1 (2-3 monolayers)	GP1	GP-AO1, Graphene Supermarket, USA	N.A.
4	Graphene, Grade 2 (~30 monolayers)	GP2	GP-AO2, Graphene Supermarket, USA	N.A.
5	Graphene oxide	GO	Graphenea, Spain	C322/GOB007/Pw1
6	Fullerene C ₆₀	C ₆₀	B1641, TCI Chemicals, Germany	ARI4C

3.3.2 Commercial UF and MF membranes

Merck Millipore Corp., USA is acknowledged for providing several commercial UF membranes in this study. The main characteristics of these UF membranes are given in Table 3.2. All membranes have non-woven support layers. The Ultracel membranes 3–100 kDa (PLH series) have a regenerated cellulose dense layer and polyethylene support layer, with a total thickness of 230 μm . The Biomax membranes (100 kDa, PBHK) have a polyethersulfone dense layer and polypropylene/ polyethylene support layer, with a total thickness of 280 μm .

Three MF and UF membrane types were used to separate nanoparticles from water in static adsorption. Regenerated cellulose (RC) 100 kDa UF membranes (code PLHHK, Merck Millipore) and polytetrafluoroethylene (PTFE) 0.45 μm MF membranes (code 11806-293-G, Sartorius, Germany), were used to separate nanoparticles except GO. These membranes were cut in small circular pieces with a diameter of 1.3 cm and then mounted in a stainless-steel membrane holder (Merck Millipore). PTFE membranes could not be used to separate GO except at very low

GO concentrations of 2 and 10 mg/L, because GO strongly adsorbs water^{277, 278} and prevents water from selectively permeating hydrophobic MF membranes. Hence, hydrophilic cellulose acetate (CA) 0.45 μm MF membranes (Minisart, Sartorius, Germany) in the supplied plastic housing were used to separate GO at concentrations 0.1–1 g/L. These CA membranes adsorbed a lot of steroid hormones at neutral pH⁴²⁵, so they caused large errors in the determined hormone concentrations. Analyte losses due to membrane adsorption are discussed in Section 4.2.5.

Table 3.2: Characteristics of commercial UF and MF membranes (generously provided by Merck Millipore, USA) used in filtration experiments.

Membrane and code	Pore size (nm)*	Dense layer porosity (%)**	Permeability (L/m ² .h.bar)	Residence time t_R at 1 bar (s)***
Regenerated cellulose (RC) UF				
3 kDa (PLHBC)	2.8	4.4–5.1	6–7 ^{a,b}	6.1
5 kDa (PLHCC)	3.7	4.7–5.9	11–14 ^{a,c}	3.5
10 kDa (PLHGC)	5.4	16–18	80–90 ^{b,c}	1.6
30 kDa (PLHTK)	9.6	13–19	200–300 ^{a,b}	0.52
100 kDa (PLHHK)	18.2	13–14	720–800 ^{a,b}	0.14
Polyethersulfone (PES) UF				
100 kDa (PBHK)	18.2	8.0**	460 ^d	0.18

^a Neale *et al.*⁴²⁶, ^b Imbrogno *et al.*⁴²⁷, ^c Aschermann *et al.*³²³, ^d Wickramasinghe *et al.*⁴²⁸.

* Calculated from MWCO using the equation $d = 4.074 \cdot 10^{-11} \cdot M^{0.53}$, in which d (nm) is the membrane pore diameter, and M (Da) is the membrane molecular weight cut-off^{326, 429}.

** Estimated from pure water flux and membrane pore size with Hagen–Poiseuille law (see Eq. (3.11)). Similar UF membranes have porosity in the range of 1–15%⁴³⁰.

*** Calculated from the pure water flux and membrane porosity (see Eq. (3.12)).

In Chapter 7, a polyvinylidene fluoride (PVDF) 0.2 μm MF membrane (code GVPP-Hydrophilic, also provided to IAMT by Merck Millipore) was placed underneath each vertically aligned carbon nanotube (VaCNT) membrane, to prevent the VaCNT membrane from cracking due to applied pressure.

3.3.3 Composite membranes

Several (adsorptive) composite membranes were used in this research project, which are single-walled carbon nanotube – ultrafiltration (SWCNT–UF) with various UF MWCOs, and VaCNT membranes.

The SWCNT–UF membranes were produced by filtering the solution through the commercial UF membrane *via* two methods, with either a vacuum filtration apparatus, and a stainless-steel stirred cell, as described in Figure 3.3 A and B. In both methods, a 7 cm membrane coupon was prepared and mounted upside-down.

The vacuum pump apparatus (model FB70155, Fisher Scientific, UK, see Figure 3.3 A) can induce a maximum pressure of 2.3 bar and is applicable for incorporating SWCNTs in the

membranes with moderate or high MWCOs (10–100 kDa). The 7 cm membrane coupon was mounted on a stainless-steel support inside a glass funnel (diameter 7.3 cm, Duran, Germany). Then, 4.2–168 mL of SWCNT suspension, which corresponds to the 0.1–4 g/m² loading, was poured into the glass funnel. The vacuum pump forces the SWCNT suspension to permeate the membrane and cause SWCNT to deposit in the UF support structure. A water trap prevents water from entering the pump.

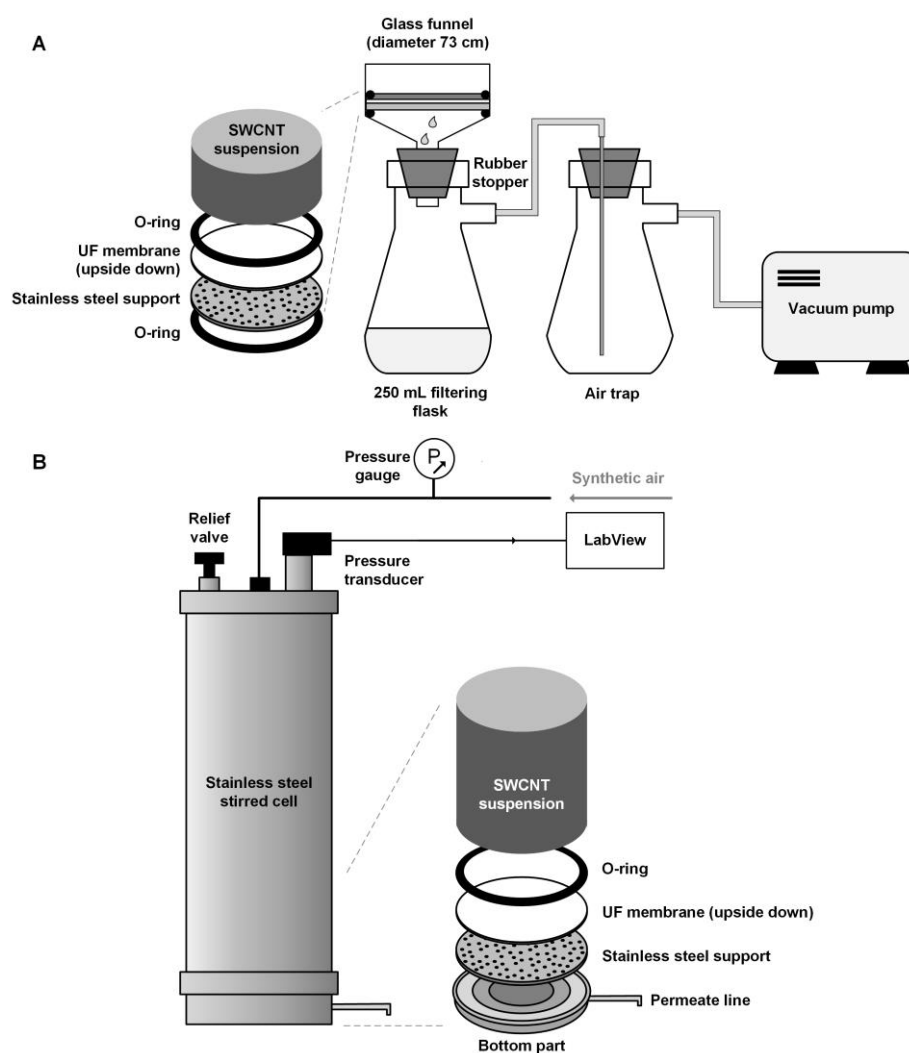


Figure 3.3: Apparatuses for SWCNT incorporation into the UF support: vacuum filtration device for 10–100 kDa UF (A) and stirred cell for 3–5 kDa UF (B).

For the low-MWCO (3–5 kDa) UF membranes, an alternative process will a stainless-steel stirred cell (see Figure 3.3 B) was used as a means to reduce the SWCNT incorporation time. The specification of this stirred cell for filtration for up to 20 bar pressure was described elsewhere⁴²². For SWCNT incorporation, the 7 cm coupon was mounted upside-down in the stirred cell, then the SWCNT suspension was added and the stirred cell was tightly sealed. A constant pressure of 4 bar was applied (which was monitored *via* a LabView 2014 program) until all the suspension in the stirred cell permeated through the UF membrane.

Vertically aligned carbon nanotube (VaCNT) membranes were fabricated at Lawrence Livermore National Laboratory (LLNL), USA, *via* a previously reported method^{195, 196, 409}. The main fabrication steps are illustrated in Figure 3.4. In brief, the fabrication steps include: 1) deposition of catalyst nanoparticles (Fe/Mo or Fe only) on a silicon support *via* a thermal evaporation process, 2) chemical vapour deposition growth of vertically aligned CNTs on the nanoparticle catalysts, 3) chemical vapour deposition of parylene-N as barrier material, and 4) plasma etching of the fabricated VaCNT membrane to open the CNT pores and functionalise the CNT tips with oxygen-containing groups.

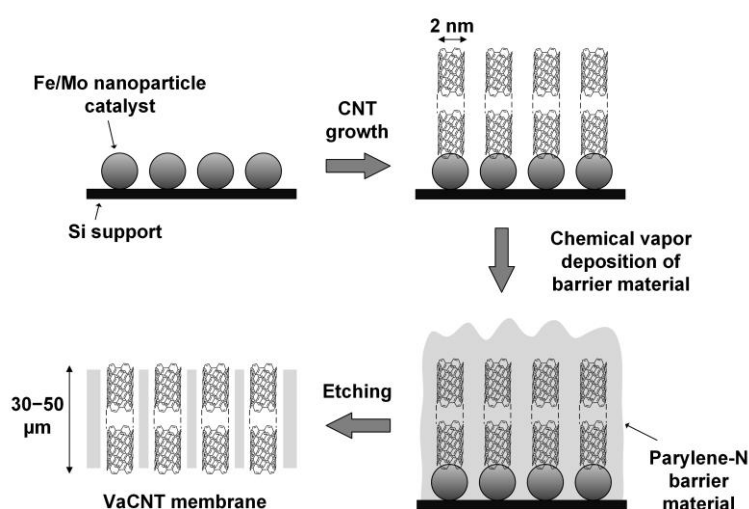


Figure 3.4: Schematic of VaCNT membrane fabrication. Adapted from Bui *et al.*¹⁹⁵.

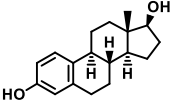
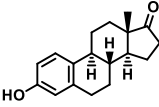
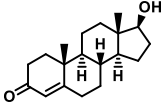
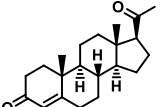
3.3.4 Solution chemistry

Radiolabelled hormones, [2,4,6,7-³H] 17 β -estradiol (E2, batches 2656306, 2695538, and 2852571), [2,4,6,7-³H] estrone (E1, batches 2155774 and 2526125); [1,2,6,7-³H] progesterone (P, batches 2151380, 2541592 and 2852581) and [1,2,6,7-³H] testosterone (T, batches 2136265 and 2502698), were supplied as 1 mCi ($3.70 \cdot 10^7$ Bq) solutions in ethanol (Perkin Elmer, USA). Alternative radiolabelled [6,7-³H] estrone (batch 210311) was supplied by BioTrend, Germany, also as 1 mCi ($3.7 \cdot 10^7$ Bq) solutions in ethanol.

From these supplied solutions, 10 μ g/L hormone stock solutions were prepared by dilution with Milli-Q water (Reference A+, Merck Millipore, USA). In experiments with E2 concentrations greater than 100 ng/L, non-radiolabelled E2 was used in addition to the radiolabelled E2. The stock non-radiolabelled E2 solution (10 mg/L) was prepared by dissolving 50 mg of powder (98% 17 β -estradiol, Sigma-Aldrich, USA) in 5 L of methanol solvent (99%, VWR, Germany).

The physiochemical properties of the steroid hormones are shown in Table 3.3.

Table 3.3: Physiochemical properties of the four steroid hormone types^{289-291, 429, 431-437}.

	E2	E1	T	P
CAS number	50-28-2	53-16-7	58-22-0	57-83-0
Chemical formula	C ₁₈ H ₂₄ O ₂	C ₁₈ H ₂₂ O ₂	C ₁₉ H ₂₈ O ₂	C ₂₁ H ₃₀ O ₂
Molecular structure				
Molecular weight without ³H label (Da)	272.4	270.4	288.4	314.5
pKa	10.2–10.7 ^{a, b, c}	10.3–10.8 ^{a, b, c}	N.A.	N.A.
Log K_{ow}	4.01 ^{c, d}	3.13 ^{c, d}	3.32 ^{c, d}	3.87 ^d
Solubility in water at 25°C (mg/L)^e	0.16–5.0	0.80–1.3	20–48	7.9–17
Solubility in methanol at 30°C (g/L)	35 ^f	5 ^{g, h}	220 ⁱ	N.D.
Solubility in ethanol (g/L)	37 (30°C) ^f	7 (30°C) ^g	N.D.	54 (21°C) ^j
Stokes radius (nm)^k	0.40	0.40	0.41	0.43
π-rings	1	1	0	0
O···H bond donors	2	1	1	0
O···H bond acceptors	2	2	2	2
Total minimum energy (kJ/mol)^{**}	112 ^{MM2} 245 ^{MMFF94}	100 ^{MM2} 213 ^{MMFF94}	159 ^{MM2} 298 ^{MMFF94}	158 ^{MM2} 309 ^{MMFF94}

^a Perrin *et al.*²⁸⁹, ^b Lewis and Archer²⁹⁰, ^c Bhandari *et al.*²⁹¹, ^d Hansch *et al.*⁴³¹, ^e Yalkowsky and He⁴³², ^f Ruchelman and Haines⁴³³, ^g Ruchelman⁴³⁴, ^h Doisy *et al.*⁴³⁵, ⁱ Ruchelman⁴³⁶, ^j Sieminska⁴³⁷, ^k calculated according to Worch⁴²⁹.
^{**} Energy minimalization was performed with MM2 and MMFF94 force-field models in Chem3D software (ChemOffice Suite 19.1, PerkinElmer, USA)

Several trends in hormone properties are determined, which may contribute to the differences in adsorption and filtration performances of CNPs and composite membranes with varied hormone types. The hydrodynamic radii of the hormones estimated from the molecular weight follow the trend E1 < E2 < T < P⁴²⁹. The pKa values of E1 and E2 were slightly higher than 10, while T and P are non-dissociable in the pH range 2–12 (Table 3.3), hence only charge interactions between the membrane or CNP with E1/E2 are relevant.

The hormone molecules can be considered hydrophobic, because of the positive and high log *K_{ow}* values, high solubilities in alcohol, and low solubilities in water. However, the trend in log *K_{ow}* (E1 < T < P < E2) does not match the trend in water solubility (E1 < E2 < P < T), therefore it is not possible to rank the steroid hormones according to hydrophobicity.

To evaluate OM interference, nine OM types were selected, which cover a broad range of size, origin, aromaticity, and hydrophobicity. These OM types are divided into four categories based on their chemical compositions and origins. Known OM properties are given in Table 3.4.

- OM types rich in humic substances: humic acid (HA technical grade, 80% purity, Sigma-Aldrich, USA), and Australian NOM (AUS, Gosford, Australia ⁴³⁸).
- OM types rich in phenols ^{439, 440}: tannic acid (TA, ACS 99.5% purity, Alfa Aesar, USA), tea extract (TEA, Indian Tata black and green tea, batch no. 09PP45-1, packaged in May 2018), and tannin (TANN, 65%, exGrape PEL, Grap'sud, France).
- Sugar-based OM types: glucose (GLU, 180 Da monosaccharide, BioUltra 99.5% purity, Sigma-Aldrich, USA), and alginate (ALG, 12–180 kDa polysaccharide ⁴⁴¹, 72–78% purity, Alfa Aesar, USA).
- Degradation products: worm farm extract (WF, raw liquid from a stacked-bin worm farm fed with food waste), and fermentation products (FP, Rechtsregulat Bio, Dr Niedermaier Pharma, Germany, consumer product from fruits and vegetables ⁴⁴²).

Table 3.4: OM types. Bio: biopolymers, HS: humic substances, BB: building blocks, LMW: low molecular-weight acids and neutrals, HOC: hydrophobic organic carbon). N.D.: not determined. Liquid chromatography – organic carbon detection (LC-OCD) separates the OM into fractions and determines the composition.

Compound	Origin	MW (Da)	Main LC-OCD fractions (%) ³⁰⁵	Diameter (nm) ^d	pKa
Humic acid (HA)	Soil	4.7k–30.4k ⁴⁴³ 780 ± 20 ^a	HS: 37%, LMW: 31%, BB: 20% (HOC: ~13%)	3.6–9.7	4.3 ⁴⁴⁴
Australian NOM (AUS)	Soil	530 ± 15 ^a	HS: 67%, LMW: 20%, BB: 14%	1.5	N.D.
Glucose (GLU)	Plants	180	LMW: ~95%	0.6	12 ⁴⁴⁵
Tannic acid (TA)	Plants	1,701	Mainly HOC	2.1	8.5 ⁴⁴⁶
Tannin (TANN)	Plants	Bio: ~23k ^b	(HOC: 63%), HS: 16%, LMW: 10%, Bio: 5%	9.3	N.D.
Alginate (ALG)	Plants	12k–180k ⁴⁴¹	Bio: 96%	5.9–25	3.4 – 3.7 ⁴⁴⁵
Tea	Plants	380 ± 10 ^a	BB: 45%, LMW: 26%, (HOC: 12%)	1.1	N.D.
Fermentation products (FP)	Degradation of plants	480 ± 15 ^a	LMW: 81%, BB: 14%	1.1	N.D.
Worm farm extract (WF)	Degradation of plants	~17k ^b	(HOC: 50%), Bio. + HS: 46%, LMW: 6%	6.4	N.D.

^a Number-average mean MW of the HS fraction determined with ChromCALC software (DOC-Labor, Germany) in LC-OCD analysis ³⁰⁵.

^b MW of the Bio fraction, estimated from the peak position calibration in the organic carbon detector of LC-OCD with polystyrene sulfonate standards 2.18–65.4 kDa ³⁰⁵.

^c With the equation $d_{OM} = 4.074 \cdot 10^{-11} \cdot M^{0.53}$, where d and M are the diameter and MW of the OM, respectively ⁴²⁹.

HA, AUS and TA in the first and second categories are rich in phenols, and hence can interact with CNPs, hormones and membranes *via* π / π stacking and hydrogen bonding^{264, 310, 316}. Non-aromatic and hydrophilic OM types in the third category can only form hydrogen bonds with the adsorbents. The properties of other OM types (TEA, TANN, FP and WF) are largely unknown prior to this work.

The background electrolytes in the feed are NaHCO₃ (1 mM) and NaCl (10 mM), which result in a simulated water matrix that is similar to natural waters. The pH of this buffered solution is around 8.1 ± 0.2 . The feed solution was prepared by diluting from 5 mM NaHCO₃ and 50 mM NaCl solutions, which were obtained by dissolving respective powders (analytical-grade 99.7% NaHCO₃, Bernd Kraft, Germany or EMSURE NaHCO₃, Merck Millipore, USA, and analytical-grade 99.9% NaCl, VWR ProLabo, Germany) in Milli-Q water. Adjustment of pH in the range of 2–12 was done with NaOH 1 M (dissolved from EMSURE (99%) pellets, Merck Millipore) and HCl 1 M (diluted from analytical-grade HCl 37%, Roth, Germany).

Triton-X100 surfactant (analytical-grade, Sigma-Aldrich, USA) was used to improve the SWCNT suspension prior to the incorporation of SWCNT in membranes.

A scintillation cocktail (Ultima Gold, PerkinElmer, USA) was used in the LSC analysis. The mobile phase for the LC-OCD analytical instrument is a buffer of 2 g/L KH₂PO₄ and 1.2 g/L Na₂HPO₄ (both dissolved in Milli-Q water from $\geq 99.5\%$ powders, EMSURE, Merck Millipore). The acidification solution for LC-OCD containing 2 g/L K₂O₈S₂ (dissolved from analytical-grade 99.5% powder, Merck Millipore) and 60.8 mM H₃PO₄ (diluted by 40 times from analytical-grade 85% solution, Merck Millipore).

The calibration of LC-OCD to determine the organic carbon content and UV absorbance was done with 0.002–10 mgC/L potassium hydrogen phthalate (KHP, dissolved from analytical-grade 99.5% powder, Merck Millipore) in the LC-OCD mobile phase. The calibration of the TOC analyzer was done with 0.002–10 mgC/L KHP in Milli-Q water. The calibration procedures for LSC and LC-OCD are described in Appendix A.

3.4 Analytical techniques

3.4.1 Liquid scintillation counting (LSC)

Liquid scintillation counting was used to quantify the radiolabelled steroid hormones at concentrations between 0.1 and 100 ng/L⁴⁴⁷. Two counters (Figure 3.5 A) were used in this research project: a Tri-Carb 2550 TR/AB and a Tri-Carb 4910 TR, both supplied by Packard, USA. In a 20 mL glass scintillation vial (Wheaton, Fischer Scientific, Germany), 1 mL of the hormone solution was mixed with 1 mL of scintillation liquid (Ultima Gold, LLT, Perkin Elmer, USA). Each sample was analysed in triplicate with each measurement lasting 10 min. Hormone concentration was determined from activity *via* linear regression obtained using steroid hormone standards (concentrations 0.2, 1, 10, 50 and 100 ng/L), *via* a procedure described in Appendix A. The calibration, analytical errors, detection limit (LOD) and limit of quantification (LOQ) are described in Section 3.6.2.

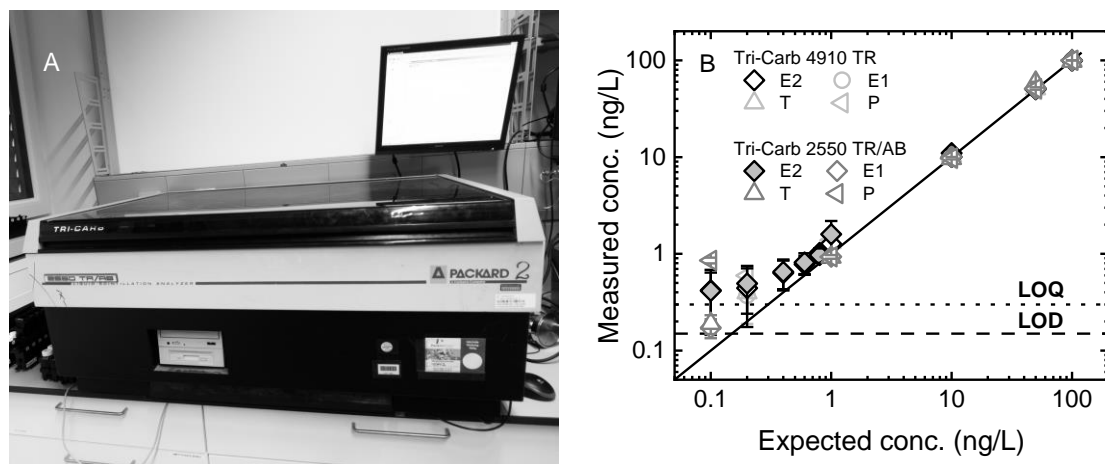


Figure 3.5: A – Photograph of the Tri-Carb 2250 TR/AB instrument (the Tri-Carb 4910 TR looks similar and is not shown). B – Calibration curves with steroid hormone standards (E1, E2, T and P) are given in log scale. The positions of the LOD and LOQ for E2 calibration are highlighted (determined *via* Method 3 in Section 3.6.2).

3.4.2 Total organic matter (TOC) analysis

The Sievers M9 TOC analyser was used to measure the OM concentration in the stock solutions between 0.2 and 10 mgC/L (Figure 3.6). The calibration with potassium hydrogen phthalate (KHP), analytical errors and detection limits (around 0.2 mgC/L) are described in Section 3.6.2. The TOC analyser was not used to analyse the feed and permeate samples that contain steroid hormones, because ethanol (the solvent for the supplied hormones) occurs at 14 mgC/L in the feed solution, and hence the OM could not be quantified.

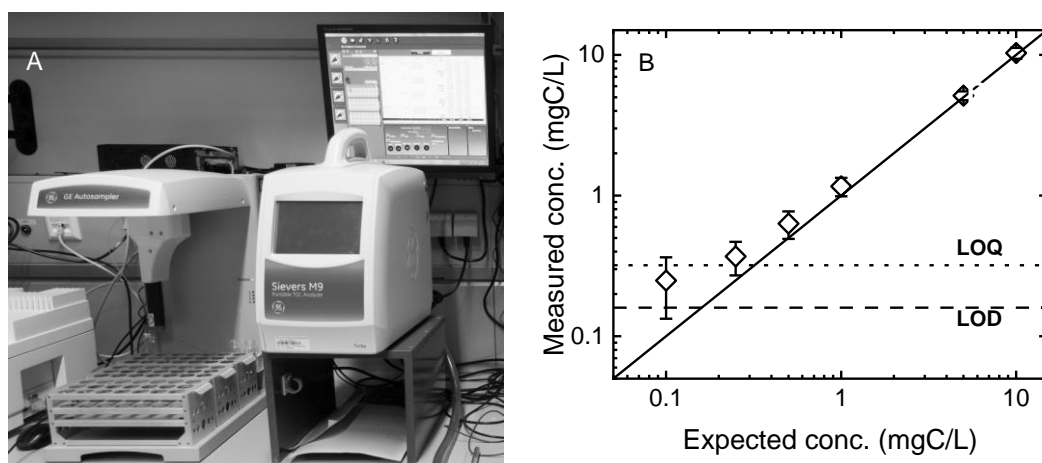


Figure 3.6: A – Photograph of the TOC analyser. B – Calibration curve with KHP standards is given in log scale. The positions of the LOD and LOQ are highlighted (determined *via* Method 3 in Section 3.6.2).

3.4.3 Liquid chromatography – organic carbon detection (LC-OCD)

LC-OCD separates OM into quantifiable fractions based on size³²⁹. The separation was achieved with a size-exclusion chromatographic column (HW-50S Toyopearl 30 μm , Tosoh Bioscience). An example chromatogram is given in Figure 3.7 A. The fractions are defined as biopolymers (>20 kDa), humic substances (around 1 kDa), building blocks (300–500 Da), and low molecular weight (LMW) acids and neutrals (<350 Da)⁴⁴⁸.

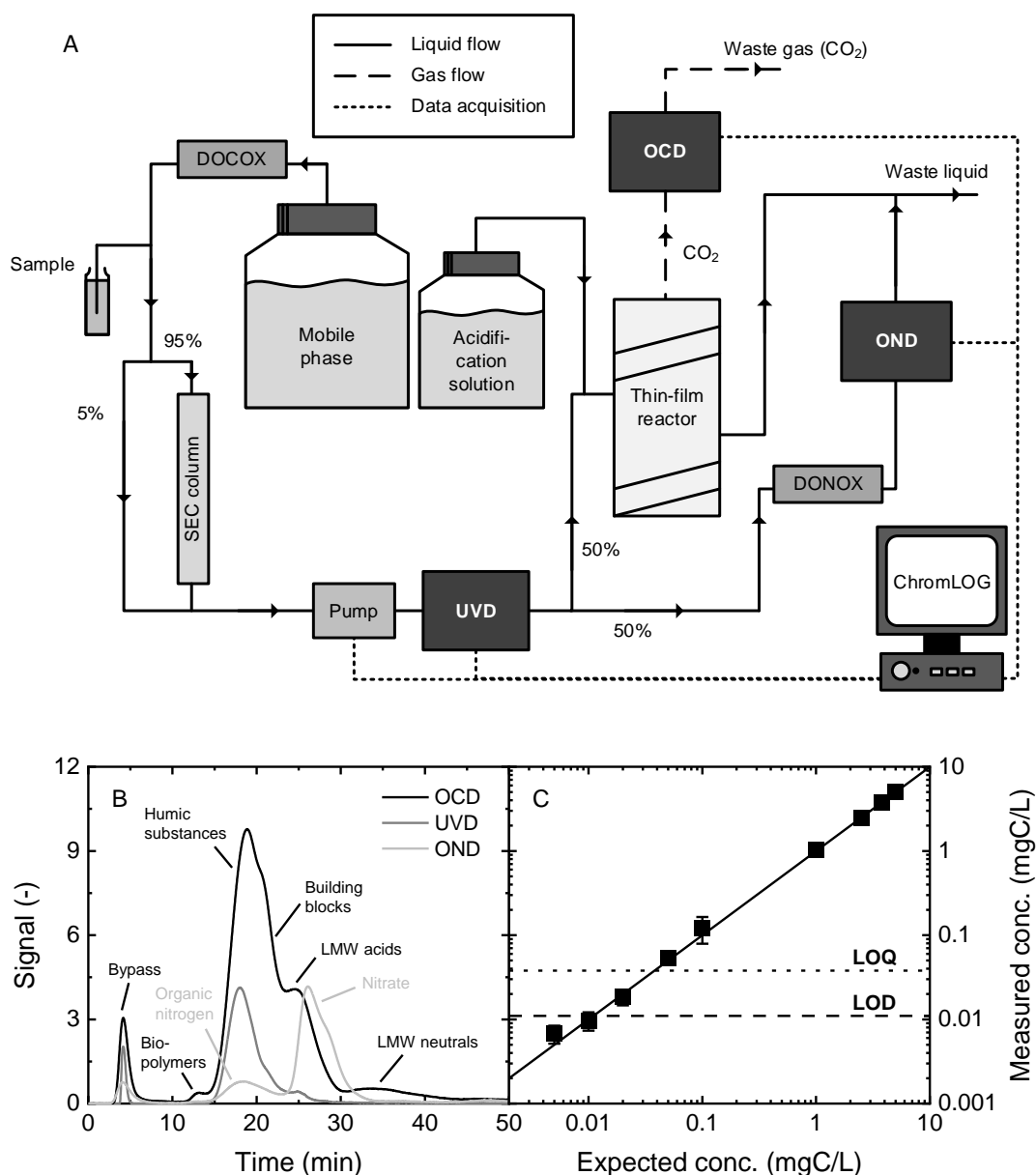


Figure 3.7: A – Schematic of VaCNT membrane fabrication. B – An example LC-OCD chromatogram of a soil extract with peak annotations (Australian natural OM). C – Calibration curve with KHP standards is given log scale. The positions of the LOD and LOQ are highlighted (determined *via* Method 3 in Section 3.6.2).

The fractions are detected with ultraviolet absorbance (UVD), organic carbon (OCD) and organic nitrogen detectors (OND). The UVD is a Knauer Azura 2.1S (Knauer, Germany) operating for the wavelength 254 nm (UV₂₅₄). The OCD consists of a Gräntzel thin-film reactor (DOC-Labor, Germany) that acidifies the measured sample and strips organic carbon as CO₂, and a non-dispersive infrared detector (AO2000 with Uras26, ABB, Switzerland) that determines the CO₂ content. The acidification solution (2 g/L K₂O₈S₂ and 60.8 mM H₃PO₄) is directly delivered to the thin-film reactor by gravity at a flow rate of ~ 0.3 mL/min. For OND, 50% of the sample was diverted as described by Huber *et al.*³²⁹, to enter a DONOX reactor (annular UV-lamp, DOC-Labor) that converts both organic and inorganic nitrogen into nitrate. The quantity of nitrate is determined from UV₂₂₀ absorbance measured with another Knauer Azura 2.1S (with a wavelength of 220 nm).

An injection system (MLE GmbH Dresden, Germany) controls the injection of samples. Each sample analysis requires an injection volume of 1 mL. The mobile phase (2 g/L KH₂PO₄ and 1.2 g/L Na₂HPO₄) and sample are delivered through the system with a total flow rate of 2 mL/min set by an HPLC pump (Knauer Azura P 4.1S, Knauer, Germany). A small portion (5%) bypasses the SEC column and gives the TOC from the peak at 5 min in the chromatogram (see Figure 3.7 B). The other 95% of the injected solution passes through the SEC column and is separated into fractions.

Calibration with 0.1–10 mgC/L KHP in mobile phase was done to determine the regression between the detected CO₂ concentration / UV absorbance and the KHP concentration. This calibration allows the determination of organic carbon concentration and the specific UV absorbance (SUVA) in each fraction of the OM samples, as described by Huber *et al.*³²⁹. Calibration with 0.1–5.0 mg/L (or 0.014–0.70 mgN/L) potassium nitrate allows the quantification of organic and inorganic nitrogen (namely nitrate and ammonium) in the OM samples, also described by Huber *et al.*³²⁹, but organic nitrogen analysis is not within the scope of the dissertation. The analytical errors and detection limits are illustrated in Figure 3.7 C and described in Section 3.6.2.

3.4.4 Other analytical techniques

The absorbance of OM in the wavelength range of 220–700 nm was determined with an UV–Vis spectroscopy instrument (Lambda 25, Perkin Elmer, USA). The absorbance in the UV range depends greatly on the aromaticity of the OM types. The absorbance of HA, TA, TEA and TANN is detectable at a UV wavelength of 254 nm. In addition, UV–Vis spectroscopy may not accurately determine the permeate OM concentration if the aromatic fractions attached to the CNPs or membrane more favourably than non-aromatic fractions. This would give an overestimation of OM removal.

UV–Vis spectroscopy is particularly useful to determine tannic acid (TA), which has a fixed molecular structure (so no fraction segregation based on aromaticity), and strong absorbance at 213 nm. In addition, TA is not detectable with LC-OCD because it is strongly adsorbed to the SEC column and capillaries, resulting in 90% analyte loss. Hence, UV–Vis spectroscopy is the only practical analytical technique for TA. Calibration of TA was done with fresh standard TA solutions in the concentration range of 0.1–5 mgC/L (Figure 3.8).

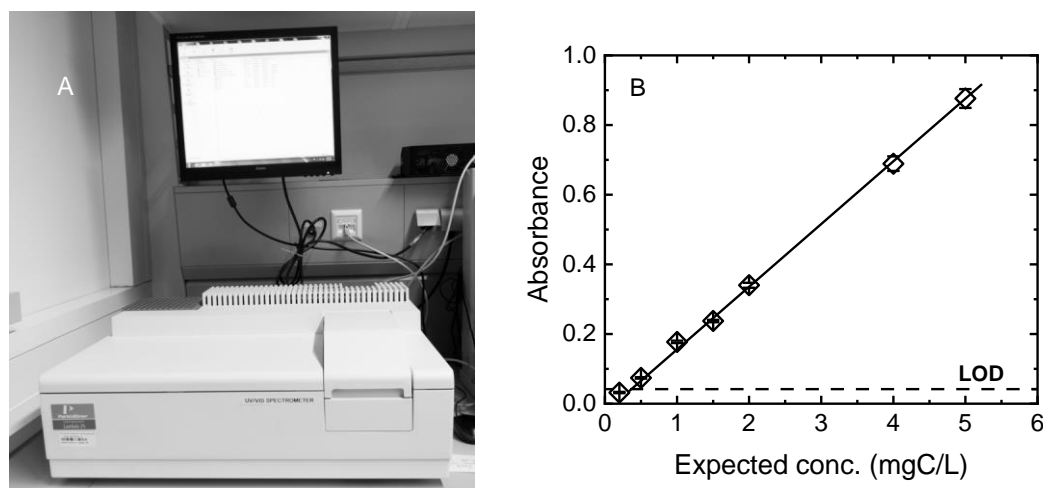


Figure 3.8: A – Photograph of the UV-Vis spectroscopy instrument. B – Calibration curve with TA standards and LOD (determined *via* Method 1 in Section 3.6.2).

The pH of the stock and feed solutions was determined with a pH electrode (InoLab pH720 or SenTix 81, WTW, Germany). The electrical conductivity of the feed solutions (of around 1000–1400 $\mu\text{S}/\text{cm}$) was determined with a TeraCon 325 electrode (WTW). Both the pH meter and conductivity electrodes are connected with a pH/Cond 3320 device (WTW).

3.5 Calculations

This sub-chapter describes the calculations to determine the adsorption and filtration properties of adsorbent materials and membranes. The kinetic and isotherm models used in static adsorption are not described here but instead in Section 4.2.3.

3.5.1 Mass balance in static adsorption and filtration

The mass balance is critically important in determining the amounts of steroid hormones or OM adsorbed to, or deposited on, the membrane and/or the nanoparticles. Specific formulae to determine the adsorbed mass / mass loss (m_{ads}), in ng or mgC/L, for each type of experiments (static adsorption, dead-end filtration and crossflow filtration) are given as follows.

Static adsorption

The adsorbed mass $m_{ads(t)}$ at time t can be determined from the liquid-phase concentrations with the simple Eq. (3.1).

$$m_{ads(t)} = (c_0 - c_t) V_0 \quad (3.1)$$

Where c_0 and c_t are the concentrations in the solution at time 0 and t , respectively. However, the above equation assumes that V_0 is constant, whereas in reality, V_0 decreases by 2.5 mL after each sample extraction. The volume at the end of the experiment is hence 12% lower than the

initial volume which is a significant source of adsorbed mass error. Eq. (3.2) is revised based on the number of extractions as follows.

$$m_{ads,n} = V_0 c_0 - V_e \sum_{i=1}^{n-1} c_i - [V_0 - (n - 1) V_e] c_n \quad (3.2)$$

where $m_{ads,n}$ is the adsorbed mass after n extractions, $V_0 = 250$ mL and $V_e = 2.5$ mL are the initial and extracted volumes, respectively. All the mass losses before the n th extraction are summed in the term $V_e \sum_{i=1}^{n-1} c_i$, and the volume of solution before the n th extraction is $V_0 - (n - 1) V_e$. With Eq. (3.2), the adsorbed mass error is reduced because the error in liquid volume is low.

Dead-end filtration

In dead-end filtration, $m_{ads(t)}$ is calculated with Eq. (3.3).

$$m_{ads(t)} = (V_f - V_{r(t)}) c_f - \sum V_{p(t)} c_{p(t)} \quad (3.3)$$

where V_f and $V_{r(t)}$ are the feed and residual volume in the feed tank at time t ; whereas c_f and $c_{p(t)}$ are the feed and permeate concentrations.

Crossflow filtration

In crossflow filtration, $m_{ads(t)}$ is equal to the difference in the mass of hormone in the feed $V_f \cdot c_f$ and the sum of the masses in the retentate $V_r \cdot c_r$ and permeates $\sum V_{p(t)} \cdot c_{p(t)}$, as shown in Eq. (3.4).

$$m_{ads(t)} = V_f c_f - V_{r(t)} c_{r(t)} - \sum V_{p(t)} c_{p(t)} \quad (3.4)$$

UF membranes do not retain steroid hormones, hence c_f is equal to $c_{r(t)}$. Eq. (3.4) can be simplified as Eq. (3.5) for steroid hormone mass balance.

$$m_{ads(t)} = [V_f - V_{r(t)}] c_f - \sum V_{p(t)} c_{p(t)} \quad (3.5)$$

Determination of specific adsorbed masses / mass losses

The specific adsorbed mass, or specific mass loss, is equal to the adsorbed mass or mass loss divided by either the membrane area, or the mass of adsorbent, as given in Eq. (3.6) and Eq. (3.7).

$$S_{ads,A}(t) = \frac{m_{ads(t)}}{A_m} \quad (3.6)$$

$$S_{ads,S}(t) = \frac{m_{ads(t)}}{m_{adsorbent}} \quad (3.7)$$

where A_m (cm²) and $m_{adsorbent}$ (g) are the effective membrane area and adsorbent mass, respectively.

3.5.2 Flux, permeability, and removal in membrane filtration

Water flux ($\text{L}/\text{m}^2\cdot\text{h}$) is determined from the permeate mass *via* Eq. (3.8).

$$J = \frac{\Delta m_p}{\Delta t \rho_{\text{wat}} A_m} \quad (3.8)$$

where Δt is the elapsed time, A_m is the membrane area, and ρ_{wat} is the density of water (equal to $1000 \pm 10 \text{ g}/\text{L}$ at $22\text{--}26 \text{ }^\circ\text{C}$ ⁴⁴⁹). The water permeability ($\text{L}/\text{m}^2\cdot\text{h}\cdot\text{bar}$) is determined from the water flux and transmembrane pressure ΔP (bar) as shown in Eq. (3.9).

$$L_p = \frac{J}{\Delta P} \quad (3.9)$$

Removal of steroid hormone or OM (%) is determined *via* Eq. (3.10).

$$R = \left(1 - \frac{c_p}{c_f}\right) 100\% \quad (3.10)$$

where c_p and c_f are the concentrations in the permeate and feed, respectively.

3.5.3 Estimation of membrane porosity, and residence time

The UF membrane porosity is calculated according to the Hagen–Poiseuille Law that determines the water velocity of an incompressible and Newtonian fluid (such as water) through a cylindrical pipe. Because the pure water flux is equal to porosity multiplied by the water velocity, the porosity can be expressed in Eq. (3.11) ⁴⁵⁰.

$$\varepsilon = \frac{32 \delta_m \mu J_0}{d_p^2 \Delta P} \quad (3.11)$$

where δ_m (m) is the separation (dense) layer thickness, μ (Pa.s) is the dynamic viscosity of water, J_0 ($\text{L}/\text{m}^2\cdot\text{h}$) is the pure water flux, d_p (nm) is the hydrodynamic diameter of the hormone, and ΔP (bar or Pa) is the pressure drop.

However, this equation is not valid to describe asymmetric membranes because of the following reasons:

- The pore sizes are not uniform, according to scanning electron microscopy (SEM), nuclear magnetic resonance cryoporometry, evapo-porometry, and liquid–liquid displacement porometry ^{428, 451–453}. The pore sizes determined from different techniques deviate from each other and from the nominal value from the manufacturer.
- The assumption of laminar flow may not be valid because the tortuosity in the membrane is not considered.
- Other effects, such as flow channelling ⁴⁵⁴ and selective permeation of solutes in larger membrane pores ⁴⁵⁵, are not considered.

In conclusion, the application of Hagen–Poiseuille Law can only give an apparent porosity that would describe membranes with cylindrical pores of the same MWCO. The residence time in the membrane t_R (s) is then estimated with Eq. (3.12).

$$t_R = \varepsilon \frac{L}{J} = \varepsilon \frac{L}{L_p \Delta P} \quad (3.12)$$

where L (m) is the membrane thickness.

Unlike asymmetric UF membranes, VaCNT membranes contain cylindrical and highly homogenous pores. As such, the porosity of these membranes is then determined from the number of pores per unit area $\frac{n_{\text{CNT}}}{A_m}$ (which is the number density of the nanotubes), and pore diameter d_p as given in Eq. (3.13).

$$\varepsilon_{\text{VaCNT}} = \frac{\pi d_p^2 n_{\text{CNT}}}{4 A_m} \quad (3.13)$$

The residence time in the VaCNT membrane t_R (s) is also calculated *via* Eq. (3.12).

3.5.4 Determination of flow enhancement in VaCNT membrane

The slippage that corresponds to the low friction slippage when the liquid–wall friction at the CNT wall is quantified *via* the slip length. The slip length is determined from the flux J_{exp} ($\text{L}/\text{m}^2 \cdot \text{h}$), applied pressure ΔP (bar), and VaCNT membrane thickness L (m) *via* Eq. (3.14)¹⁹⁴.

$$b = \frac{J_{\text{exp}} \mu L}{16 \pi \Delta P \varepsilon d_p} - \frac{d_p}{8} \quad (3.14)$$

The relationship between VaCNT membrane permeability and slip length is rewritten as shown in Eq. (3.15).

$$L_{p,\text{exp}} = \frac{J_{\text{exp}}}{\Delta P} = \frac{\varepsilon}{8 \mu L} \left[\left(\frac{d_p}{2} \right)^2 + 4 \left(\frac{d_p}{2} \right) b \right] \quad (3.15)$$

The flow enhancement in VaCNT can be determined by comparing the theoretical permeability determined *via* the Hagen–Poiseuille equation, and the experimentally determined pure water permeability (see Eq. (3.9)). The theoretical permeability $L_{p,\text{HP}}$ is determined *via* Eq. (3.16).

$$L_{p,\text{HP}} = \frac{\varepsilon}{8 \mu \alpha L} \left(\frac{d_p}{2} \right)^2 \quad (3.16)$$

where α is the tortuosity factor. In UF/NF membranes, α can take the value between 1.5 and 2.5⁴¹⁸. The enhancement factor (EF) is then determined *via* Eq. (3.17).

$$\text{EF} = \frac{L_{p,\text{exp}}}{L_{p,\text{HP}}} = 1 + \frac{8b}{d_p} \quad (3.17)$$

For a VaCNT membrane with pore diameter of ~ 2 nm, slip length b can range between 140 and 1400 nm, and EF can range between 550 and 8500¹⁹⁴.

3.6 Error analysis

3.6.1 Determination of the error sources

A thorough list of error / uncertainty sources encountered in the adsorption and filtration experiments are summarised in Table 3.5. The errors are categorised based on the steps: sample preparation, experiment operation, analytical operation, and calculation & reporting. Several parts of the list (analytical error, error propagation methods, and interference to hormone analysis) will be discussed in the next sections.

Table 3.5: Error sources, and a list of methods to notice and tackle the errors.

Step	Error source	How to notice the issue	What to do
Sample preparation	Sensor / instrument sensitivity (balance, volumetric flask), materials (membranes)	Check instrument specifications, verify periodically	Revise sensor specifications and experimental protocol
	Human error (calculations, pipetting, weighing)	Document thoroughly, verify with other experiments, monitor experimental parameters	<i>Avoid making errors</i> , repeat the experiment 2–3 times to confirm anomalies
Experiment operation	Sensor / instrument sensitivity (temperature, pressure sensors, and balance)	Monitor of experimental parameters (pay attention to the range of fluctuations)	Revise sensor items and experimental protocol
	Uncontrolled parameters (room temperature and humidity etc.)	Monitor experimental parameters (pay attention to any non-linear trends over time)	Revise experimental protocol, implement control, <i>e.g.</i> use a water chiller, integrate these errors in error calculations, make assumptions for the surrounding environments
	Interference from apparatus (<i>e.g.</i> adsorption to filters)	Document thoroughly, verify with other experiments	Investigate systematically, revise experimental protocol
Analytical operation	Analytical error	Check instrument specifications, document thoroughly, verify with other analyses	Revise analytical protocol
	Human error – calculations, pipetting / weighing	Document thoroughly, verify with other analyses	<i>Avoid making errors</i> , repeat the analysis multiple times to confirm anomalies
	Interference from water matrix	Document thoroughly, verify with other analyses	Investigate systematically, revise analytical protocol, integrate these errors in error calculations
Calculations and reporting	Human error – calculations	Verify with other data, double-check calculations	<i>Avoid making errors</i> , thoroughly check and validate results

Error propagation method	Verify with other data and with literature, double-check calculation	Apply the correct error propagation methods (explained in this Sub-chapter)
--------------------------	--	---

3.6.2 Errors from sample preparation

The errors from sample preparation comes from the tolerances (*i.e.* the total allowable error marked by the manufacturers of the measuring tools) of the analytical balance (± 0.1 mg), volumetric flasks (around 0.1–0.2%), and pipettes (around 1% for the 0.2–5 mL pipettes). These errors can be negligible when compared with other error sources, such as experimental and analytical operations described below. For the tolerances to be valid, the measurement tools need to be checked and calibrated correctly before the sample preparation.

3.6.3 Errors from experimental operation

The errors coming from experimental operation include the range of fluctuation in an experiment, and the variation between experiments, and determined from the maximum and minimum recorded values. The surrounding environments (varied room temperature, humidity, *etc.*) add up to the variation of monitored parameters and can elevate the experimental errors. The varied operational parameters include applied pressure (around $\pm 4\%$), feed solution temperature (± 2 °C without a water chiller and ± 0.2 °C with the water chiller) and permeate flow rate (around $\pm 4\%$, calculated from the slope of permeate volume increase with time). Interferences from membrane filters and OM with trace hormone analysis are discussed in Sections 4.2.5 and 6.2.5, respectively.

3.6.4 Analytical errors

In this section, the errors and detection limits of LSC and LC-OCD analytical instrument are given, while the error determination method for LC-OCD is discussed in detail. The analytical error is determined as the standard deviation from multiple calibrations with calibration standards. These standards include steroid hormone standards in LSC analysis, and KHP standards in TOC and LC-OCD analyses. A linear regression is observed in the calibration range of 0.1–100 ng/L (LSC), 0.1–5 mgC/L with LC-OCD, and 0.25–10 mgC/L with TOC analyser. Analytical errors (as standard deviations) are illustrated in Figure 3.9. The LODs are shown in Sub-chapter 3.4.

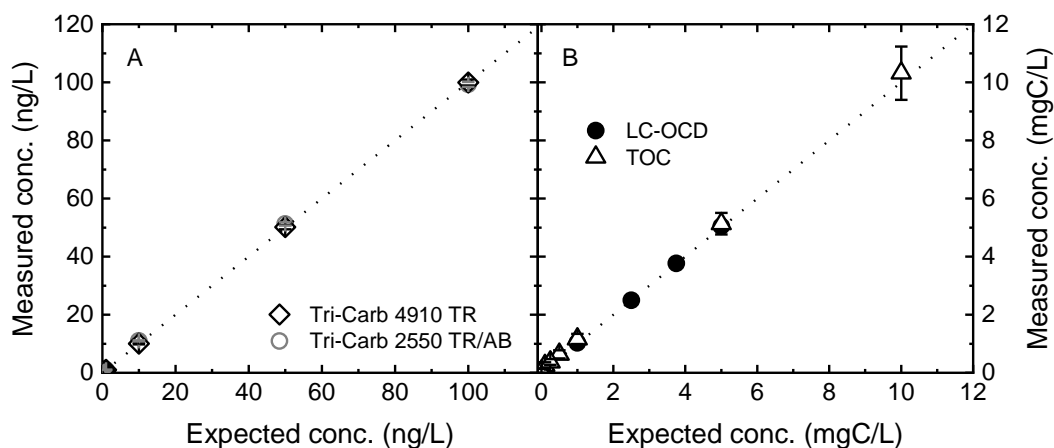


Figure 3.9: Calibration of steroid hormones (A) and organic matter (B). The dotted lines indicate the regressions of the calibration.

The three methods to determine the LOD are: i) eye inspection of the break in calibration slope, ii) signal-to-noise ratio evaluation, and iii) calculation from the standard deviation (valid only with 30–40 repeats⁴⁵⁶) of blank signals and calibration slope⁴⁵⁷.

In Method 1 (eye inspection), LOD estimation will require multiple measurements at the low concentration range. The LOD is estimated when a break in linearity of the regression is observed. Figure 3.5 B, Figure 3.6 B, Figure 3.7 C and Figure 3.8 B clearly shows these breaks in the respective calibrations with LSC, TOC analyser, LC-OCD, and UV–Vis spectroscopy.

Method 2 can be applied when the raw data of the signal and the noise are accessible, such as in the case of LC-OCD (Figure 3.10). The intensity of the noise is determined when no analyte is present. The LOD and limit of quantification (LOQ) are determined as the concentrations at which the peak intensities are 3 and 10 times higher than the intensity of the noise, respectively. Multiple calibrations can increase the accuracy of LOD and LOQ estimation.

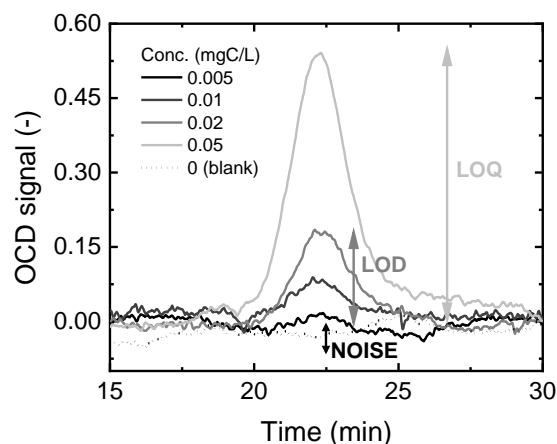


Figure 3.10: Organic carbon signal as function of elution time between 15 and 30 min at concentrations of 0.005–0.05 mgC/L. Results from only one repeat per concentration is illustrated.

Signal corresponding to KHP at 22 min is distinguishable from the noise (i.e. signal is >3 times higher than the noise) from concentration 0.01 mgC/L. At 0.01 mgC/L, the signal is not distinguishable from the noise, so LOD is estimated to be 0.02 mgC/L. LOQ is defined as where the signal is 10 times higher than the noise and it is about 0.05 mgC/L.

Method 3 gives a mathematical representation for Method 2, with which the LOD and LOQ are more precisely determined than with Method 1. In addition, Method 3 does not require the raw signal and noise data as in Method 2 (*e.g.* for the TOC analyser, the raw peak intensities are not reported). The LOD and LOQ are determined *via* Eqs. (3.18) and (3.19).

$$\text{LOD} = c_{\text{blank}} + 3 \sigma_{\text{blank}} \quad (3.18)$$

$$\text{LOQ} = c_{\text{blank}} + 10 \sigma_{\text{blank}} \quad (3.19)$$

where c_{blank} and σ_{blank} (both have the units of ng/L in LSC or mgC/L in TOC analyser and LC-OCD) are the measured concentration of the blank (without analytes) and its standard deviation. With Method 3, at least 40 measurements of the blank samples are needed to determine the mean concentration c_{blank} and standard deviation σ_{blank} . Table 3.6 compares the LOD and LOQ determined with the three methods.

It is observed that the precise LOD determined with Method 3 is not significantly different from the estimations with Method 1 and 2. The LOQ of LSC can be as low as 0.2–0.5 ng/L, which allows a determination of steroid hormone removal of 99.5–99.8% from a 100 ng/L feed solution. In contrast, the TOC analyser allows a determination of TOC removal of 97–99% from the 10 mgC/L feed solution. The removal threshold is not discussed for LC-OCD because the organic matter is separated in various fractions, although the detection limits of this method is one order of magnitude lower than in the TOC analyser.

Table 3.6: Detection limits (LOD) and limits of quantifications (LOQ) of analytical instrument determined with the three methods. The detection limits for LSC are ~2 times higher than previously reported with a smaller set of data ¹¹². N.A.: not available, because the raw data of signal and noise are not accessible.

Analytical instrument	Method 1 *	Method 2		Method 3	
	(eye inspection)	(signal to noise ratio)	(signal to noise ratio)	(Eq. (3.18) and (3.19))	(Eq. (3.18) and (3.19))
	LOD	LOD	LOQ	LOD	LOQ
TOC analysis (units: mgC/L)					
TOC analyser	0.2	N.A.	N.A.	0.13	0.31
LC-OCD	0.05	0.01	0.05	0.01	0.04
Steroid hormone analysis (units: ng/L)					
Tri-Carb 2550 TR/AB	0.3	N.A.	N.A.	0.32	0.58
Tri-Carb 4910 TR	0.2	N.A.	N.A.	0.21	0.38

* With Method 1, only the LOD is estimated.

3.6.5 Error calculations – Determination of measured and calculated parameters

Filtration (or static adsorption / diffusion) is a complex process, and the uncertainty in determined concentration depends not only on the analytical instrument sensitivity, but also on sample preparation and membrane process control. In a general crossflow filtration experiment performed in this project, the relationships between all parameters (including those measured and calculated) are as described in Figure 3.11.

The measured parameters include temperature – from which the water density can be correlated, solution pH, permeate mass, and applied pressure; the corresponding errors do not only come from sensor or balance sensitivity but also on the variability between different experiments and membrane coupons. The calculated parameters (determined *via* error propagation) include permeate flux, permeability, residence time, permeate / retentate / feed concentrations, removal, and adsorbed mass.

Some relationships between the parameters are straightforward, such as those between permeate mass and permeate flux / permeability, or between concentrations and removal / adsorbed mass. On the other hand, some relationships are complex as a result of membrane characteristics and adsorbent–adsorbate interactions, which require careful assumptions.

Permeate concentration, which is used to characterise steroid hormone adsorption by composite membranes, depends on several factors: surface area for adsorption, residence time in membrane, and adsorption affinity of the membrane material. Both the surface area and residence time depends on the membrane thickness, pore size and porosity, while the residence time also depends on the flow rate. With the assumptions of cylindrical pores with uniform pore diameter in the dense layer (*i.e.* $\Delta d_p = 0$), and uniform dense layer thickness ($\Delta \delta_m = 0$), the relative errors in membrane porosity (see Eq. (3.11)), residence time (see Eq. (3.12)) and surface area for adsorption will be equal to the relative error in permeate flux / membrane permeability.

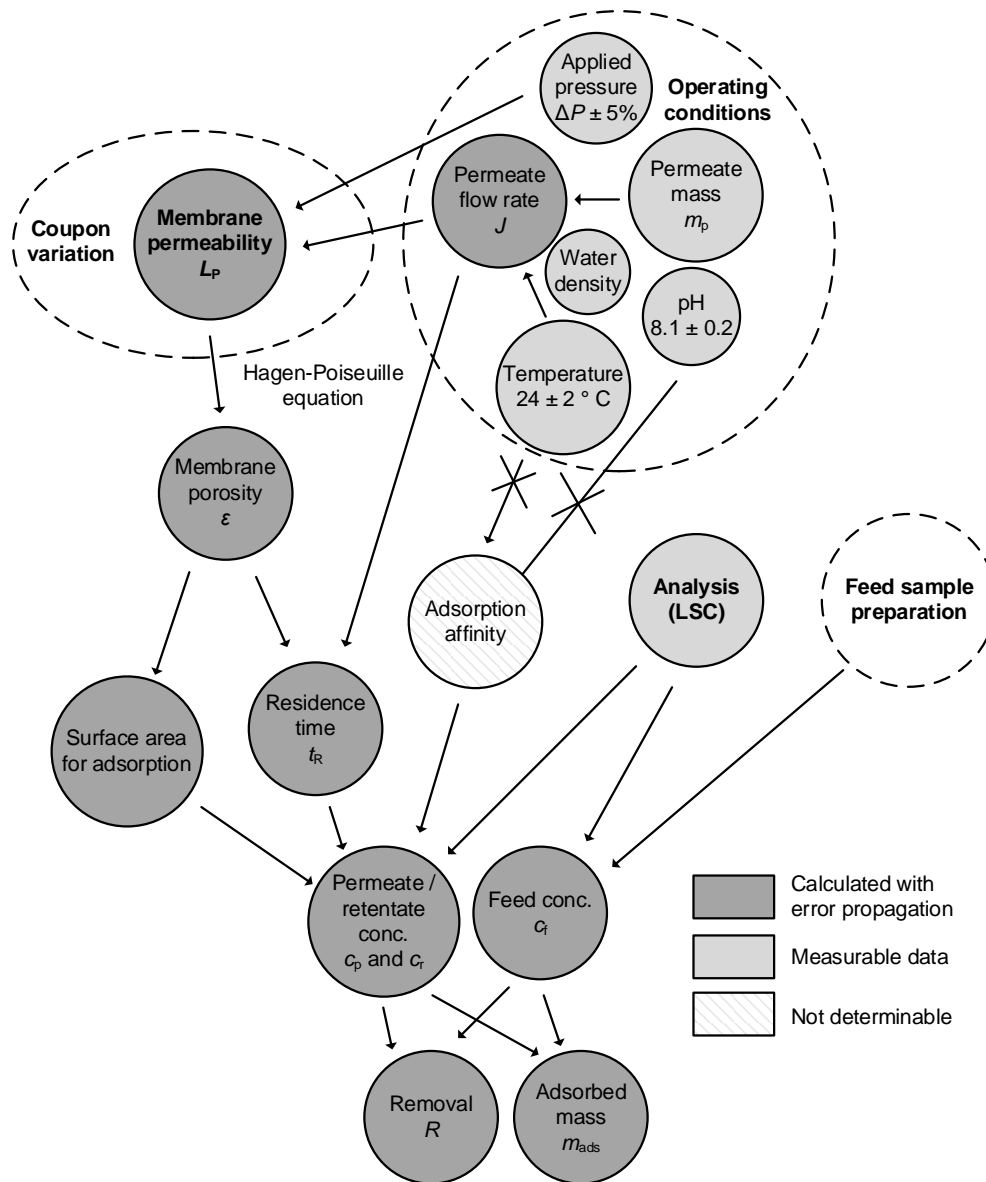


Figure 3.11: Illustration of the relationships between measured and calculated parameters in a typical filtration experiment with CNP-UF membranes.

Adsorption affinity is hard to quantify, although the solution pH affects the charge interactions between hormones and adsorbents (CNPs and membrane), while temperature impacts both the kinetics and thermodynamics of the adsorption, as well as the diffusion of steroid hormones. In this regard, the variation in pH and temperature should be minimised to assume no variation in adsorption affinity. Because all steroid hormones are uncharged at $\text{pH} < 10$, a small variation in pH between experiments of 8.1 ± 0.2 is assumed to not affect adsorption. It is also assumed a variation in temperature between experiments of $\pm 2^\circ \text{C}$ does not impact adsorption. In Chapter 7 experiments, the temperature variation was decreased to $\pm 0.2^\circ \text{C}$ with a water chiller. The adsorption affinity of the composite membrane is hence assumed to be unaffected by the varying experimental conditions and does not affect the permeate concentration.

In summary, the permeate and retentate concentrations are affected by the analytical method, solution preparation, and filtration process, where the error contribution from the filtration process is directly linked with the error in membrane permeability. The assumption of cylindrical membrane pores and overlooking of membrane coupon variability may result in error underestimation. Sufficient number of experiments with the same conditions (30–40 repeats) can give more accurate errors, although performing many repeats is not practical in the laboratory.

3.6.6 Error propagation

The errors of measurable data are determined as follows. When the measurements are statistically significant (*i.e.* when there are sufficient repeats N of 30–40⁴⁵⁶, such as the concentration of standards in calibration), the absolute error Δx is equal to the standard deviation of σ_x ⁴⁵⁸ as shown in Eq. (3.20).

$$\Delta x = \sigma_x = \sqrt{\frac{\sum(x_i - \bar{x})^2}{N}} \quad (3.20)$$

where \bar{x} is the average value. The value + error is reported as $\bar{x} \pm \Delta x$. When the measurements are not statistically significant (such as pressure and temperature variation in multiple filtration experiments at the same set conditions), the absolute error must be determined as half the range between maximum (x_{max}) and minimum (x_{min}) values, as shown in Eq. (3.21).

$$\Delta x = \frac{x_{max} - x_{min}}{2} \quad (3.21)$$

The value + error is reported as $\tilde{x} \pm \Delta x$, where \tilde{x} is the median value.

Error propagation is needed to determine the error of an *unmeasurable data* from the errors of *measurable data* (for example, determine the error in removal from the analytical errors in concentrations). The error propagation methods are thoroughly documented in literature⁴⁵⁸. The most important error propagation equations are given in Appendix B.

3.7 Membrane and nanoparticle characterisation

3.7.1 Surface analysis with Argon adsorption / desorption

Argon adsorption and desorption tests were carried out by Peter G. Weidler (IFG, KIT) with membrane fragments and CNPs in solid phase using the Autosorb 1-MP instrument (Quantachrome, USA). First, the membrane fragments and powdered particles were degassed in liquid nitrogen at 343 K in vacuum for 24 h °C, and then dried in vacuum at elevated temperatures (70 °C for 24 h for the CNPs, and 40 °C for 72 h for the membrane fragments). Then, the degassed samples were transferred into the sample holders, in which Argon adsorption and desorption took place. The adsorption/desorption data were obtained, and the Brunauer–Emmett–Teller (BET) and Quenched Solid Density Functional Theory (QSDFT) models were then applied to these data. Surface analysis according to both models was performed with ASiQwin v5.2 software, and the

surface area (BET and QSDFT), and the distribution of surface area and pore volume for different pore sizes (QSDFT) were then determined.

The BET model is a simple model that considers only the physical adsorption on any kind of surface ⁴⁵⁹. The QSDFT model considers also the pore geometries, capillary condensation in pores, and pore structure complexity and heterogeneity ⁴⁶⁰. It was reported that DFT models give more reliable surface area results for microporous carbons than the BET model ⁴⁶¹.

With the QSDFT model, different pore geometries can be chosen for the fitting of the Argon adsorption data, which are cylindrical pores, slit pores, and a combination of cylindrical and spherical pores. The criteria for selecting which QSDFT model is suitable are based on the fitting error (%), which represents the standard deviation of the fit. The lower the fitting error, the better model fitting.

3.7.2 Surface visualization with Helium Ion Microscopy (HIM) and Scanning Electron Microscopy (SEM)

To visualise the membrane morphology, field-emission scanning electron microscopy (FESEM) was carried out by Claus J. Burkhardt (a collaborator from NMI, Germany), using a ZEISS GeminiSEM (Carl Zeiss Research Microscopy Solutions, Germany) equipped with an Everhart–Thornley Secondary Electron Detector. Prior to characterisation, the dry membranes were sputtered with a 5 nm layer of platinum, using a Sputter Coater 208HR (Cressington, UK). FESEM was operated with an acceleration voltage of 3 keV.

Helium Ion Microscopy (HIM) for CNPs and membranes was carried out by Ruth Schwaiger (IAM, KIT) and Claus J. Burkhardt (NMI) at different places (Karlsruhe and Reutlingen) using the same type of instrument (Zeiss Orion NanoFab, Carl Zeiss AG, Germany, with an Everhart–Thornley Secondary Electron Detector). The operation voltage and beam current were in the range of 25–30 kV and 0.02–10 pA, respectively. For the CNPs, small amounts of powder samples were deposited on transmission electron microscopy grids and characterised without any sputtering. Similarly, the dry membrane pieces were directly characterised with no sputtering. To observe the support layer of the membranes, the membrane surface was cleaved using a focused ion beam (this operation was done by Claus Burkhardt). Without sputtering, nanostructures, such as the individual strands or small bundles of SWCNTs and the stacks of graphene layers, can be resolved with HIM.

3.7.3 Elemental composition analysis with X-ray Photoelectron Spectroscopy (XPS)

X-ray Photoelectron Spectroscopy (XPS) was carried out by Michael Bruns and Christian Njel (IAM, KIT) using a K-Alpha+ Spectrometer (Thermo-Fisher Scientific, UK). The CNP samples in solid form were irradiated with a mono-chromated Aluminium K-Alpha X-ray beam, and the electrons photo-emitted from the top surface (penetration depth of only 3 nm) were captured by the instrument detector, giving a spectrum ⁴⁶². The spectra were then fitted with a probability distribution (Voigt) profile; and the elemental composition were determined through the analyser

transmission function, Scofield sensitivity factors and TPP-2M standard for effective photoelectron attenuation lengths^{463, 464}. All spectra were referenced to the C1s peaks of graphite (binding energy 284.4 eV) and of hydrocarbon (binding energy 285.0 eV).

3.7.4 Particle size and charge analysis with Dynamic and Electrophoretic Light Scattering (DLS / ELS)

Both Dynamic Light Scattering and Electrophoretic Light Scattering (DLS / ELS) were carried out with a Litesizer 500 (Anton Paar, USA) in IMT laboratory, KIT, to characterise the CNP size and surface charge, respectively.

For DLS, the CNP was suspended in Milli-Q water at an initial concentration of 0.2 g/L. To evaluate the dependence of solution chemistry on the aggregate size, three different preparation methods were used.

- Method 1 (which follows CNP preparation for static adsorption experiments): CNPs in 50 mL of Milli-Q water were sonicated for 1 hour, then background electrolytes were added within 30 min, to make up a 100 mL of 0.1 g/L CNP suspension in 1 mM NaHCO₃ and 10 mM NaCl.
- Method 2: The CNP suspension in water and background electrolytes was prepared as in Method 1, but then this suspension was sonicated again for 1 hour to allow interactions between the electrolytes and CNPs.
- Method 3: No background electrolytes were added after the one-hour sonication.

In all three methods, there was always a 30 min period when each suspension was allowed to equilibrate (and settle), before they were shaken at 260 rpm for 7 hours on a bench shaker (code 980181EU, Talboys, UK). Small suspension aliquots of around 2.5 mL were taken at intervals for particle size determination. The focal point and scattering angle (90° or 175°), and number of measurements per sample were automatically determined. The characterisation temperature was 20 °C. The DLS returns a number-weighted distribution of particle sizes; a Gaussian model was applied to this distribution to determine the mean and full-width-at-half-maximum (FWHM) values. The FWHM values were reported as error bars.

Electrophoretic Light Scattering (ELS) returns the values of CNP zeta potential, of which sign and magnitude indicate whether the particles surface was positively-charged, neutral or negatively-charged at different pH. Solutions of 1 M HCl or 1M NaOH were used to adjust the pH in the range 2–12. Following pH adjustment, the CNP suspension was transferred to a Ω-shaped capillary tube (Anton Paar, USA) for characterisation. The number of measurements per sample were automatically determined; the characterisation temperature was 20 °C.

4 Influence of Adsorbent Surface on Hormone Adsorption

This chapter is adapted from a publication in Journal of Hazardous Materials (2020) entitled “Interactions between carbon-based nanoparticles and steroid hormone micropollutants in water”, by Minh N. Nguyen, Peter G. Weidler, Ruth Schwaiger and Andrea I. Schäfer³⁰³.

This chapter aims to investigate the steroid hormone adsorption performance of six types of carbon-based nanoparticles (multi- and single-walled carbon nanotubes, two grades of graphene, graphene oxide, and fullerene C₆₀), and determine which nanoparticles are promising for the later incorporation in an adsorptive composite membrane. The adsorption performance of these nanoparticles is linked to the surface properties (such as surface area, accessibility, and chemistry). Varied experimental parameters include the nanoparticle and steroid hormone concentrations, steroid hormone type, water temperature and pH. Finally, the adsorption mechanisms and limiting factors to adsorption are evaluated, and the most capable adsorbent will be selected for incorporation in membranes.

The contributions of co-authors are indicated as follows. Peter G. Weidler (IFG, KIT) and Ruth Schwaiger (IAM, KIT) assisted with nanoparticle characterisation in Argon adsorption tests and helium ion microscopy, respectively. Andrea I. Schäfer is the corresponding author of the project and conceptualised the research. All co-authors participated in revising and editing the manuscript. The authors acknowledge Michael Bruns and Christian Njel (IAM) for performing particle characterisation with X-ray photoelectron spectroscopy; Deski Beri and Andrey Turshatov (IMT, KIT), and Johannes Lützenkirchen (INE, KIT) for helping with dynamic light scattering methodology and problem-solving; and Jinju Zhang and Luiza von Sperling (IAMT) for assisting with sample collection and pH adjustment.

4.1 Literature summary of the surface characteristics of CNPs

Adsorption technology with carbon-based nanoparticles (CNPs) has been extensively investigated for environmental applications¹⁵². The favourable characteristics of CNPs include high surface-to-volume ratios, diverse structures that contain predominantly external surface, high thermal stability, and tuneable chemistry *via* functionalisation^{152, 257, 259, 465, 466}. Good adsorption of steroid hormones, such as E2, EE2, and the xenoestrogen BPA by CNPs has been observed¹⁶⁹⁻¹⁷⁵. The reported fast adsorption kinetics and high adsorption capacities displayed are consistent with the Langmuir and Freundlich isotherm models. However, all these reports prior to this work were performed at elevated hormone concentrations of several $\mu\text{g/L}$ to several mg/L , which are a few orders of magnitude higher than their expected concentrations in waters (see Table 1.1). If hormone adsorption is investigated at relevant concentrations in wastewater (*e.g.* 100 ng/L), the quantity of adsorption sites is not a limiting factor as it may be excessive compared to the quantity of hormones.

Certain CNPs such as carbon nanotubes and graphenes, have predominantly external surface (50–88% for SW-/MWCNTs^{222, 223} and ~100% for graphenes and fullerenes) as such intra-particle diffusion (IPD)²²⁹ is irrelevant. Without IPD (which is considered a slow mass transfer process in activated carbons (ACs))²²⁹, some CNPs display faster kinetics of micropollutant adsorption than ACs, as such the adsorption equilibrium is reached in shorter residence times²⁴². The adsorbed mass by CNPs is likely influenced by film diffusion and/or the energetic interactions at the surface (described in Sub-chapter 2.4). If the residence time is long enough (several hours, for instance) to eliminate the mass transfer limitation caused by film diffusion, the surface characteristics can be considered as the main factor that determines the adsorbed mass.

Apart from the amount of total surface area, the follow surface characteristics are important for the adsorption performance of CNPs: i) the amount of external and highly accessible surface, ii) surface hindrance caused by aggregation, and iii) the surface chemistry that dictates the interactions between the hormone and CNPs^{168, 169, 252, 264}.

This chapter gives an evaluation of steroid hormone adsorption at a relevant concentration (100 ng/L) by six types of CNPs, namely multi-walled carbon nanotube (MWCNT), single-walled carbon nanotube (SWCNT), graphene Grade 1 (2–3 monolayers, GP1), graphene Grade 2 (~30 monolayers, GP2), graphene oxide (GO), and fullerene C₆₀. Samples were taken at residence times ranging from 5 min to 26 h, which ensures that adsorption equilibrium was attained by the end of every experiment. The primary objective is to determine how surface characteristics influence the adsorption of steroid hormones by CNPs. This study can hence complement several other works with ACs at more relevant steroid hormone concentrations (of ~100 ng/L)^{108, 109, 112, 246}. The secondary objective is to determine which CNP has the potential to perform well in a sub-millimetre thin layer of a composite membrane (where fast adsorption kinetics is crucial). The key research interests are: i) which CNPs display fast adsorption kinetics and high capacity for steroid hormones, ii) which CNP surface characteristics (surface area, charge, composition, and hydrophobicity) are responsible for hormone adsorption, and iii) which are the hormone adsorption mechanisms of CNPs at the accessible surface.

4.2 Experimental methods to characterise CNP surface and hormone adsorption

4.2.1 Static adsorption

The investigated parameters in this chapter are steroid hormone type (E1, E2, T and P), CNP concentration (from 2 mg/L to 1 g/L), steroid hormone concentration (from 10 ng/L to 1 mg/L), temperature (from 5 to 80 °C, and solution pH (from 2 to 12). For each investigated parameter, experiments with all the six CNPs were performed. The summary of the experimental design and conditions is given in Table 4.1.

Table 4.1: Overview of the static adsorption experiment design and conditions. For each investigated parameter, experiments with all the six CNPs were performed.

Investigated parameter	Hormone type	CNP conc. (g/L)	Hormone conc. (ng/L)	Temperature (°C)	Solution pH
Hormone type	E1, E2, T, P	0.1	100	20	8
CNP concentration	E2	0.002–1	100	20	8
Hormone concentration	E2	0.1	10–10 ⁶	20	8
Temperature	E2	0.1	100	5–80	8
Solution pH	E2	0.1	100	20	2–12

The static adsorption protocol is described in Appendix C. The analytical technique (liquid scintillation counting) is described in Section 3.4.1 and the error in trace contaminant determination caused by membrane filters is discussed later in Section 4.2.5. In the experiments with varying E2 concentration, the initial E2 concentrations were between 10 ng/L and 1 mg/L; higher concentrations than 1 mg/L were not studied because these concentrations are close to the solubility of E2 in pure water (0.2–5.0 mg/L at 25 °C, see Table 3.3) and hence not realistic in the water environment.

4.2.2 Determination of the adsorbed mass of hormones

In static adsorption, the adsorbed mass as a function of time was calculated according to Eq. (3.2) (see Section 3.5.1). The specific adsorbed mass is determined as the ratio of the adsorbed mass by the weight of adsorbent (see Eq. (3.7)).

The kinetic models can be applied to various data points of specific adsorbed mass of hormone vs. time. The isotherm models are applied to the data of hormone adsorbed mass vs. liquid-phase concentration after the adsorption equilibrium has been attained. The selection of kinetic and isotherm models is described in the next section.

4.2.3 Kinetic models

Three kinetic and four isotherm models have been applied to characterise the evolution of hormone adsorbed mass per mass of adsorbent over time with the ‘*Non-linear curve fitting*’ option of the Origin Pro 2017 / 2020 software (OriginLab, USA).

The evaluated adsorption kinetic models include intra-particle diffusion (IPD), first-order and second-order kinetic models. IPD model developed by Weber and Morris²³⁷ has been commonly applied to characterise micropollutant adsorption by activated carbons. According to this model, IPD is the limiting factor, which determines the rate of adsorption. The specific adsorbed mass $s_{ads,S(t)}$ (ng/g) is linked to residence time t (in h) as shown in Eq. (4.1).

$$q_{ads,S(t)} = K_d \cdot t^{0.5} \quad (4.1)$$

where K_d (g/ng.h^{0.5}) is the intra-particle diffusion coefficient.

The first-order and second-order kinetic models define that the rate of adsorption (or any chemical reaction) is relevant to the concentrations of involving species. With this definition, the phase change of hormones from liquid phase to sorbed phase (*i.e.* the mass action process), could be the rate limiting factor⁴⁶⁷. These models are empirical and do not indicate explicitly which mechanism is limiting (the adsorptive interaction, film diffusion, or IPD). The first-order model fits better when the quantity of adsorption sites is low, while the second-order one fits better when the quantity of accessible adsorption sites is high relative to the quantity of adsorbates⁴⁶⁸⁻⁴⁷⁰.

The first-order model⁴⁷¹ fits with the adsorption when the rate of reaction is proportional to the adsorbate mass (rate_(t) = $K_1 \cdot s_{ads,S(t)}$ where K_1 (1/h) is the rate constant). The adsorbed mass is linked to residence time as shown in Eq. (4.2).

$$q_{ads,S(t)} = q_E \cdot (1 - e^{-K_1 \cdot t}) \quad (4.2)$$

where q_E is the adsorbed mass at equilibrium.

The second-order model⁴⁷² fits when the rate of reaction is proportional to the square of the adsorbate concentration in the solid phase (rate_(t) = $K_2 \cdot s_{ads,S(t)}^2$ where K_2 (g/ng.h) is the rate constant). The adsorbed mass is linked to residence time as shown in Eq. (4.3).

$$\frac{1}{q_{ads,S(t)}} = \frac{1}{K_2} \frac{1}{q_E^2} \frac{1}{t} + \frac{1}{q_E} \quad (4.3)$$

4.2.4 Isotherm models

The empirical Freundlich model^{473, 474} indicates multi-layer coverage of adsorbates and is applicable for the adsorption on a heterogeneous surface. The relationship between the adsorbed mass and liquid-phase concentration, both at equilibrium, is given in Eq. (4.4).

$$q_E = K_F (c_E)^{n_F} \quad (4.4)$$

where K_F ($\text{ng}^{n-1} \cdot \text{g/L}^n$) and n are the Freundlich constants.

The Langmuir isotherm model ^{474, 475} requires the assumption of monolayer coverage of adsorbates and homogeneous adsorption surface only, and that the adsorption sites are identical. The Langmuir-type relationship is given in Eq. (4.5).

$$q_E = q_{max} \cdot \frac{b_L c_E}{1 + b_L c_E} \quad (4.5)$$

where q_{max} (ng/g) is the adsorption capacity (*i.e.* the maximum adsorbed mass that can be achieved by the adsorbents) and b_L (L/ng) is the equilibrium constant. The ratio $\frac{b_L c_E}{1 + b_L c_E}$ is the fractional surface coverage.

The Henry isotherm ⁴⁷⁶ describes the linear relationship between the specific adsorbed mass and liquid-phased concentration at equilibrium, as such adsorption is not limited by number of adsorption sites. This model implies that the adsorbed mass attained is below 10% of the adsorption capacity ⁴⁷⁶ and is presented in Eq. (4.6).

$$q_E = K_H c_E \quad (4.6)$$

where K_H (L/g) is the Henry constant. The Henry model also indicates the special cases of Freundlich model with $n_F = 1$ and Langmuir model with $b_L c_E \ll 1$. The adsorption capacity q_{max} cannot be determined with this model.

The Polanyi–Mane isotherm model ⁴⁷⁷ is applicable for both pore filling and flat surface adsorption and hence useful in characterising adsorption by CNPs. Instead of being fixed to the adsorption sites as described in the Langmuir model, the adsorbate molecules near the surface are attracted to the surface due to an adsorption potential $RT \ln(C_S/C_E)$, where C_S (ng/L) is the solubility of the adsorbate. The Polanyi–Mane isotherm is illustrated as in Eq. (4.7).

$$q_E = q_{max} \exp(Z_{PM} [RT \ln(C_S/C_E)]^{d_{PM}}) \quad (4.7)$$

Where d_{PM} and Z_{PM} ($\text{J}^{1/d}$) are the Polanyi–Mane model constants. The adsorption capacity q_{max} can be determined with this model. This model was based on the theory that adsorbed molecules are not rigidly attached to the adsorbent (which is the condition for Langmuir model) but have an affinity or chemical potential towards the adsorbent. The advantage of the Polanyi theory is that the adsorption capacity can be predicted from adsorbent and adsorbate properties that are commonly available ⁴⁷⁸. Yang and Xing summarised that the Polanyi–Mane model fit better than both Langmuir and Freundlich models for the adsorption by various CNPs ⁴⁷⁷.

4.2.5 Remarks on the use of membrane filters to separate CNPs

The use of membrane filters to separate CNPs has two limitations.

First, it is impossible to confirm that CNPs are completely removed through filtration. The whole or broken CNPs occur in a wide range of sizes as a matter of their natural aggregation, and some small nanoparticles may pass through the MF or even UF pores. This limitation also relates to some well-founded concerns over the toxicity of CNPs, because it is difficult to guarantee zero leakage of CNPs when these are immobilised in a membrane, whereas detection of any leaked CNPs in waters using current analytical techniques is impossible³⁷¹.

It was assumed that the amount of leaked CNPs would be small enough to not significantly impact steroid hormone determination although there is no guarantee that the interference did not happen. Any leakage of CNP did not cause randomness in results because, as reported later, the concentrations of hormones after filtering do not lie outside the concentration error range determined from the use of membranes.

Second, the use of membranes may interfere with the micropollutant analysis⁴⁷⁹. This interference due to the adsorption by membranes was investigated by comparing the decrease in E2 concentration before (*i.e.* in the feed) and after filtration (*i.e.* in the permeate) in six consecutive filtration steps with a single membrane (Figure 4.2). Aliquots of 25 drops were collected in each filtration following the main static adsorption protocol (see Appendix C). With an assumption that each drop had a rough volume of 50 μL ⁴⁸⁰, the permeate volume is estimated to be 1.25 mL. More accurate volume values could be obtained from the permeate mass determined by weighing the container before and after the filtration.

The same permeate concentrations were collected from six filtration steps with PTFE 0.45 μm and RC 100 kDa membranes, hence these membrane filters could be recycled up to six times without the concerns over increasing error caused by adsorption. It appears that the saturation point was not reached, hence the adsorbed mass increased linearly with permeate volume. In contrast, the CA 0.45 μm membrane adsorbed more E2 in the first two filtrations. As such, the CA filters were not recycled. Significant amounts of steroid hormone adsorbed can impact the adsorption data.

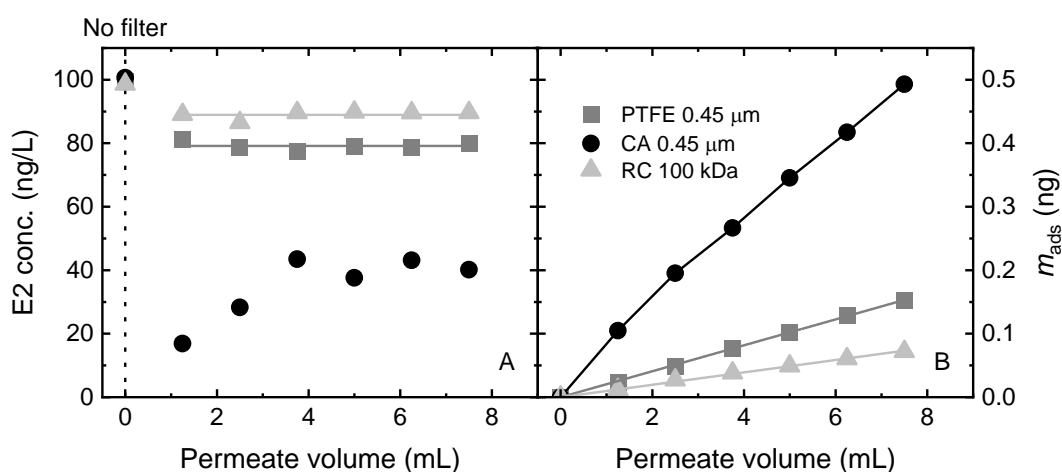


Figure 4.1: Permeate E2 concentration (A) and adsorbed mass (B) after recycling the membranes up to 6 times. Total filtered volume 7.5 mL, 100 ng/L E2, 1 mM NaCO_3 , 10 mM NaCl , pH 8.2 ± 0.1 . Permeate volume is roughly determined from the number of drops. Adapted from Nguyen *et al.*³⁰³.

The hydrophilic cellulose acetate (CA) MF membranes were used to separate GO; hydrophobic membranes such as the PTFE ones do not work for higher GO concentrations than 10 mg/L because the GO is hydrophilic and the interaction between GO and water is strong^{277, 278}. CA membranes adsorbed a lot more steroid hormones than the PTFE membranes, which is an issue for hormone determination.

The interference was then evaluated for different initial E2 concentrations (1–100 ng/L) in Figure 4.3. In static adsorption, the hormone concentration decreased from 100 ng/L when it is adsorbed by CNPs.

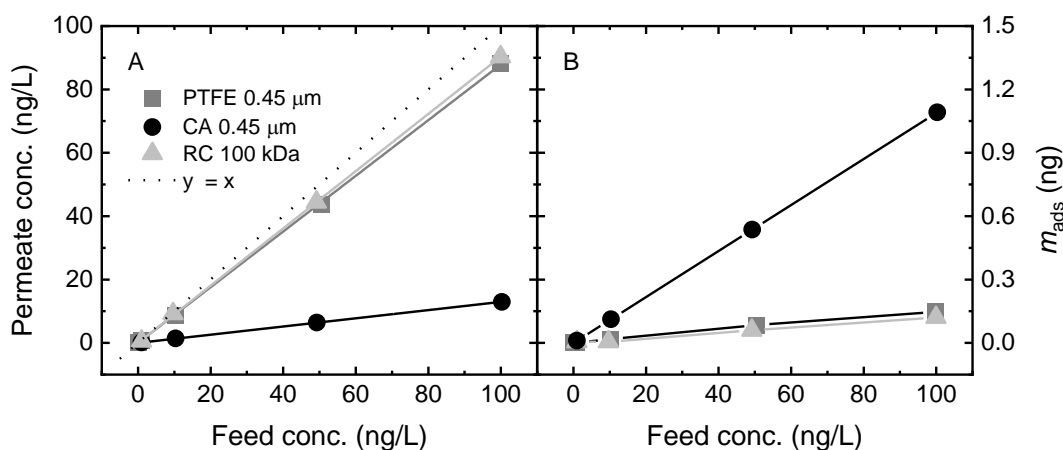


Figure 4.2: Permeate E2 concentration and adsorbed mass by the membrane filters with different feed concentrations. Adsorbed mass was calculated for a rough value of filtered volume of 1.25 mL, 1 mM NaCO₃, 10 mM NaCl, pH 8. Adapted from Nguyen *et al.*³⁰³.

A linear relationship between the feed and permeate E2 concentrations was observed for all three membranes. The decrease in E2 concentration caused by the CA membrane is very high (80%), because CA membrane adsorbed E2 strongly. This decrease was <10% for PTFE and RC membranes. The relative error due to E2 adsorption by membrane is 680% for CA, 10.7% for RC and 13.4% for PTFE membranes. The adsorption percentages vary between E1, E2, T and P but follow the same membrane order CA > PTFE ≈ RC (data not shown in this dissertation).

pH can have an influence on E2 adsorption by CA membranes. Figure 6.1 shows the E2 removal and adsorbed mass by CA membrane at pH 8, 11 and 12.

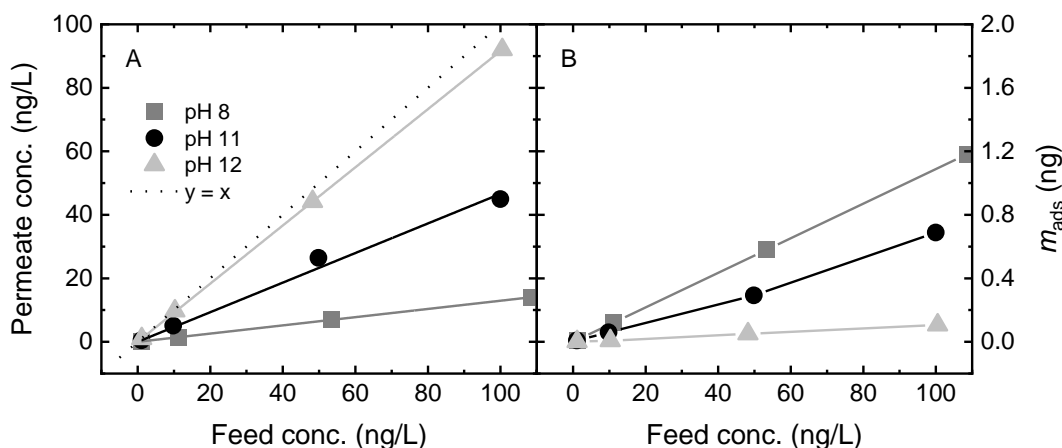


Figure 4.3: Permeate E2 concentration (A) and adsorbed mass (B) at pH 8, 11 and 12 with different feed concentrations. Adsorbed mass was calculated for a rough value of filtered volume of 1.25 mL. 1 mM NaCO_3 , 10 mM NaCl . Adapted from Nguyen *et al.* ³⁰³.

The CA membrane adsorbed only 50% and 3% at pH 11 and 12, respectively, because of the electrostatic repulsion between the negatively charged membrane material and the deprotonated hormone. Therefore, the error is significantly lower at the high pH. In contrast, very little E2 (<13%) was adsorbed by the PTFE and RC membrane in the whole pH range of 2–12 (data not shown in this dissertation).

Although the adsorbed mass of hormones by GO at pH 8 can be determined within an acceptable error range as reported later, some trends in steroid hormone adsorption by GO cannot be concluded as a result of strong interference from the membrane filters. A potential solution to achieve lower error with CA membrane is by elevating the pH to >10; deprotonated E1 and E2 may interact less with the CA membrane because of electrostatic repulsion, but this solution may not work for T and P. Besides, CA degrades at high pH so the membranes may not be recyclable. Separation of GO with more hydrophobic membranes such as PTFE may be possible if the suspension is diluted to contain only 10 mg/L of GO, but the analytical sensitivity for hormones will be reduced.

4.2.6 Nanoparticle characterisation

The surface morphologies of CNPs were visualised with Helium Ion Microscopy (HIM) with the instrument operation provided by Ruth Schwaiger (IAM, KIT). X-ray Photoelectron Spectroscopy was performed by Christian Njel and Michael Bruns (IAM, KIT) to determine the elemental composition of the CNP surface. Argon adsorption and desorption tests were performed by Peter G. Weidler (IFG, KIT) to determine the surface area and pore size distribution of CNPs. Dynamic and electrophoretic light scattering (DLS/ELS) was performed by M.N. with the helps from Deski Beri, Andrey Turshatov (IAM, KIT) and Johannes Lützenkirchen (INE, KIT) to determine the size and zeta potential of the CNP aggregates. All the characterisation methods are described in Sub-chapter 3.7.

4.3 Steroid hormone adsorption performance

This Sub-chapter gives an assessment of steroid hormone adsorption by all the six CNPs in static adsorption experiments. Firstly, the adsorption kinetics and capacity of the CNPs are determined. Then, hormone adsorption by CNPs was evaluated in different water conditions (varying steroid hormone type, solution temperature and solution pH).

4.3.1 Adsorption kinetics of CNPs

The adsorption kinetics is determined for six CNPs, which quantifies how fast the CNPs adsorb steroid hormones and may imply the limiting transfer mechanism encountered with these materials. If the adsorbed mass vs. time can be fitted with the IPD model (see Eq. (4.1)), the adsorption process is controlled by the slow diffusion of hormones into the pores⁴⁸¹. If the IPD model does not fit, and the first- and/or second-order kinetic models fit (Eqs. (4.2) and (4.3)), mass action (*i.e.* the transfer of steroid hormone molecules from liquid to solid phase), it is loosely implied that film diffusion instead of IPD is the limiting process. Better fitting of second-order model compared with the first-order one implies that the quantity of active sites is in excess compared to the quantity of the adsorbates⁴⁶⁹, which is case for the adsorption of hormones in trace concentrations.

Figure 4.4 shows the specific adsorbed mass of E2 as a function of time for six CNPs. The fitting parameters and R^2 for the first-order, second-order and IPD models are given in Appendix D.

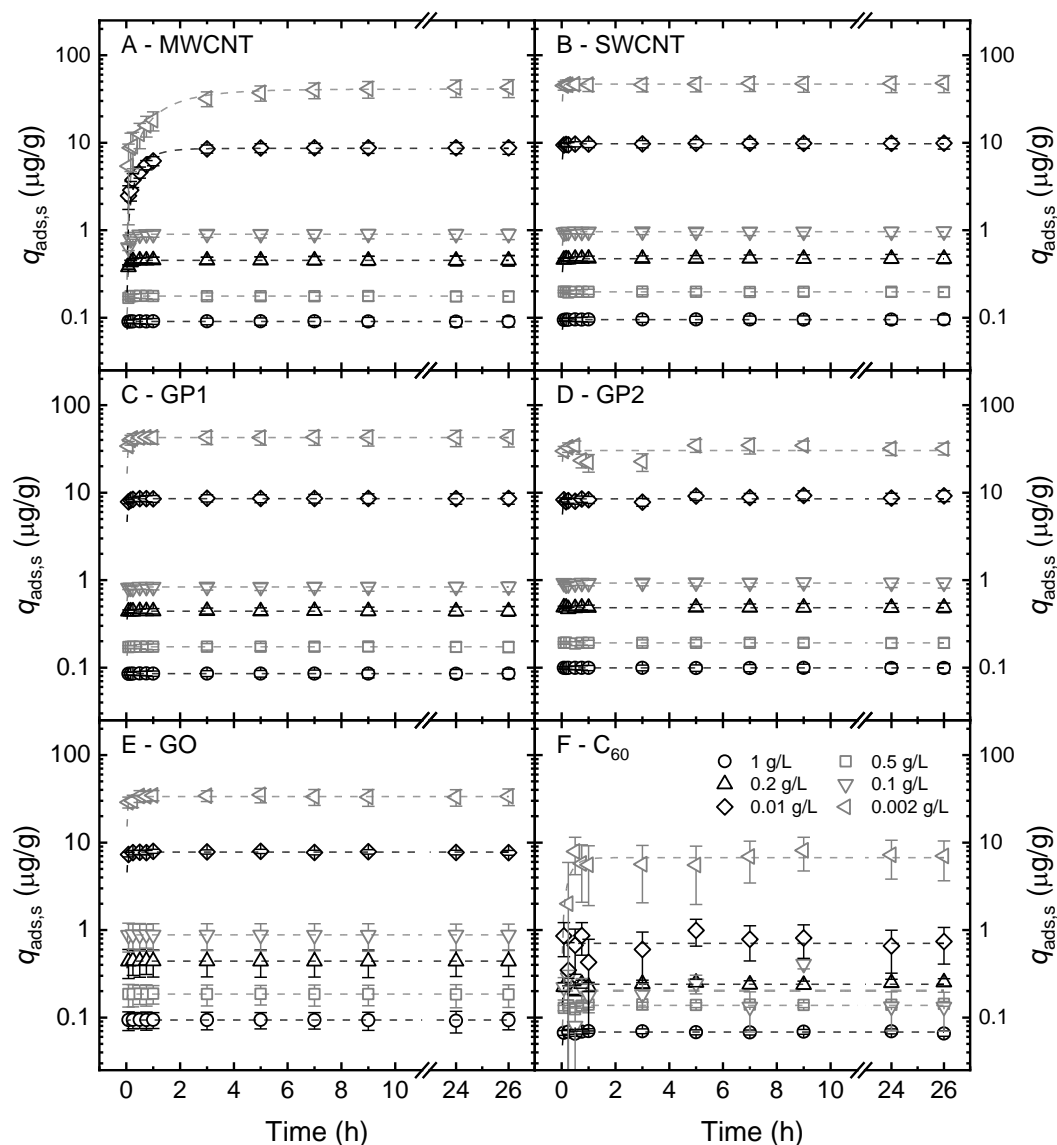


Figure 4.4: E2 adsorbed mass a function of time with varied CNP doses. Data are fitted with the first-order kinetics model. Conditions: 100 ng/L E2, 1 mM NaHCO_3 , 10 mM NaCl, 20.0 ± 0.5 °C, pH 8.0 ± 0.1 . Adapted from Nguyen *et al.*³⁰³.

Generally, E2 adsorption by CNPs was fast, where the adsorption equilibrium (*i.e.* no more increase in specific adsorbed mass) was reached in <5 h for MWCNT and <1 h for all other CNPs. This means the hormone molecules could readily approach the surface of CNPs and implies that the mass transfer was not significantly limited. Adsorption by C_{60} was also fast but the adsorbed masses at equilibrium with C_{60} was generally lower than that those with other CNPs. From Appendix D, the IPD model poorly fits the adsorption, which indicates that the diffusion into the CNP pores did not limit adsorption even at the lowest CNP doses (10 and 2 mg/L). In addition, from Appendix D, the first- and second-order models both fit very well, suggesting that film diffusion may be a relevant rate limiting mechanism.

The adsorption rate constants (Appendix D) generally increased with CNP concentration maybe because at higher CNP concentration, more external surface becomes readily available to E2 molecules, but this trend can also be due to a fitting issue when the adsorption equilibrium was achieved very quickly.

When the above results were compared to those for polymer-based spherical activated carbon (PBSAC) obtained by Tagliavini *et al.*¹¹², the difference in adsorption mechanisms is highlighted. For PBSAC, the IPD model fitted well with $R^2 = 0.96$. The adsorption sites of these relatively large particles are mainly (99%) located in the pores^{112, 193}, as such the diffusion of hormones into the pores can be rate controlling. In CNPs, the majority of adsorption sites are exposed and accessible to steroid hormones (50–88% for MW-/SWCNTs^{222, 223} and ~100% for graphenes), hence the external surface of CNPs may be in excess and hormone adsorption is fast.

Fast adsorption kinetics is encouraging when the CNPs are incorporated in a composite membrane. The residence time in a membrane is only from several seconds to a minute¹⁷⁹, so the adsorbents need to adsorb micropollutants within the same time frame. For SWCNT, GP1, GP2 and GO, the E2 adsorption equilibrium was reached within minutes, so these CNPs are strong candidates for membrane incorporation. E2 adsorption by MWCNT was slower, so MWCNT is a less promising candidate than SWCNT and the graphenes.

4.3.2 Adsorption isotherms of CNPs

The adsorption capacity q_{max} determines the amount of hormone that can be taken up before the limit of surface area for adsorption is reached and the CNPs need regeneration / replacement. The value of q_{max} was investigated for six CNPs *via* the adsorption isotherm, gives the relationship between the specific E2 adsorbed mass at equilibrium q_E and liquid-phase concentration at equilibrium c_E (Figure 4.5). All adsorption experiments reached equilibrium within a few hours.

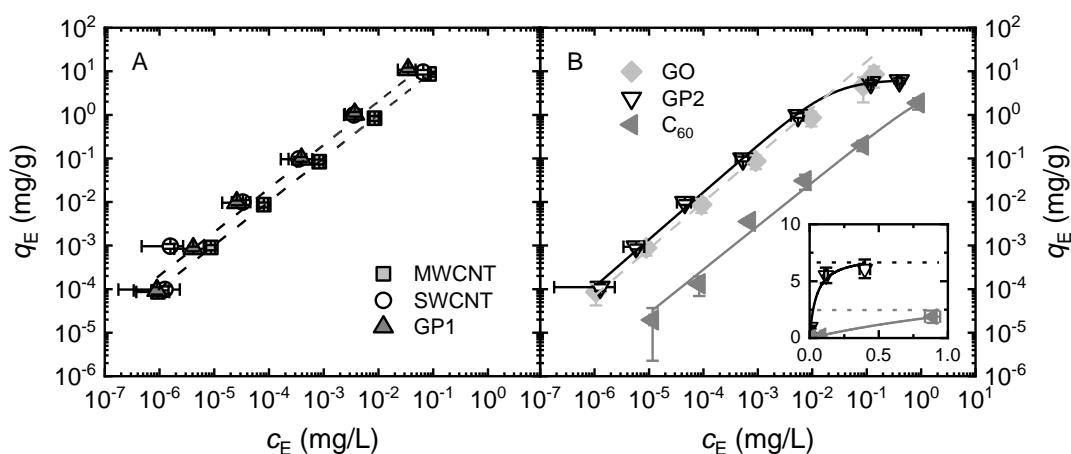


Figure 4.5: A and B – Specific adsorbed mass of E2 q_E vs. E2 concentration at equilibrium c_E . Henry model was applied for MW-/SWCNT, GP1 and GO (dashed lines). Langmuir model was applied for GP2 and C_{60} (solid curves). Inset of B shows the GP2 and C_{60} data in linear scale. Conditions: 0.1 g/L CNP, 1 mM NaHCO_3 , 10 mM NaCl , 20.0 ± 0.5 °C, $\text{pH } 8.0 \pm 0.1$. Adapted from Nguyen *et al.*³⁰³.

From Figure 4.5 A, SWCNT, MWCNT and GP1 show a linear relationship between adsorbed mass and liquid-phase. In the log scale, the Henry model can be fit if the slope of the best fit line is equal to 1 (see Eq. (4.8), noting that the respective units must be eliminated before the logarithmic transformation).

$$\log \frac{q_E}{\text{ng/g}} = \log \frac{K_H}{\text{L/g}} + \log \frac{c_E}{\text{ng/L}} \quad (4.8)$$

Henry model suggests that only <10% of the CNP surface was covered by the adsorbates and the E2 was depleted prior to adsorption site saturation⁴⁷⁶. This assertion is valid for SWCNT, MWCNT and GP1. According to the estimations with CNPs, the estimated q_{max} based on their ideal shapes (77–650 mg/g, see Appendix E) were 1–2 orders of magnitude higher than the maximum value that was attained experimentally, which is 10 mg/g. Very high Langmuir-type q_{max} for steroid hormones have been reported in literature (for example, 100 and 300 mg/g for MW- and SWCNT, respectively¹⁶⁹. Some reports pointed out that E2 adsorption by several CNP types followed the Freundlich isotherm that is characteristic for multilayer adsorption^{172, 174}. However, this empirical model will not describe multi-layer adsorption when a large quantity of CNP adsorption sites is unoccupied.

As seen in Figure 4.5 B and its inset, q_{max} of GP2 is determinable. The Langmuir isotherm fits well ($R^2 > 0.99$), and the corresponding q_{max} of GP2 is 6.6 mg/g. The Polanyi–Mane model also gives a higher q_{max} of 53 mg/g. According to both Langmuir and Polanyi–Mane isotherms, the adsorbate (E2) forms a monolayer on the adsorbent (GP2) surface. The theoretical q_{max} based on the assumption of monolayer E2 coverage on ideal GP2 shapes (35 mg/L, see Appendix E) is around 5 times higher than the q_{max} determined with the Langmuir model (6.6 mg/g).

Both Langmuir and Henry isotherms could fit E2 adsorption by C₆₀ with $R^2 > 0.99$. The roughly estimated Langmuir-type q_{max} of C₆₀ is 1.8 mg/L. The E2 adsorbed mass with C₆₀ is 1–2 orders of magnitude lower than with other CNPs, indicating again the poor adsorption by C₆₀. The theoretical q_{max} of GO is around 300 mg/g (see Appendix E) and a Langmuir isotherm could not be determined in Figure 4.5 B. Large errors in both c_E (not indicated with horizontal error bars in Figure 4.5) and q_E are the results of strong hormone adsorption by the CA membrane filter (as much as 70%, see Section 4.2.5). Therefore, q_{max} of GO could not be determined.

In summary, the shorter list of suitable CNPs for membrane incorporation includes SWCNT, GP1 and probably GO. Their high q_{max} could indicate abundant surfaces and long adsorption times before regeneration or replacement is required. The isotherms indicated here are specific for E2; other steroid hormones (E1, T and P) may interact with CNPs differently according to their structural and chemical differences (see Table 3.3). However, if adsorption is not limited by the amount of accessible surface, high q_{max} of MWCNT, SWCNT and GP1, and lower q_{max} of GP2 and C₆₀ can be expected for all steroid hormones.

4.3.3 Adsorption of different steroid hormone types

After the characterisation of the adsorption kinetics and capacity, it is then necessary to determine the adsorption performance for different types of steroid hormones (E1, E2, T and P). Static

adsorption was performed for each CNP and hormone pair at the same concentrations of the hormone (of 100 ng/L) and CNP (of 0.1 g/L). The relative hormone concentration and specific adsorbed mass at equilibrium are given in Figure 4.6. The properties of the four hormones are as described in Table 3.3. All adsorption experiments reached equilibrium within a few hours.

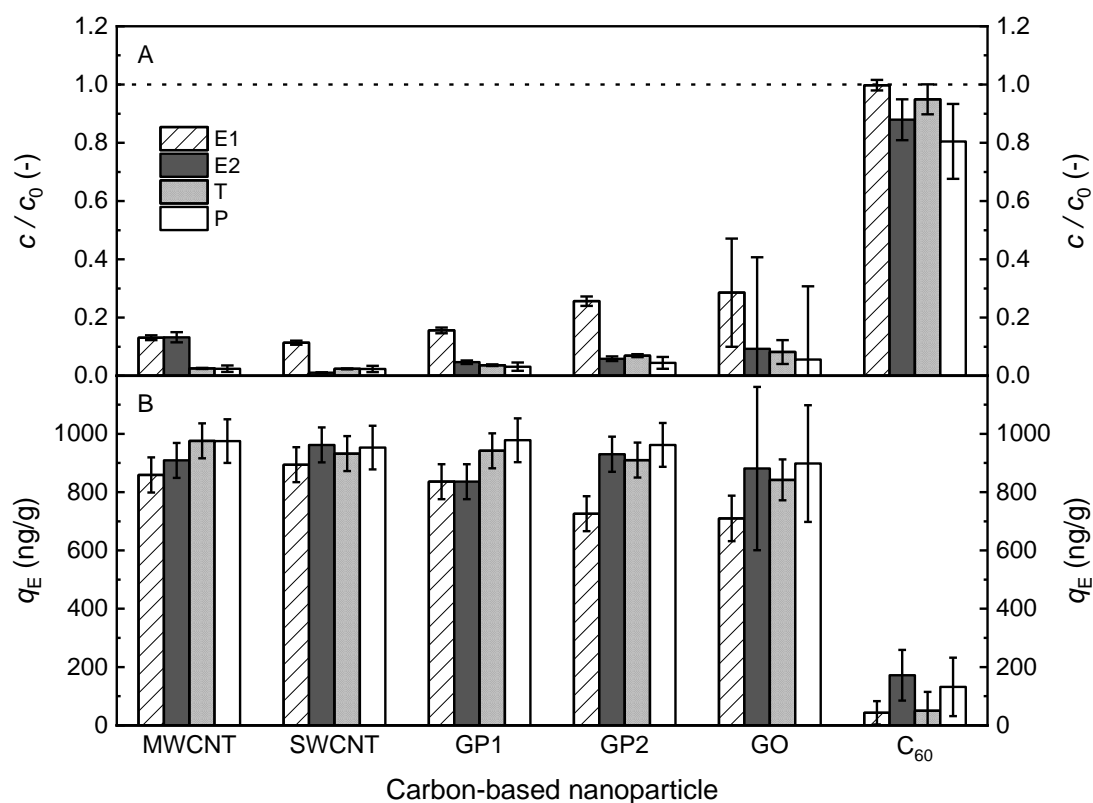


Figure 4.6: Relative hormone concentration c/c_0 (A) and specific adsorbed mass at equilibrium q_E (B) of four hormones. Conditions: 0.1 g/L CNPs, 100 ng/L hormone (E1, E2, T and P), 1 mM NaHCO_3 , 10 mM NaCl , 20.0 ± 0.5 °C, $\text{pH } 8.0 \pm 0.1$. Adapted from Nguyen *et al.* ³⁰³.

As observed in Figure 4.6 A, C_{60} removed the four steroid hormones very little (removal was between 5 and 20%). In contrast, MW-/SWCNT, GP1, GP2 and GO removed a lot of steroid hormones (70–99%). The concentrations of steroid hormones in most experiments with MW-/SWCNTs and graphenes approached the European guideline limit for E2 in drinking water (1 ng/L, corresponding to a relative concentration of 0.01). Figure 4.6 B reveals that the hormone masses adsorbed by C_{60} (<200 ng/g) was several times than the masses adsorbed by the other CNPs (700–1000 ng/g). Therefore, C_{60} is a poor adsorbent regardless of hormone type, and it is not a good choice for incorporation in the composite membrane.

Figure 4.6 B also shows that the variation in adsorption of different hormone types was not significant. GP2 is an exception where the adsorbed mass of E1 (700 ng/g) was significantly lower than those of E2, T and P (around 900 ng/g). With other CNPs, the adsorbed masses of four hormones varied within the error. When the amount of surface and mass transfer are not the limiting factors, steroid hormone adsorption depends on the affinity of the adsorbent surface for the hormone molecules. However, this affinity does not vary significantly between the hormone

types. It is speculated that π - π stacking is not a decisive factor, because T and P do not have any π -ring (see Table 3.3) but were strongly adsorbed. This result contradicts those from several computational studies (molecular dynamics) on E2 and EE2 adsorption by graphene, GO and MW-/SWCNT^{173, 276, 482, 483}, where π - π stacking was suggested to be the most important adsorption mechanism. To date, the adsorption of T or P by CNPs have not been simulated and compared with that of E2 or E1.

4.3.4 Influence of solution temperature on adsorption

The solution temperature may affect the E2 adsorbed mass because it shifts both the kinetics and thermodynamics of the adsorbent-adsorbate interaction. Varying the temperature can confirm whether diffusional processes (both film diffusion and IPD, see Figure 2.5) control adsorption because the diffusivity of adsorbates (E2) increases with temperature according to the Worch equation⁴²⁹. E2 adsorption by the six CNPs at different temperatures (between 5 and 80 °C) are given in Figure 4.7. All adsorption experiments reached equilibrium within a few hours.

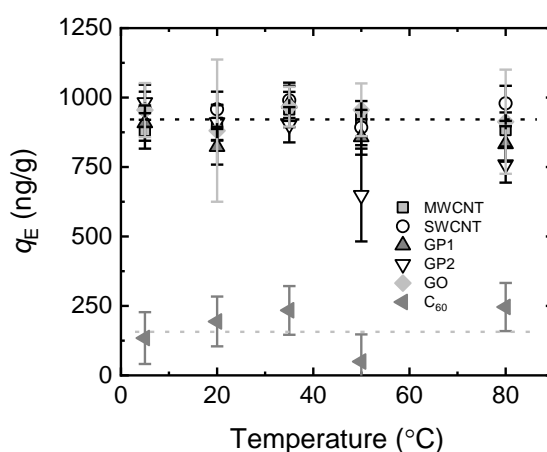


Figure 4.7: Specific adsorbed mass of E2 at equilibrium (q_E) vs. temperature. Conditions: 0.1 g/L CNP, 100 ng/L E2, 1 mM NaHCO₃, 10 mM NaCl, pH 8.0 ± 0.1. Adapted from Nguyen *et al.*³⁰³.

According to Figure 4.7, E2 adsorbed mass was independent of temperature for all CNPs (the adsorption by C₆₀ was poor at all temperatures). These results agree with the remarks on the adsorption kinetics results in Section 4.3.1, where IPD was deemed irrelevant, and film diffusion was a facile process. The diffusivity of hormones depends greatly on temperature (for example, the bulk diffusivity of E2 calculated with the Worch equation⁴²⁹ increases from $2.7 \cdot 10^{-10}$ m²/s at 5 °C to $1.5 \cdot 10^{-9}$ m²/s at 80 °C, *i.e.* by six times), but the limitation in hormone mass transfer from the bulk to the sorbed phase is too small to observe strong adsorbed mass variation with temperature.

It also appears that hormones cannot be desorbed by elevating the temperature to 80 °C, therefore hydrothermal regeneration at this temperature is not possible with CNPs. Hot water has been applied to desorb some pollutants from expired activated carbon in an adsorber but at a more elevated temperature (125 °C)^{354, 355}. To obtain a water temperature of above 100 °C, an induced

pressure of 1 bar is needed (in a pressure cooker, for instance), which could not be achieved in the current study.

4.3.5 Influence of solution pH on adsorption

To determine the influence of surface on hormone adsorption by the six CNPs at different pH, static adsorption with E2 was performed at pH varying from 2 to 12. E2 deprotonation (*i.e.* the process of losing an H^+ to form a negative ion) occurs at pH 10.2–10.7²⁸⁹⁻²⁹¹. If the surface of CNP is negatively charged, electrostatic repulsion occurs between the CNP surface and the deprotonated E2, resulting in low adsorption. The specific adsorbed mass of E2 at equilibrium was plotted against pH as shown in Figure 4.8. All adsorption experiments reached equilibrium within a few hours.

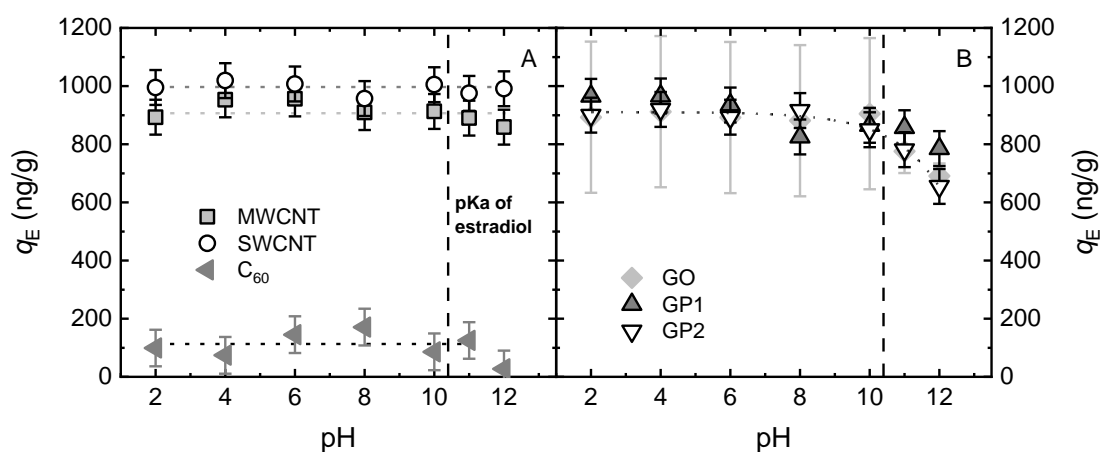


Figure 4.8: A and B – E2 adsorbed mass at equilibrium q_E as a function of pH (100 ng/L E2, 1 mM $NaHCO_3$, 10 mM $NaCl$, 20.0 ± 0.5 °C, pH 2–12). Vertical line indicates the pK_a of E2²⁸⁹. Adapted from Nguyen *et al.*³⁰³.

As observed in Figure 4.8 A, the adsorbed mass with MW- and SWCNT was independent of pH and stays at around 900 and 1000 ng/g, respectively. The insignificant change in adsorption at $pH \geq 10$ implies that the surfaces of MW-/SWCNT are uncharged. C_{60} adsorbed very little E2 (< 200 ng/g) in the pH range of 2–12, so the impact of pH could not be concluded.

According to Figure 4.8 B, GP1 and GP2 adsorbed less hormone at $pH \geq 10$. E2 adsorbed mass achieved with GO was not accurately determined because E2 adsorption by the CA membrane filters was very strong at pH 2–10 (see Section 4.2.5) and caused high error. At pH 11–12, CA adsorbed much less E2, and E2 adsorbed mass by GO at pH 11 was higher than that at pH 12.

At high pH of 11–12, E2 adsorption by GO, GP1 and GP2 is dictated by two phenomena: i) electrostatic repulsion between the negatively-charged surface and E2 ions, and ii) exfoliation of the stacked graphene sheets because of increasing repulsion between the functional groups and/or adsorbed hydroxyl ions, giving more surface for E2 adsorption⁴⁸⁴⁻⁴⁸⁶. Phenomenon 1 may be relevant as the graphenes are not purely carbon and may contain deprotonable oxygen-containing groups. Adsorption with varying pH was not performed for T and P but given that these steroid

hormones cannot form negative ions, their adsorption by graphenes could increase with pH according to Phenomenon 2.

In summary, E2 adsorption by GP1, GP2 and GO was more sensitive to the variation in water chemistry (pH) than that by MW-/SWCNT. In consideration of the complex water matrices in water treatment, and the fast adsorption kinetics displayed by SWCNT, SWCNT may be the best candidate for membrane incorporation. Another conclusion is that, because the impact of a wide range of pH is generally low, manipulating the solution pH to regenerate CNPs seems impractical.

4.4 Relationship between surface accessibility and adsorption

To find the relationship between surface accessibility and adsorption, the specific surface area (SSA), pore characteristics, and state of aggregation of CNPs will be determined. High surface areas and large pores / spaces are beneficial for adsorption. Aggregation limits the access of molecules to the surface, which reduces adsorption.

4.4.1 Specific surface area

Argon adsorption / desorption experiments (done by Peter G. Weidler) provide the results of the SSA along with the size and volume of the CNP pores. The SSAs determined with the BET and QSDFT models, and pore volume determined with the QSDFT model are given in Table 4.2. With QSDFT, the cylindrical pore configuration fitted best with the carbon nanotubes, and the slit pore with the graphenes and C_{60} . A theoretical correlation was established in Appendix E between the measured SSA and the adsorption capacity for E2.

The SSA according to the BET and QSDFT models both followed the trend $GP1 > SWCNT \geq MWCNT > GP2 > GO > C_{60}$. From assumptions with ideal CNP shapes (see Appendix E), the SSA followed the trend $C_{60} > SWCNT > GP1 = GO > GP2 > MWCNT$.

The experimental and theoretical surfaces of C_{60} are vastly different: the ideal-shape SSA (1250 m^2/g) was 500–5000 times larger than the BET- / QSDFT-derived SSA (0.5–3 m^2/g). The low measured SSA of C_{60} here consistent with the value reported in another work (1.1 m^2/g)²¹⁹. It appears that the penetration of Argon to the C_{60} surface was very limited due to strong supramolecular interactions within a C_{60} ‘cluster’ (nC_{60}). The distance between C_{60} molecules is around 0.2 nm²⁰⁵, which is shorter than the typical distance of intermolecular interactions (0.3–0.5 nm, see Section 2.4.4), giving nC_{60} a crystalline structure. As a result, the spaces in an nC_{60} cluster are not accessed by the bigger Argon molecules that have a van der Waals diameter of 0.4 nm. This exclusion is also relevant for steroid hormone molecules that have a hydrodynamic diameter of 0.8 nm.

With the assumption of ideal shapes, GP1, GP2, GO and C_{60} possess no internal surface, so the theoretical pore volumes is equal to zero. The experimental pore volumes V_{pore} were in the range of 0.007–5.6 cm^3/g , and these values can only be attributed to the pores created by aggregation. Aggregation is implied *via* the tri-modal distribution of pore volume in the pore diameter range

4 Influence of Adsorbent Surface on Hormone Adsorption

of 1–5 nm (see the pore profile graphs in Appendix F). In contrast, MW-/SWCNTs have defined pores, which corresponds to a surge in pore volume in the pore diameter range of 1.3–1.8 nm (Appendix F).

Table 4.2: Surface area, pore characteristics and adsorption capacities (experimental and theoretical) of CNPs. PBSAC is also included for comparison ¹¹². N.D.: not determined. Adapted from Nguyen *et al.* ³⁰³.

	MWCNT	SWCNT	GP1	GP2	GO	C ₆₀	PBSAC
BET model							
SSA (m ² /g)	639	775	1750	24	10	< 0.5	1500
SSA correlation coefficient	0.9999	0.9998	0.9999	0.9999	0.9995	0.8676	N.D.
DFT model							
SSA (m ² /g)	801	796	2270	29	8.5	3	1332
Pore volume V_{pore} (cm ³ /g)	1.28	1.25	5.56***	0.057	0.013	0.007	1.3
Average pore size (nm)	1.6	7.1	5.5	1.5	1.6	2.5	1.3–2.3
Fitting error (%)	0.386	0.686	1.252	1.201	1.183	2.620	N.D.
Ideal shape assumptions*							
SSA (m ² /g)	14	960	330	150	330	1250	N.D.
External surface (m ² /g)	12†	490	330	150	330	1250	N.D.
Internal surface (m ² /g)	2†	470	~0	~0	~0	~0	N.D.
Adsorption capacity (mg/g)							
Experimental	>10	>10	>10	6.6	>10	~1.8	>10
Theoretical** – based on DFT SSA	330	410	860	12	5.2	0.25	850
Theoretical** – based on ideal shapes	13.2	834	296	35	296	1040	N.D.

* Ideal shapes of CNPs: tube-like shape for MW/SWCNTs, planar shape for GP1, GP2 and GO, and spherical shape for C₆₀ (see Appendix E).

** Assuming that all the surface of E2 was in contact with the CNP surface forming a monolayer; the cross-sectional surface area of each E2 molecule was 0.5 nm² (calculated from the hydrodynamic radius of 0.4 nm).

*** The mass of GP1 was relatively low (6 mg, 10 times lower than other CNPs) so a rough pore volume value was obtained (~20% error).

† MWCNT surface areas based on the ideal shape was underestimated probably because the assumed MWCNT density (33 g/cm³, see Appendix E) is much higher than the reported value in literature (1–2 g/cm³) ⁴⁸⁷.

As opposed to activated carbons (such as PBSAC), CNPs contain predominantly external surfaces. The DFT-derived pore diameters of PBSAC (diameters of 200–450 nm) narrowly

distributed between 1.2 and 2.3 nm, which are only marginally larger than the size of hormones, hence IPD of adsorbate molecules is relevant and can control the kinetics¹¹². In contrast, the lack of ‘pores’ in CNPs confirms that IPD is not relevant, although the aggregation of CNPs may undermine the surface area and adsorption capacity q_{max} . Aggregation leads to the difference between the experimental and theoretical SSAs because Argon atoms (and hormone molecules) might not penetrate some adsorption sites²⁵². The aggregated CNPs will be visualised with helium ion microscopy (HIM) in the next section.

4.4.2 Surface morphology

The surface morphology of CNPs can explain the trends in SSA and hence the adsorption performance. The HIM micrographs of CNPs are shown in Figure 4.9. The insets show parts of CNPs with higher resolution.

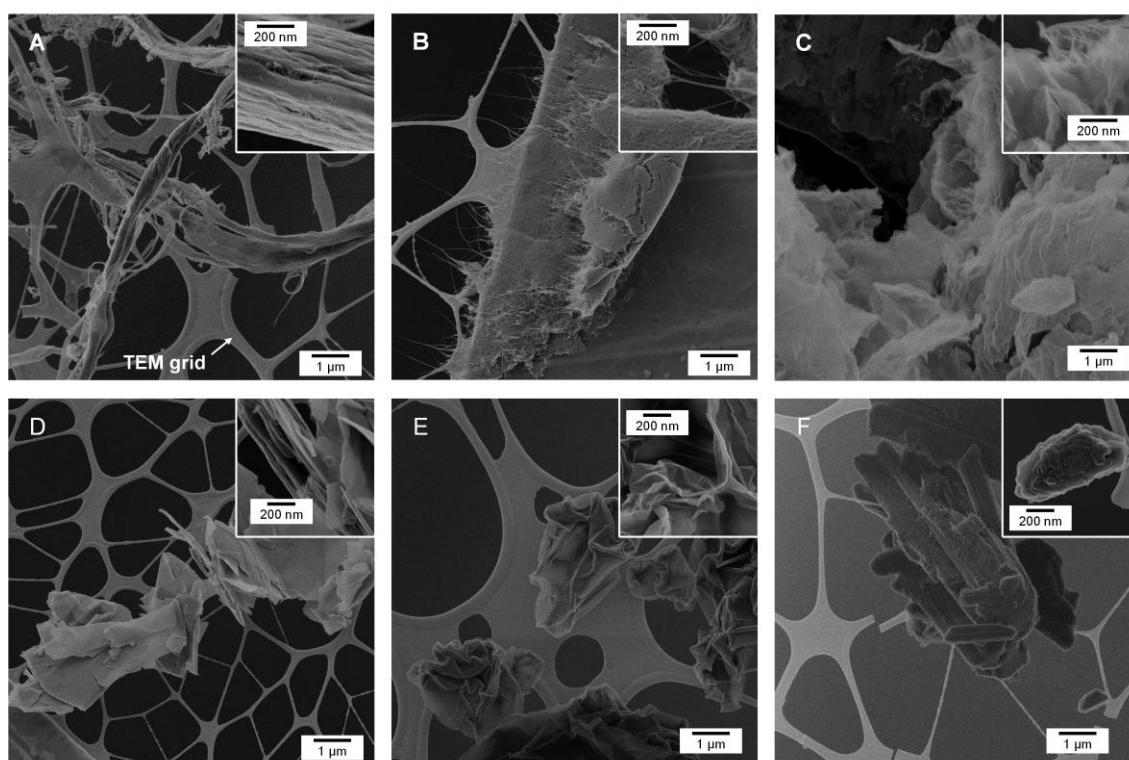


Figure 4.9: HIM micrographs of MWCNT (A), SWCNT (B), GP1 (C), GP2 (D), GO (E) and C₆₀ (F). The TEM grid on which the CNPs were deposited can be seen in the background. Reprinted from Nguyen *et al.*³⁰³.

The aggregation of the CNPs is observed in all the micrographs, as the shapes of CNPs are vastly different from the theoretical ones (which are described in Appendix E). Micrographs of MWCNT (Figure 4.9 A) and SWCNT (Figure 4.9 B) show entangled and bundled rod-like structures, although the inset SWCNT micrograph shows some distinctive individual nanotubes of several nanometres in tube diameter. In contrast, only thick nanotube bundles with diameters of up to several micrometres were observed with MWCNTs. It is clear that SWCNT exposes more surface

for adsorption than MWCNT; and any adsorption hindrance will likely depend on the amount of less accessible surface in the aggregates.

The 2D structures of individual GP1 (Figure 4.9 C) and GO (Figure 4.9 E) nanosheets were not observed; instead, the appearances resemble crumpled papers of several micrometres in size. The wrinkles, crumples and folds of such structures can improve for adsorption as they give rise to high-energy surfaces⁴⁸⁸⁻⁴⁹⁰. GP2 (Figure 4.9 D) that contains more monolayers than GP1 and appears like graphite and without any observable wrinkles and crumples, as a result of the thick stacked sheets of 50–200 nm. C₆₀ (Figure 4.9 F) showed only aggregate structures of several micrometres in size. In another work, X-ray diffraction studies confirmed that solid C₆₀ form densely-packed structures with covalent-like intermolecular bonds at room temperature²⁰⁵. It seems that the bulky and non-porous aggregates of C₆₀ could consist of millions of individual C₆₀ of diameter <1 nm; where most surface is not accessible for adsorption.

4.4.3 Aggregation of CNPs in solution

In solution, CNP aggregation varies with time, shear forces and solution chemistry, which inevitably affects the adsorption of steroid hormones. DLS can measure the aggregate size of CNPs but inaccurately, because this technique requires the particles or aggregates to be spherical and monodispersed⁴⁹¹. In contrast, CNP aggregates have complicated geometries and random orientations in water. Furthermore, big aggregates of CNPs can settle and will not be detected⁴⁹². The sizes of CNP aggregates that are suspended in the solution as a function of time are reported in Figure 4.10. The three CNP suspension preparation methods that impact the size measurements are described in Section 3.7.4.

The aggregate sizes of CNPs vary with time because aggregation process is dynamic but thermodynamically driven process, where hydrophobic particles (all CNPs probably except GO) tend to gather to minimise the contact area with water^{493,494}. The presence of dilute electrolytes (1 mM NaHCO₃ and 10 mM NaCl) in preparation methods 1 and 2 can enhance CNP aggregation according to the Derjaguin–Landau–Verwey–Overbeek (DLVO) theory^{288, 495-498}. Such an enhancement is a result of the *squeezing-out effect* where the electrolyte ions readily penetrate the diffuse double layer around the aggregates, reducing the inter-aggregate repulsion and causing the aggregates to be more compact³²¹.

Aggregate sizes obtained *via* preparation method 2 (in which electrolytes were added before sonication) were 2 orders magnitude higher than those obtained *via* preparation method 1 (where electrolytes were added after sonication), because the total sonication time was doubled, which could increase the CNP breakdown into smaller aggregates, before the electrolytes prevented the reaggregation and settling of dispersed CNPs^{499,500}. A continuous increase of particle sizes over time was not observed in all three methods because the bigger aggregates settle, which signifies the complexity of the tested systems.

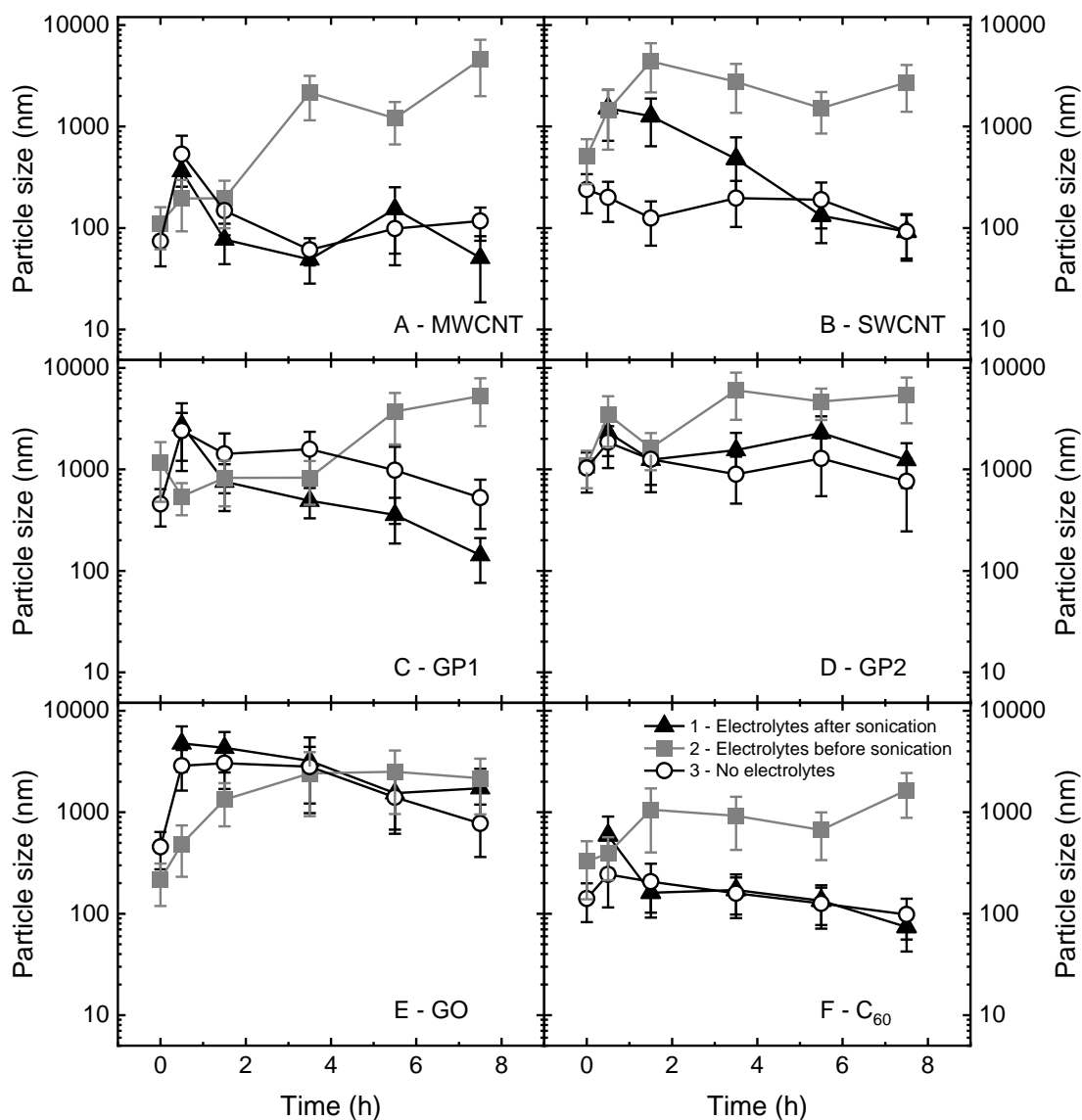


Figure 4.10: Aggregate size of CNPs vs. time where the suspensions were prepared *via* three methods indicated in Section 3.7.4. Adapted from Nguyen *et al.* ³⁰³.

In summary, the combined effects of CNP properties, solution chemistry, and preparation method can impact the dispersion of CNPs in water and resulting in unavoidable bias in adsorption evaluation. The settling of CNP aggregates in adsorption experiments was overcome to some extent by continuous shaking. Methods to reduce aggregation include surface treatment ^{501, 502}, use of surfactants ^{503, 504}, or solvent exchange ⁵⁰⁵. However, the additives potentially interact with adsorbates and may complicate the CNP performance evaluation.

4.4.4 Remarks on the surface accessibility – adsorption relationship

To summarise the CNP surface features and their connection with adsorption, Figure 4.11 schematically illustrates the possible regions created by aggregated CNP structures that are accessible to steroid hormones.

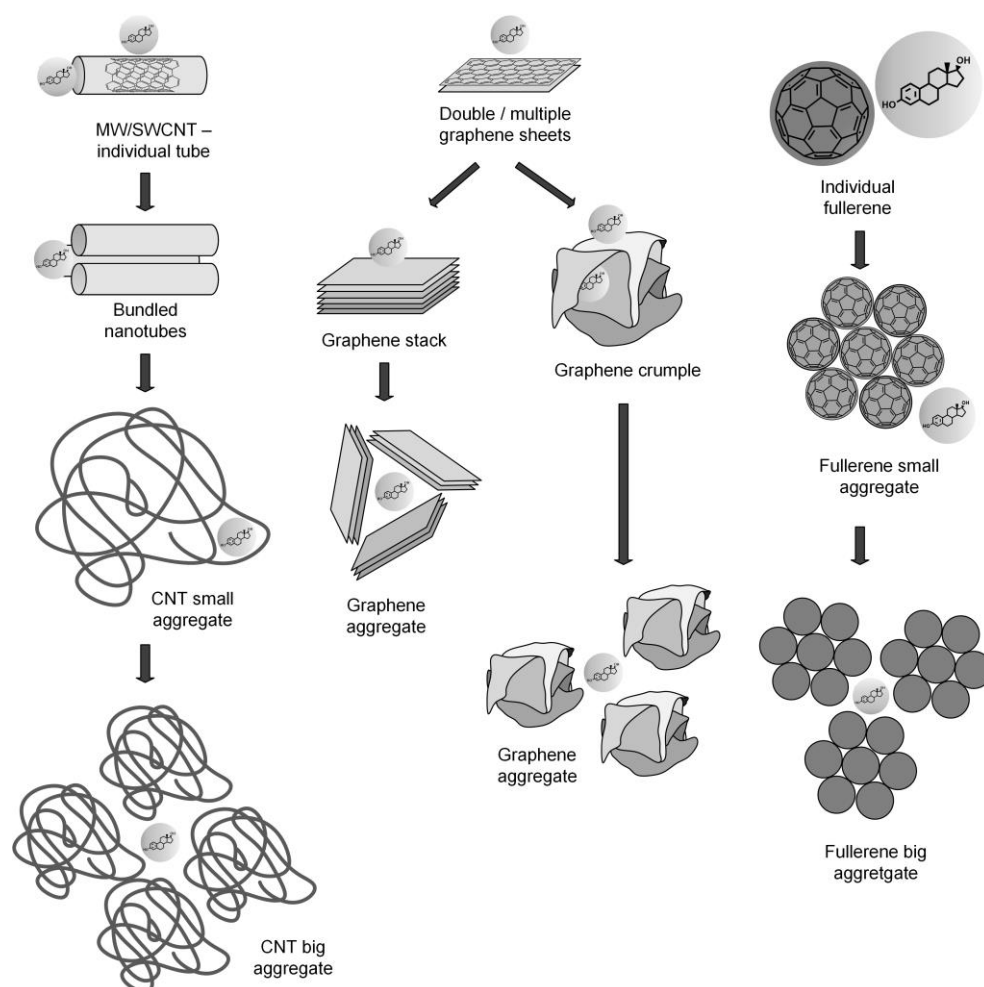


Figure 4.11: Geometries of MW-/SWCNT, graphene, GO and C₆₀ molecules and aggregates. Different adsorption sites are illustrated with E2 molecules. Only the size of C₆₀ is to scale with the size of E2. Adapted from Nguyen *et al.*³⁰³.

With MW-/SWCNTs, the external nanotube walls are the primary adsorption sites. It is still unclear whether the internal surface (enclosed inside the nanotubes) is practically available for adsorption. The internal nanotube diameter is around 2 nm, while the diameter of an E2 molecule (0.8 nm) can be smaller. However, because the external surface area of MW-/SWCNTs is a few thousand times larger than the area of pore entrance (see Appendix E), the hormone will likely adsorb to the external surface instead of penetrating the pores. The secondary adsorption sites are the grooves between the nanotubes in a bundle, and the vacancies created by coiling nanotubes, and the spaces between the small aggregates of the nanotubes.

The primary adsorption site of graphene is the graphitic planes. Aggregation of graphene materials results in two structures: stacked sheets (observed in the case of GP2) and crumples (observed in the cases of GP1 and GO). E2 cannot occupy the spaces between the graphene sheets in a stack because the inter-sheet distance (0.3 nm) is smaller than the size of E2. In contrast, E2 can occupy the space created by the crumpling of GO and GP1.

The curved surface of C_{60} are the primary accessible areas for adsorption. The crystal-like aggregate of C_{60} provides no internal surface areas for E2 due to the high packing density, with an inter- C_{60} distances of only 0.2 nm²⁰⁵. The surface for adsorption is limited in this regard.

In the next sub-chapter, the relationship between surface chemistry and adsorption is elucidated, which highlights the contribution of several adsorption mechanisms (electrostatic interaction and O...H hydrogen bonding) to the overall adsorption.

4.5 Relationship between surface chemistry and adsorption

4.5.1 Elemental composition of the CNP surfaces

The elemental composition implies whether the CNP surface is hydrophilic and capable of forming electrostatic interaction and hydrogen bonds with the hormone. The percentages of surface carbon and oxygen, including those of the different electronic states, were determined with X-ray photoelectron spectroscopy (XPS) and reported in Table 4.3.

Table 4.3: Percentages of carbon and oxygen, and their respective electronic states at the CNP surface. Reprinted from Nguyen *et al.*³⁰³.

No.	CNP	Total C (%)	Total O (%)	Carbon (%)					Oxygen (%)	
				sp ² -C	sp ³ -C	C-O	C=O	π - π^*	C=O	C-O
1	MWCNT	97.4	2.6	89.5	0.0	1.2	0.8	5.9	0.9	1.7
2	SWCNT	98.1	1.9	90.7	0.0	1.1	1.1	5.1	0.9	1.0
3	GP1	98.6	1.4	89.1	3.5	0.6	0.7	4.7	0.8	0.6
4	GP2	97.9	2.1	89.5	0.1	1.6	0.6	6.1	0.7	1.4
5	GO	69.1	30.9	6.4	25.8	32.0	4.9	–	0.4	30.5
6	C_{60}	98.3	1.7	89.0	0.0	1.1	0.9	7.1	0.8	0.9

MW-/SWCNTs, GP1, GP2 and C_{60} were hydrophobic because they contained mostly carbon (97–99%) on the surface. Most of the carbon atoms (~90% of the total carbon) of these CNPs were in the sp^2 hybridisation state implying the abundance of aromatic rings¹⁵². Hence, hormone adsorption by these CNPs involves directional π / π and X-H / π interactions, as well as non-directional hydrophobic effect as the hormones are hydrophobic (with high K_{OW} values, see Table 3.3).

In contrast, GO had a high oxygen composition of 31%; most of these oxygen atoms (99% of the total oxygen) formed a single bond with carbon atoms. The prevalence of C–O bonds could indicate –OH and epoxy functionalities on the graphitic planes. GO has a relatively low number of carbon atoms in the sp^2 hybridisation state (~10% of the total carbon and 6.4% of the total elements), indicating that the honeycomb structure was disrupted by the oxygen-containing groups⁵⁰⁶. This disruption potentially reduces π / π and X–H / π interactions and intensifies hydrophilic interactions such as O···H hydrogen bonding. In addition, electrostatic repulsion is bound to be an important limitation to E2 adsorption by GO at high pH. Hormone adsorption by GO is also affected by direct competition from water^{278, 281, 507}.

4.5.2 Surface charge

The surface charge indicates the significance of electrostatic interaction. CNPs once in dispersion can behave as colloids^{288, 496-498}, hence the surface charge can be determined in the form of zeta potential. According to the colloidal dispersion (DLVO) theory, a zeta potential higher than 30 mV or lower than –30 mV indicates that the colloids are stable and disperse well in the water⁵⁰⁸. Zeta potential measured with ELS as a function of solution pH is given in Figure 4.12.

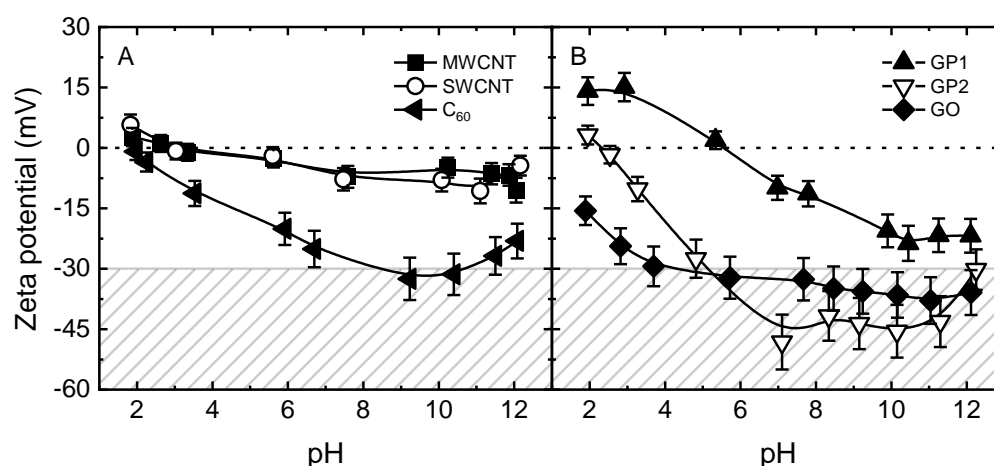


Figure 4.12: Zeta potential as function of pH. Colloids are expected to be stable if the magnitude of zeta potential exceeded 30 mV (grey region) according to Everett⁵⁰⁸. Reprinted from Nguyen *et al.*³⁰³.

As observed in Figure 4.12 A, MW- and SWCNT have insignificant zeta potential in the pH range 2–12. Therefore, electrostatic interactions could contribute little to adsorption. In contrast, the zeta potential values of C₆₀ were more negative than those of MW-/SWCNTs at pH 4–12; at pH 8–11, C₆₀ falls into the colloidal stability regime.

From Figure 4.12 B, GP1, GP2 and GO have a negative surface charge at neutral and high pH, thus the dispersion of these CNPs is enhanced by electrostatic repulsion. At pH \geq 5, GP2 and GO can form stable colloidal suspensions. The isoelectric point (at which the zeta potential is equal to zero) of GP1, GP2 and C₆₀ is between pH 2 and 6. E2 adsorption of these graphenes and C₆₀ may be lower at pH \geq 10 where electrostatic repulsion occurs between the charged surface and hormones.

The zeta potential of GO was negative at all pH, which was expected because the oxygen-containing functional groups such as $-OH$ and $-COOH$ are deprotonable and give the surface an overall negative charge. In contrast, the negative zeta potential values of GP1, GP2 and C_{60} were unexpected for carbon-rich surfaces. These negative zeta potential values can be attributed to the charges at defects and edges^{509, 510}, or hydroxyl ion adsorption^{511, 512}. Because the quantity of hydroxyl ions depends on the solution chemistry, the surface charge analysis is complicated. According to the DLVO theory⁵⁰⁸, GP2, GO and C_{60} have zeta potential values smaller than -30 mV and should form stable colloids / aggregates at pH 8, but these stable aggregates were not identified in DLS because their sizes were large and varied with time.

4.6 Examination of the adsorption mechanisms and limiting factors

4.6.1 Adsorption mechanisms

The adsorption process can now be speculated based on the distance between the hormone adsorbates and the CNP surface. This process is schematically illustrated in Figure 4.13.

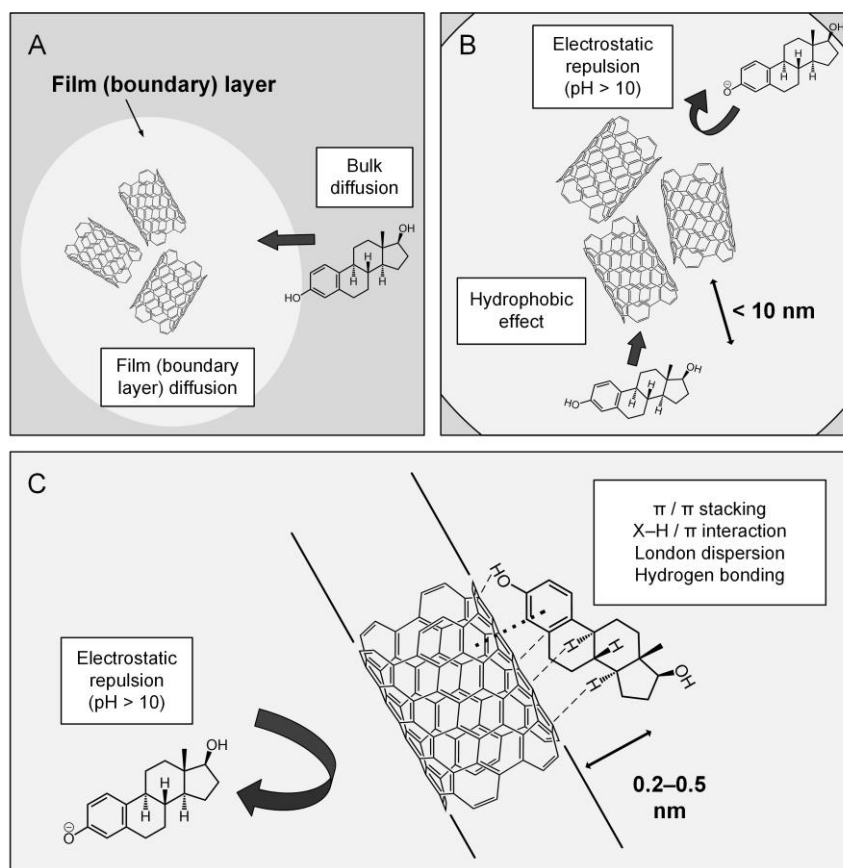


Figure 4.13: Mechanisms of steroid hormone adsorption by CNPs based on the proximity (CNP–hormone distance follows the order $A > B > C$). CNP aggregates are represented as SWCNT segments as an example. Adapted from Nguyen *et al.*³⁰³.

Figure 4.13 A illustrates the mass transfer mechanisms (bulk diffusion and film diffusion) at relatively large distances between CNP and the steroid hormone. When the hormone enters the film layer of CNPs, a resistance is provided against hormone diffusion to the external surface. The thickness of this film layer of CNP aggregates have not been determined but can be reduced *via* vigorous shaking. All experimental results pointed out that because the adsorption equilibrium was reached very quickly (hence very fast adsorption kinetics), the film diffusion process did not limit the adsorption significantly.

Figure 4.13 B shows the occurrence of non-directional forces when the hormone–CNP distance is below 10 nm. Relatively long-range hydrophobic effect²⁹⁵ assist hormone diffusion through the film (boundary) layer. If the CNP surface is negatively charged, at $\text{pH} \geq 10$, long-range electrostatic repulsion between E2 ions and the CNP surface can hinder this diffusion and potentially result in low adsorption. According to the experimental results at varying pH, different CNPs can repel the deprotonated E2 to specific extent, which explains the different trends of E2 adsorbed mass with pH.

According to Figure 4.13 C, when hormones are in very close proximity with CNPs (sub-nanometre distances), the film (boundary) layer resistance is elevated, but many directional forces become active, such as aromatic interactions (π / π stacking and X–H / π interaction), O \cdots H hydrogen bonding (dominant in GO) and short-range electrostatic interactions. The balance between these forces and the repulsive force between the electrons of adsorbent and adsorbate explains the highly-ordered ‘gap’ between solutes and the CNP surface of 0.3–0.5 nm^{513, 514}. Hence, the minimum hormone–CNP distance is determined to be around 0.3 nm.

4.6.2 Limiting factors to adsorption

In the next sub-section, the limiting factors to adsorption will be summarised based on similar static adsorption studies with different carbon-based adsorbents, namely CNPs (this research project³⁰³), PBSAC (Tagliavini *et al.*¹¹² and AC fibres (Zhang *et al.*²⁴⁶).

The surface composition is very similar between the CNPs (except GO), PBSAC and AC fibres (according to this work, Tagliavini *et al.*¹¹² and Zhang *et al.*²⁴⁶), so the energetic interactions between the hormone and adsorbent surface are expected to be similar. The variation in adsorption is hence attributed to the difference in surface accessibility (*i.e.* the mass transfer processes). Four cases of surface accessibility are described as follows.

Case 1: Internal surface is dominant (PBSAC). In PBSAC, the composition of external surface is around 1%¹⁹³, similar to those of PBSAC with similar particle sizes²¹⁶. The pore diameters of PBSAC from Argon adsorption / desorption analysis are 1.3–2.3 nm. These are larger than the diameter of steroid hormones (0.8 nm), so the hormones can penetrate these pores¹¹². At low doses of PBSAC of 2–10 mg/L, IPD (*mass transfer*) limits the adsorption and the adsorption equilibrium was not observed after 26 h; at higher doses of PBSAC (>10 mg/L), IPD appears less important to adsorption as the equilibrium was reached within a few hours¹¹².

Case 2: Internal surface is less dominant (AC fibres). When E2 adsorption was evaluated with smaller AC fibres (10–30 μm in size) at the low doses of 2–10 mg/L, IPD controlled the

adsorption only in the first 30 min²⁴⁶. The SSA (1600 m²/g) and pore volume (1.5 cm³/g) of AC fibres⁵¹⁵ are similar to those of PBSAC (see Table 4.2 for PBSAC data). The pore sizes of AC fibres (~3.4 nm) were larger than those of PBSAC, which is beneficial for E2 diffusion into the pores. Adsorption equilibrium was achieved quickly afterwards (in a few hours), indicating that AC fibres display faster adsorption kinetics than PBSAC.

Hence, IPD limits the adsorption by AC fibres to a smaller extent compared with PBSAC because the percentage of external surface of AC fibres is probably higher than that of PBSAC. The data for AC fibres were not reported by Zhang *et al.*⁵¹⁵, but a negative relationship between particle size and external surface area had been established for PAC and superfine PAC²¹⁶.

Case 3: External surface is dominant (MW-/SWCNT and graphenes). Carbon nanotubes (MW-/SWCNTs) and graphenes (GP1, GP2 and GO) adsorb steroid hormones mainly on the abundant external surface. In the CNP concentration range of 2–10 mg/L, the quantity of surface adsorption sites is not a limiting factor. Adsorption was fast with the adsorption equilibrium reached within a few minutes (except for MWCNT where at the lowest concentrations of 10 and 2 mg/L, the equilibrium was reached in 3 h). Only the nanotube entrances of MW-/SWCNTs are intrinsic ‘pores’, although the access of E2 to these pores is not likely. Hence, IPD is not relevant while the mass transfer limitation caused by film diffusion is low. The slower adsorption kinetics with MWCNT is explained by the adsorbate diffusion into less accessible regions of MWCNT aggregates.

Case 4: Very little surface is available (fullerenes, C₆₀). For C₆₀, the aggregates are too strong and dense, which significantly limits the surface accessibility. This limitation caused by surface is determined *via* the low SSA for Argon adsorption, of <0.5 m²/g, compared with the high theoretical SSA of over 1000 m²/g. Adsorption of steroid hormones was very low due to the poor surface access. In other words, the amount of surface is the main limiting factor for adsorption.

From the above cases, it is concluded that the accessible surface (or external surface) overcomes the mass transfer limitation and dictates the adsorption performance of carbon-based adsorbents. The promising adsorbents in adsorptive composite membranes must exhibit very fast adsorption kinetics, where IPD is not relevant and film diffusion does not strongly limit the adsorption. Carbon nanotubes (especially SWCNT) and graphenes are promising materials for incorporation in membranes.

4.7 Concluding remarks on the adsorption at the CNP surface

In this chapter, the steroid hormone adsorption performance of six types of CNPs, which are MWCNTs, SWCNTs, two grades of graphene, graphene oxide, and fullerene C₆₀ was evaluated in static adsorption, where the residence time ranges between 5 min and 26 h (i.e. longer than in adsorptive composite membranes). The following points are obtained from this investigation.

- All CNPs adsorbed steroid hormones very fast as a result of low mass transfer limitation, as the adsorption equilibrium was attained in <1 h at CNP concentrations of 0.05–1 g/L. IPD is irrelevant while film diffusion is facile and does not immensely limit adsorption.
- The accessible surface influences adsorption and depends on the aggregation state, which varies with time and is affected by solution chemistry. When the residence time and surface area were not limiting factors, good hormone removal (up to 99%) was attained in varied water conditions.
- SWCNT is the most capable material for membrane incorporation due to the high amount of accessible surface, which results in its fast adsorption kinetics, high adsorption capacity, and good performance in varied water conditions, even in the aggregate form.

The experimental results show that when steroid hormone micropollutants were present at realistic concentrations (*e.g.* 100 ng/L), adsorption by CNPs can be effective to reach the European guideline E2 concentration in drinking water (1 ng/L) if i) the residence time is long (*i.e.* in the order of minutes or hours), and ii) the surface area provided by CNPs is in excess and accessible by the hormone molecules. Good surface accessibility is attained when the CNP has high quantity of external surface area, and the aggregation of CNPs does not significantly obstruct the surface. Good adsorbent materials (such as SWCNT) for the incorporation in the membrane need to display very good surface accessibility, because the residence time and hence mass transfer will become limiting factors in the ACMs.

5 Influence of Mass Transfer Limitation on Steroid Hormone Adsorption

This chapter is adapted from a publication in Separation and Purification Technology (2021) entitled “Incorporation of single-walled carbon nanotubes in ultrafiltration support structure for the removal of steroid hormone micropollutants”, by Minh N. Nguyen, Phuong B. Trinh, Claus J. Burkhardt and Andrea I. Schäfer³⁰².

In the previous chapter, the influence of adsorbent surface on hormone adsorption was evaluated for six types of carbon-based nanoparticles, and single-walled carbon nanotube (SWCNT) has been selected for the incorporation in adsorptive composite membranes. This chapter continues the evaluation of steroid hormone adsorption performance, but with the SWCNT–UF membrane, the mass transfer of hormones from the bulk to the sorbed phase is limited by the short residence times in membrane filtration.

Quantitative evaluation of membrane performance is based on the steroid hormone removal and adsorbed mass (the latter is determined via mass balance). Varied experimental parameters for the characterisation of mass transfer limitation include adsorbent loading, residence time, steroid hormone type, and solution pH.

The contributions of co-authors are indicated as follows. Phuong Trinh, a Master student, participated in protocol development and performed 60% of filtration experiments and data analysis (for SWCNT–RC10 and SWCNT–PES100 membranes). Claus J. Burkhardt (NMI, Germany) performed helium ion and scanning electron microscopies to visualise the control and SWCNT composite membranes. Andrea I. Schäfer is the corresponding author of the project and conceptualised the research and provided membrane expertise. All co-authors participated in revising and editing the manuscript.

5.1 Mass transfer limitation in ACMs

Steroid hormone removal with micro-/ultrafiltration (MF/UF) membranes may be feasible if an adsorption functionality from powdered activated carbon (PAC) and carbon-based nanoparticles (CNPs) is incorporated, which result in an adsorptive composite membrane (ACM). Prior to this study, variants of PAC have been deposited on the surface or held separately in the permeate side of MF/UF membranes to remove micropollutants dynamically^{192, 226, 246}. In contrast, because of their smaller sizes¹⁵², CNPs can be deposited directly into the MF structure or UF support layer. With the permeate-side incorporation of CNPs, the adsorption performance loss caused by particle aggregation is partially avoided. As discussed in the previous chapter, certain CNPs, namely single-walled carbon nanotube (SWCNT) and graphenes, are good adsorbents and can be suitable for such incorporation.

The slow IPD process is a limiting mass transfer mechanism in the porous PAC^{112, 229}, which means the residence times need to be sufficiently long for the micropollutants to diffuse into the adsorbent pores. As a result, in dynamic membrane adsorption, the adsorbed amount of micropollutants (steroid hormones) with PAC decreases with decreasing residence times^{192, 246}. In contrast, IPD is not a limiting mass transfer mechanism in certain CNPs that have dominant external and accessible surfaces such as SWCNT²²². Good adsorption may be achieved with adsorptive composite membranes (ACMs) that incorporate SWCNT, because of the high external surface areas and good intrinsic mass transfer of the material^{169, 516}. In this regards, good adsorption performance can be anticipated within relatively short residence times in membrane technology (sub-seconds to a minute)¹⁷⁹.

However, despite the good accessibility of hormones to the adsorbent surface, hormone removal in dynamic membrane adsorption may not be as high as those in static adsorption. Beside the great difference in residence times between the two experiment types (at least 5 min in static adsorption vs. below 1 min in dynamic membrane adsorption), hormone adsorption can be affected by the i) surface inhomogeneity caused by aggregation^{168, 169, 252} (as such some adsorbent surface is concealed and not accessible), and ii) water / solute channelling⁴⁵⁴ through less dense regions of the adsorbent (SWCNT) layer. The mass transfer limitation caused by the above processes may limit adsorption.

In this chapter, a simplistic SWCNT–UF composite membrane with a sub-millimetre adsorbent layer is evaluated for hormone removal. The objective of this chapter is to determine how the design (SWCNT loading), operational (pressure) and water quality factors (pH and hormone type) influence the mass transfer and steroid hormone adsorption by the SWCNT–UF. With this research objective, the chapter seek to determine: i) the required SWCNT loading for effective steroid hormone adsorption, ii) whether hormone adsorption is limited by the residence time, and iii) how hormone adsorption is affected by varying the water quality, namely pH and hormone type.

5.2 Experimental methods to determine hormone adsorption

5.2.1 Composite membrane (SWCNT–UF) preparation

The base UF membranes are the described in Section 3.3.2, which have regenerated cellulose (RC) or polyethersulfone (PES) dense layer, and polyolefin support structures. The particular membranes used in this chapter investigation are the RC 10 kDa (code PLHGC), RC 100 kDa (code PLHHK) and PES 100 kDa (code PBHK), all supplied by Merck Millipore, USA. The corresponding composite membranes with SWCNT incorporation are named SWCNT–RC10, SWCNT–RC100, and SWCNT–PES100.

The preparation of these SWCNT–UF membranes is described in Section 3.3.3. A single preparation method with the vacuum filtration apparatus was used as shown in Figure 3.3 A. In brief, the base membrane (with a diameter of 7 cm) was mounted upside-down in the vacuum filtration funnel, and 4.2–168 mL aliquots of SWCNT suspension (0.1 g/L SWCNT and 0.1 wt.% Triton-X100 surfactant) was poured onto this membrane to obtain SWCNT loadings in SWCNT–UF membranes of 0.1–4 g/m². The SWCNT was deposited into the support structure of the UF as visualised in Figure 5.1, where both the rod-like structures (diameter 2–3 nm) and aggregates of SWCNTs were attached to the non-woven membrane support fibre.

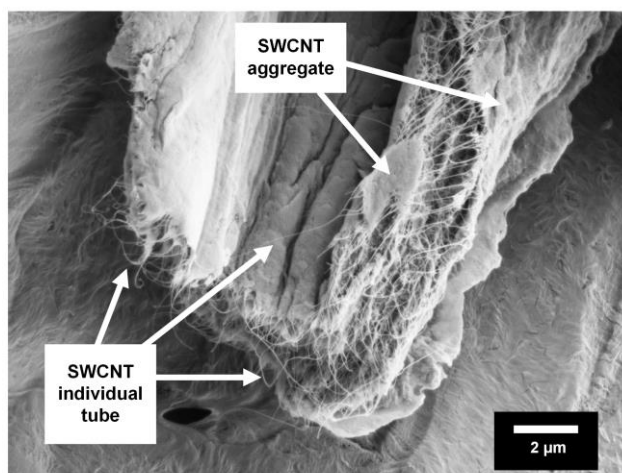


Figure 5.1: High-resolution micrograph of SWCNT deposits on a support structure of an UF support structure (loading 2 g/m²), showing SWCNTs as individual rod-like structures (with diameters of around 2–3 nm), and in aggregate form. Reprinted from Nguyen *et al.*³⁰².

5.2.2 Filtration experiments

The investigated parameters in this chapter are loading (from 0.1 to 4 g/m²) and pressure (from 0.5 to 4 bar) with all three composite membranes, and solution pH (from 2 to 12) and steroid hormone type (E1, E2, T and P) for SWCNT–RC10 membrane. The summary of the experimental design and conditions is given in Table 5.1.

Table 5.1: Overview of the filtration experiment design and conditions.

Investigated parameter	Membrane type	Loading (g/m ²)	Pressure (bar)	Solution pH	Hormone type
Loading	RC 10 kDa RC 100 kDa PES 100 kDa	0.1–4	1	8.1	E2
Pressure	RC 10 kDa RC 100 kDa PES 100 kDa	2	0.5–4	8.1	E2
pH	RC 10 kDa	2	10–10 ⁶	2–12	E2
Hormone type	RC 10 kDa	2	100	8.1	E1, E2, T, P

The micro-crossflow filtration system described in Sub-chapter 3.1 was operated in crossflow mode, with a uniform pump flow rate of 30 mL/min, which is equivalent to a crossflow velocity of nearly 0.1 m/s. The filtration protocol is provided in Appendix G. The exposed surface area of the SWCNT layer is assumed to be the same as the membrane filtration area (2 cm²), as discussed in Appendix H.

A drawback of this filtration protocol is that the permeate samples were collected according to time instead of permeate volume. The total permeate volume obtained after a certain filtration time of 3 h varied because these are specific for the membrane type and operating condition (especially applied pressure). Hence, adsorbed masses at the same permeate volume had to be estimated from the breakthrough curves so that the comparison of adsorption between membranes can be valid. The filtration protocol was improved in the subsequent research project with SWCNT–UF membranes (as presented in the next chapter).

The analytical technique (liquid scintillation counting, LSC) for steroid hormone determination is described in Section 3.4.1.

5.2.3 Membrane characterisation

Scanning electron microscopy (SEM) and helium ion microscopy (HIM) were performed by Claus J. Burkhardt (from NMI, Reutlingen, Germany) to visualise the membrane structures and morphologies (for the dense layer, middle support layer, and non-woven support structure), and the deposition of SWCNT in non-woven support layer. The description of these microscopic techniques is given in Section 3.7.2.

5.3 Filtration property of the single-walled carbon nanotube – ultrafiltration membrane (SWCNT–UF)

5.3.1 Pure water permeability of SWCNT–UF

The incorporation of SWCNTs might obstruct the water flow through the UF membrane and increase the membrane resistance. To determine whether this flow obstruction is relevant, pure water permeabilities of the single blank (SB, single membrane without SWCNTs) and double blank (DB, two membranes stacked on top of each other without SWCNTs) were compared with those of SWCNT–UF membranes, as shown in Figure 5.2.

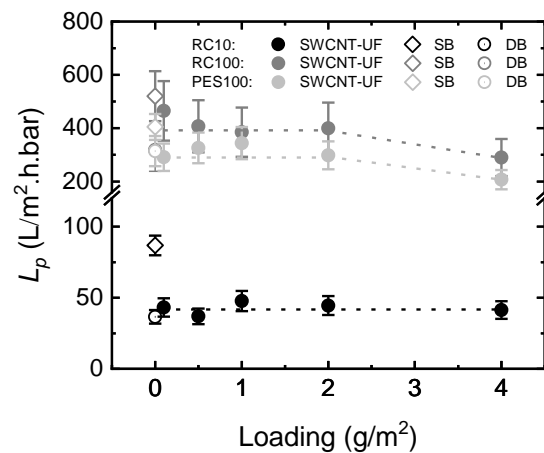


Figure 5.2: Pure water permeability L_p of the single blank (SB), double blank (DB), and SWCNT–UF membranes at different SWCNT loadings. Adapted from Nguyen *et al.*³⁰².

The permeability of the DB was approximately half of that of the SB, which is expected because the membrane thickness and hence resistance was doubled in the DB^{402, 403}. However, SWCNT incorporation did not cause any further noticeable flux decline, because the permeabilities of composite membranes with different SWCNT loadings were similar to those of the pristine DB. To explain this observation, two hypotheses are proposed: i) pore blockage was not relevant, and/or ii) the SWCNT packing was loose enough and caused no significant obstruction to the water flow.

For pore blockage to occur, the size of the incorporated particles must be in the same magnitude as that of the membrane pores. A decrease in membrane permeability has been reported when the membrane pore and particle sizes are similar. For example, Ellerie *et al.* investigated the deposition of various carbon particles in MF membranes (pore size 0.1 μm), and observed flux declines of 4% and 17% with the deposition of MWCNTs and superfine PAC, respectively²²⁶. Pore blockage was more relevant for superfine PAC with a particle size of $\sim 0.24 \mu\text{m}$, compared with MWCNTs where the aggregate sizes varying from 200 μm to several millimetres. Similarly, Ajmani *et al.* reported that pore blocking occurred when MWCNTs were stabilised with surfactants before its deposition in MF 0.45 μm membranes; the baseline permeability reduced from a few thousands to 130 $\text{L}/\text{m}^2\cdot\text{h}$ (*i.e.* the UF range)⁵¹⁷.

In this work, the UF pore sizes are between 5–18 nm, while SWCNTs in suspension could form much larger aggregates. In addition, SWCNTs were deposited in the much more open support structure of the asymmetric UF, and the SWCNT aggregates might not penetrate the dense layer during incorporation. In the next section, the deposition of SWCNT in the UF support structure will be confirmed *via* scanning electron microscopy (SEM).

5.3.2 Visualisation of the SWCNT–UF membrane layers

To link the permeability results with the morphology of the SWCNT layer, the distribution and penetration depth of SWCNTs were visualised *via* scanning electron microscopy (SEM). SEM was performed by Claus. J. Burkhardt (NMI) with the support structures and cross-sections of SWCNT–UF membranes. A selection of micrographs is given in Figure 5.3.

Figure 5.3 A, C and E show the support structures of the RC 10 kDa, RC 100 kDa and PES 100 kDa membranes, respectively. The RC and PES membranes have similar non-woven support structures where SWCNT can be deposited on the fibres and in the spaces between fibres. However, the spaces between the fibres of PES 100 kDa were partially filled by membrane support material, so the loading capacity of this membrane may be less than those of the RC.

As observed in Figure 5.3 B, D and F, the distribution of SWCNTs is uneven, because of the insufficient loading and/or aggregation of the SWCNTs. This uneven distribution is clear in the cross-section micrograph of an SWCNT–UF (Figure 5.3 G). Because of the loose packing, water can flow through the SWCNT layer with little or no resistance, which explains the high water permeabilities of the SWCNT–UF membranes relative to the DB ones. However, the selective flow paths of water may result in poor contact between the SWCNT and hormones, and hence the adsorption efficiency cannot be as high as in static adsorption. This flow selectivity has been extensively characterised for microporous structures⁴⁵⁴, and the same phenomenon is expected in the support structure of UF where SWCNTs are deposited.

Overloading may occur at the higher loading of 4 g/m². This phenomenon can be observed in Figure 5.3 H where a layer of SWCNTs covered the top of the support structure. The loading capacity in theory is determined to be around 11 g/m² (see Appendix I), but in practice this value is lower and may depend on two factors. Firstly, SWCNT aggregation prevents the penetration of SWCNT into narrower spaces, leading to lower loading capacity and poorer contact between the SWCNT and adsorbates (as mentioned above). Secondly, the penetration of SWCNTs in vacuum filtration was not controlled, as such denser membranes (RC 10 kDa) was penetrated more slowly than the looser membranes (RC and PES 100 kDa). Hence, SWCNT–RC10 may have lower loading capacity than SWCNT–RC100 and SWCNT–PES100.

Overloading increases the risk of SWCNT leakage, which leads to a less effective contact for adsorption, causes irreproducible results and raises toxicological concerns. As such, there is a small window for SWCNT loading that may limit the applicability of these ACMs. In the next section, steroid hormone adsorption by SWCNT–UF with a range of SWCNT loadings (0.1–4 g/m²) will be evaluated.

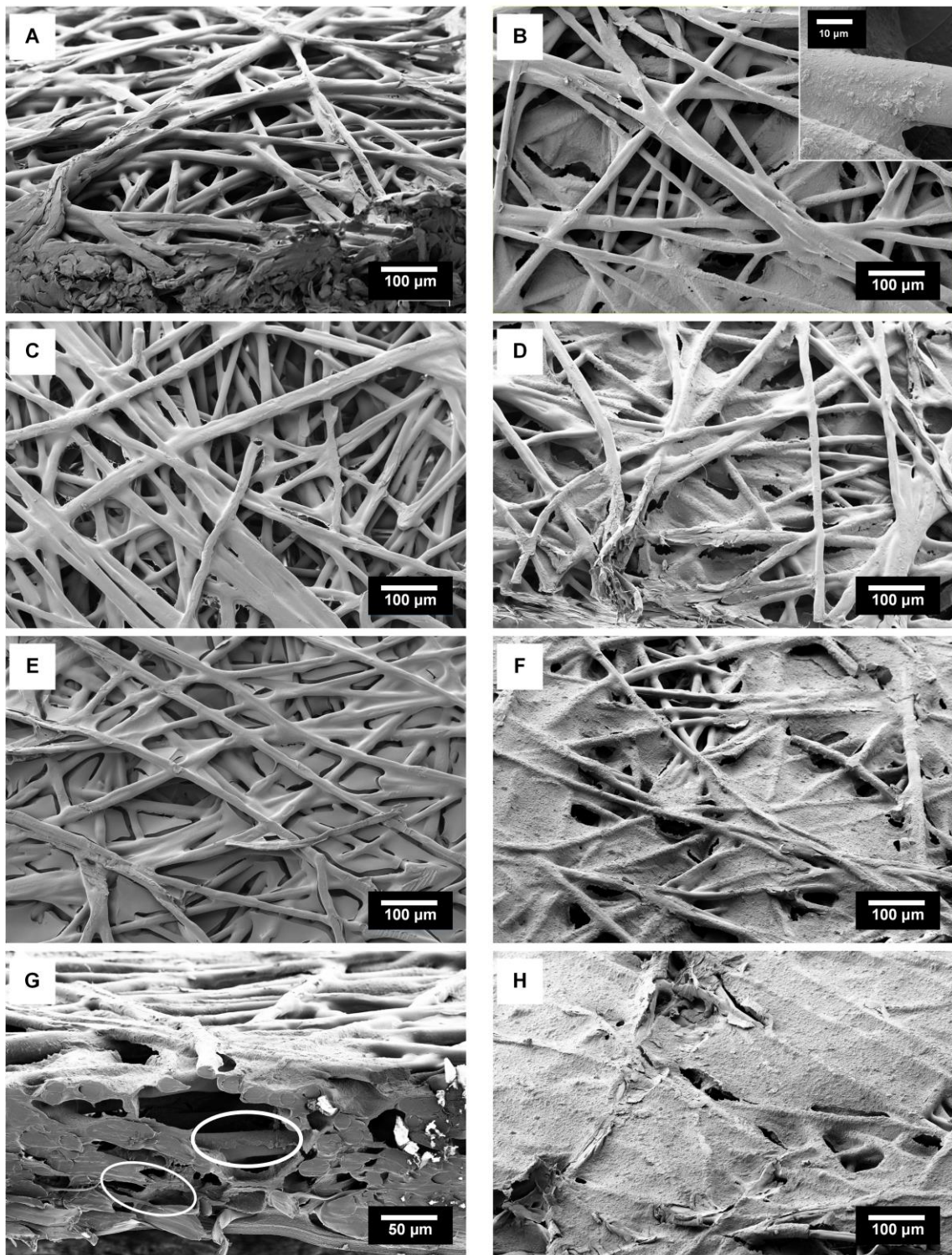


Figure 5.3: A, C and E – Respective surfaces of the support layer of RC 10 kDa, RC 100 kDa and PES 100 kDa; B, D and F – Respective surfaces of the support layer of SWCNT-RC10, -RC100 and -PES100 at 2 g/m^2 (the inset in B shows the coating of SWCNTs); G – Cross-section of SWCNT-RC100 at 2 g/m^2 ; H – Surface of SWCNT-PES100 at 4 g/m^2 that shows overloading. Adapted from Nguyen *et al.*³⁰².

5.4 Influence of SWCNT loading on hormone adsorption

5.4.1 Breakthrough of steroid hormone

The evolution of hormone concentration with filtration time or total permeate volume is referred to as the hormone breakthrough. The shape of this breakthrough curve allows a qualitative evaluation of the dynamic adsorption process. For UF membranes, a full hormone breakthrough (where the membranes materials are fully saturated with steroid hormone) is indicated when the permeate hormone concentration is equal to the feed concentration. The breakthrough curves corresponding to E2 adsorption by the pristine membranes (SB and DB) and SWCNT–UF at varied loadings are given in Figure 5.4 and Figure 5.5.

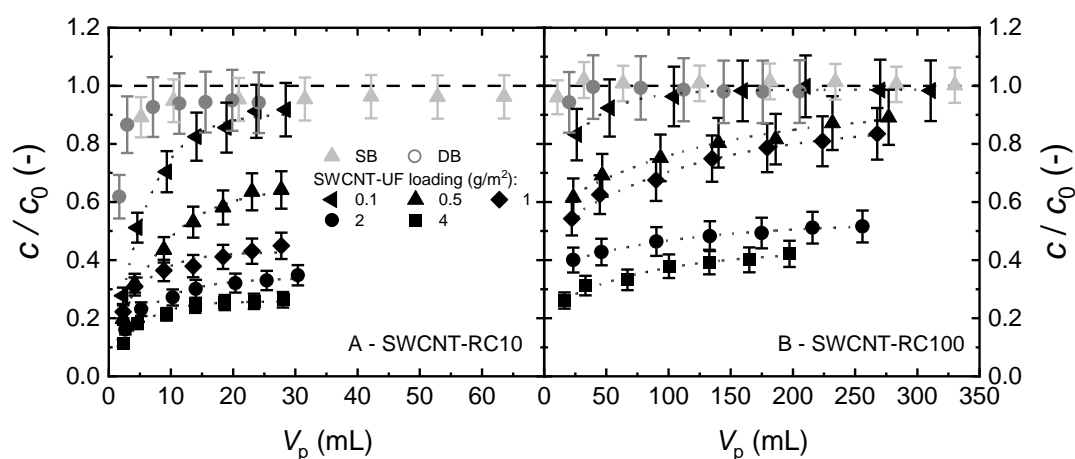


Figure 5.4: E2 breakthrough of SB, DB, and SWCNT–UF at different loadings. 100 ng/L E2, 1 mM NaHCO₃, 10 mM NaCl, 24 ± 2 °C, pH 8.2 ± 0.1, pressure 1 bar. Volume scale is different between 10 kDa and 100 kDa membranes. Reprinted from Nguyen *et al.*³⁰².

As seen from Figure 5.4 A and B, the SB and DB of RC membranes (10 and 100 kDa) adsorbed very little E2, where a complete breakthrough was observed and the saturation point was reached after only 10–15 mL of treated volume. With the corresponding SWCNT–RC10 and SWCNT–RC100 membranes at loadings >0.1 g/m², the breakthrough was incomplete and characteristic for early-stage adsorption. At any given permeate volume, the permeate concentration decreases with increasing SWCNT loading. With the 0.1 g/m² loading, adsorption saturation was approached after 30 mL and 100 mL of treated volume in SWCNT–RC10 and SWCNT–RC100, respectively.

From the above findings, it is implied that E2 removal was limited by the accessibility of the SWCNT surface. At the very low loading (0.1 g/m²), the contact between the hormone and adsorbent is especially poor because SWCNTs distribute non-uniformly, and water channels through the less dense SWCNT regions.

Unlike the RC membranes, the pristine PES 100 kDa membranes already adsorbed significant amounts of steroid hormones (Figure 5.5). Adsorption saturation was not reached in 3 h, or around 200–250 mL of treated volume, for both the SB and DB. E2 removal at 200 mL (or 1000 L/m²)

is around 70% for SB and 90% for DB. This is in vast contrast to RC 10 and 100 kDa DB in Figure 5.4, where the breakthrough curve was complete within a significantly less volume (40 mL, or 200 L/m²). It appears that the filtration time in this study was not long enough to overcome the interference of the PES material with adsorption. As such, the adsorption contributed by SWCNTs was not determined.

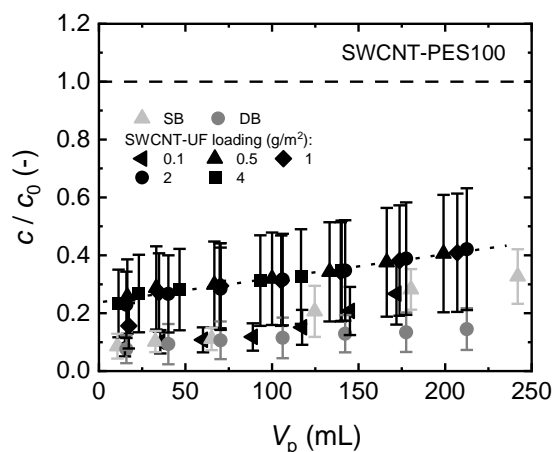


Figure 5.5: E2 breakthrough of SB and DB of PES 100 kDa, and SWCNT-PES100 at different loadings. 100 ng/L E2, 1 mM NaHCO₃, 10 mM NaCl, 24 ± 2 °C, pH 8.2 ± 0.1, pressure 1 bar. Adapted (extracted) from Nguyen *et al.* ³⁰².

Several other works also report good hormone adsorption by PES membranes. Jermann *et al.* pointed out that E2 removal by the same PES 100 kDa was consistently high at 80% from 100 ng/L feed, until 215 L/m² of permeate was collected. Zhang *et al.* also determined that E2 removal by the PES 100 kDa DB gradually decreased from very high (>90%) at 180 L/m² to around 20% at 1800 L/m²; adsorption saturation was not reached in this experiment ²⁴⁶.

In summary, the loading appears to control the adsorption performance of SWCNT-UF, because the higher loading, the more accessible surface of SWCNT is available for adsorption. If the base membrane material (such as PES) can adsorb much hormone, the contribution from SWCNTs in the permeate side is not significant, and a longer filtration time may be needed to observe the enhancement.

5.4.2 Influence of SWCNT loading on E2 adsorption

The breakthrough curves only provide an impression of how E2 was adsorbed by the composite membranes. A quantitative analysis requires the determination of E2 adsorbed mass from the mass balance. E2 removal R_{E2} and specific adsorbed mass $q_{ads,s}$ (as mass of E2 per mass of SWCNTs) at fixed treated volumes, 25 mL for 10 kDa and 180 mL for 100 kDa membranes, are plotted as functions of loading in Figure 5.6.

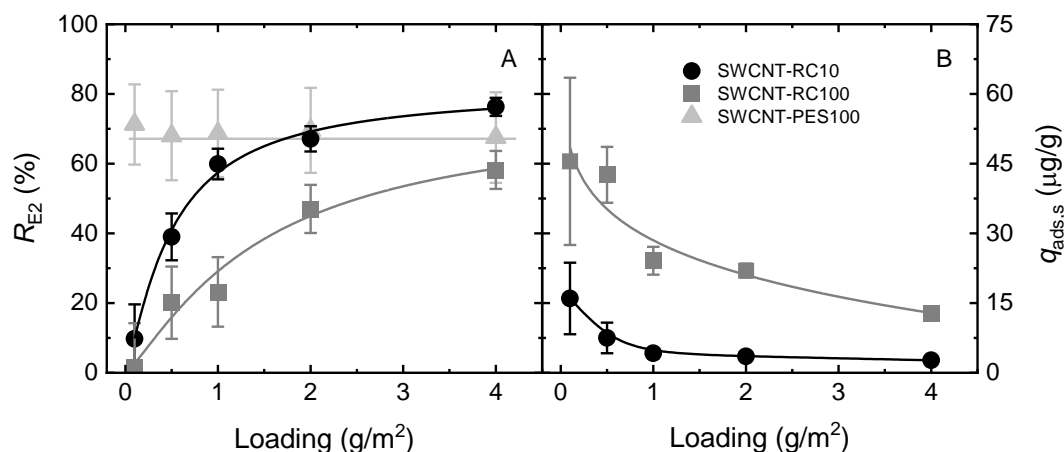


Figure 5.6: E2 removal R_{E2} and specific adsorbed mass by SWCNTs $q_{ads,s}$ at a permeate volume of 25 mL for 10 kDa and 180 mL for 100 kDa membranes. Adsorbed mass for SWCNT–PES100 was not determined because of the strong adsorption by the blank membranes. 100 ng/L E2, 1 mM NaHCO₃, 10 mM NaCl, 24 ± 2 °C, pH 8.2 ± 0.1, pressure 1 bar. Adapted (extracted) from Nguyen *et al.* ³⁰².

Figure 5.6 A shows an increasing trend in E2 removal of SWCNT–RC10 and SWCNT–RC100 with loading, implying that E2 adsorption was limited by the amount of SWCNTs. In Figure 5.6 B, the specific adsorbed mass per SWCNT mass decreases with loading because at higher loadings, the adsorption sites of SWCNT are less likely a limiting factor. In contrast, for SWCNT–PES100, E2 removal was independent of the SWCNT loading (Figure 5.6 A), because the adsorption sites of SWCNT is not limiting where the blank membranes contributed much to adsorption.

To explain how the SWCNT loading controlled E2 adsorption, two hypotheses can be given: i) the number of total adsorption sites of SWCNTs were too low to accommodate the E2, or ii) the diffusion of E2 into the less accessible adsorption sites of SWCNTs was the limiting factor.

The first hypothesis cannot be correct, because the theoretical adsorption capacity was 360 mg/g (see Appendix J), which is around 10⁵ times higher than the maximum adsorbed mass (0.05 mg/g) determined in the experiment with the lowest (0.1 g/m²) loading. Therefore, the total surface of SWCNTs cannot be a limiting factor for the dynamic adsorption.

Only the second hypothesis is appropriate. In static adsorption where the residence time ranged between 5 min to 26 h, E2 removal at equilibrium was high (97–99%) and independent of the SWCNT concentration (see previous Chapter 4). E2 access to the SWCNT surface was not a limiting factor because the long residence time overcame the mass transfer resistance and provided sufficient contact for adsorption. In a dynamic membrane process (in this chapter), the residence times in SWCNT–UF are relatively short (3.3 s for SWCNT–RC10 and 0.3 s for SWCNT–RC100, see Section 3.5.3 for the calculation), hence E2 did not have enough time to diffuse i) from the open channel to the SWCNT surface (as a result of water channelling⁴⁵⁴), and ii) from the SWCNT proximity to the more obstructed adsorption sites. As a result, only a fraction of the SWCNT surface was accessed by the hormones.

The above explanation is not valid for SWCNT–PES100 because a significant amount of E2 had been adsorbed by the top PES membrane and only little amount of E2 reached the SWCNT layer.

To improve E2 adsorption, the SWCNT loading may be increased and/or alternative materials to these SWCNTs with higher external surfaces need to be found. For SWCNT–UF, the theoretical maximum loading is only 11.5 g/m² (see Appendix I), so a redesign of composite membrane is needed to achieve a significantly higher adsorbent loading. In the PBSAC–UF hybrid system where PBSAC were arranged in a 2 mm layer, Tagliavini *et al.* achieved very low permeate concentrations of E2 that approach the European guideline (of 1 ng/L)¹⁹³. The ‘loading’ of PBSAC was around ~1000 g/m², which is impossible to attain with an ACM.

In the next experiments with a fixed SWCNT loading, the 2 g/m² loading was selected instead of the 4 g/m² one because the latter resulted in modest increase in E2 removal at the expense of twice the adsorbent quantity. In addition, SWCNT leakage and irreproducible results may happen if overloading occurs.

5.5 Influence of residence time on hormone adsorption

5.5.1 The link between flux, pressure, and residence time

E2 adsorption by SWCNT–RC10 and SWCNT–RC100 was evaluated with varying hydraulic residence time, to determine whether E2 diffusion to the SWCNT surface limits adsorption. The residence time was varied *via* adjusting the pressure in the range of 0.5–4 bar. The relationship between the pressure, flux and residence time is shown in Section 3.5.3. With the assumption that the UF membrane consists of cylindrical pores with a uniform porosity, pressure is proportional to flux and inversely proportional to residence time as illustrated in Figure 5.7.

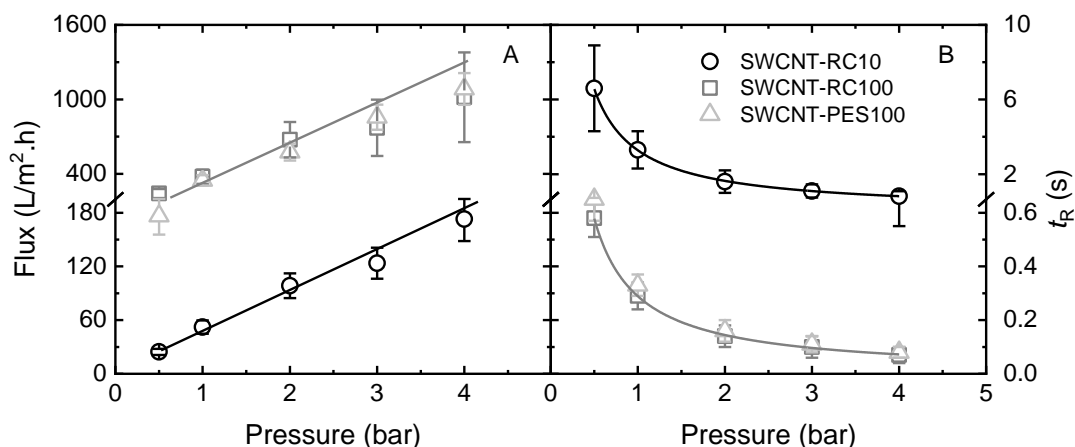


Figure 5.7: Flux and residence time in SWCNT–UF vs. pressure (100 ng/L E2, 2 g/m² loading, 1 mM NaHCO₃, 10 mM NaCl, 24 ± 2 °C, pH 8.2 ± 0.1). Adapted from Nguyen *et al.*³⁰².

Figure 5.7 A confirms that pressure is proportional to the flux derived from the change in permeate mass in experiments. A flux decline of ~25% in the three hours of filtration with 100 kDa

membranes at 3 and 4 bar was observed, which may be caused by system instability when operating a high-MWCO UF membrane at relatively high pressures (it is noteworthy that the pressure range for all UF is 0.1–5 bar¹²⁹). This flux variation is presented as the average value \pm error in Figure 5.7 A. The corresponding hydraulic residence time data in SWCNT–UF were given in Figure 5.7 B. As the pressure increased from 0.5 bar to 4 bar, the residence time decreased reciprocally from 7.1 to 0.8 s for 10 kDa membranes, and from 0.6 to 0.08 s for 100 kDa membranes. The residence time difference between 3 bar and 4 bar pressures is no longer clear.

5.5.2 Influence of flux / residence time on hormone adsorption

To determine whether E2 adsorption was limited by the residence time, E2 removal and adsorbed mass after a three-hour filtration was determined as functions of pressure and residence time in Figure 5.8. Because of the higher pressure, the more solution filtered after a fixed filtration time, the mass of E2 in contact with SWCNT–UF was not controlled. Hence, in Figure 5.8, the adsorbed mass was corrected with the total permeate volume (V_p), which allows comparison between membranes.

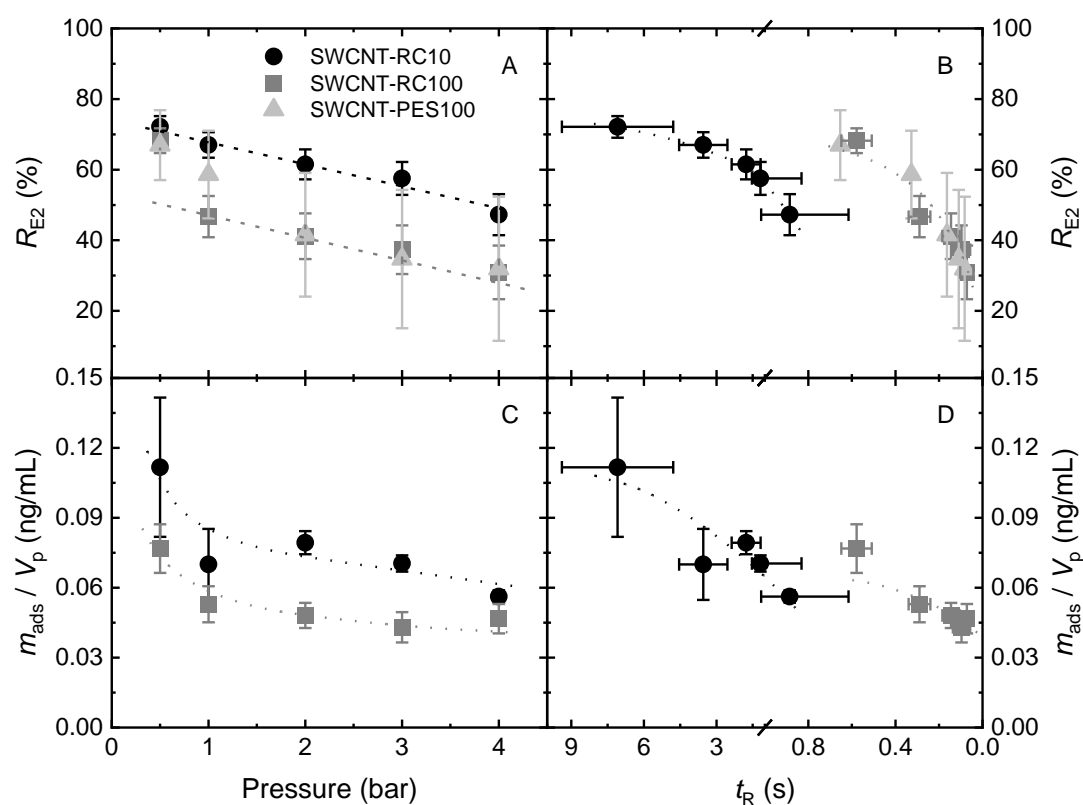


Figure 5.8: E2 removal R_{E2} (A and B) and adsorbed mass corrected by the treated volume m_{ads} / V_p (C and D) after three hours vs. pressure and residence time. Adsorbed mass with SWCNT–PES100 was not determined because of the strong adsorption by the blank membranes. 100 ng/L E2, 2 g/m² loading, 1 mM NaHCO₃, 10 mM NaCl, 24 \pm 2 $^{\circ}$ C, pH 8.2 \pm 0.1. Adapted from Nguyen *et al.*³⁰².

According to Figure 5.8 A and B, E2 removal after 3 h by both the SWCNT–RC100 and RC100 decreased with increasing pressure and decreasing residence time. Because E2 removal at a given time was driven by the amount of E2 that had been taken up, it is confirmed that the accessible surface area of SWCNTs could limit adsorption. The volume-corrected adsorbed mass slightly decreased with increasing pressure and decreasing residence time as seen in Figure 5.8 C and D. However, adsorption saturation (where E2 removal is 0%) was not achieved in any of the experiments with SWCNT–RC10 and SWCNT–RC100, which emphasised that SWCNT–UF will continue to adsorb E2 after a treated volume of 650 mL (or 3200 L/m²).

In the next step, E2 removal and adsorbed mass were compared at the same treated volumes, of 14 mL for 10 kDa and 100 mL for 100 kDa membranes, (see Figure 5.9). These volumes were the respective volumes of E2 solution treated in three hours at 0.5 bar.

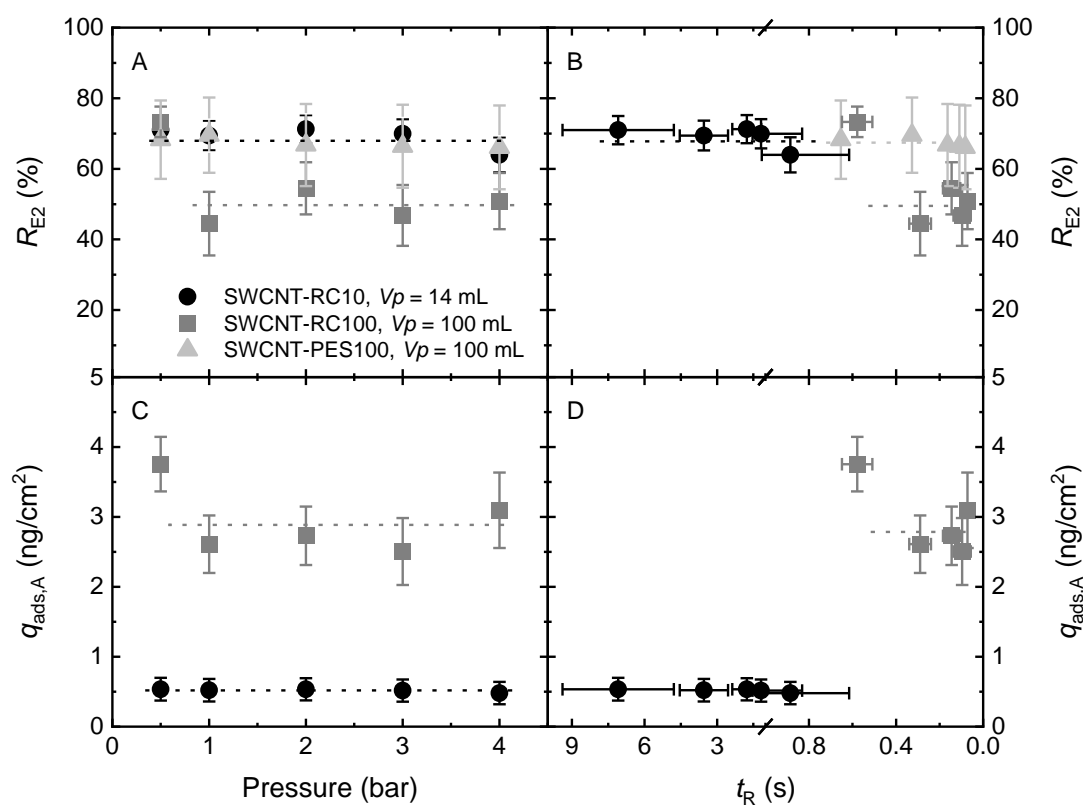


Figure 5.9: E2 removal R_{E2} (A and B) and specific adsorbed mass $q_{ads,A}$ (C and D) by SWCNT–UF membranes at the same treated volumes (indicated in the legend) vs. pressure and residence time t_R . Adsorbed mass for SWCNT–PES100 was not determined because of the strong adsorption by the blank membranes. 100 ng/L E2, 2 g/m² loading, 1 mM NaHCO₃, 10 mM NaCl, 24 ± 2 °C, pH 8.2 ± 0.1. Adapted from Nguyen *et al.* ³⁰².

When the treated volumes were standardised, E2 removal and adsorbed mass were independent of pressure in the range of 0.5–4 bar. The corresponding hydraulic residence time range in SWCNT–UF was 7.1–0.08 s. It appears that the adsorption kinetics was very fast and did not limit E2 adsorption at the most accessible surface of SWCNTs. Therefore, the mass transfer

resistance was not important, even when the residence times were only several seconds or sub-seconds.

Similar conclusion was reached in Chapter 4 for hormone adsorption by SWCNTs but with longer residence times (of minutes or hours) in static adsorption. Unlike the SWCNT–UF, the PBSAC–UF hybrid system showed a decrease in E2 adsorption with increasing flux¹⁹², where mass transfer resistance was a limiting mechanism with PBSAC because the short residence times prevent E2 from finding surface inside the PBSAC pores. The SWCNT–UF in this work could be advantageous because SWCNTs possess higher amount of external and immediately accessible surface than PBSAC.

5.6 Influence of water chemistry on hormone adsorption

5.6.1 Influence of pH on E2 adsorption

In this section, the impact of water quality (pH) on E2 removal by an SWCNT–UF will be assessed. Water pH can influence charge interactions and hence steroid hormone adsorption by SWCNT–UF. Therefore, E2 adsorption by SWCNT–RC10 was evaluated in the pH range of 2–12. The pH of natural waters is typically between 6.5 and 9.5, and the pH of drinking water according to the WHO guideline is between 6.5 and 8.5⁵¹⁸. However, extreme pH can be found in effluents from mining or alkaline scrubbing processes^{519,520}. E2 removal and adsorbed mass at 25 mL of treated volume are shown in Figure 5.10.

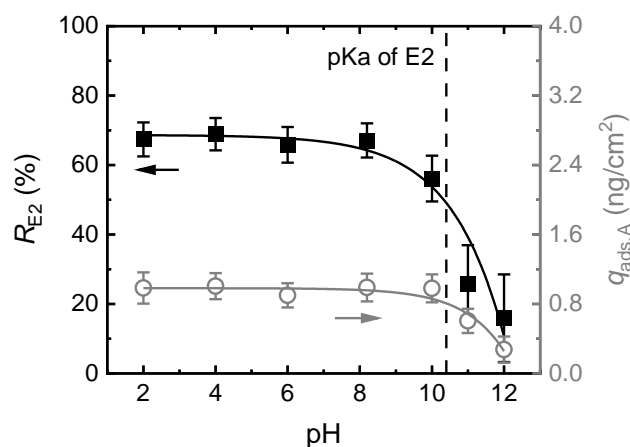


Figure 5.10: E2 removal R_{E2} and specific adsorbed mass $q_{ads,A}$ by SWCNT–RC10 at 25 mL vs. pH. Vertical line indicates the pKa of E2 according to Perrin²⁸⁹. 100 ng/L E2, 2 g/m² loading, 1 mM NaHCO₃, 10 mM NaCl, 24 ± 2 °C, pressure 1 bar. Adapted from Nguyen *et al.*³⁰².

From Figure 5.10, E2 removal was high (~70%) and independent of pH in the range of 2–8.2. The isoelectric point of the RC10 membrane was 3.3³²⁴, so E2 adsorption was not affected by whether the UF surface was charged or neutral. At pH 10–12, E2 removal decreased from 60%

to 15–20%, which is connected to the deprotonation of E2 at pH 10.2–10.7²⁸⁹⁻²⁹¹. In summary, pH has a significant impact on the E2 adsorption by the SWCNT composite membranes.

It is noted that the surface of SWCNTs has an overall close-to-zero charge at all pH (see Chapter 4). Hence, E2 adsorption by SWCNTs is based on hydrophobic interactions²⁵⁷, and expected to not depend on the charge of E2. In static adsorption, this E2 charge independence was found following expectations (Chapter 4). However, in the dynamic membrane process where the residence time is short, E2 is likely adsorbed only at the most accessible surface, and some local characteristics of such surface (at the tips and defects) may result in poorer adsorption of deprotonated E2 ions. When E2 is deprotonated at high pH, its capacity of donating hydrogen decreases and the chance of its repulsion by a negatively-charged local surface is more significant (see Section 2.4.4).

5.6.2 Impact of hormone type on E2 adsorption

To determine the capability of SWCNT–RC10 to adsorb different hormone types, four hormones (E1, E2, T and P) were tested with this membrane in filtration experiments. The main differences between the hormones include molecular weight, aromaticity (*i.e.* the presence of π -ring), dipole moment and number of hydrogen bond donors (see Table 3.3). Hormone removal and adsorbed mass after 25 mL of permeate volume are given in Figure 5.11.

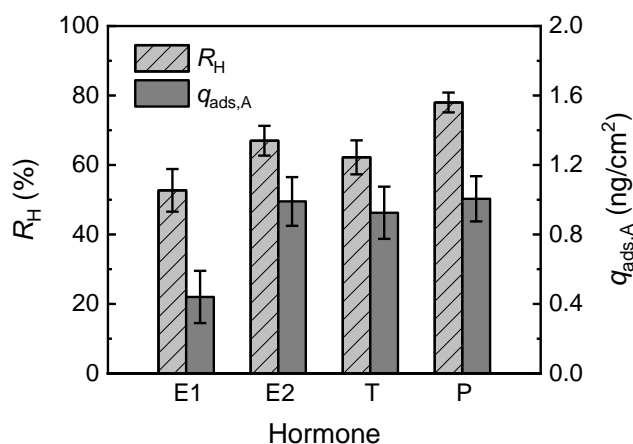


Figure 5.11: Hormone removal R_H and specific adsorbed mass $q_{ads,A}$ at 25 mL by SWCNT–RC10. 100 ng/L hormone, 2 g/m² loading, 1 mM NaHCO₃, 10 mM NaCl, 24 ± 2 °C, pH 8.2 ± 0.1, pressure 1 bar. Adapted from Nguyen *et al.*³⁰².

As seen from Figure 5.11, hormone removal varied between 50% and 75% in the following order: E1 < T ≈ E1 < P. Hormone adsorbed mass followed the same trend as hormone removal, although the error bars in adsorbed mass overlapped for E2, T and P and prevented the comparison between these three hormones. An adsorbed mass of 1.0 ng/cm² was then reported for E1, E2 and P.

In contrast, E1 adsorbed mass was significantly lower, at 0.4 ng/cm². The above trends in removal and adsorbed mass were explained by the different physiochemical properties of the four hormones. However, it was unclear which property was the most impactful to adsorption. In static

adsorption, the adsorbed mass of all four hormones were similar (see Figure 4.6), therefore it can be implied that the short residence times lead to a small degree of selectivity of the steroid hormones.

5.7 Concluding remarks on the mass transfer limitation

This chapter evaluates the steroid hormone adsorption performance of a simplistic ACM (SWCNT–UF) where SWCNTs were mechanically incorporated between two UF membranes. Steroid hormone removal was achieved indicating the feasibility of this ‘sandwich’ membrane. The following points are obtained from this investigation:

- With an SWCNT loading of 2 g/m², SWCNT–UF removed 50–75% of steroid hormones after 3 h, which is lower than hormone removal by SWCNT in static adsorption. This finding indicates that mass transfer limitation plays an important role.
- Hormone (E2) adsorption by SWCNT–UF is limited by the hormone accessibility to the SWCNT surface. Adsorption increases with SWCNT loading because the higher loadings provide more external surface for hormone access with low mass transfer limitation.
- At the most accessible surface of SWCNT, hormone adsorption was not influenced by varying residence time in SWCNT–UF between 7.1 and 0.08 s. At this surface, the mass transfer limitation caused by limited residence times is overcome.

The above experimental results indicate that, even when the total surface area of adsorbents is in excess compared to the amount of adsorbed hormone, the mass transfer limitation is relevant in controlling adsorption because of the i) uneven distribution of adsorbents in ACMs / SWCNT–UF, ii) presence of less accessible surface, and iii) short residence times in the membrane. Achieving the European drinking water guideline value of 1 ng/L for E2⁵²¹ will require further optimisation of membranes and adsorbents. To improve steroid hormone removal, the following strategies can be considered: i) increasing the adsorbent loading with alternative membrane designs to increase the amount of accessible surface, and/or ii) using alternative adsorbents that afford higher accessible surface and/or better mass transfer than SWCNTs. When such improvements are realised, the composite can excel over NF/RO because of the lower specific energy consumption typical for UF membranes.

6 Mass Transfer Limitation Caused by Organic Matter

This chapter is adapted from a publication in Water Research Journal (2021) entitled “Organic matter interference with steroid hormone removal by single-walled carbon nanotubes - ultrafiltration composite membrane”, by Minh N. Nguyen, Rubén Hervás-Martínez and Andrea I. Schäfer³⁰⁵.

This chapter investigates the interference of organic matter (OM) with steroid hormone adsorption by the SWCNT–UF described in the previous chapter. Liquid chromatography – organic carbon detection (LC-OCD) was employed to determine the OM characteristics. Quantitative evaluation of hormone adsorption is based on the steroid hormone removal and adsorbed mass (the latter is determined via mass balance).

OM can reduce the steroid hormone adsorption performance via two interference mechanisms: direct competition as the OM blocks the hormone access to surface, and indirect competition as the OM binds with the hormone and this OM–hormone complex has lower accessibility to the adsorbent surface. Both mechanisms can be involved in limiting the mass transfer of hormone from the bulk to the sorbed phase. Varied parameters for the characterisation of OM interference include nine OM types (glucose, alginate, humic acid, Australian natural organic matter, tannic acid, tannin, tea extract, worm farm extract and fermentation products), four steroid hormone types (E1, E2, T and P), residence time, and membrane MWCO. The membrane MWCO was evaluated as an interference control strategy, as such a low membrane MWCO may retain the interfering OM and maintain good hormone adsorption by the permeate-side SWCNTs.

The contributions of co-authors are indicated as follows. Rubén Hervás-Martínez, a Master student, assisted by performing the majority (around 70%) of filtration experiments, with varying UF MWCO (ten experiments), OM type (six types out of nine), hormone type (four experiments) and residence time (five experiments). Andrea I. Schäfer is the corresponding author of the project and conceptualised the research and provided membrane expertise. All co-authors participated in revising and editing the manuscript.

6.1 Interference of organic matter (OM) with steroid hormone adsorption

Incorporation of adsorbents in high-permeability MF/UF membranes to remove micropollutants from water is an interesting and feasible concept. In the previous chapter, good removal of steroid hormones with a simplistic SWCNT–UF composite membrane has been demonstrated, although the water matrix was simple with only 1 mM NaHCO₃ and 10 mM NaCl. In real water matrices, compounds such as organic matter (OM) that are present in mg/L concentrations can interfere with steroid hormone adsorption in a more significant way.

As reviewed in Section 2.5.3, OM can interact with both adsorbents (here SWCNTs) and hormones in respective OM–SWCNT and OM–hormone binary systems. MW-/SWCNTs have a high exposed surface for interaction with OM³⁰⁶ *via* hydrogen bonding, π / π stacking and hydrophobic effect^{307,308}. Aromatic OM such as HA and tannic acid (TA) can be adsorbed by the carbon nanotubes at capacities of hundreds of mg/g^{307,310-312}, while hydrophilic and non-aromatic OM types are adsorbed much less than the hydrophobic ones^{304,314,315}.

Similarly, OM–hormone interactions include π / π stacking, hydrogen bonding and hydrophobic effect³¹⁶, along with electrostatic interaction when the steroid hormones are charged at high pH³¹⁷. OM–hormone interactions are strong where the OM types are highly aromatic, such as TA and HA, as opposed to the weak OM–hormone interactions where the OM are hydrophilic and non-aromatic^{317-320,522}. Because of the similar interactions between OM and adsorbents and between OM and hormones, potential interference of OM (especially the aromatic ones) with hormone adsorption by CNTs in ternary systems can be expected⁵²³.

The extent of OM interference may depend on the large difference in concentration between OM (in mgC/L) and MP / hormone (in ng/L) in real waters³²¹, and the residence time for OM–hormone, OM–CNT and/or hormone–CNT interactions³¹⁴. OM interference acts *via* two mechanisms: i) direct competition of OM with hormones for CNT adsorption sites, and ii) indirect competition where the OM–hormone complex has lower accessibility for the CNTs than the free hormones. Both mechanisms can elevate the mass transfer limitation that hinders hormone adsorption.

To prevent OM interference, the UF MWCO can be tailored to allow the retention of some OM fractions based on size and prevent OM interference with permeate-side adsorption. For example, UF MWCO of 5–10 kDa can remove humic substances^{323,326-328} that are the main constituent (40–60%) of natural OM (NOM)³²⁵ *via* size exclusion. Humic substances also contain high quantities of aromatic OM³²⁵, so a dominant source of interference is prevented with 5–10 kDa UF membranes. However, LMW compounds (MW <350 Da) can pass through all UF membranes³²⁸, and adsorption by CNTs in the permeate side can still be compromised by these compounds.

The main objective of this chapter is to evaluate the OM interference with steroid hormone removal by SWCNT–UF *via* mass transfer limitation, when considering a broad range of OM types. The primary research interests are: i) whether OM interfere significantly with steroid hormone adsorption by SWCNT–UF, ii) which OM characteristics that result in strongest interference, and iii) whether this interference is controlled by the UF MWCO.

6.2 Experimental methods to examine OM interference

6.2.1 Static adsorption experiments

Static adsorption was performed with the ternary system of E2, SWCNT, and OM (10 mgC/L of varying OM type) to determine the interference of OM with E2 adsorption given the long residence time of minutes or hours.

The static adsorption protocol described in Appendix B was followed. At different time intervals between 5 min and 26 h, a 2.5 mL aliquot was extracted from the hormone–OM–SWCNT mixture and filtered through a 1.3 cm membrane filter (Ultracel 100 kDa, code PLHHK, Merk Millipore, USA) for steroid hormone analysis.

6.2.2 Composite membrane preparation

For the preparation of the 10–100 kDa composite membranes, a vacuum filtration process was followed as described in Sections 3.3.3 and 5.2.1. To obtain a loading of 2 g/m², a volume of 84 mL of 0.1 g/L SWCNT suspension was completely filtered through a 7 cm circular membrane coupon that had been mounted upside-down in the in the vacuum filtration funnel. A vacuum pump assisted the deposition of SWCNT with an air pressure of around 2.3 bar.

For the preparation of the 3 and 5 kDa composite membranes, a stirred cell filtration process was applied (see Section 3.3.3). The 7 cm membrane coupon was mounted upside-down in the stainless-steel stirred cell. A pressure of 4 bar was induced inside the stirred cell with the synthetic air, and nanoparticle deposition was complete when 84 mL of the SWCNT suspension had been filtrated. The corresponding loading of SWCNT was 2 g/m².

6.2.3 Filtration experiments

The investigated parameters in this chapter are OM type (nine OM types, as described in Table 3.4), hormone type (E1, E2, T and P), pressure (from 0.5 to 4 bar) and UF MWCO. The experiments with varying hormone type, pressure and UF MWCO were only performed with the strongest OM interferants. The summary of the experimental design and conditions is given in Table 6.1.

In all filtration experiments, the micro-crossflow filtration system described in Sub-chapter 3.1 was operated in crossflow mode with a pump flow rate of 30 mL/min. The filtration protocol is provided in Appendix G. An improvement of this protocol from the one described in Chapter 5 is that the permeate samples were collected according to permeate volume. As such, the final permeate volume was fixed in the same set of experiments, which allows the comparison of adsorption.

Table 6.1: Overview of the filtration experiment design and conditions. The loading of SWCNTs in all SWCNT-UF membranes is 2 g/m² and the OM concentration was fixed at 10 mgC/L. The solution pH in all experiments is 8.1 ± 0.2.

Investigated parameter	UF MWCO (kDa)	OM type	Pressure (bar)	Hormone type
OM type	100	HA, AUS, TA, TEA, TANN, ALG, GLU, WF, FP	1	E2
Hormone type	100	TA	1	E1, E2, T, P
Pressure	10	TA	0.5–4	E2
MWCO	3, 5, 10, 30, 100	HA, TA	3–5 kDa: 4 10–100 kDa: 1	E2

6.2.4 Analytical techniques

Various analytical techniques had been used in this project and described in Sub-chapter 3.4. A liquid scintillation counter (LSC, 2550 TR/AB, Packard, USA) was used to quantify tritium-labelled hormones (E1, E2, T and P) in the range of 0.1–100 ng/L. A TOC analyser (Sievers M9, SUEZ, France) determined the carbon content of stock OM solutions. The feed, permeate and concentrate containing steroid hormones also contained ethanol at concentrations as high as 14 mgC/L, hence the TOC analyzer could not determine the OM concentration in these solutions. LC-OCD (DOC-Labor, Germany) was used instead because this technique gave a single carbon signal for ethanol at 40 min, which was distinguishable from most OM signals. The detection limit of LC-OCD was 0.02 mgC/L (see Section 3.4.3). Reproducibility evaluation for LC-OCD analysis of the nine OM types is reported in Appendix L. An UV-Vis spectroscopy instrument (Lambda 25, Perkin Elmer, USA) determined the absorbance of OM in the wavelength range 200–700 nm. The solution pH was determined with a pH electrode (InoLab pH720, WTW, Germany).

The presence of certain OM types at high concentrations (up to 10 mgC/L) can quench the activity of the radiolabelled steroid hormone measured with LSC. This quenching had been investigated with various OM types (nine) and concentrations (from 1 to 100 mgC/L), at two E2 concentrations of 10 and 100 ng/L, as described in Section 6.2.5. The main result of this investigation is that OM concentrations of ≤10 mgC/L does not cause a severe reduction in steroid hormone activity (*i.e.* below 10%). Hence, appropriately account for the quenching, an additional relative error of 10% was applied to the determined hormone concentrations when the feed solution contained OM.

6.2.5 Influence of OM on steroid hormone analysis

LSC works based on the detection of light pulses deflected by the sample-containing mixture⁵²⁴, several OM types (Table 3.4) can reduce the detected signals and hence interfere with the LSC analyses. This interference was quantified by measuring the E2 activity without OM and with five concentrations of OM (1, 10, 20, 50 and 100 mgC/L). Two concentrations of E2 were tested: 100

ng/L (which is the concentration feed solution) and 10 ng/L (which is the concentration at a practical E2 removal of 90%). The E2 concentrations related to the activities are shown in Figure 6.1.

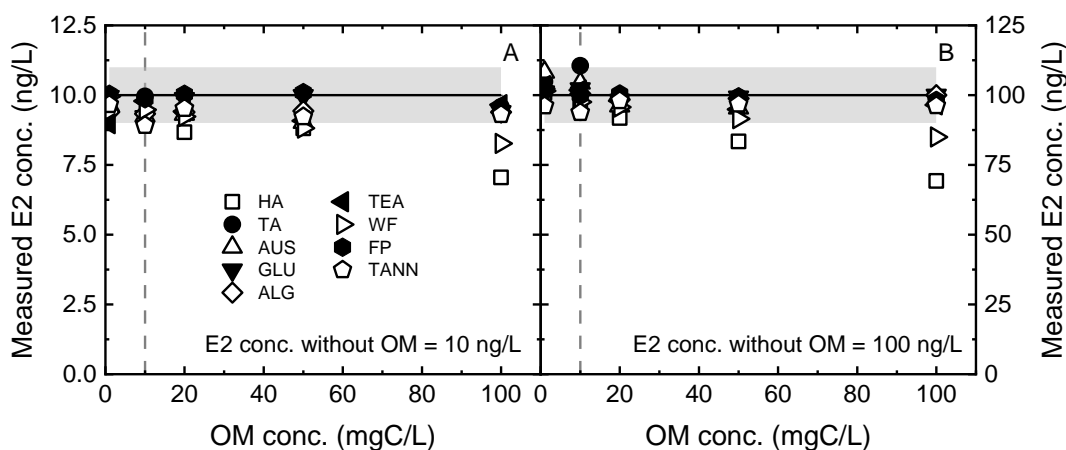


Figure 6.1: Measured E2 concentration in the presence of OM as a function of OM concentration. The horizontal solid line indicates the E2 concentration without OM. The vertical dashed line indicates the maximum OM concentration where interference is low (< 10%). Adapted from Nguyen *et al.*³⁰⁵.

The maximum deviation in E2 concentration was 10% at OM concentrations up to 10 mgC/L. This percentage was considered as an error in feed and permeate concentrations and would be propagated in concentration error calculations. For WF and HA, at higher concentrations than 10 mgC/L, the E2 signal is quenched by 10–50%, indicating that severe quenching of E2 activity occurred. As a result, E2 concentration was not accurately determined at high TA and HA concentrations. Similar quenching caused by HA had also been reported in previous studies^{112, 324}. In contrast, the seven other OM types did not cause significant quenching even at OM concentrations higher than 10 mgC/L.

6.2.6 Remarks on the exposure times in filtration experiments

In filtration experiments, the OM and hormone were mixed together 30 min before the filtration with the SWCNT–UF started, so these components were exposed to each other for a longer time than to SWCNT. It is worth repeating that the residence time in SWCNT–UF is typical in membrane filtration and short (less than 1 min).

Because of the longer exposure between OM and hormone, the OM–hormone interaction (or indirect interference mechanism) is more favoured than the OM–SWCNT interaction (or direct interference mechanism). To avoid intensifying the bias, the exposure time between OM and hormone was deliberately fixed at 30 min.

6.3 Interference of various OM types with hormone adsorption

6.3.1 Interference of OM types in static adsorption

To determine if different OM types affect the adsorption of E2 by SWCNTs, static adsorption experiments were performed with ternary mixtures that contained 100 ng/L E2, 10 mgC/L OM and 0.1 g/L SWCNTs. E2 adsorbed mass at equilibrium and kinetic rate constant (k_{E2}) are shown in Figure 6.2.

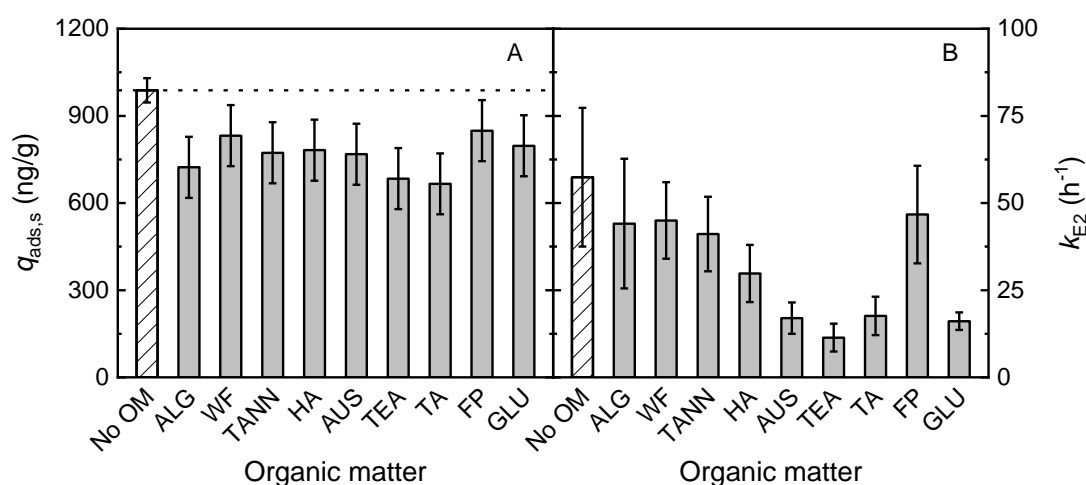


Figure 6.2: E2 adsorbed mass at equilibrium $q_{ads,s}$ (A) and kinetic rate constant k_{E2} (B) vs. OM type. 100 ng/L E2, 10 mgC/L OM, 0.1 g/L SWCNTs, 1 mM $NaHCO_3$, 10 mM NaCl, 20 ± 1 °C, pH 8.1 ± 0.2 . Adapted from Nguyen *et al.* ³⁰⁵.

From Figure 6.2 A, the interference of OM with E2 adsorption can be observed. In the control (*i.e.* without OM) experiment, the E2 adsorbed mass at equilibrium was 980 ng/g. When OM was introduced, this value decreased to 750–870 ng/g. The variation in E2 adsorbed mass between the experiments with nine OM types was not significant and within the error range. Therefore, the characteristics of OM could not be linked with adsorption interference in these experiments.

In contrast, several other studies found the link between the high aromaticity of OM and the strong interactions of OM with both CNTs and small organic molecules ^{312, 316, 525, 526}. However, with a large sample set, the correlation between OM aromaticity and OM adsorption by CNTs could not be concluded ⁵²³. The concentration difference between E2 and OM was five orders of magnitude, which could enhance the direct competition of OM (regardless of the characteristics) with E2 for the adsorption sites ³²¹.

The impact of OM on the E2 adsorption kinetics can be observed in Figure 6.2 B. ALG, TANN and WF did not cause a significant deviation of k_{E2} from the control value (57 ± 20 h^{-1}). On the other hand, k_{E2} values were significantly lower (between 7 and 23 h^{-1}) with TA, TEA, GLU and AUS. These OM types are small (see Table 3.4), indicating that the E2 adsorption kinetics could

be dictated by the OM size. Small OM compounds could diffuse into the less accessible surface of SWCNTs²⁵⁷ and compete more strongly with E2 for the adsorption sites. As a result, the adsorption speed of E2 is low in the presence of such small compounds.

The adsorption kinetics could be a limiting factor to E2 removal in the filtration with SWCNT-UF, where residence times were only seconds (between 0.3 and 3.3 s). In the next section, E2 breakthrough with SWCNT-UF is then investigated to determine the interference in these short residence times.

6.3.2 Interference of OM types in dynamic membrane adsorption

E2 breakthrough curves offer a qualitative view of the OM interference in a dynamic membrane adsorption process (Figure 6.3). The MWCO of SWCNT-UF is 100 kDa because these membranes would not retain OM except some high-MW fractions. As a result, little or no OM shielding were expected with most OM types.

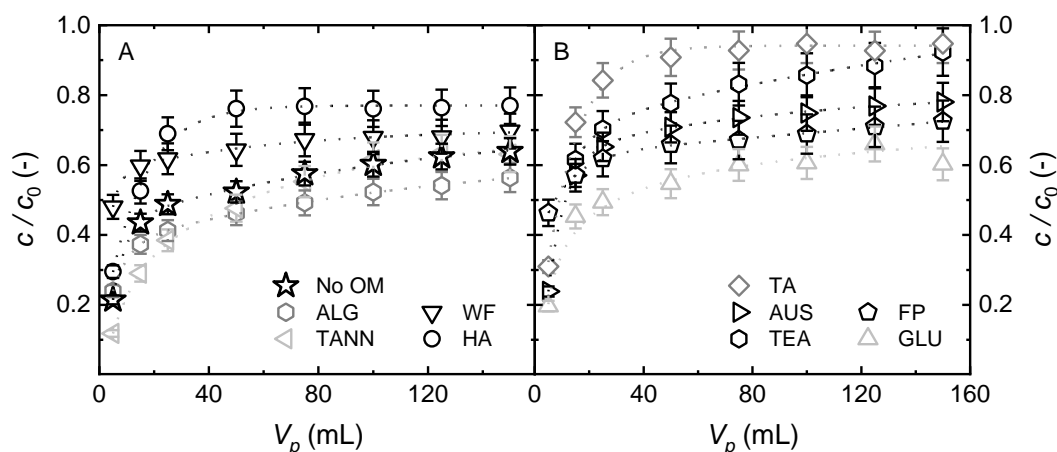


Figure 6.3: Relative permeate E2 concentration c/c_0 vs. permeate volume V_p (A and B) with SWCNT-UF 100 kDa. Dotted curves are the guides for the eye. 100 ng/L E2, 10 mgC/L OM, pressure 1 bar, 1 mM NaHCO_3 , 10 mM NaCl , 24 ± 2 °C, pH 8.1 ± 0.2 . Adapted from Nguyen *et al.*³⁰⁵.

Figure 6.3 (both A and B) shows that the adsorption saturation points where $c/c_0 = 1$ were not determined in all experiments, with or without OM. The stronger OM interference, the more deviated E2 breakthrough from that of the control experiment (indicated with the star symbols in Figure 6.3 A). With this qualitative evaluation, AUS, ALG, GLU, TANN and WF had only minor influence on E2 adsorption.

In contrast, HA, TEA, FP, and TA interfered more strongly, because the corresponding experiments indicate higher permeate E2 concentrations and hence poorer E2 removal. TA causes the strongest interference, because the respective c/c_0 at 150 mL was 0.87, which is 30% higher than the c/c_0 of the control (0.59). TA contained a high density of aromatic rings and could induce strong π / π interactions with both SWCNTs³¹⁰ and E2³¹⁸. As such, TA can interfere with E2 adsorption by SWCNT-UF *via* both direct and indirect competition mechanisms.

E2 adsorbed mass determined from the mass balance can offer a more quantitative analysis of OM interference. This parameter, along with E2 removal, OM removal and OM mass loss at 150 mL permeate volume, are given in Figure 6.4. OM concentration was determined as the sum of carbon concentrations in the humic substance, building block and LMW fractions in LC-OCD. Analytical issues were encountered with TA, TANN, TEA and WF, because these OM types were partly adsorbed by the capillaries and SEC column of LC-OCD (50–90%, see Appendix K), as such the removals of TANN, TEA and WF were not reliable. For TA, the analytical issue was resolved with the use of UV–Vis spectroscopy at a UV wavelength of 213 nm.

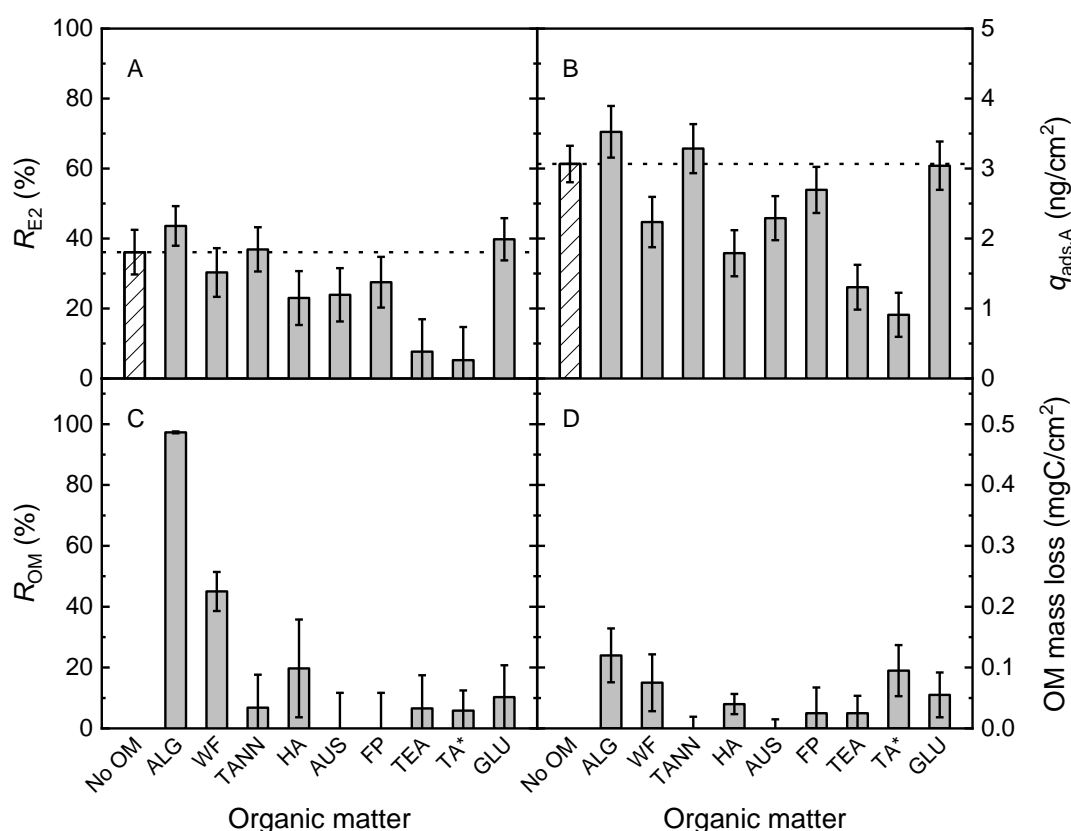


Figure 6.4: E2 removal R_{E2} (A), E2 adsorbed mass $q_{ads,A}$ (B), OM removal R_{OM} (C) and OM mass loss (D) with SWCNT–UF 100 kDa vs. OM type. The dotted horizontal lines indicate R_{E2} and $q_{ads,A}$ without OM. *TA was quantified from the UV absorbance (213 nm). 100 ng/L E2, 10 mgC/L OM, 1 mM NaHCO₃, 10 mM NaCl, 24 ± 2 °C, pH 8.1 ± 0.2. Adapted from Nguyen *et al.*³⁰⁵.

Figure 6.4 A and B shows that when TA, HA and TEA were introduced, E2 removal and adsorbed mass respectively decreased from 36% and 3.1 ng/cm² in the control experiment to around 10% and 0.8–1.7 ng/cm². In contrast, AUS, FP, GLU and TANN had a moderate negative or no influence on E2 adsorption; the corresponding adsorbed masses were ≥ 2.2 ng/cm².

According to Figure 6.4 C, the OM types that were retained by the 100 kDa UF included ALG (95%) and WF (45%). The mass losses of these OM types are significant as seen from Figure 6.4 D, which could indicate pore blocking. The high retentions could be linked to high MWs, and hence the interference evaluation was not conclusive for these two OM types. Increasing the

membrane MWCO can allow high-MW OM types to pass through but escalate the risk of SWCNT leakage. From Figure 6.4 D, the remaining seven OM types appeared to permeate completely through the 100 kDa UF. Figure 6.4 D shows that the adsorbed mass (or mass loss) of TA was significant, which suggests direct competition of TA with E2 for adsorption sites. In contrast, the adsorbed masses of HA and TEA were low, so direct competition appeared to be less important.

The difference in OM interference between dynamic membrane (Figure 6.4) and static adsorption (Figure 6.2) is caused by the mass transfer or residence time. In static adsorption, the residence time was long (up to several hours) and the SWCNT surface was not limited (see Chapter 4), and hence the surface access is an important factor. Therefore, varying the OM type leads to stronger variation in E2 adsorption kinetics than E2 adsorbed mass at equilibrium. In contrast, when the residence time is less than a minute in dynamic membrane adsorption, E2 adsorption occurred where the SWCNT surface is most accessible (see Chapter 5). As such, the OM and hormone compete for these limited adsorption sites, and hence the affinity of OM for SWCNTs and/or E2 is bound to impact E2 adsorption.

6.4 Relationship between OM characteristics and interference

6.4.1 Relationship between OM size and interference

To link the OM size and OM interference with E2 adsorption, LC-OCD analyses were performed, in which the OM was fractionated mainly based on size, into biopolymer (> 20 kDa), humic substance (around 1 kDa), building block (300–500 Da), and LMW acid and neutral (< 350 Da) fractions⁴⁴⁸. The organic carbon content of each fraction was then quantified from the area under the curves³²⁹ (which are in different shades in Figure 6.5). The concentrations of individual fractions are reported in Appendix K.

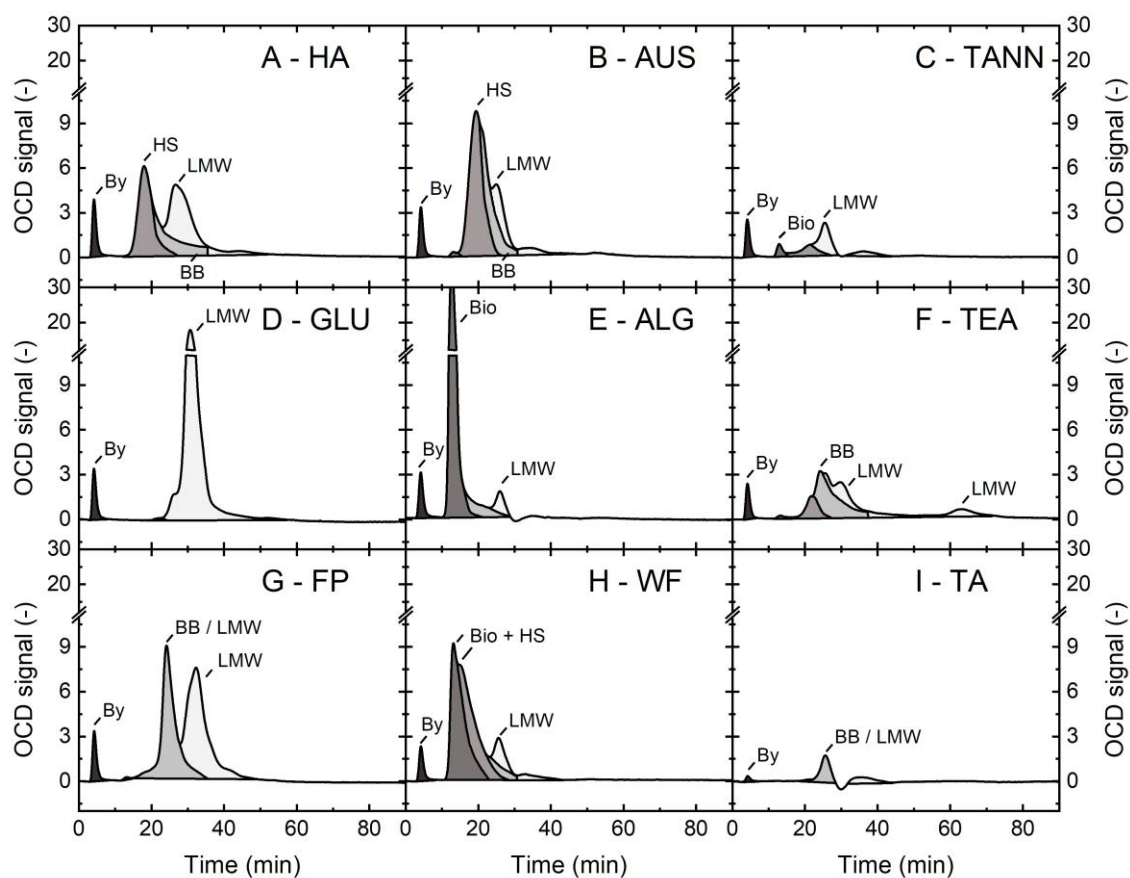


Figure 6.5: Raw organic carbon (OCD) signal (without normalization) of the nine OM types at 5 mgC/L (By: bypass, Bio: biopolymers, HS: humic substances, BB: building blocks, LMW: low molecular-weight substances). Adapted from Nguyen *et al.*³⁰⁵.

From Figure 6.5 A and B, HA and NOM are similar in size composition, because both contain mainly fractions in the humic substance region (~ 1 kDa)³²⁵. These two OM types interfered to the same extent with E2 adsorption by SWCNT-UF (see Figure 6.4).

There is a fascinating difference between FP and WF (Figure 6.5 G and H), although both are products of biodegradation. The two peaks (left and right) in the FP chromatograph can be interpreted as LMW acid and LMW neutral. In contrast, the home-made WF showed a double peak at 10–22 min corresponding to a mix of biopolymers and humic substances. FP is an industrial product that undergoes several steps of filtration⁴⁴², as a result the high-MW fractions are depleted. As observed in Figure 6.4, the size difference between WF and FP only slightly affected E2 adsorption in the filtration with SWCNT-UF.

From Figure 6.5 C, F and I, the total peak areas of the phenol-rich compounds, TEA, TANN, and TA, are relatively small because parts of these OM types were adsorbed by the LC-OCD instrument. The respective losses were estimated in Appendix K to be 50, 80, and 90%, respectively. The SEC column adsorbs hydrophobic components and leads to non-ideal mass loss⁵²⁷; the size characteristics of lost compounds cannot be determined. When only the eluted components are evaluated, TANN shows a characteristic peak at 8 min that indicates biopolymer-

like compounds (> 20 kDa in size). In contrast, TA and TEA contains mainly building blocks and LMW acids and neutrals. As shown in Figure 6.4, the smaller TA and TEA showed the strongest interference with E2 adsorption, whereas TANN showed only insignificant interference.

In summary, the OM size affects the interference in static adsorption and filtration to specific extents. In filtration experiments, OM size does not seem to control OM interference, where the residence time was short and adsorption occurred at the most accessible surface. In static adsorption where the residence time was long, small OM types, such as AUS, TEA, TA and GLU, diffuses the less accessible surface of SWCNTs and causes the directly competing E2 or micropollutants to be adsorbed in a longer time ²⁵⁷ (Figure 6.2).

6.4.2 Relationship between OM aromaticity and interference

The aromaticity of different OM types was determined to assess the link between this characteristic and interference. Aromaticity is commonly characterised with the specific ultraviolet absorbance ($SUVA_{254}$), which is determined as the UV absorbance (254 nm) divided by the TOC concentration ^{528, 529}. The $SUVA_{254}$ of the nine OM types measured with the UV–Vis spectroscopy and TOC analyser are given in Figure 6.6.

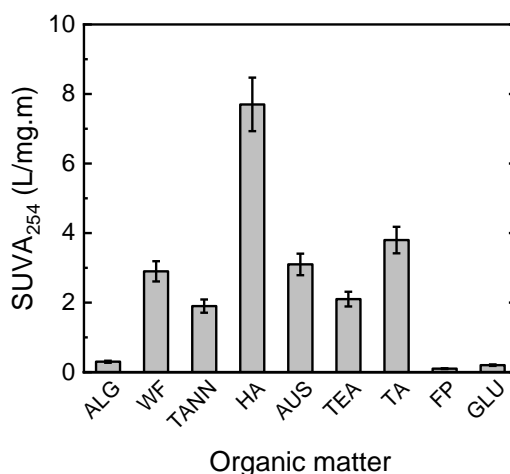


Figure 6.6: Specific ultraviolet absorbance ($SUVA_{254}$) of the nine OM types. Reprinted from Nguyen *et al.* 2021 ³⁰⁵.

The highest $SUVA_{254}$ of 7.7 L/mg.m was found for HA. The $SUVA_{254}$ values of TA, TANN, TEA, WF and AUS were lower than that of HA, at 2–4 L/mg.m. A $SUVA_{254} > 2$ L/mg.m indicates the occurrence of aromatic and hydrophobic compounds ⁵³⁰. Among the above OM types, TA, TEA, HA and AUS interfered strongly with E2 adsorption by SWCNT–UF (see Figure 6.4). As such, π / π stacking can be the key interactions between OM and SWCNT or E2. In contrast, the $SUVA_{254}$ of FP, ALG and GLU are near-zero. These OM types have little impact on E2 adsorbed mass by SWCNT–UF, suggesting that hydrophilic interactions (*e.g.* OH hydrogen bonding) may not control OM interference within short residence times.

In conclusion, the presence of aromatic rings in OM causes the greatest interference with E2 adsorption by SWCNT–UF. In contrast, OM size does not directly control interference, although small aromatic OM compounds, such as TEA and TA, appeared to affect E2 adsorption more strongly than big aromatic ones such as TANN. TA causes the strongest interference *via* where its structure contains abundant phenolic rings and will be the main target of investigation in the next sections.

6.5 Determination of the OM interference mechanisms

Direct interference displayed by TA (which is the strongest interferant) has already been confirmed from the significant mass loss of this OM type with SWCNT–UF 100 kDa. This sub-chapter then evaluates the relevance of the indirect interference mechanism, from the dynamic membrane adsorption results with varying hormone type and residence time.

6.5.1 Influence of hormone type on OM interference

Different steroid hormones can form specific interactions with SWCNTs and OM owing to their distinct characteristics (see Table 3.3). To evaluate the adsorption of other hormone types (E1, T and P) by SWCNT–UF, filtration experiments were carried out with four steroid hormones in the presence and absence of TA. With SWCNT–RC100, hormone removal, hormone adsorbed mass, and TA removal and TA mass loss / adsorbed mass at 150 mL of permeate volume are illustrated in Figure 6.7.

From Figure 6.7 A and B, without TA, E2 removal and adsorbed mass with SWCNT–RC100 follow the trend: E1 < T \approx E2 < P. A similar trend had been reported with SWCNT–RC10 at the same loading (2 g/m²) in Chapter 5. It is then implied that hormone adsorption was controlled by the specific interactions between the hormone and the most accessible surface of SWCNTs. Figure 6.7 A and B also show that TA interfered with the adsorption of all four hormones. In particular, hormone removal dropped drastically from 20–40% to below 10% for E1, E2 and T, and slightly from 80% to 70% for P.

According to Figure 6.7 C, the difference in TA removal was only within error, although TA was significantly removed in the experiments with (T) and P. Figure 6.7 D confirmed that TA adsorption in the presence of E1, E2 and P was significant, and the highest TA adsorbed mass was found in the experiment with P. TA seemed to interact with P and both were adsorbed by SWCNTs. Neale *et al.*³¹⁷ reported that TA–P and TA–E1 interactions were stronger than TA–E2 and TA–T interactions and suggested that the hydrogen-accepting ketone groups of P and E1 (see Table 3.3) enhanced the hormone interactions with TA. In this study, the interference caused by TA–E1 interactions was not assumed because the adsorption of both E1 and TA by SWCNT–UF was poor. Only with the specific case of P, the relevance of TA–hormone interactions (and hence indirect interference) could be indicated. It can be summarised that TA can compete with steroid hormones *via* both the direct and indirect mechanisms.

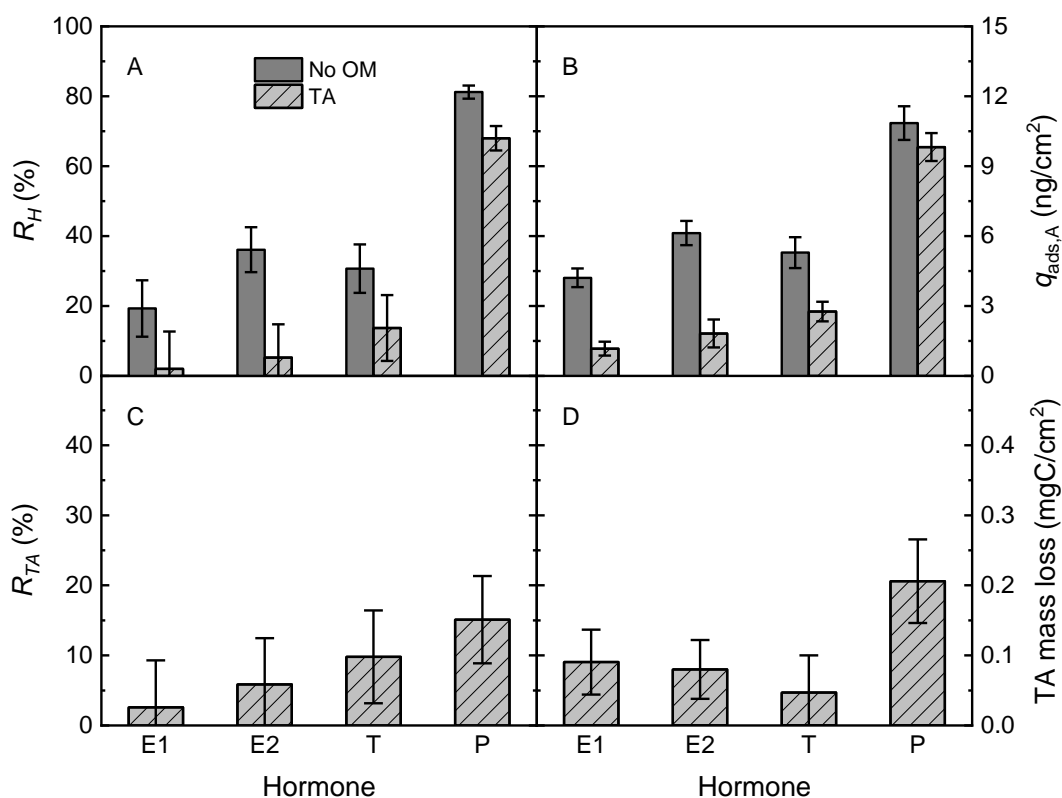


Figure 6.7: Hormone removal R_H (A), adsorbed mass of hormone $q_{ads,A}$ (B), TA removal R_{TA} (C) and TA mass loss with SWCNT-UF 100 kDa. 100 ng/L hormone, 10 mgC/L TA, 1 mM NaHCO₃, 10 mM NaCl, 24 ± 2 °C, pH 8.1 ± 0.2 . Adapted from Nguyen *et al.* 2021³⁰⁵.

6.5.2 Influence of flux / residence time on OM interference

The residence time t_R of the hormones in SWCNT-UF can affect the hormone adsorption efficiency. To determine whether E2 adsorption by SWCNT-RC10 was limited by a range of t_R between 6.6 to 0.8 s in the presence of TA, E2 filtration experiment was performed at different pressures ranging from 0.5 to 4 bar. The dependence between pressure, flux and residence time is given in the previous chapter. E2 removal, E2 adsorbed mass, TA removal and TA mass loss at 30 mL of permeate volume are shown in Figure 6.8 as functions of flux and t_R .

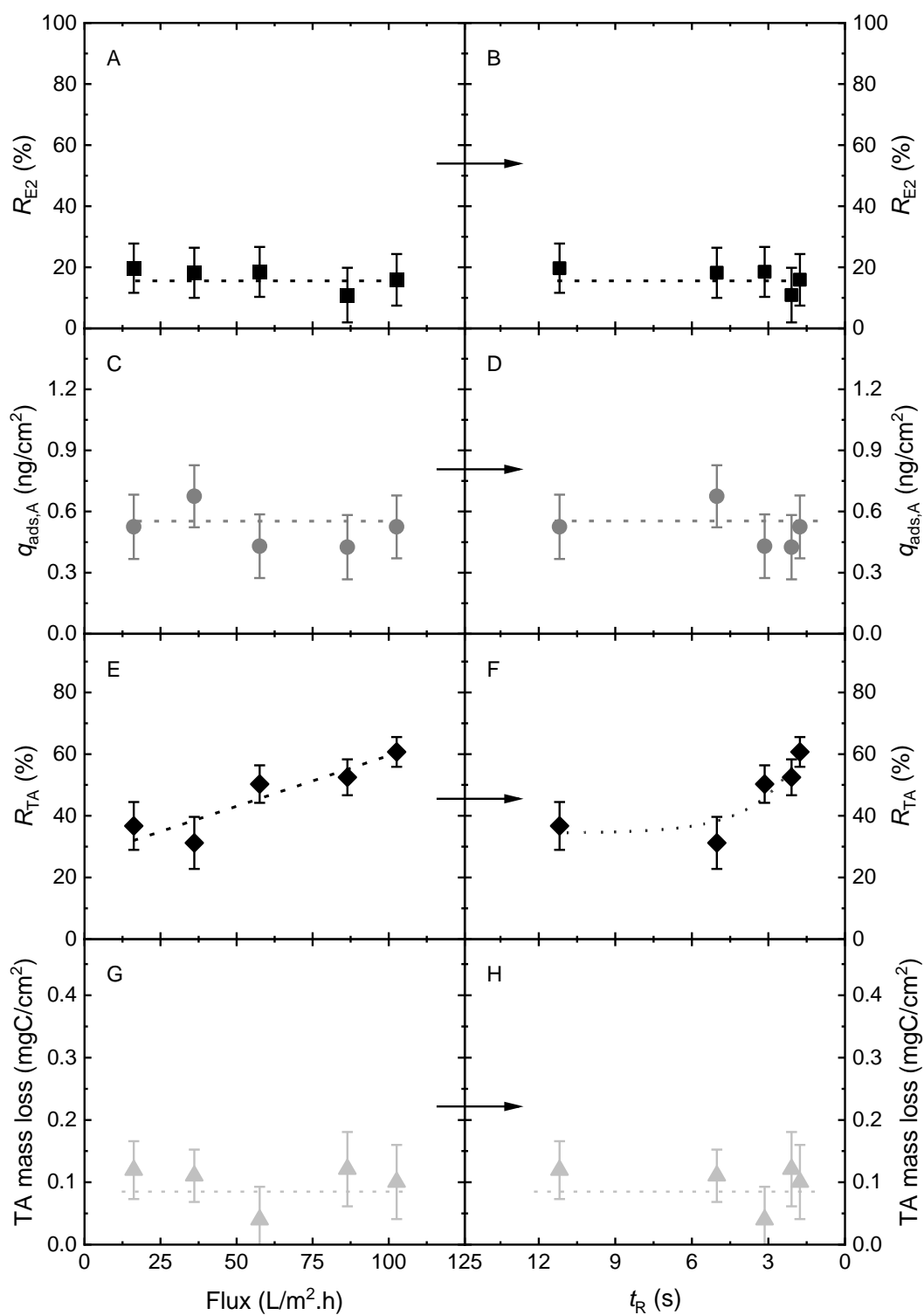


Figure 6.8: E2 removal R_{E2} (A and B), E2 adsorbed mass $q_{ads,A}$ (C and D), TA removal R_{TA} (E and F) and TA mass loss (G and H) with SWCNT-UF 10 kDa vs. flux and residence time, respectively. 100 ng/L E2, 10 mgC/L, 1 mM NaHCO₃, 10 mM NaCl, 24 ± 2 °C, pH 8.1 ± 0.2. Adapted from Nguyen *et al.*³⁰⁵.

From Figure 6.8 A and B, E2 removal and adsorbed mass were constant at 20% and 0.5 ng/cm², respectively, regardless of the flux and t_R . Similar observations of E2 adsorption were reported in Chapter 5 in the absence of OM, where the SWCNT surface was excessive, and E2 adsorption at the most accessible surface was fast and not controlled by t_R . In this study, although TA reduced E2 removal with SWCNT–UF, this OM did not appear to control the kinetic process of E2 adsorption. It then appears that TA favours indirect competition and reduces the affinity of E2 for SWCNTs *via* TA–E2 interactions. Feed solution preparation already caused bias toward this interference mechanism when the TA was exposed to E2 for 30 min before filtration.

As shown in Figure 6.8 C, TA (size of 1.7 kDa) was partially removed by SWCNT–UF 10 kDa, and TA removal increased from 37 to 61% with an increasing flux from 16 to 103 L/m².h. Adsorbed mass of TA did not vary significantly (0.1 mgC/cm²) with flux (see Figure 6.8 D), so it appears that a portion of TA was retained by the membrane. TA retention occurred because the flux of TA was lower than that of water, and this flux difference increases with applied pressure.

In summary, E2 removal and adsorption did not depend on residence time in the presence of TA. This is disadvantageous to the membrane filtration process because the interference cannot be reduced *via* increasing flow rate or pressure. However, it seems possible that TA can be retained and its interference can be controlled by an UF MWCO of <10 kDa.

6.6 Shielding of the UF membrane against OM interference

In this sub-chapter, the UF MWCO of the SWCNT–UF was varied between 3 and 100 kDa, to determine if interference can be controlled when the interfering fractions of OM are retained by the top membrane. Beside TA (molecular weight 1.7 kDa), HA (molecular weight 4.7–30.4 kDa, see Table 3.4) was also selected because the UF may retain HA better than TA. The total permeate volume was 30 mL for 1–10 kDa membranes and 150 mL for 30–100 kDa membranes. E2 removal, E2 adsorbed mass, TA / HA removal and TA / HA mass loss vs. UF MWCO are given in Figure 6.9.

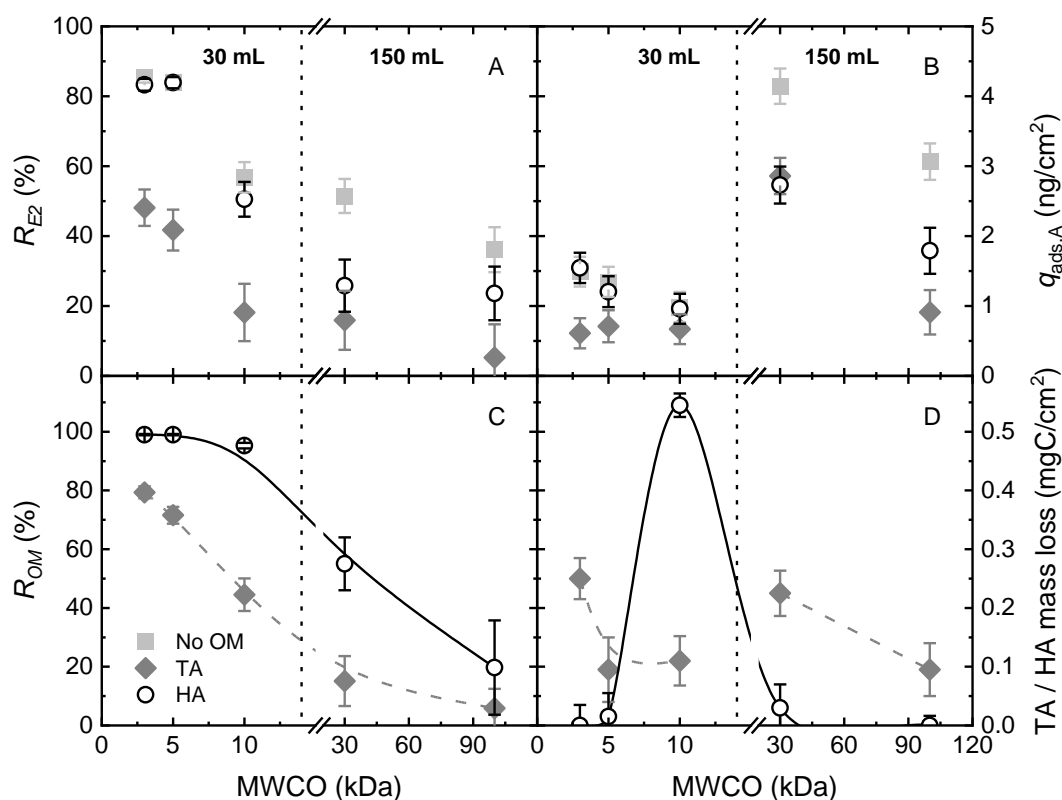


Figure 6.9: E2 removal R_{E2} (A), E2 adsorbed mass $q_{ads,A}$ (B), TA / HA removal R_{OM} (C) and TA / HA mass loss (D) vs. UF MWCO. Permeate volume 30 mL for 1–10 kDa membranes, and 150 mL for 30–100 kDa membranes, 100 ng/L E2, 1 mM NaHCO_3 , 10 mM NaCl, 24 ± 2 °C, pH 8.1 ± 0.2 . Adapted from Nguyen *et al.*³⁰⁵.

As opposed to TA, HA was almost completely retained (95–99% removal) by SWCNT–UF 3–10 kDa (Figure 6.9 C), which agrees with previous works on HA retention by UF membranes^{324, 327, 531}. With an efficient shielding against HA by 3–10 kDa UF membranes, E2 removal and adsorbed mass were similar between the HA and control (no OM) experiments (Figure 6.9 A and B).

While the formation of E2–OM ‘clusters’ is possible, E2 removal did not increase with the retention of HA / TA (Figure 6.9 A), which seems to contradict with other experimental investigations. With dead-end filtration, Jermann *et al.*⁵³² reported a small increase in E2 removal with 100 kDa UF membranes when the solution contained 10 mgC/L HA. In another work, 18% of E2 was partitioned to HA and increased E2 removal by 1–100 kDa UF membranes by 2–3 times⁴²⁶. As opposed to this study, the above investigations were performed with base membranes instead of ACMs. The base membranes adsorbed very little amounts of hormones. In this study, E2 may be retained if it is portioned to TA / HA, but the amount of permeating E2 does not significantly affect the amount of E2 adsorbed to the SWCNT layer, so any enhancement in E2 removal was not observed.

Because the main fractions of NOM are humic substances that can also be found dominantly in HA, the low UF MWCO of 3–10 kDa may prevent the interference of a relatively wide range of OM in surface water and wastewater. However, higher operating pressures and costs may be

required to achieve the productivity of the higher-MWCO membranes. In addition, small and hydrophobic compounds that reassemble TA cannot be controlled by the UF MWCO. If occurring at high concentrations, these compounds may decrease the micropollutant adsorption performance of SWCNT–UF.

6.7 Concluding remarks on the mass transfer limitation caused by OM

In this work, the influence of OM with different characteristics on steroid hormone adsorption by the SWCNT–UF was examined. The following points are obtained from this investigation:

- All the nine OM types resulted in a decrease in hormone (E2) adsorbed mass by SWCNT–UF to specific extents. Aromatic OM types (especially with low MW such as TA) hindered adsorption most drastically.
- TA competed with hormone for adsorption sites (direct interference) and might also form interactions with hormone, which reduced the hormone accessibility to and affinity for the SWCNT surface (indirect interference).
- TA (1.7 kDa) shielding was not effective with UF MWCO as low as 3 kDa, but HA (4.7–30.4 kDa) shielding was effective with UF MWCO between 3 and 10 kDa. As a result, interference caused by HA can be controlled.

The experimental results show aromatic OM types in feed water can cause a significant additional mass transfer limitation to the ACM, as such steroid hormone adsorption is poorer than in control (no OM) conditions. OM needs to be controlled to maintain a good performance of ACMs. With permeate-side incorporation of adsorbents (*e.g.* in SWCNT–UF), the top UF membrane can remove aromatic humic substances and results in very good adsorption by the ACM, although some small aromatic compounds similar to TA may cause undesirable performance loss.

7 Influence of the Forces on Steroid Hormone Adsorption

This chapter is adapted from a submitted manuscript to ACS Nano (June 2022) entitled “Adsorption of steroid hormone micropollutants in vertically aligned single-walled carbon nanotube membranes”, by Minh N. Nguyen, Melinda L. Jue, Steven F. Buchsbaum, Sei Jin Park, Florian Vollnhals, Silke Christiansen, Francesco Fornasiero, and Andrea I. Schäfer⁴¹⁴.

As shown in the previous chapters, steroid hormone adsorption by adsorptive composite membranes is affected by the mass transfer limitation. Reducing this limitation may allow good adsorption performance. This chapter presents a scenario where the mass transfer distance between the solute and the adsorbent surface is effectively zero.

The membranes in this research project are the vertically aligned carbon nanotube membranes, in which the only conducting channels of water and solutes are the CNT ‘pores’ with pore diameters of 1.7–3.3 nm. These pores permit fast water permeation because of ultralow friction between the water molecules and the hydrophobic CNT wall. The factors that impact adsorption at the CNT wall will be investigated in this chapter.

The contributions of co-authors are indicated as follows. The development and integrity testing of the VaCNT membranes was performed by Melinda L. Jue, Steven F. Buchsbaum, Sei Jin Park, and Francesco Fornasiero at the Lawrence Livermore National Laboratory (LLNL), California, USA. Florian Vollnhals and Silke Christiansen (INAM, Germany) characterised the membrane surface with helium ion microscopy. Andrea I. Schäfer is the corresponding author of the project and conceptualised the research and provided membrane expertise. All co-authors participated in revising and editing the manuscript.

7.1 Utilisation of vertically aligned carbon nanotube (VaCNT) membranes to investigate the forces

In recent years, advanced membranes have been designed and built from the molecular level^{405, 406}. These membranes target to overcome the trade-off between water permeability and solute retention in UF and NF membranes^{533, 534}. Vertically aligned carbon nanotube (VaCNT) membranes are those membranes that offer rapid water transport in pressure-driven processes^{194, 408, 412}. Good separation of solute molecules and ions is allowed *via* size and charge exclusion^{535, 536}, and the selectivity is modulated by adjusting the pore diameter⁴¹⁰ and through tip functionalisation^{535, 537}.

The water flow enhancement with VaCNT membranes (pore diameter around 2 nm) is from 10^3 to 10^4 , which is determined as the experimental flow rate divided by the calculated flow rate with the Hagen–Poiseuille equation¹⁹⁴. The enhanced flow results from a very low viscous friction experienced by water on a smooth and hydrophobic pore wall²⁹⁷. This low friction originates from the electronic effects at the carbon nanotube (CNT) surface⁵³⁸⁻⁵⁴¹, while any (hypothetical) surface roughness, even at a size of a water molecule, will diminish the flow enhancement in CNTs^{542, 543}. The VaCNT membrane pores have low tortuosity (1.1–1.25^{195, 408}). Therefore, the contact between the adsorbate and pore surface of VaCNT membranes is low compared with that between the adsorbate and the pore surface of UF/NF membranes (pore tortuosity of 1.5–2.5⁴¹⁸).

The VaCNT membranes can be deemed as a special case of (adsorptive) composite membranes with high structural and chemical homogeneity⁴⁰⁵, where the mass transfer distance between the adsorbates and surface is effectively zero. Unlike water that interacts very weakly with the CNT wall and flows inside the CNT in a near-frictionless manner, a hormone molecule can interact more strongly with the CNT wall, hence the hormone moves at a lower velocity than water and, if the velocity is very low, the hormone is *apparently retained* the wall. The significance of this ‘adsorption’ can be explained *via* the interplay of forces that act on the hormone (Figure 7.1).

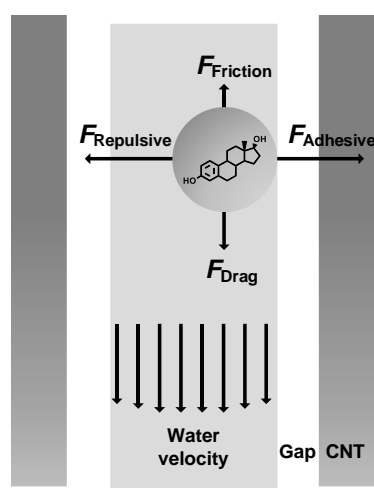


Figure 7.1: Schematic of the forces acting on a hormone molecule inside a VaCNT membrane pore: adhesive, repulsive, hydrodynamic drag, and friction forces. The hormone diameter (0.8 nm), gap thickness (0.3 nm) and pore diameter (2 nm) are approximately to scale. The magnitudes of the forces are not to scale.

The drag and adhesive forces can be quantified *via* equations. In VaCNT membranes, the *high slip condition* can be applied, where the water flow velocity at the fluid–wall interface is close to that in the pore centre (*i.e.* a plug-like flow condition)^{544,545}. F_A then is calculated with the Stokes equation⁵⁴⁶ (see Eq. (7.1)), with the assumption that the hormone molecule is spherical, the fluid flow is considered as ‘unbound’ due to the very high slip⁵⁴⁷, and the water viscosity in the pores is not significantly deviated from the bulk value^{548,549}.

$$F_H = 3\pi \mu d_{SH} v_{water} \quad (7.1)$$

where v_{water} (m/s) is the plug-like flow velocity in the pore and d_{SH} (nm) is the hydrodynamic diameter of the steroid hormone.

The adhesive van der Waals force F_A is determined *via* Eq. (7.2)^{415,416}. It is assumed that the van der Waals interaction²⁹⁸ is independent of the molecular geometries of the interacting molecules, but in reality some specific groups (*e.g.* the π -rings) can form stronger interactions²⁶¹.

$$F_A = \frac{H d_{SH}^3}{16 \left(z - \frac{1}{2}d_{SH}\right)^4} \quad (7.2)$$

where H (J) and z (m) are the Hamaker constant specific for the molecule–surface pair-wise interaction, and distance between the hormone molecule centre and the wall, respectively. F_A balances F_R at a separation between the hormone and wall of 0.3 nm⁴¹⁶, which keeps the molecule static in the direction perpendicular to the flow.

The hormone–wall friction F_F is weak by nature because of the high slip but it is not precisely determined. However, two scenarios can occur depending on the magnitude of F_F . If the water flow velocity is high, F_H is significantly higher than F_F , and the hormone molecule quickly moves in the pores and exits the VaCNT membrane. If the water flow velocity is sufficiently low, the hormone molecule either sticks to the CNT wall, or moves at a very low velocity so that an apparent retention / ‘adsorption’ is observed.

In summary, with the VaCNT membrane, the forces F_A , F_H and F_R can be quantified and a threshold for F_H ⁴²¹ can be estimated where adsorption becomes significant. The objective of this study is to link the force interplay to steroid hormone ‘adsorption’ by VaCNT membranes and relate these findings to the design of adsorptive composite membranes (ACMs). The specific research interests are: i) whether steroid hormones are adsorbed in the cylindrical and straight VaCNT membrane pores, ii) adsorption is significant allowed at which hydrodynamic condition (that is quantifiable *via* the drag force) is and iii) how the affinity between the hormone and wall (that is quantifiable *via* the adhesive force) controls adsorption.

7.2 Experimental methods to quantify adsorption and the forces

7.2.1 Characteristics of the VaCNT membranes

The main properties of VaCNT membranes used are given in Table 7.1. In brief, three types of VaCNT membranes were prepared at LLNL with average pore diameters of 1.7 ± 0.7 , 2.6 ± 0.7 and 3.3 ± 0.8 nm. Pore diameter determination was based on image analysis of a large set (>200) of transmission electron microscopic images as described elsewhere¹⁹⁶.

Table 7.1: List of VaCNT membranes. Adapted from Nguyen *et al.*⁴¹⁴, copyright 2022 American Chemical Society.

No.	CNT diameter (nm)		CNT density (10^{12} cm^{-2}) ^c	Porosity ^d (%)	VaCNT membrane thickness (μm) ^a
	External ^a	Internal ^b			
1	2.02 ± 0.71	1.68 ± 0.71	1.52	3.4 ± 2.0	Batch 1: 53 ± 2 Batch 2: 45 ± 2 Batch 3: 56 ± 2
2	2.93 ± 0.75	2.59 ± 0.75	0.67	3.5 ± 1.4	26 ± 2
3	3.64 ± 0.75	3.30 ± 0.75	0.22	1.9 ± 0.6	69 ± 1

^a Analysed from a large set of TEM images *via* a procedure described elsewhere¹⁹⁶.

^b Equal to external diameter subtracted by two times the van der Waals radius of carbon (0.17 nm).

^c Determined with the weight gain method described elsewhere⁵⁵⁰.

^d Calculated from the number density of CNTs and internal CNT diameter.

7.2.2 Analytical techniques

A Tri-Carb 4910 TR liquid scintillation counter (Packard, USA) was used to quantify steroid hormone as described in Section 3.4.1. The SenTix 81 and TeraCon 325 electrodes (WTW, Germany) measured the pH of the feed samples, and electrical conductivity (EC) of the feed and permeate samples.

7.2.3 Static adsorption

To determine steroid hormone adsorption by the VaCNT membrane with the condition of no convective flow, static adsorption was performed with small membrane pieces with a total mass of 2.5 ± 0.1 mg. The experimental protocol is described elsewhere¹¹². The membrane pieces were added to the steroid hormone solution that contained 100 ng/L E2, 1 mM NaHCO_3 , and 10 mM NaCl, in a 250 mL conical flask. This mixture was shaken at 260 rpm in an incubator shaker (described in Sub-chapter 3.2) at 20 °C. Sample aliquots of 2.5 mL were taken at different time intervals (5, 10, 15, 30 and 45 min; 1, 3, 5, 7, 9, 24 and 26 h) for analysis.

7.2.4 Filtration experiments

Filtration was performed in dead-end mode with the system described in Sub-chapter 3.1. The filtration protocol is as described in Appendix G. The dead-end mode was set by fully closing the needle valve that connects the retentate outlet of the membrane cell and the feed bottle (item 7 in Figure 7.2). In the experiment with the lowest flux ($6 \text{ L/m}^2\cdot\text{h}$) that corresponds to a lower flow rate than the pump specifications, the needle valve was partially open. The pressure was not controlled and increased during most experiments. The remarks on this are given in the next section. In addition, because no pressure dampener was used, the pressure fluctuated to some extent due to pump pulsation.

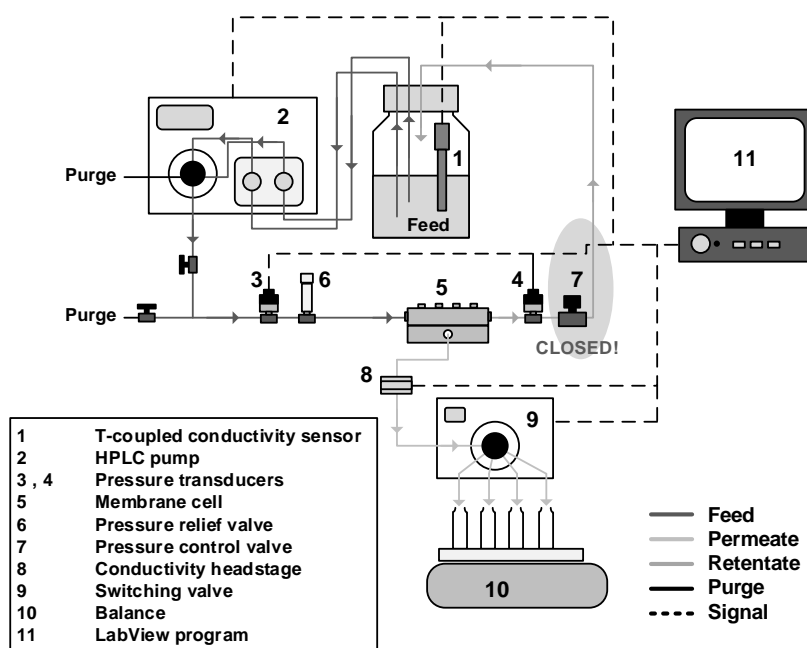


Figure 7.2: Schematic of the filtration system; when pressure control valve (item 7) is closed, the system is operated in dead-end mode.

7.2.5 Remarks on the pressure increase throughout the filtration

The transmembrane pressure increased in most filtration experiments that lasted 15–50 h, which corresponds to a decrease in membrane permeability of up to 95%. This phenomenon can be attributed to several reasons: i) internal pore blocking caused by the adsorption of hormones and/or ethanol, ii) external pore blocking caused by the retention of hormone-ethanol clusters, or contaminants such as dust and bacteria, and iii) deformation of the VaCNT membrane caused by the applied pressure. The schematics of these mechanisms are given in Figure 7.3.

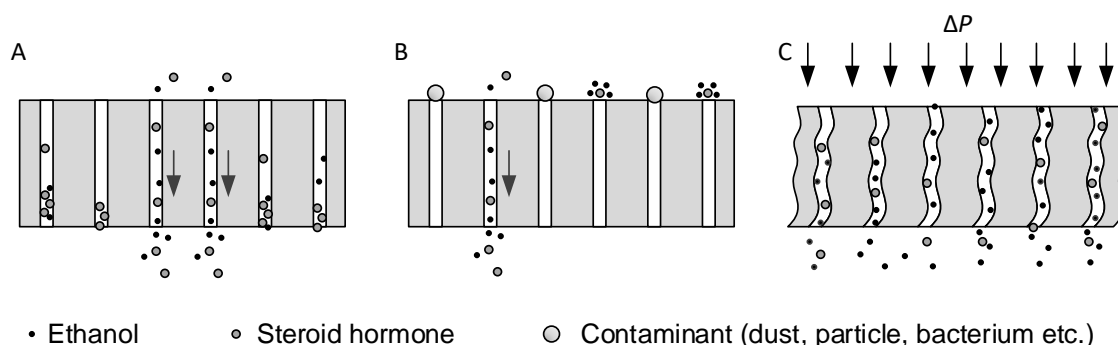


Figure 7.3: Potential reasons for the pressure increase in the filtration experiments: internal pore blocking (A), external pore blocking (B), and membrane deformation (C). Membrane thickness, pore size, and the sizes of ethanol, hormone and contaminant are not to scale.

In the first two cases, pore blocking reduces the number of conducting channels for water and solutes. In the last case, the pore tortuosity increases and may result in more energy dissipation, and the number of conducting channels may decrease if some pores are obstructed (buckled) by severe membrane compression.

To determine which was the main reason for the pressure increase, an experiment was performed with a 2.6 nm VaCNT membrane, at a constant flux of 30 L/m².h. This experiment contains three parts.

- In part 1, filtration with Milli-Q water was performed until 100 mL of permeate was obtained.
- In part 2, filtration with simulated background (1 mM NaHCO₃, 10 mM NaCl and 30 mg/L ethanol) was performed with the same membrane until 100 mL of permeate was obtained.
- In part 3, filtration with 1,000 ng/L feed E2 including 1 mM NaHCO₃, 10 mM NaCl and around 300 mg/L ethanol was performed with the same membrane until 65 mL of permeate was obtained.

The results of this experiment are given in Appendix O, showing that pressure increase and permeability loss was observed in all the steps. It appears that the permeability loss was not a direct consequence of the water quality, while both membrane compression and pore blocking are possible mechanisms.

Because of the high flow enhancement provided with VaCNT membranes, the enhancement factor calculated *via* Eq. (3.17) is still in the order of 10² and 10³, and the plug flow condition is still assumed despite the permeability loss.

7.2.6 Force assumptions

The assumptions about the drag and adhesive forces are described in bullet points as follows.

Hydrodynamic drag force

- The continuum hydrodynamics of water does holds for CNT channel sizes >1 nm²⁹⁷, hence the Stokes equation to calculate F_A in this work is valid.
- In ~ 2 nm CNT pores, the viscosity of water is assumed to be the same as the bulk viscosity^{548, 549}.
- Ethanol present at 15–30 mg/L concentrations is assumed to be a part of the continuum. The viscosity of water–ethanol mixture is assumed to be the same as that of water.
- The Coulombic drag force acting on charged and polar solutes caused by the flow of water in the conductive CNT pore^{551, 552} is not considered. Hormone molecules are uncharged.
- As described in the Introduction, the steroid hormone is considered as spherical with a hydrodynamic diameter of 0.8 nm¹³⁸. The actual estimated width, length, and height of E2 for instance are 0.5, 0.6 and 1.0 nm, respectively, estimated from the Chem3D model (PerkinElmer Informatics, USA).
- The plug-like flow condition is assumed, as such the flow velocities at the wall and in the pore centre are the same⁵⁴⁵.
- The wall correction factor induced when the hormone is at a close proximity to the wall is not considered as the fluid in a plug-like flow is considered to be ‘unbound’⁵⁴⁷.

Adhesive force

- The adhesive force F_A that is applied to evaluate hormone adsorption is primarily van der Waals interaction²⁹⁸.
- The hormone is treated as a homogenous sphere, where the orientation and specific interactions induced by specific groups are not considered in the calculation of the Hamaker constant and F_A .
- The Hamaker constant that is specific for the interaction between a hormone molecule and CNT pore wall corrected for the water medium is calculated according to Eq. (7.3).

$$H = (\sqrt{H_{\text{CNT}}} - \sqrt{H_{\text{water}}})(\sqrt{H_{\text{SH}}} - \sqrt{H_{\text{water}}}) \quad (7.3)$$

where H_{CNT} , H_{water} , and H_{hormone} are the Hamaker constants for the pair-wise interaction between two molecules of CNT, water, and hormone, respectively.

- $H_{\text{water}} = 3.7 \cdot 10^{-20}$ J according to literature⁵⁵³.
- H_{CNT} related to the interaction between SWCNTs with an external diameter of 2 nm⁵⁵⁴ takes the value of $1.8 \cdot 10^{-19}$ J, although this H_{CNT} is estimated for the external CNT surface instead of the internal one.
- H_{SH} has not been reported in literature and is hence assumed to be around $(3-10) \cdot 10^{-20}$ J, which are the Hamaker constant values of non-conducting organic liquids⁵⁵⁵.
- With the component Hamaker constants determined as above, H is approximated to be $3.5 \cdot 10^{-20}$ J and is a fixed value for the four hormones. Note that with a fixed H , F_A is not accurately determined for the four hormones with varied diameters.
- With the above assumptions for H and at a fix CNT–hormone distance (for instance, 0.3 nm), the trend in F_A follows the trend in the hormone diameter according to Eq. (7.2).

7.3 Adsorption performance of VaCNT membranes

7.3.1 Comparison between VaCNT membrane and CNPs

To determine whether the VaCNT membrane qualifies as an adsorbent, static adsorption of this membrane with a mass of 2.5 mg. The specific adsorbed mass of VaCNT was compared to those of CNPs at the same mass (2.5 mg/L) in Figure 7.4 A to elucidate the surface accessibility. The relative affinity for hormones between the external and internal CNT surfaces was estimated by comparing the adsorption performance of the VaCNT membrane and SWCNT (Figure 7.4 B).

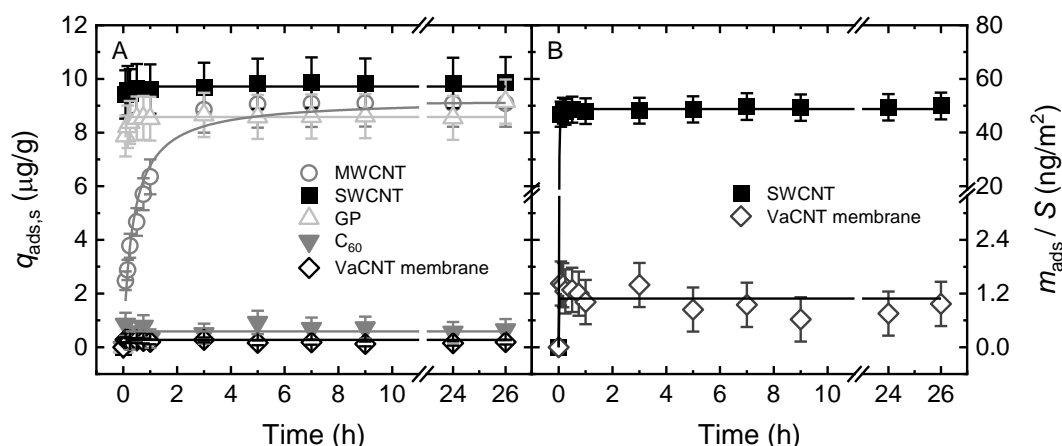


Figure 7.4: Specific E2 adsorbed mass $q_{ads,s}$ vs. time for four types of CNPs and VaCNT membrane at the same concentration of 0.01 g/L (A), and E2 adsorbed mass per adsorbent surface area $m_{ads,s} / S$ between SWCNT and VaCNT membrane (B). 100 ng/L E2, 1 mM NaHCO_3 , 10 mM NaCl, 20 °C, pH 8. Reprinted from Nguyen *et al.* ⁴¹⁴, copyright 2022 American Chemical Society.

The results of CNPs were obtained in Chapter 4 and serves here as the benchmarks for the VaCNT membrane. From Figure 7.4 A, adsorption by SWCNT and GP was fast and efficient, because their surfaces are available and readily accessible. In contrast, the lower adsorption kinetics displayed by MWCNT may imply good surface availability but poorer surface accessibility. Adsorption by C_{60} is low because of the poor surface access.

The specific adsorbed mass obtained with the VaCNT membrane is very low (around 0.22 $\mu\text{g/g}$, or 0.45 ng per cm^2 of filtration area), which may imply the weak adsorptive interaction. The adsorbed mass at equilibrium is even lower than that of C_{60} (nearly 1 $\mu\text{g/g}$). C_{60} has very poor surface access due to aggregation. In contrast, the low adsorption by the VaCNT membrane may be instead attributed to the low-affinity surface.

When the surface area is fixed for VaCNT membrane and SWCNT, the hormone adsorbed mass with VaCNT membrane is 30 times lower than that with SWCNT. This result implies that the internal surface of CNT does not interact as strongly with adsorbates as the external surface. The low affinity of the internal surface for hormones (E2) adsorption could be the result of the low electronic density at the concave internal CNT surface ⁵⁵⁶ that impedes the van der Waals

interaction with E2. In the next section, the adsorption by VaCNT membrane will be evaluated in a pressure-driven filtration.

7.3.2 Comparison between VaCNT, UF, NF and SWCNT-UF membranes

Hormone adsorption by the VaCNT membrane in the VaCNT-MF is compared with that by a UF, an SWCNT-UF (single-walled carbon nanotube – ultrafiltration membrane, see Chapter 5) and an NF membrane at a relevant flux of 60–80 L/m².h as shown in Figure 7.5. The same micro-crossflow filtration system was used with an effective filtration area of 2 cm². The results of UF and SWCNT-UF membrane (RC 10 kDa) were obtained from Chapter 5, and the results for the NF membrane (NF270, Dupont, USA) at 5 bar pressure was taken from Imbrogno *et al.*⁵⁵⁷.

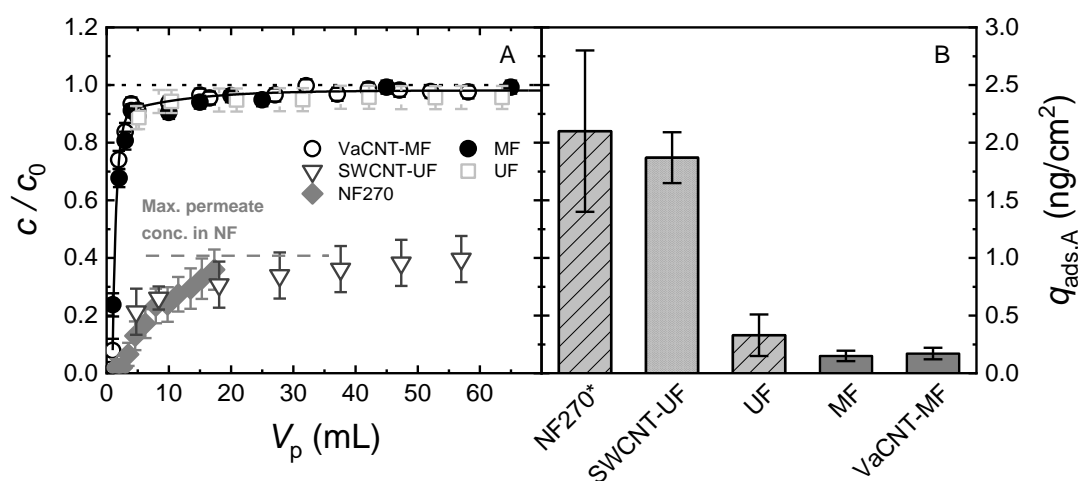


Figure 7.5: Relative E2 concentration c/c_0 vs. permeate volume V_p (A), and specific adsorbed mass $q_{ads,A}$ of VaCNT and UF membrane at 65 mL, and NF270 membrane at 18 mL (B; star symbol indicates the lower permeate volume). Dashed line in A indicates the maximum permeate concentration due to retention by NF⁵⁵⁷. In VaCNT-MF and MF experiments: CNT pore diameter 1.7 nm, flux 57 ± 3 L/m².h, 100 ng/L E2, 1 mM NaHCO₃, 10 mM NaCl, pH 8.2 ± 0.1 , 23.0 ± 0.2 °C. Reprinted from Nguyen *et al.*⁴¹⁴, copyright 2022 American Chemical Society. SWCNT-UF data are taken from Nguyen *et al.*³⁰².

From Figure 7.5 A, the breakthrough curves of the VaCNT-MF, MF and UF overlap, resulting in a similar adsorbed mass of 0.2–0.3 ng/cm². The adsorbed mass of VaCNT membrane (without the MF support) is determined by subtracting the adsorbed mass of MF by that of VaCNT-MF. This adsorbed mass is negligible (Figure 7.5 B).

The adsorbed mass with the UF 10 kDa is significant at 0.20 ± 0.08 ng/cm². Both E2 adsorption and retention were achieved with the NF270 membrane because the relative permeate concentration does not reach above 0.4 (this is not indicated from Figure 7.5 with the 5 bar pressure data, but confirmed in the original paper with the data at higher pressures⁵⁵⁷). The adsorbed mass with NF270 is much higher than that of the VaCNT and UF membranes, and similar to that of SWCNT-UF membrane, at 1.15 ± 0.35 ng/cm².

The absence adsorption by the VaCNT membrane is explained by the dominating flow hydrodynamics, which drives the hormone from the fixed adsorption site and out or the nanopores. The same phenomenon was not observed with UF and NF membranes, where the pores are non-uniform and tortuous⁴¹⁸. As such, the flow hydrodynamics at the wall is drastically reduced, and the drag force is not strong enough to reduce adsorption. To investigate this hypothesis further, E2 breakthrough with varying flux will be examined with the VaCNT membrane in the next section.

7.4 Influence of the drag force on adsorption

The hydrodynamic drag force scales with the flow velocity v_{water} in the pores via Eq. (7.1), and v_{water} in turn scales with transmembrane flux J_{exp} in the filtration experiments with VaCNT membranes via the relationship $v_{\text{water}} = \frac{J_{\text{exp}}}{\varepsilon}$, where ε is the VaCNT membrane porosity. Hence, the drag force can be controlled by controlling the transmembrane flux.

7.4.1 Breakthrough of hormone at varying flux

In this section, the breakthrough of E2 with the VaCNT membrane is provided at varying flux between 6 and 60 L/m².h, to determine whether adsorption is achieved upon reducing the flux (see Figure 7.6).

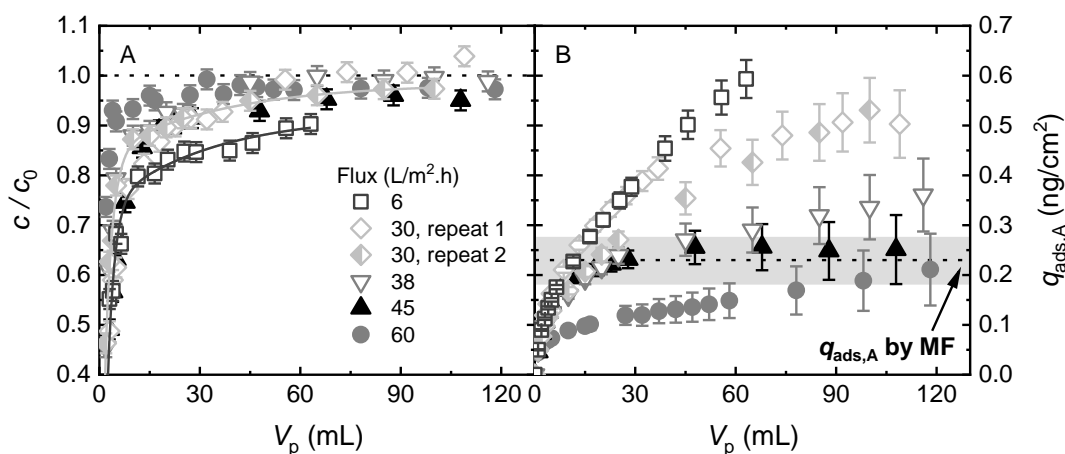


Figure 7.6: Relative E2 concentration c/c_0 (A) and specific adsorbed mass $q_{\text{ads,A}}$ (B) vs. permeate volume V_p with varying flux. The dashed line and grey box in B indicate the adsorbed mass by MF and error bar at 100 mL. CNT pore diameter 1.7 nm, 100 ng/L E2, 1 mM NaHCO₃, 10 mM NaCl, pH 8.2 ± 0.1, 23.0 ± 0.2 °C. Reprinted from Nguyen *et al.*⁴¹⁴, copyright 2022 American Chemical Society.

From Figure 7.6 A, it appears that the VaCNT membrane did not retain E2 with a hydrodynamic diameter of 0.8 nm. The hydrodynamic diameter of E2 is twice smaller than the average pore diameter of 1.7 nm. With the 6 L/m².h flux, adsorption was not complete after 65 mL of permeate was obtained. With the fluxes of 30–60 L/m².h, adsorption saturation was observed where the permeate concentration approached the feed concentration after 100 mL.

In Figure 7.6 B, the adsorbed mass of E2 by MF membrane is indicated by the dotted horizontal line. At the higher fluxes of 38–60 L/m².h, the adsorbed mass obtained with the VaCNT–MF was not significantly above the dotted line, which implies that E2 adsorption by VaCNT membrane is insignificant. Adsorption became significant when the flux was reduced to 6–30 L/m².h. From these breakthrough results, the relationship between F_H and adsorption will be elucidated in the next section.

7.4.2 Influence of hydrodynamic drag force on adsorption

The trend in adsorption with varying flux is determined *via* the specific E2 adsorbed mass at 65 mL as a function of flux, flow velocity and hydrodynamic drag force F_H as given in Figure 7.7. F_H is proportional to the flow velocity in the VaCNT pores *via* Eq. (7.1).

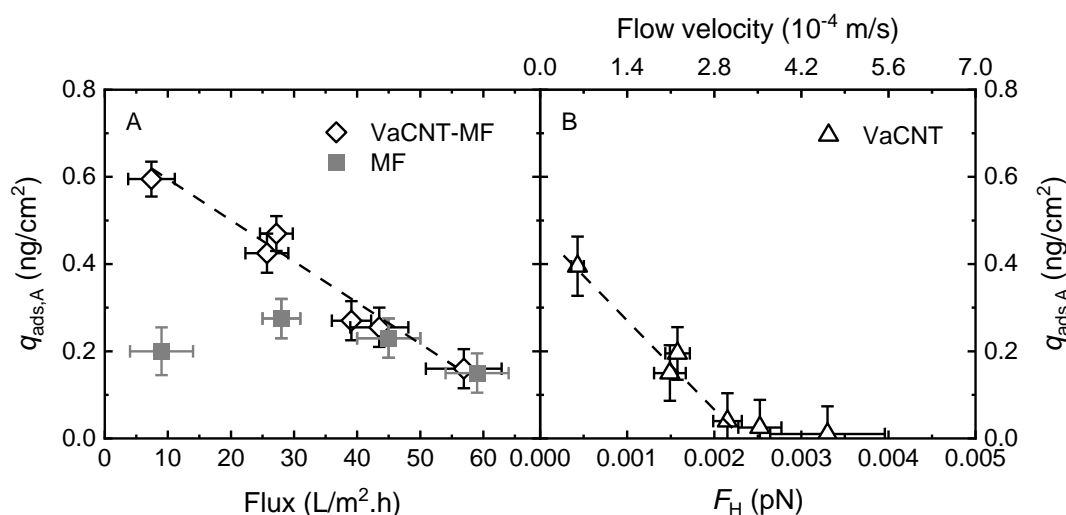


Figure 7.7: Specific E2 adsorbed mass $q_{ads,A}$ of VaCNT–MF and MF vs. flux (A), and $q_{ads,A}$ of VaCNT membrane vs. hydrodynamic drag force F_H and flow velocity (B) at 65 mL permeate volume. The dashed lines are guides for the eye. CNT pore diameter 1.7 nm, 100 ng/L E2, 1 mM NaHCO₃, 10 mM NaCl, pH 8.2 ± 0.1, 23.0 ± 0.2 °C. Reprinted from Nguyen *et al.* ⁴¹⁴, copyright 2022 American Chemical Society.

As seen in Figure 7.7 A, the specific E2 adsorbed mass of the MF support was 0.22 ± 0.05 ng/cm² and appears independent of flux, whereas the specific adsorbed mass of VaCNT–MF increased from 0.20 to 0.60 ng/cm² when reducing the flux from 57 to 6 L/m².h. From Figure 7.7 B, at high fluxes of 38–60 L/m².h, the adsorbed mass of the VaCNT membrane is insignificant where the error bar was higher than the value.

The adsorbed mass is related to F_H as shown in Figure 7.7 B. Significant E2 adsorption was achieved when F_H was below 2.2 · 10⁻³ pN corresponding to a flow velocity of 3.0 · 10⁻⁴ m/s. The adsorbed mass increased with decreasing F_H from 2.2 · 10⁻³ to 4.3 · 10⁻⁴ pN and decreasing flow velocity from 3.0 · 10⁻⁴ to 6.2 · 10⁻⁵ m/s.

In the VaCNT membrane pores, the adsorbate (E2) is very close to the wall, and the diffusional limitation relevant in the bulk phase is eliminated in such nanoconfinement ⁵⁵⁸. According to molecular dynamics simulation, adsorption (*i.e.* the energetic interactions between the hormone

and CNT surface) is a very fast process and occurs within nanoseconds²⁵⁵. Because diffusion and energetic hormone–wall interaction do not pose significant limitation to adsorption, the hydrodynamics that results in the convective flow appears to dictate whether the hormone is adsorbed or slips along the pore wall and exits the pore. In particular, if F_H is above $2.2 \cdot 10^{-3}$ pN, the hormone–wall friction F_F is no longer significant, and the adsorption of the hormone molecule is no longer apparent.

7.5 Influence of adhesive force on adsorption

At the condition where adsorption is permitted, *i.e.* when F_H is below the $2.2 \cdot 10^{-3}$ pN threshold, hormone adsorbed mass may be influenced by the adhesive (van der Waals) force F_A between the hormone and the CNT wall. To verify this influence, the adsorbed masses of E1, E2, T and P with varied hydrodynamic diameters were compared at the same F_H of $1.6 \cdot 10^{-3}$ pN (Figure 7.8).

The Hamaker constant used to calculate F_A (see Eq. (7.2)) was corrected for the hormone–CNT pair-wise interaction. If a uniform Hamaker constant ($3.5 \cdot 10^{-20}$ J, see Section 7.2.6) is applied to calculate F_A for the four hormones, F_A will follow the trend in hormone size (E1 < E2 < T < P).

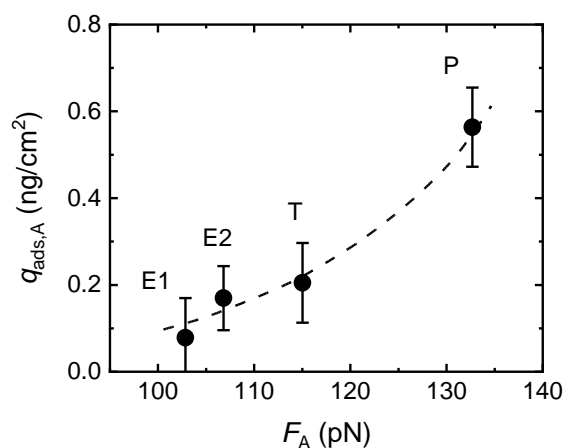


Figure 7.8: Specific hormone adsorbed mass $q_{ads,A}$ vs. adhesive force F_A . The dashed curve is a guide for the eye. CNT pore diameter 1.7 nm, flux 27 ± 3 L/m².h, 100 ng/L E2, 1 mM NaHCO₃, 10 mM NaCl, pH 8.2 ± 0.1 , 23.0 ± 0.5 °C. Reprinted from Nguyen *et al.*⁴¹⁴, copyright 2022 American Chemical Society.

The specific adsorbed mass follows the order E1 (insignificant) < E2 ≤ T < P, which also follows the trend in F_A . The hormone molecule is held static in the direction perpendicular to the water flow *via* the balance between F_A and the repulsive force F_R between the CNT and hormone electrons at a distance of ~ 0.3 nm⁴¹⁶. However, F_A (and F_R) can influence the movement of hormone molecules at the fluid–wall interface in the perpendicular direction.

The stronger the hormone–wall interaction, the stronger the resistance against the movement of the hormone. In particular, F_A influences the hormone–wall friction force F_F . The correlation between hormone adsorbed mass and F_A highlights an interplay of forces that act not only in the

flow direction but also the direction perpendicular to the flow. F_A (~ 100 pN) is five orders of magnitude higher than the F_H threshold (around $2 \cdot 10^{-3}$ pN), which implies that the hormone–wall friction is ultralow and the CNT surface is effectively lubricated⁵⁵⁹.

7.6 Influence of membrane pore diameter on adsorption

To determine whether varying the VaCNT membrane pore diameter impacts hormone adsorption, the E2 adsorbed masses obtained with three pore diameters of 1.7 ± 0.7 , 2.6 ± 0.7 and 3.3 ± 0.8 nm are compared in Figure 7.9. The flux was controlled at 27 ± 3 L/m².h, and the corresponding water flow velocities were $(2.2 \pm 0.2) \cdot 10^{-4}$ for the 1.7 and 2.6 nm diameter membranes, and $(3.6 \pm 0.1) \cdot 10^{-4}$ m/s for the 3.3 nm diameter membrane. The plug flow could be assumed where the enhancement factor (EF) is 2–3.5 orders of magnitude (Figure 7.9). It appears that the drag force F_H does not vary significantly (25%) between the three membranes, while F_A at the fluid–wall interface is constant and specific for the E2–CNT pair (at around 110 pN). Hence, the similar values of adsorbed mass (0.25 ± 0.10 ng/cm²) obtained for the three VaCNT membrane diameters is consistent with expectations. In summary, the pore diameter in the range of 1.7–3.3 nm does not impact adsorption if the pores are hydrophobic and smooth.

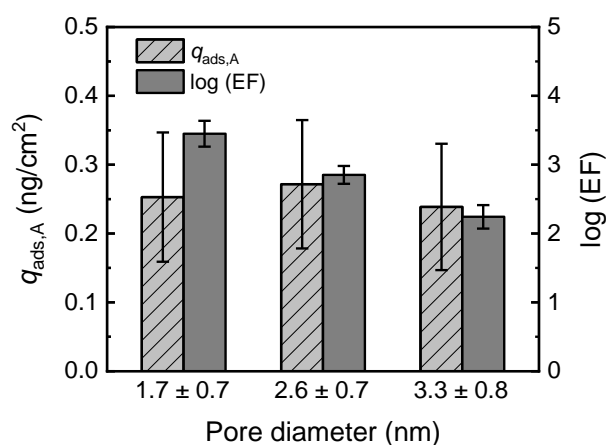


Figure 7.9: Specific E2 adsorbed mass $q_{ads,A}$ and relative membrane resistance R/R_{HP} vs. pore diameter. Flux 27 ± 3 L/m².h, permeate volume 100 mL, 100 ng/L E2, 1 mM NaHCO₃, 10 mM NaCl, pH 8.2 ± 0.1 , 23.0 ± 0.5 °C. Reprinted from Nguyen *et al.*⁴¹⁴, copyright 2022 American Chemical Society.

7.7 Concluding remarks on the interplay of forces

In this experimental study, the adsorption of steroid hormone micropollutants by the VaCNT membrane was evaluated. The following points are obtained from this investigation:

- The VaCNT membrane shows low adsorption of hormone in static adsorption, and zero adsorption in pressure-driven filtration at a relevant flux in UF and NF. The observation in filtration is explained by the interplay of forces.
- Hormones were adsorbed when the hydrodynamic drag force F_H is below $2.2 \cdot 10^{-3}$ pN as the effect of the opposing hormone-wall friction force F_F becomes significant. Further decreasing F_H from this point increased the E2 adsorbed mass from zero to 0.4 ng/cm^2 .
- When F_H was fixed at $1.6 \cdot 10^{-3}$ pN (which allows adsorption), the adsorbed mass of four steroid hormones was correlated to the adhesive force F_A . This force F_A drives the hormone towards the nanotube wall until it balances the repulsive force F_R , while influencing F_F that resists hormone movement with the flow.

An important message is drawn from the experimental investigation of VaCNT membranes for the development of ACMs. Even when the surface is abundant and mass transfer is non-existent, good adsorption by the ACM is not guaranteed without an analysis of the forces acting on the adsorbate. In an atomically smooth and hydrophobic surface such as the VaCNT membrane pore surface, the adsorbed molecules can slip easily in the presence of water flow leading to poor adsorption. Adsorption will be better if i) the pore tortuosity or the surface roughness is high, and ii) the surface has strong affinity for adsorbates. These directions may be considered in designing adsorptive composite membranes with low or negligible mass transfer limitation.

8 Conclusions and Outlook

8.1 Summary and conclusions

The dissertation investigates the possibility of removing steroid hormone micropollutants with low-pressure ultrafiltration (UF) membranes. Typical UF membranes do not allow hormone removal unless adsorbents, namely carbon-based nanoparticles (CNPs), are incorporated into these membranes to remove hormones *via* adsorption. This dissertation is dedicated to evaluating the CNP characteristics, composite membrane designs, and operating conditions, to develop effective adsorptive composite membranes (ACMs). So far, ACMs have not been employed at industrial scale, and the results gained from this study bring these membranes one step closer to the application.

The literature review in Chapter 2 first highlights the difference between ACMs and hybrid membrane systems. The latter contain separate adsorption and membrane filtration modules and have been applied in industry to remove micropollutants. For example, with a hybrid membrane system, good removal of steroid hormones has been achieved in a powdered activated carbon (PAC) contactor, whereas an UF module placed downstream of the adsorption module retains the loose PAC⁸⁵. The main drawbacks of these hybrid systems are the high footprint, and long residence times required for the pollutants to overcome the mass transfer limitation, and access the internal surface that is dominant in porous PAC. In contrast, ACMs allow the use of CNPs with vast external surface, hence these membranes promise to remove micropollutants with low adsorbent requirements and in short residence times (several seconds to a minute).

Chapter 2 then discussed five technical considerations (adsorbed mass at saturation, adsorption kinetics, interference of water components, regeneration measures and leakage / toxicological concerns), and several designs of ACMs. Several CNPs may be appropriate for the incorporation in the ACMs because of their fast adsorption kinetics and high adsorption capacity for steroid hormones, which results in low mass transfer limitation. However, prior to this study, all adsorption experiments were performed with elevated concentrations of steroid hormones (sub-mg/L to several mg/L), so they do not reflect the adsorbent performance at realistic conditions.

Some organic matter (OM) types can interfere with steroid hormone adsorption by CNPs, both directly (*via* competing with the hormones for the adsorption sites) and indirectly (*via* forming the OM–hormone clusters that have lower affinity for the CNPs or cannot access the CNP surface). Prior to this study, a thorough evaluation of OM interference at relevant hormone concentrations (sub- $\mu\text{g/L}$) had been missing. Adsorbent regeneration, possibility of leakage and toxicological concerns are also discussed in the literature review. These aspects are not within the experimental investigation of this dissertation but need to be considered in the later phases of the ACM development. Especially, the toxicity concerns prevent ACM application in water treatment.

Several designs of ACMs have been reviewed in Chapter 2. Feed-side deposition of superfine PAC and CNPs on the MF or UF surface is commonly reported. Permeate-side deposition of

CNPs (for example, deposition in the support layer of asymmetric UF membranes) may partly overcome some mass transfer limitation of feed-side deposition. An added benefit is that, by retaining the OM, the UF can prevent OM interference with micropollutant removal by the CNP layer. This shielding effect of UF membranes had not been specified prior to this work. Vertically aligned carbon nanotube (VaCNT) membranes are a special case of composite membranes, where adsorption may not be relevant in the molecularly smooth and hydrophobic nanopores, even when mass transfer limitation is non-existent. This special case allows the investigation of the forces acting on an adsorbed hormone molecule and provides interesting insight into the design of effective ACMs.

In Chapter 4, static adsorption was performed with six types of CNPs and VaCNT membrane to evaluate the adsorption performance where the residence time was not a limiting factor. In Chapters 5 to 7, filtration with ACMs (where the adsorbents are incorporated in the permeate side) and VaCNT membranes allows the hormone removal investigation where the residence time is constrained to several seconds or sub-seconds. Breakthrough curve evaluation and adsorbed mass determination *via* the mass balance are central in this study. A wide range of membranes were covered in this study, including CNP–UF membranes with pore diameters of 2.8–18.2 nm, and VaCNT membrane with pore diameters of 1.7, 2.6 and 3.3 nm of VaCNT. Four steroid hormones (E1, E2, T and P) were evaluated in all Chapters.

The objective in Chapter 4 is to understand the influence of surface characteristics on adsorption *via* evaluate the adsorption performance of several CNP types (multi- and single-walled carbon nanotubes, two grades of graphene, graphene oxide and fullerene C₆₀) in static adsorption with relevant steroid hormone concentrations (100 ng/L, except in the adsorption isotherm investigation). Adsorption (Figure 8.1) was quantified with two parameters: the adsorbed mass at equilibrium, and the adsorption kinetics determined by the time taken by the CNP to reach the adsorption equilibrium. The impacts of CNP and hormone types, CNP and hormone concentrations, and water conditions (temperature and pH) on the adsorption were investigated.

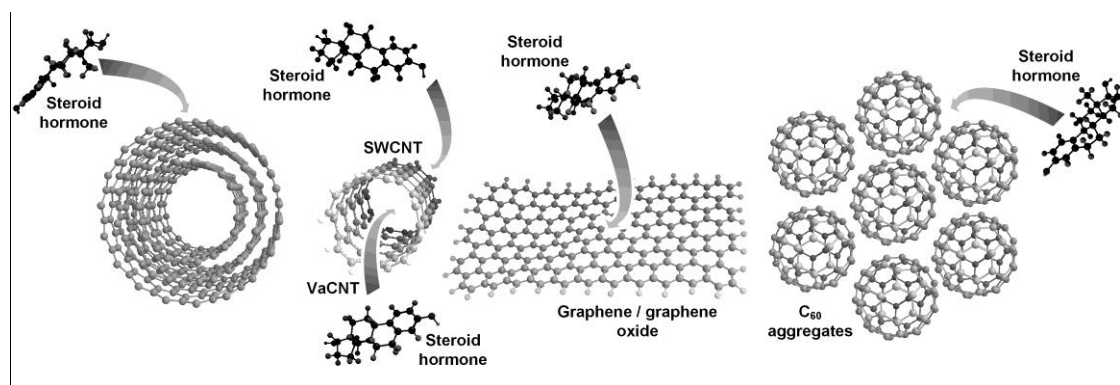


Figure 8.1: Adsorption of steroid hormone molecules by CNPs. From left to right: MWCNT, SWCNT / VaCNT membrane pore, graphene, and fullerene (C₆₀) aggregates.

All four steroid hormones were quickly adsorbed by all the CNPs at a CNP concentration of 0.1 g/L. When the CNP concentration was varied between 0.05 and 1 g/L, the E2 adsorption equilibrium was reached in less than an hour, indicating a low limitation of hormone mass transfer from the bulk to the sorbed phase. Because fast adsorption kinetics are important in ACMs where

the residence times are very short, materials that adsorb hormones quickly are promising candidates for membrane incorporation.

MW-/SWCNTs and the first-grade graphene (GP1) had very high adsorption capacities that were undetermined in the isotherm experiments. The adsorption capacities of second-grade graphene GP2 and C_{60} were determined to be 6.6 and 1.8 mg/g, respectively. High-capacity adsorbents are preferred in the ACM because the adsorption capacity (or the adsorbed mass at equilibrium) is linked to the abundance of CNP surface and related to the adsorption time before the material must be regenerated or replaced. The amount of surface that is accessible by hormone adsorbates depends on CNP aggregation, which varies with time and depends on solution chemistry. Without the limitation of residence time (that can reach 26 h) and surface area (that is in excess), good hormone removal of up to 99% was attained in varied water conditions (hormone type, solution pH and solution temperature).

Chapter 4 gives a comprehensive evaluation of six CNPs when the residence time is long (in the order of minutes or hours), in contrast with the residence time in ACMs (from sub-seconds to a minute). Good adsorbents for the incorporation in ACMs require a low mass transfer limitation. Single-walled carbon nanotube (SWCNT) is the most capable material for this incorporation because the residence time and hence mass transfer will become limiting factors in the ACMs, and the fast adsorption kinetics displayed by SWCNT may correlate with good surface accessibility.

A simplistic ACM (SWCNT-UF) was then evaluated for steroid hormone removal in Chapter 5, in which SWCNTs were mechanically incorporated between two UF membranes (Figure 8.2).

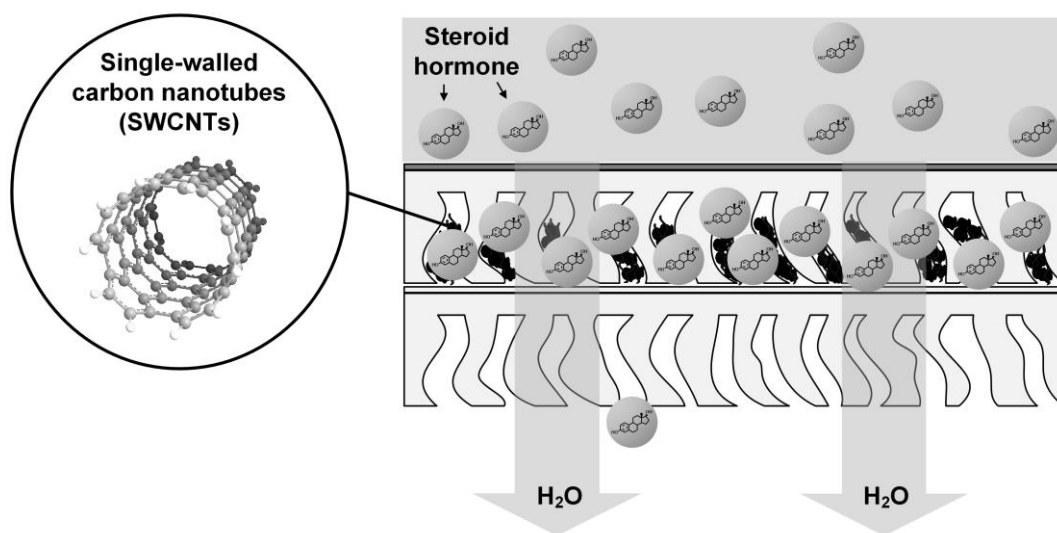


Figure 8.2: Steroid hormone removal with the SWCNT-UF membrane.

The feasibility of this SWCNT-UF was established, and with an SWCNT loading of 2 g/m^2 , SWCNT-UF removed 50–75% of steroid hormones in three-hour experiments. Complete breakthrough of steroid hormones was not achieved owing to the high adsorption capacity of SWCNTs. The above removals are lower than in static adsorption, which indicates that when the

residence time is below a minute, the mass transfer limitation may influence adsorption more significantly.

The surface accessibility is a limiting factor for steroid hormone (E2) removal / adsorption by the SWCNT–UF. This is evidenced by the increase in adsorbed mass with SWCNT loading. The distribution of SWCNTs in the membrane material was not uniform, hence a lower loading may correspond to less contact between hormones and SWCNTs, as water and solutes flow selectively through less dense adsorbent portions. However, at the highly accessible surface of SWCNTs, hormone adsorption was not influenced by the varying residence time in SWCNT–UF between 7.1 and 0.08 s. An explanation is that some surface of SWCNT is readily accessed by the hormone molecules as such the mass transfer limitation caused by short residence times does not result in a significant adsorption trend.

While steroid hormone removal with the SWCNT–UF has been demonstrated, enhancements are required to achieve the ambitious European drinking water target of 1 ng/L⁸⁴, which is equivalent to 99% removal from a 100 ng/L feed solution. Potential improvements include i) increasing the adsorbent loading and reducing water channelling with alternative membrane designs, and/or ii) using other particles that afford higher surface areas and/or better mass transfer than SWCNTs. When these improvements are realised, the ACMs may excel over NF/RO because of the lower specific energy consumption that is typical for UF membranes.

In Chapter 6, the interference of nine OM types with steroid hormone adsorption by the SWCNT–UF was examined (Figure 8.3). The OM has potential to cause an additional mass transfer limitation, because they can bind with the SWCNT or the hormone and prevent the access of the hormone to the highly accessible SWCNT surface.

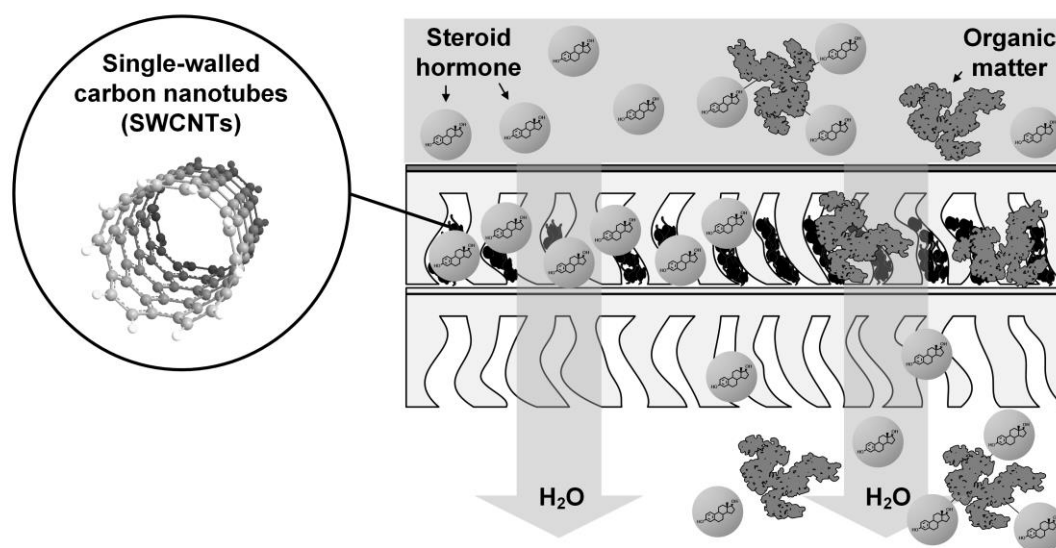


Figure 8.3: Interference of OM and shielding of UF with the SWCNT–UF membrane. Adapted from the graphical abstract of Nguyen *et al.*³⁰⁵.

The nine OM types with varying size and aromaticity interfered with E2 adsorption by SWCNT–UF to varying extents. Aromatic OM types, especially those with low MW such as

tannic acid (TA), interfered with E2 adsorption most drastically. Both E2 and TA were adsorbed by SWCNT–UF, implying that TA could compete directly with E2 for the adsorption sites. TA also strongly decreased E1 and T adsorption and slightly affected P adsorption. Reducing the residence time from 6.6 to 0.8 s did not affect E2 adsorption in the presence TA, which implies that TA affected the affinity of E2 for SWCNTs, or the accessibility of E2 to the SWCNT surface.

OM needs to be controlled to prevent the additional mass transfer limitation and maintain a good hormone adsorption performance of ACMs. The shielding against TA (1.7 kDa) was not effective with the UF molecular weight cut-off (MWCO) as low as 3 kDa. However, humic acid (HA, 4.7–30.4 kDa) was mostly retained (95–99%) with the UF MWCOs between 3 and 10 kDa. Consequently, high E2 removals of >80% were achieved, similar to the control experiment without any OM. Because HA contains mostly humic substances that constitute the majority of natural OM, successful control of interference was demonstrated with the SWCNT–UF.

The experimental results show that aromatic OM types in feed water can cause a significant mass transfer limitation to the ACM, as such steroid hormone adsorption is poorer than in control (no OM) conditions. OM needs to be controlled to maintain a good performance of ACMs. With permeate-side incorporation of adsorbents (*e.g.* in SWCNT–UF), the top UF membrane can remove aromatic humic substances and results in very good adsorption by the ACM, although some small aromatic compounds similar to TA may cause performance loss.

Short mass transfer distances are not the only requirement of an effective ACM. In the next chapter (Chapter 7), hormone adsorption was investigated with VaCNT membranes, where the mass transfer distance was effectively zero. However, the membrane pores had low tortuosity, and their surface was molecularly smooth and hydrophobic. Because of these, water flows through the VaCNT membrane pores rapidly. Unfortunately, the same pore characteristics prevent steroid hormone adsorption. The objective of this study is to understand the mechanisms of force interplay inside such pores and propose the limiting factors against adsorption where the mass transfer limitation does not exist.

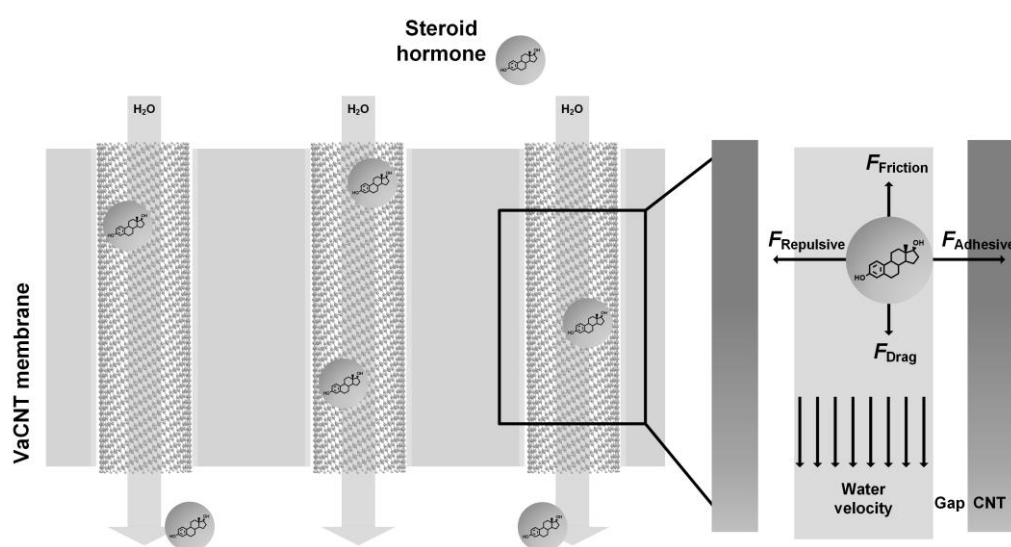


Figure 8.4: Transfer of hormone through the nanopores of a VaCNT membrane. Reprinted from the graphical abstract of Nguyen *et al.*⁴¹⁴, copyright 2022 American Chemical Society.

The VaCNT membrane adsorbed very little steroid hormones in static adsorption (30 times lower than SWCNT), and zero adsorption in pressure-driven filtration at a flux relevant in UF and NF. The flux was then reduced to determine where hormone adsorption was significant. Hormones are *apparently* adsorbed if their movement along the CNT wall is greatly hindered by the low water flow velocity resulting in a weak drag force. Hormone adsorption was observed when the hydrodynamic drag force F_H decreased with the flux to $2.2 \cdot 10^{-3}$ pN. At this drag force value, the hormone–wall friction threshold F_F became significant and prevented the movement of hormone along the CNT pore wall. Further decreasing F_H from this point to $4.4 \cdot 10^{-4}$ pN increased the E2 adsorbed mass from 0 to 0.4 ng/cm^2 .

When F_H was fixed at $1.6 \cdot 10^{-3}$ pN where adsorption was allowed, the adsorbed mass of four steroid hormones (E1, E2, T and P) followed the trend in the adhesive (van der Waals) force F_A between the hormone and the pore wall. The normal force F_A play two roles: it drives the hormone towards the pore wall until it balances with the hormone–wall repulsive force F_R ; and influences the friction force F_F that resists the hormone movement.

An important message is drawn from the experimental investigation of VaCNT membranes for the development of ACMs. Even when the surface is abundant and mass transfer is non-existent, good adsorption by the ACM is not guaranteed without an analysis of the forces acting on the adsorbate. In an atomically smooth and hydrophobic surface such as the VaCNT membrane pore, the adsorbed molecules can slip easily in the presence of water flow leading to poor adsorption. Adsorption will be better if i) the pore tortuosity or the surface roughness is high, and ii) the surface has strong affinity for adsorbates. These directions may be considered in designing adsorptive composite membranes with low or negligible mass transfer limitation.

From the studies described above, several key messages can be given. Mass transfer limitation is a critical consideration for ACMs. Hormone adsorption is limited by the diffusion through the ‘sparse’ SWCNT layer in SWCNT–UF (Figure 8.5 B). However, when there is no mass transfer limitation, the interplay of forces inside the (nano)channels dictate adsorption (Figure 8.5 A). In the VaCNT membrane, hormone adsorption depends on the affinity of steroid hormones for the surface, and the flow dynamics that causes the hormone molecule to slide along the nanopore.

An ideal ACM should possess nanoscale water channels where the mass transfer limitation is low or non-existent, while the surface of these channels has high affinity for steroid hormones and is sufficiently rough and tortuous (Figure 8.5 C). A high surface roughness and pore tortuosity improve the retention of steroid hormone at the adsorption sites and prevent the negative effect of flow hydrodynamics on adsorption.

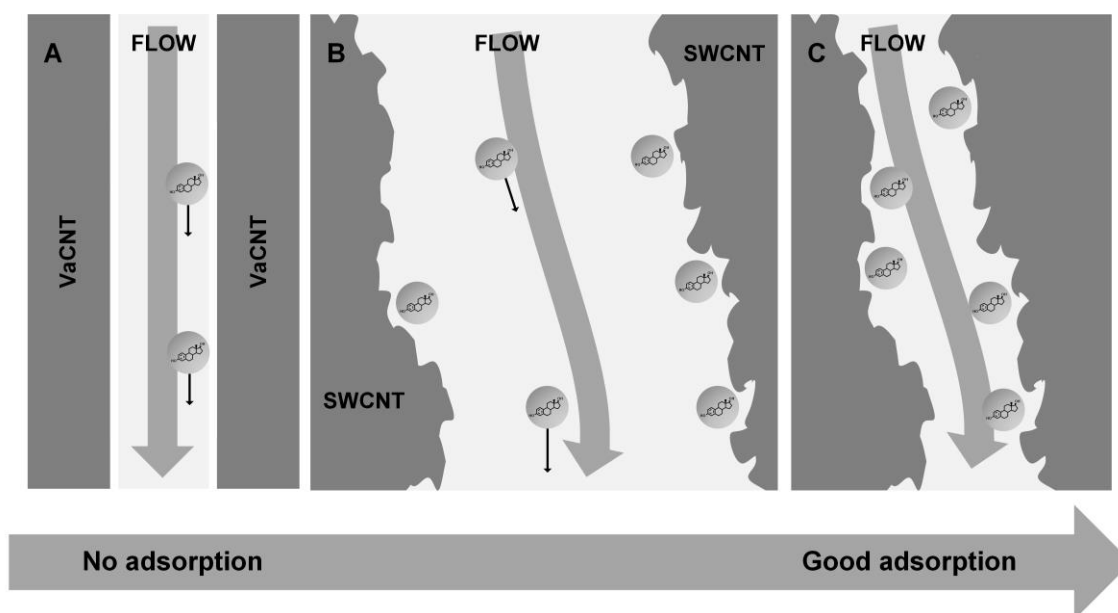


Figure 8.5: Schematics of steroid hormone transport through the adsorbent layer of VaCNT membrane (A), SWCNT–UF (B) and an untested carbonaceous membrane in which adsorption may be effective (C).

8.2 Outlook

Valuable lessons are gained from this study to achieve the long-term goal of using ACMs. Single-walled carbon nanotubes are capable adsorbents, but the composite membranes are not considered a safe option, because the toxicological impacts and possibility of leakage of SWCNTs are still unidentified. The adoption of ACMs will require tremendous investigation efforts. Regeneration strategies, nanoparticle leakage prevention, cost analysis, and public acceptance of CNP-based treatments must be considered beyond this study.

CNPs can be applied in ACMs once the toxicological concerns of CNPs are addressed and/or a fail-safe method to retain these adsorbents is provided. The dominance of external surface results in a modest mass transfer limitation, which is appreciated as the residence time in membranes is very short. However, the simplistic CNP–UF (such as SWCNT–UF) does not incorporate a higher quantity of CNPs than 11.5 g/m^2 . Alternative membrane designs (such as those with large finger-like voids in the support structure⁵⁶⁰) are needed in this regard. A drawback of ACMs is that they must be regenerated more often and hence require more energy to operate compared with activated carbons. Non-thermal regeneration techniques are needed to verify the lifetime of the ACMs.

The permeate-side deposition is a good idea to prevent the interference of water components, especially the hydrophobic and aromatic OM types. A dense membrane is required (10 kDa), which requires more energy to achieve the same productivity as the looser UF membranes (30–100 kDa). Hence, further investigations are needed for reducing the energy consumption of denser UF membranes. In addition, simulations will improve the understanding of OM interference in a dynamic adsorption process. Most OM compounds in the water environment

have unknown structures and provide a barrier against model implementation. Some surrogates, such as tannic acid and glucose, can be used instead of natural OM to simplify the simulations.

Lastly, the reported results provide a comprehensive insight into the most important ingredient of an effective ACM: **the contact between the micropollutants and surface**. A way to quantify this 'contact' has not been defined, although a good contact depends on three aspects: i) low mass transfer resistance, ii) abundance of adsorbent surface that have high affinity for micropollutants, and iii) the capability of retaining the micropollutants at the adsorption sites characterised with the interplay of forces. To increase the ACM efficiency, this contact must be improved.

Bibliography

- [1] United Nations, Goal 6 - Ensure availability and sustainable management of water and sanitation for all, <https://sdgs.un.org/goals/goal6>, accessed on 12 March 2022.
- [2] L. Mays, Water resources sustainability: An ecological-economics perspective, in: *Water Resources Sustainability*, McGraw Hill, New York, USA, 2006, pp. 55-72.
- [3] W.J. Cosgrove, D.P. Loucks, Water management: Current and future challenges and research directions, *Water Resources Research*, 51 (2015) 4823-4839.
- [4] M. Flörke, C. Schneider, R.I. McDonald, Water competition between cities and agriculture driven by climate change and urban growth, *Nature Sustainability*, 1 (2018) 51-58.
- [5] S. Batterman, J. Eisenberg, R. Hardin, M.E. Kruk, M.C. Lemos, A.M. Michalak, B. Mukherjee, E. Renne, H. Stein, C. Watkins, M.L. Wilson, Sustainable control of water-related infectious diseases: a review and proposal for interdisciplinary health-based systems research, *Environmental Health Perspectives*, 117 (2009) 1023-1032.
- [6] World Health Organization, Diarrhoeal disease fact sheet, <https://www.who.int/news-room/fact-sheets/detail/diarrhoeal-disease>, accessed on 29 March 2022.
- [7] WHO/UNICEF, Progress on drinking water, sanitation and hygiene (WASH), <https://washdata.org/>, accessed on 17 November 2021.
- [8] W.J. Weber, Distributed optimal technology networks: an integrated concept for water reuse, *Desalination*, 188 (2006) 163-168.
- [9] G. Wade Miller, Integrated concepts in water reuse: managing global water needs, *Desalination*, 187 (2006) 65-75.
- [10] V.G. Gude, Desalination and sustainability – An appraisal and current perspective, *Water Research*, 89 (2016) 87-106.
- [11] M.E. Hacker, C. Binz, Institutional barriers to on-site alternative water systems: A conceptual framework and systematic analysis of the literature, *Environmental Science & Technology*, 55 (2021) 8267-8277.
- [12] J.A. William, H. Vaux, The role of science in solving the world's emerging water problems, *PNAS*, 102 (2005) 15715-15720.
- [13] M.A. Shannon, P.W. Bohn, M. Elimelech, J.G. Georgiadis, B.J. Marinas, A.M. Mayes, Science and technology for water purification in the coming decades, *Nature*, 452 (2008) 301-310.
- [14] L.F. Greenlee, D.F. Lawler, B.D. Freeman, B. Marrot, P. Moulin, Reverse osmosis desalination: Water sources, technology, and today's challenges, *Water Research*, 43 (2009) 2317-2348.
- [15] E. Jones, M. Qadir, M.T.H. van Vliet, V. Smakhtin, S.-m. Kang, The state of desalination and brine production: A global outlook, *Science of the Total Environment*, 657 (2019) 1343-1356.
- [16] A. Subramani, M. Badruzzaman, J. Oppenheimer, J.G. Jacangelo, Energy minimization strategies and renewable energy utilization for desalination: A review, *Water Research*, 45 (2011) 1907-1920.
- [17] World Bank, The role of desalination in an increasingly water-scarce world, <https://openknowledge.worldbank.org/bitstream/handle/10986/31416/W18059.pdf?sequence=5&isAllowed=y>, accessed on 29 March 2022.
- [18] H. Lee, T.P. Tan, Singapore's experience with reclaimed water: NEWater, *International Journal of Water Resources Development*, 32 (2016) 611-621.
- [19] O. Lefebvre, Beyond NEWater: An insight into Singapore's water reuse prospects, *Current Opinion in Environmental Science & Health*, 2 (2018) 26-31.
- [20] A.I. Schäfer, J. Shen, B.S. Richards, Renewable energy-powered membrane technology in Tanzanian communities, *npj Clean Water*, 1 (2018) 24.
- [21] X. Zhou, H. Lu, F. Zhao, G. Yu, Atmospheric water harvesting: A review of material and structural designs, *ACS Materials Letters*, 2 (2020) 671-684.
- [22] R.P. Schwarzenbach, B.I. Escher, K. Fenner, T.B. Hofstetter, C.A. Johnson, U. von Gunten, B. Wehrli, The challenge of micropollutants in aquatic systems, *Science*, 313 (2006) 1072-1077.
- [23] M. Clara, B. Strenn, O. Gans, E. Martinez, N. Kreuzinger, H. Kroiss, Removal of selected pharmaceuticals, fragrances and endocrine disrupting compounds in a membrane bioreactor and conventional wastewater treatment plants, *Water Research*, 39 (2005) 4797-4807.

- [24] V. Turusov, V. Rakitsky, L. Tomatis, Dichlorodiphenyltrichloroethane (DDT): Ubiquity, persistence, and risks, *Environmental Health Perspectives*, 110 (2002) 125-128.
- [25] T. Wang, Y. Wang, C. Liao, Y. Cai, G. Jiang, Perspectives on the inclusion of perfluorooctane sulfonate into the stockholm convention on persistent organic pollutants, *Environmental Science & Technology*, 43 (2009) 5171-5175.
- [26] C.P. Silva, M. Otero, V. Esteves, Processes for the elimination of estrogenic steroid hormones from water: A review, *Environmental Pollution*, 165 (2012) 38-58.
- [27] S. Mompelat, B. Le Bot, O. Thomas, Occurrence and fate of pharmaceutical products and by-products, from resource to drinking water, *Environment International*, 35 (2009) 803-814.
- [28] Y.L. Luo, W.S. Guo, H.H. Ngo, L.D. Nghiem, F.I. Hai, J. Zhang, S. Liang, X.C.C. Wang, A review on the occurrence of micropollutants in the aquatic environment and their fate and removal during wastewater treatment, *Science of the Total Environment*, 473 (2014) 619-641.
- [29] M.L. Scala-Benuzzi, E.A. Takara, M. Alderete, G.J.A.A. Soler-Illia, R.J. Schneider, J. Raba, G.A. Messina, Ethinylestradiol quantification in drinking water sources using a fluorescent paper based immunosensor, *Microchemical Journal*, 141 (2018) 287-293.
- [30] E. Diamanti-Kandarakis, J.-P. Bourguignon, L.C. Giudice, R. Hauser, G.S. Prins, A.M. Soto, R.T. Zoeller, A.C. Gore, Endocrine-disrupting chemicals: An endocrine society scientific statement, *Endocrine Reviews*, 30 (2009) 293-342.
- [31] L. Trasande, R.T. Zoeller, U. Hass, A. Kortenkamp, P. Grandjean, J.P. Myers, J. DiGangi, M. Bellanger, R. Hauser, J. Legler, N.E. Skakkebaek, J.J. Heindel, Estimating burden and disease costs of exposure to endocrine-disrupting chemicals in the European Union, *Journal of Clinical Endocrinology and Metabolism*, 100 (2015) 1245-1255.
- [32] T.M. Attina, R. Hauser, S. Sathyanarayana, P.A. Hunt, J.-P. Bourguignon, J.P. Myers, J. DiGangi, R.T. Zoeller, L. Trasande, Exposure to endocrine-disrupting chemicals in the USA: A population-based disease burden and cost analysis, *The Lancet Diabetes & Endocrinology*, 4 (2016) 996-1003.
- [33] C.D. Kassotis, L.N. Vandenberg, B.A. Demeneix, M. Porta, R. Slama, L. Trasande, Endocrine-disrupting chemicals: economic, regulatory, and policy implications, *The Lancet Diabetes & Endocrinology*, 8 (2020) 719-730.
- [34] W. Chatuphonprasert, K. Jarukamjorn, I. Ellinger, Physiology and pathophysiology of steroid biosynthesis, transport and metabolism in the human placenta, *Frontiers in Pharmacology*, 9 (2018).
- [35] The Endogenous Hormones and Breast Cancer Collaborative Group, Endogenous sex hormones and breast cancer in postmenopausal women: Reanalysis of nine prospective studies, *JNCI: Journal of the National Cancer Institute*, 94 (2002) 606-616.
- [36] B.B. Yeap, H. Alfonso, S.A.P. Chubb, D.J. Handelsman, G.J. Hankey, P.E. Norman, L. Flicker, Reference ranges and determinants of testosterone, dihydrotestosterone, and estradiol levels measured using liquid chromatography-tandem mass spectrometry in a population-based cohort of older men, *The Journal of Clinical Endocrinology & Metabolism*, 97 (2012) 4030-4039.
- [37] H.W. Vesper, J.C. Botelho, M.L. Vidal, Y. Rahmani, L.M. Thienpont, S.P. Caudill, High variability in serum estradiol measurements in men and women, *Steroids*, 82 (2014) 7-13.
- [38] H. Kuhl, Pharmacology of estrogens and progestogens: influence of different routes of administration, *Climacteric*, 8 (Suppl. 1) (2005) 3-63.
- [39] J. Corrales, L.A. Kristofco, W.B. Steele, B.S. Yates, C.S. Breed, E.S. Williams, B.W. Brooks, Global assessment of Bisphenol A in the environment: Review and analysis of its occurrence and bioaccumulation, *Dose-Response*, 13 (2015) 1-29.
- [40] L.N. Vandenberg, T. Colborn, T.B. Hayes, J.J. Heindel, D.R. Jacobs, D.-H. Lee, T. Shioda, A.M. Soto, F.S. vom Saal, W.V. Welshons, R.T. Zoeller, J.P. Myers, Hormones and endocrine-disrupting chemicals: Low-dose effects and nonmonotonic dose responses, *Endocrine Reviews*, 33 (2012) 378-455.
- [41] A.M. Soto, C. Sonnenschein, Environmental causes of cancer: Endocrine disruptors as carcinogens, *Nature Reviews Endocrinology*, 6 (2010) 364-371.
- [42] K. Dahlman-Wright, V. Cavailles, S.A. Fuqua, V.C. Jordan, J.A. Katzenellenbogen, K.S. Korach, A. Maggi, M. Muramatsu, M.G. Parker, J.A. Gustafsson, International Union of Pharmacology. LXIV. Estrogen receptors, *Pharmacological Reviews*, 58 (2006) 773-781.
- [43] M.O. Barbosa, N.F. Moreira, A.R. Ribeiro, M.F. Pereira, A.M. Silva, Occurrence and removal of organic micropollutants: An overview of the watch list of EU Decision 2015/495, *Water Research*, 94 (2016) 257-279.

- [44] D.J. Caldwell, F. Mastrocco, P.D. Anderson, R. Lange, J.P. Sumpter, Predicted-no-effect concentrations for the steroid estrogens estrone, 17 β -estradiol, estriol, and 17 α -ethinylestradiol, *Environmental Toxicology and Chemistry*, 31 (2012) 1396-1406.
- [45] W. Young, P. Whitehouse, I. Johnson, *Proposed predicted-no-effect-concentrations (PNECs) for natural and synthetic steroid oestrogens in surface waters*, Great Britain Environment Agency, 2002.
- [46] N.K. Nagpal, C.L. Meays, Water quality guidelines for pharmaceutically-active compounds (PhACs): 17 α -ethinylestradiol (EE2), *Ministry of Environment, Province of British Columbia (Technical Appendix)*, (2009).
- [47] G.G. Ying, R.S. Kookana, Y.J. Ru, Occurrence and fate of hormone steroids in the environment, *Environment International*, 28 (2002) 545-551.
- [48] A. Pal, K.Y.-H. Gin, A.Y.-C. Lin, M. Reinhard, Impacts of emerging organic contaminants on freshwater resources: Review of recent occurrences, sources, fate and effects, *Science of the Total Environment*, 408 (2010) 6062-6069.
- [49] M. Gardner, S. Comber, M.D. Scrimshaw, E. Cartmell, J. Lester, B. Ellor, The significance of hazardous chemicals in wastewater treatment works effluents, *Science of the Total Environment*, 437 (2012) 363-372.
- [50] Y. Zhou, J. Zha, Y. Xu, B. Lei, Z. Wang, Occurrences of six steroid estrogens from different effluents in Beijing, China, *Environmental Monitoring and Assessment*, 184 (2012) 1719-1729.
- [51] A.Z. Aris, A.S. Shamsuddin, S.M. Praveena, Occurrence of 17 α -ethinylestradiol (EE2) in the environment and effect on exposed biota: A review, *Environment International*, 69 (2014) 104-119.
- [52] N.H. Tran, M. Reinhard, K.Y.-H. Gin, Occurrence and fate of emerging contaminants in municipal wastewater treatment plants from different geographical regions - A review, *Water Research*, 133 (2018) 182-207.
- [53] R. Sacdal, J. Madriaga, M.P. Espino, Overview of the analysis, occurrence and ecological effects of hormones in lake waters in Asia, *Environmental Research*, 182 (2020) 109091.
- [54] L.M. Madikizela, S. Ncube, L. Chimuka, Analysis, occurrence and removal of pharmaceuticals in African water resources: A current status, *Journal of Environmental Management*, 253 (2020) 109741.
- [55] Z. Tang, Z.-h. Liu, H. Wang, Z. Dang, H. Yin, Y. Zhou, Y. Liu, Trace determination of eleven natural estrogens and insights from their occurrence in a municipal wastewater treatment plant and river water, *Water Research*, 182 (2020) 115976.
- [56] K.M. Sta. Ana, M.P. Espino, Occurrence and distribution of hormones and bisphenol A in Laguna Lake, Philippines, *Chemosphere*, 256 (2020) 127122.
- [57] B. Ng, N. Quinete, S. Maldonado, K. Lugo, J. Purrinos, H. Briceño, P. Gardinali, Understanding the occurrence and distribution of emerging pollutants and endocrine disruptors in sensitive coastal South Florida Ecosystems, *Science of the Total Environment*, 757 (2021) 143720.
- [58] S. Lu, C. Lin, K. Lei, M. Xin, B. Wang, W. Ouyang, X. Liu, M. He, Endocrine-disrupting chemicals in a typical urbanized bay of Yellow Sea, China: Distribution, risk assessment, and identification of priority pollutants, *Environmental Pollution*, 287 (2021) 117588.
- [59] C. Purdom, P. Hardiman, V. Bye, N. Eno, C. Tyler, J. Sumpter, Estrogenic effects of effluents from sewage treatment works, *Chemistry and Ecology*, 8 (1994) 275-285.
- [60] J.L. Parrott, B.R. Blunt, Life-cycle exposure of fathead minnows (*Pimephales promelas*) to an ethinylestradiol concentration below 1 ng/L reduces egg fertilization success and demasculinizes males, *Environmental Toxicology*, 20 (2005) 131-141.
- [61] A.D. Vethaak, J. Lahr, S.M. Schrap, A.C. Belfroid, G.B.J. Rijs, A. Gerritsen, J. de Boer, A.S. Bulder, G.C.M. Grinwis, R.V. Kuiper, J. Legler, T.A.J. Murk, W. Peijnenburg, H.J.M. Verhaar, P. de Voogt, An integrated assessment of estrogenic contamination and biological effects in the aquatic environment of The Netherlands, *Chemosphere*, 59 (2005) 511-524.
- [62] F. Gagné, C. Blaise, M. Salazar, S. Salazar, P.D. Hansen, Evaluation of estrogenic effects of municipal effluents to the freshwater mussel *Elliptio complanata*, *Comparative Biochemistry and Physiology Part C: Toxicology & Pharmacology*, 128 (2001) 213-225.
- [63] J.A. Leonard, W.G. Cope, M.C. Barnhart, R.B. Bringolf, Metabolomic, behavioral, and reproductive effects of the synthetic estrogen 17 α -ethinylestradiol on the unionid mussel *Lampsilis fasciola*, *Aquatic Toxicology*, 150 (2014) 103-116.
- [64] G. Levy, I. Lutz, A. Krüger, W. Kloas, Bisphenol A induces feminization in *Xenopus laevis* tadpoles, *Environmental Research*, 94 (2004) 102-111.

- [65] Y. Li, Y. Shen, J. Li, M. Cai, Z. Qin, Transcriptomic analysis identifies early cellular and molecular events by which estrogen disrupts testis differentiation and causes feminization in *Xenopus laevis*, *Aquatic Toxicology*, 226 (2020) 105557.
- [66] M. Adeel, X. Song, Y. Wang, D. Francis, Y. Yang, Environmental impact of estrogens on human, animal and plant life: A critical review, *Environment International*, 99 (2017) 107-119.
- [67] R.I.L. Eggen, J. Hollender, A. Joss, M. Schärer, C. Stamm, Reducing the discharge of micropollutants in the aquatic environment: The benefits of upgrading wastewater treatment plants, *Environmental Science & Technology*, 48 (2014) 7683-7689.
- [68] B. Kasprzyk-Hordern, R.M. Dinsdale, A.J. Guwy, The occurrence of pharmaceuticals, personal care products, endocrine disruptors and illicit drugs in surface water in South Wales, UK, *Water Research*, 42 (2008) 3498-3518.
- [69] H.M. Kuch, K. Ballschmiter, Determination of endocrine-disrupting phenolic compounds and estrogens in surface and drinking water by HRGC-(NCI)-MS in the picogram per liter range, *Environmental Science & Technology*, 35 (2001) 3201-3206.
- [70] A. Wenzel, J. Müller, T. Ternes, Study on endocrine disrupters in drinking water, *Final Report, ENV.D.1/ETU/2000/0083*, (2003).
- [71] M.J. Benotti, R.A. Trenholm, B.J. Vanderford, J.C. Holady, B.D. Stanford, S.A. Snyder, Pharmaceuticals and endocrine disrupting compounds in U.S. drinking water, *Environmental Science & Technology*, 43 (2009) 597-603.
- [72] D.J. Caldwell, F. Mastrocco, E. Nowak, J. Johnston, H. Yekel, D. Pfeiffer, M. Hoyt, B.M. DuPlessie, P.D. Anderson, An assessment of potential exposure and risk from estrogens in drinking water, *Environmental Health Perspectives*, 118 (2010) 338-344.
- [73] A. Azzouz, E. Ballesteros, Influence of seasonal climate differences on the pharmaceutical, hormone and personal care product removal efficiency of a drinking water treatment plant, *Chemosphere*, 93 (2013) 2046-2054.
- [74] R.H. Gee, L.S. Rockett, P.C. Rumsby, Considerations of endocrine disrupters in drinking water, in: P.D. Darbre, *Endocrine Disruption and Human Health*, Academic Press, Boston, 2015, pp. 319-341.
- [75] Japanese Ministry of Environment, Strategic Programs on Environmental Endocrine Disruptors '98 (SPEED '98), <https://www.env.go.jp/en/chemi/ed/speed98/sp98.html>, accessed on 17 November 2021.
- [76] The Swiss Federal Council, Gewässerschutzverordnung (GSchV), 2016.
- [77] F. Metz, K. Ingold, Sustainable wastewater management: Is it possible to regulate micropollution in the future by learning from the past? A policy analysis, *Sustainability*, 6 (2014) 1992-2012.
- [78] C. Stamm, R.I.L. Eggen, J.G. Hering, J. Hollender, A. Joss, M. Schärer, Micropollutant removal from wastewater: Facts and decision-making despite uncertainty, *Environmental Science & Technology*, 49 (2015) 6374-6375.
- [79] National Health and Medical Research Council, Natural Resource Management Ministerial Council, Australian drinking water guidelines, 2011.
- [80] Australian Environment Protection and Heritage Council, National Health and Medical Research Council, Natural Resource Management Ministerial Council, Australian Guidelines for water recycling: Managing health and environmental risks (Phase 2) - Augmentation of drinking water supplies, 2008.
- [81] European Parliament and Council, Directive 2013/39/EU of the European Parliament and of the Council of 12 August 2013 amending Directives 2000/60/EC and 2008/105/EC as regards priority substances in the field of water policy, 2013.
- [82] European Commission, Proposal for a Directive of the European Parliament and of the Council amending Directives 2000/60/EC and 2008/105/EC as regards priority substances in the field of water policy, <https://eur-lex.europa.eu/legal-content/EN/TXT/?uri=CELEX:52011PC0876>, 2011.
- [83] European Commission, Commission implementing Decision (EU) 2015/495 of 20 March 2015 establishing a watch list of substances for Union-wide monitoring in the field of water policy pursuant to Directive 2008/105/EC of the European Parliament and of the Council, 2015.
- [84] European Parliament and Council, Directive 2020/2184 of the European Parliament and of the Council of 16 December 2020 on the quality of water intended for human consumption (recast), 2020.
- [85] J. Margot, C. Kienle, A. Magnet, M. Weil, L. Rossi, L.F. de Alencastro, C. Abegglen, D. Thonney, N. Chevre, M. Scharer, D.A. Barry, Treatment of micropollutants in municipal wastewater: Ozone or powdered activated carbon?, *Science of the Total Environment*, 461-462 (2013) 480-498.
- [86] J. Altmann, A.S. Ruhl, F. Zietzschmann, M. Jekel, Direct comparison of ozonation and adsorption onto powdered activated carbon for micropollutant removal in advanced wastewater treatment, *Water Research*, 55 (2014) 185-193.

- [87] Kompetenzzentrum Spurenstoffe BW, Kläranlagenausbau in Baden-Württemberg, <https://koms-bw.de/cms/content/media/2021-05%20Karte%20BW%20Ausbau%20Spurenstoffelimination.pdf>, accessed on 17 November 2021.
- [88] LGL-BW, Open Data für Geobasisdaten, <https://www.lgl-bw.de/unsere-themen/Produkte/Open-Data/>, accessed on 17 November 2021.
- [89] A. Shahmansouri, C. Bellona, Nanofiltration technology in water treatment and reuse: applications and costs, *Water Science and Technology*, 71 (2015) 309-319.
- [90] R.R.Z. Tarpani, A. Azapagic, Life cycle costs of advanced treatment techniques for wastewater reuse and resource recovery from sewage sludge, *Journal of Cleaner Production*, 204 (2018) 832-847.
- [91] World Health Organization, Potable reuse: Guidance for producing safe drinking-water, http://www.who.int/water_sanitation_health/publications/potable-reuse-guidelines/en/, accessed on 6 September 2020.
- [92] U. von Gunten, Ozonation of drinking water: Part I. Oxidation kinetics and product formation, *Water Research*, 37 (2003) 1443-1467.
- [93] S. Irmak, O. Erbatur, A. Akgerman, Degradation of 17 β -estradiol and bisphenol A in aqueous medium by using ozone and ozone/UV techniques, *Journal of Hazardous Materials*, 126 (2005) 54-62.
- [94] P. Westerhoff, Y. Yoon, S. Snyder, E. Wert, Fate of endocrine-disruptor, pharmaceutical, and personal care product chemicals during simulated drinking water treatment processes, *Environmental Science & Technology*, 39 (2005) 6649-6663.
- [95] Y. Wolf, S. Oster, A. Shuliakovich, I. Brückner, R. Dolny, V. Linnemann, J. Pinnekamp, H. Hollert, S. Schiwy, Improvement of wastewater and water quality via a full-scale ozonation plant? – A comprehensive analysis of the endocrine potential using effect-based methods, *Science of the Total Environment*, 803 (2022) 149756.
- [96] M.M. Huber, A. Göbel, A. Joss, N. Hermann, D. Löffler, C.S. McArdell, A. Ried, H. Siegrist, T.A. Ternes, U. von Gunten, Oxidation of pharmaceuticals during ozonation of municipal wastewater effluents: A pilot Study, *Environmental Science & Technology*, 39 (2005) 4290-4299.
- [97] E.C. Wert, F.L. Rosario-Ortiz, D.D. Drury, S.A. Snyder, Formation of oxidation byproducts from ozonation of wastewater, *Water Research*, 41 (2007) 1481-1490.
- [98] H. Mestankova, A.M. Parker, N. Bramaz, S. Canonica, K. Schirmer, U. von Gunten, K.G. Linden, Transformation of Contaminant Candidate List (CCL3) compounds during ozonation and advanced oxidation processes in drinking water: Assessment of biological effects, *Water Research*, 93 (2016) 110-120.
- [99] Y. Kurokawa, A. Maekawa, M. Takahashi, Y. Hayashi, Toxicity and carcinogenicity of potassium bromate—a new renal carcinogen, *Environmental Health Perspectives*, 87 (1990) 309-335.
- [100] C.K. Schmidt, H.-J. Brauch, N,N-dimethylsulfamide as precursor for N-nitrosodimethylamine (NDMA) formation upon ozonation and its fate during drinking water treatment, *Environmental Science & Technology*, 42 (2008) 6340-6346.
- [101] J. Hollender, S.G. Zimmermann, S. Koepke, M. Krauss, C.S. McArdell, C. Ort, H. Singer, U. von Gunten, H. Siegrist, Elimination of organic micropollutants in a municipal wastewater treatment plant upgraded with a full-scale post-ozonation followed by sand filtration, *Environmental Science & Technology*, 43 (2009) 7862-7869.
- [102] D. Stalter, A. Magdeburg, J. Oehlmann, Comparative toxicity assessment of ozone and activated carbon treated sewage effluents using an in vivo test battery, *Water Research*, 44 (2010) 2610-2620.
- [103] R.d.O. Pereira, M.L. de Alda, J. Joglar, L.A. Daniel, D. Barceló, Identification of new ozonation disinfection byproducts of 17 β -estradiol and estrone in water, *Chemosphere*, 84 (2011) 1535-1541.
- [104] X.-Y. Zhang, Y. Du, Y. Lu, W.-L. Wang, Q.-Y. Wu, Characteristics of the formation and toxicity index of nine newly identified brominated disinfection byproducts during wastewater ozonation, *Science of the Total Environment*, 824 (2022) 153924.
- [105] J. Li, H. Zhang, J. Wang, Z. Yu, H. Li, M. Yang, Identification of unknown disinfection byproducts in drinking water produced from Taihu Lake source water, *Journal of Environmental Sciences*, 113 (2022) 1-11.
- [106] X.-Y. Zhang, Y. Lu, Y. Du, W.-L. Wang, L.-L. Yang, Q.-Y. Wu, Comprehensive GC \times GC-qMS with a mass-to-charge ratio difference extraction method to identify new brominated byproducts during ozonation and their toxicity assessment, *Journal of Hazardous Materials*, 403 (2021) 124103.
- [107] B. Haist-Gulde, G. Baldauf, H.J. Brauch, Removal of organic micropollutants by activated carbon, in: J. Hrubec, *Water Pollution: Drinking Water and Drinking Water Treatment*, Springer, Berlin, Heidelberg, 1995, pp. 103-128.

- [108] M. Fuerhacker, A. Dürauer, A. Jungbauer, Adsorption isotherms of 17 β -estradiol on granular activated carbon (GAC), *Chemosphere*, 44 (2001) 1573-1579.
- [109] Y. Yoon, P. Westerhoff, S.A. Snyder, M. Esparza, HPLC-fluorescence detection and adsorption of bisphenol A, 17 β -estradiol, and 17 α -ethynyl estradiol on powdered activated carbon, *Water Research*, 37 (2003) 3530-3537.
- [110] T. Fukuhara, S. Iwasaki, M. Kawashima, O. Shinohara, I. Abe, Adsorbability of estrone and 17 β -estradiol in water onto activated carbon, *Water Research*, 40 (2006) 241-248.
- [111] Y. Zhang, J.L. Zhou, Removal of estrone and 17 β -estradiol from water by adsorption, *Water Research*, 39 (2005) 3991-4003.
- [112] M. Tagliavini, F. Engel, P.G. Weidler, T. Scherer, A.I. Schäfer, Adsorption of steroid micropollutants on polymer-based spherical activated carbon (PBSAC), *Journal of Hazardous Materials*, 337 (2017) 126-137.
- [113] E. Worch, Chapter 3. Adsorption equilibrium I: General aspects and single-solute adsorption, in: *Adsorption Technology in Water Treatment: Fundamentals, Processes, and Modeling*, De Gruyter, 2012, pp. 41-76.
- [114] T. Fundneider, V. Acevedo Alonso, G. Abbt-Braun, A. Wick, D. Albrecht, S. Lackner, Empty bed contact time: The key for micropollutant removal in activated carbon filters, *Water Research*, 191 (2021) 116765.
- [115] E. Worch, Chapter 7. Fixed-bed adsorber design, in: *Adsorption Technology in Water Treatment: Fundamentals, Processes, and Modeling*, De Gruyter, 2012, pp. 197-252.
- [116] F. Meinel, A.S. Ruhl, A. Sperlich, F. Zietzschmann, M. Jekel, Pilot-scale investigation of micropollutant removal with granular and powdered activated carbon, *Water, Air, & Soil Pollution*, 226 (2014) 2260.
- [117] F. Zietzschmann, C. Stützer, M. Jekel, Granular activated carbon adsorption of organic micropollutants in drinking water and treated wastewater – Aligning breakthrough curves and capacities, *Water Research*, 92 (2016) 180-187.
- [118] I.N. Najm, V.L. Snoeyink, B.W. Lykins Jr, J.Q. Adams, Using powdered activated carbon: A critical review, *Journal - AWWA*, 83 (1991) 65-76.
- [119] C. Stoquart, P. Servais, P.R. Bérubé, B. Barbeau, Hybrid Membrane Processes using activated carbon treatment for drinking water: A review, *Journal of Membrane Science*, 411-412 (2012) 1-12.
- [120] L. Kovalova, H. Siegrist, U. von Gunten, J. Eugster, M. Hagenbuch, A. Wittmer, R. Moser, C.S. McArdell, Elimination of micropollutants during post-treatment of hospital wastewater with powdered activated carbon, ozone, and UV, *Environmental Science & Technology*, 47 (2013) 7899-7908.
- [121] C. Schwaller, G. Hoffmann, C.X. Hiller, B. Helmreich, J.E. Drewes, Inline dosing of powdered activated carbon and coagulant prior to ultrafiltration at pilot-scale – Effects on trace organic chemical removal and operational stability, *Chemical Engineering Journal*, 414 (2021) 128801.
- [122] S.A. Snyder, S. Adham, A.M. Redding, F.S. Cannon, J. DeCarolis, J. Oppenheimer, E.C. Wert, Y. Yoon, Role of membranes and activated carbon in the removal of endocrine disruptors and pharmaceuticals, *Desalination*, 202 (2007) 156-181.
- [123] B. Ledesma, S. Román, A. Álvarez-Murillo, E. Sabio, J.F. González, Cyclic adsorption/thermal regeneration of activated carbons, *Journal of Analytical and Applied Pyrolysis*, 106 (2014) 112-117.
- [124] P.A. Quinlivan, L. Li, D.R.U. Knappe, Effects of activated carbon characteristics on the simultaneous adsorption of aqueous organic micropollutants and natural organic matter, *Water Research*, 39 (2005) 1663-1673.
- [125] D.J. de Ridder, A.R.D. Verliefde, S.G.J. Heijman, J.Q.J.C. Verberk, L.C. Rietveld, L.T.J. van der Aa, G.L. Amy, J.C. van Dijk, Influence of natural organic matter on equilibrium adsorption of neutral and charged pharmaceuticals onto activated carbon, *Water Science and Technology*, 63 (2011) 416-423.
- [126] G. Aschermann, F. Zietzschmann, M. Jekel, Influence of dissolved organic matter and activated carbon pore characteristics on organic micropollutant desorption, *Water Research*, 133 (2018) 123-131.
- [127] C.T. Cleveland, Big advantages in membrane filtration, *Journal - AWWA*, 91 (1999) 10-10.
- [128] A. Yusuf, A. Sodiq, A. Giwa, J. Eke, O. Pikuda, G. De Luca, J.L. Di Salvo, S. Chakraborty, A review of emerging trends in membrane science and technology for sustainable water treatment, *Journal of Cleaner Production*, 266 (2020) 121867.
- [129] B. Van der Bruggen, C. Vandecasteele, T. Van Gestel, W. Doyen, R. Leysen, A review of pressure-driven membrane processes in wastewater treatment and drinking water production, *Environmental Progress*, 22 (2003) 46-56.

- [130] G.K. Pearce, UF/MF pre-treatment to RO in seawater and wastewater reuse applications: a comparison of energy costs, *Desalination*, 222 (2008) 66-73.
- [131] F. Prézélys, L. Tiruta-Barna, J.-C. Remigy, C. Guigui, Process-based LCA of ultrafiltration for drinking water production, *Water Research*, 199 (2021) 117156.
- [132] H. Rosentreter, M. Walther, A. Lerch, Partial desalination of saline groundwater: Comparison of nanofiltration, reverse osmosis and membrane capacitive deionisation, *Membranes*, 11 (2021).
- [133] M. Giagnorio, S. Steffenino, L. Meucci, M.C. Zanetti, A. Tiraferri, Design and performance of a nanofiltration plant for the removal of chromium aimed at the production of safe potable water, *Journal of Environmental Chemical Engineering*, 6 (2018) 4467-4475.
- [134] J. Kim, K. Park, D.R. Yang, S. Hong, A comprehensive review of energy consumption of seawater reverse osmosis desalination plants, *Applied Energy*, 254 (2019) 113652.
- [135] S.-Y. Pan, A.Z. Haddad, A. Kumar, S.-W. Wang, Brackish water desalination using reverse osmosis and capacitive deionization at the water-energy nexus, *Water Research*, 183 (2020) 116064.
- [136] R. Singh, Analysis of energy usage at membrane water treatment plants, *Desalination and Water Treatment*, 29 (2011) 63-72.
- [137] EUROSTAT, Electricity price statistics, https://ec.europa.eu/eurostat/statistics-explained/index.php?title=Electricity_price_statistics, accessed on 17 April 2022.
- [138] A.J.C. Semião, A.I. Schäfer, Removal of adsorbing estrogenic micropollutants by nanofiltration membranes. Part A—Experimental evidence, *Journal of Membrane Science*, 431 (2013) 244-256.
- [139] A.I. Schäfer, L.D. Nghiem, T.D. Waite, Removal of the natural hormone estrone from aqueous solutions using nanofiltration and reverse osmosis, *Environmental Science & Technology*, 37 (2003) 182-188.
- [140] L.D. Nghiem, A. Manis, K. Soldenhoff, A.I. Schäfer, Estrogenic hormone removal from wastewater using NF/RO membranes, *Journal of Membrane Science*, 242 (2004) 37-45.
- [141] Y. Yoon, P. Westerhoff, J. Yoon, S.A. Snyder, Removal of 17 β estradiol and fluoranthene by nanofiltration and ultrafiltration, *Journal of Environmental Engineering - Asce*, 130 (2004) 1460-1467.
- [142] L.D. Nghiem, A.I. Schäfer, M. Elimelech, Removal of natural hormones by nanofiltration membranes: Measurement, modeling, and mechanisms, *Environmental Science & Technology*, 38 (2004) 1888-1896.
- [143] Y. Yoon, P. Westerhoff, S.A. Snyder, E.C. Wert, J. Yoon, Removal of endocrine disrupting compounds and pharmaceuticals by nanofiltration and ultrafiltration membranes, *Desalination*, 202 (2007) 16-23.
- [144] S. Weber, M. Gallenkemper, T. Melin, W. Dott, J. Hollender, Efficiency of nanofiltration for the elimination of steroids from water, *Water Science and Technology*, 50 (2004) 9-14.
- [145] Y. Yoon, P. Westerhoff, S.A. Snyder, E.C. Wert, Nanofiltration and ultrafiltration of endocrine disrupting compounds, pharmaceuticals and personal care products, *Journal of Membrane Science*, 270 (2006) 88-100.
- [146] I. Koyuncu, O.A. Arıkan, M.R. Wiesner, C. Rice, Removal of hormones and antibiotics by nanofiltration membranes, *Journal of Membrane Science*, 309 (2008) 94-101.
- [147] S.J. Khan, T. Wintgens, P. Sherman, J. Zaricky, A.I. Schäfer, Removal of hormones and pharmaceuticals in the Advanced Water Recycling Demonstration Plant in Queensland, Australia, *Water Science and Technology*, 50 (2004) 15-22.
- [148] A.I. Schäfer, I. Akanyeti, A.J.C. Semião, Micropollutant sorption to membrane polymers: A review of mechanisms for estrogens, *Advances in Colloid and Interface Science*, 164 (2011) 100-117.
- [149] K. Arola, B. Van der Bruggen, M. Mänttari, M. Kallioinen, Treatment options for nanofiltration and reverse osmosis concentrates from municipal wastewater treatment: A review, *Critical Reviews in Environmental Science and Technology*, 49 (2019) 2049-2116.
- [150] L.D. Nghiem, A.I. Schäfer, Critical risk points of nanofiltration and reverse osmosis processes in water recycling applications, *Desalination*, 187 (2006) 303-312.
- [151] W. Guo, H.-H. Ngo, J. Li, A mini-review on membrane fouling, *Bioresource Technology*, 122 (2012) 27-34.
- [152] M.S. Mauter, M. Elimelech, Environmental applications of carbon-based nanomaterials, *Environmental Science & Technology*, 42 (2008) 5843-5859.
- [153] R. Mailler, J. Gasperi, Y. Coquet, S. Deshayes, S. Zedek, C. Cren-Olivé, N. Cartiser, V. Eudes, A. Bressy, E. Caupos, R. Moilleron, G. Chebbo, V. Rocher, Study of a large scale powdered activated carbon pilot: Removals of a wide range of emerging and priority micropollutants from wastewater treatment plant effluents, *Water Research*, 72 (2015) 315-330.

- [154] A.M. Kennedy, A.M. Reinert, D.R.U. Knappe, I. Ferrer, R.S. Summers, Full- and pilot-scale GAC adsorption of organic micropollutants, *Water Research*, 68 (2015) 238-248.
- [155] P. Kokkinos, D. Mantzavinos, D. Venieri, Current trends in the application of nanomaterials for the removal of emerging micropollutants and pathogens from water, *Molecules*, 25 (2020).
- [156] J. Kim, B. Van der Bruggen, The use of nanoparticles in polymeric and ceramic membrane structures: Review of manufacturing procedures and performance improvement for water treatment, *Environmental Pollution*, 158 (2010) 2335-2349.
- [157] D.S. Dlamini, B.B. Mamba, J. Li, The role of nanoparticles in the performance of nano-enabled composite membranes – A critical scientific perspective, *Science of the Total Environment*, 656 (2019) 723-731.
- [158] S. Hao, Z. Jia, J. Wen, S. Li, W. Peng, R. Huang, X. Xu, Progress in adsorptive membranes for separation – A review, *Separation and Purification Technology*, 255 (2021) 117772.
- [159] C. Grandclément, I. Seyssiecq, A. Piram, P. Wong-Wah-Chung, G. Vanot, N. Tiliacos, N. Roche, P. Doumenq, From the conventional biological wastewater treatment to hybrid processes, the evaluation of organic micropollutant removal: A review, *Water Research*, 111 (2017) 297-317.
- [160] K. Kimura, G. Amy, J.E. Drewes, T. Heberer, T.-U. Kim, Y. Watanabe, Rejection of organic micropollutants (disinfection by-products, endocrine disrupting compounds, and pharmaceutically active compounds) by NF/RO membranes, *Journal of Membrane Science*, 227 (2003) 113-121.
- [161] B. Mathon, J.-M. Choubert, C. Miege, M. Coquery, A review of the photodegradability and transformation products of 13 pharmaceuticals and pesticides relevant to sewage polishing treatment, *Science of the Total Environment*, 551-552 (2016) 712-724.
- [162] B. Mathon, M. Ferreol, M. Coquery, J.-M. Choubert, J.-M. Chovelon, C. Miège, Direct photodegradation of 36 organic micropollutants under simulated solar radiation: Comparison with free-water surface constructed wetland and influence of chemical structure, *Journal of Hazardous Materials*, 407 (2021) 124801.
- [163] G.K. Ramesha, A.V. Kumara, H.B. Muralidhara, S. Sampath, Graphene and graphene oxide as effective adsorbents toward anionic and cationic dyes, *Journal of Colloid and Interface Science*, 361 (2011) 270-277.
- [164] V.K. Gupta, R. Kumar, A. Nayak, T.A. Saleh, M.A. Barakat, Adsorptive removal of dyes from aqueous solution onto carbon nanotubes: A review, *Advances in Colloid and Interface Science*, 193-194 (2013) 24-34.
- [165] K. Pyrzynska, Carbon nanotubes as sorbents in the analysis of pesticides, *Chemosphere*, 83 (2011) 1407-1413.
- [166] S.M. Maliyekkal, T.S. Sreepasad, D. Krishnan, S. Kouser, A.K. Mishra, U.V. Waghmare, T. Pradeep, Graphene: A reusable substrate for unprecedented adsorption of pesticides, *Small*, 9 (2013) 273-283.
- [167] C. Jung, A. Son, N. Her, K.-D. Zoh, J. Cho, Y. Yoon, Removal of endocrine disrupting compounds, pharmaceuticals, and personal care products in water using carbon nanotubes: A review, *J. Ind. Eng. Chem.*, 27 (2015) 1-11.
- [168] F.F. Liu, J. Zhao, S. Wang, P. Du, B. Xing, Effects of solution chemistry on adsorption of selected pharmaceuticals and personal care products (PPCPs) by graphenes and carbon nanotubes, *Environmental Science & Technology*, 48 (2014) 13197-13206.
- [169] B. Pan, D.H. Lin, H. Mashayekhi, B.S. Xing, Adsorption and hysteresis of bisphenol A and 17 α -ethinyl estradiol on carbon nanomaterials, *Environmental Science & Technology*, 42 (2008) 5480-5485.
- [170] L. Joseph, J. Heo, Y.-G. Park, J.R.V. Flora, Y. Yoon, Adsorption of bisphenol A and 17 α -ethinyl estradiol on single walled carbon nanotubes from seawater and brackish water, *Desalination*, 281 (2011) 68-74.
- [171] A. Kiran Kumar, S. Venkata Mohan, Removal of natural and synthetic endocrine disrupting estrogens by multi-walled carbon nanotubes (MWCNT) as adsorbent: Kinetic and mechanistic evaluation, *Separation and Purification Technology*, 87 (2012) 22-30.
- [172] L. Jiang, Y. Liu, S. Liu, G. Zeng, X. Hu, X. Hu, Z. Guo, X. Tan, L. Wang, Z. Wu, Adsorption of estrogen contaminants by graphene nanomaterials under natural organic matter preloading: Comparison to carbon nanotube, biochar, and activated carbon, *Environmental Science & Technology*, 51 (2017) 6352-6359.
- [173] Q. Zaib, I.A. Khan, N.B. Saleh, J.R.V. Flora, Y.-G. Park, Y. Yoon, Removal of bisphenol A and 17 β -Estradiol by single-walled carbon nanotubes in aqueous solution: Adsorption and molecular modeling, *Water, Air, & Soil Pollution*, 223 (2012) 3281-3293.

- [174] W. Sun, K. Zhou, Adsorption of 17 β -estradiol by multi-walled carbon nanotubes in natural waters with or without aquatic colloids, *Chemical Engineering Journal*, 258 (2014) 185-193.
- [175] L. Jiang, Y. Liu, G. Zeng, S. Liu, X. Hu, L. Zhou, X. Tan, N. Liu, M. Li, J. Wen, Adsorption of estrogen contaminants (17 β -estradiol and 17 α -ethynylestradiol) by graphene nanosheets from water: Effects of graphene characteristics and solution chemistry, *Chemical Engineering Journal*, 339 (2018) 296-302.
- [176] A. Freixa, V. Acuna, J. Sanchis, M. Farre, D. Barcelo, S. Sabater, Ecotoxicological effects of carbon based nanomaterials in aquatic organisms, *Science of the Total Environment*, 619-620 (2018) 328-337.
- [177] R. Das, B.F. Leo, F. Murphy, The toxic truth about carbon nanotubes in water purification: A perspective view, *Nanoscale Research Letters*, 13 (2018) 183.
- [178] Y. Zhu, X. Liu, Y. Hu, R. Wang, M. Chen, J. Wu, Y. Wang, S. Kang, Y. Sun, M. Zhu, Behavior, remediation effect and toxicity of nanomaterials in water environments, *Environmental Research*, 174 (2019) 54-60.
- [179] W. Kulcke, A. Knabbe, G. Brunner, Characterization of a microfiltration membrane by use of residence time distribution, *Journal of Membrane Science*, 161 (1999) 263-273.
- [180] A.G. Fane, Membranes for water production and wastewater reuse, *Desalination*, 106 (1996) 1-9.
- [181] J. Löwenberg, A. Zenker, M. Baggenstos, G. Koch, C. Kazner, T. Wintgens, Comparison of two PAC/UF processes for the removal of micropollutants from wastewater treatment plant effluent: Process performance and removal efficiency, *Water Research*, 56 (2014) 26-36.
- [182] K. Ebie, F. Li, Y. Azuma, A. Yuasa, T. Hagishita, Pore distribution effect of activated carbon in adsorbing organic micropollutants from natural water, *Water Research*, 35 (2001) 167-179.
- [183] F. Zietzschmann, E. Worch, J. Altmann, A.S. Ruhl, A. Sperlich, F. Meinel, M. Jekel, Impact of EfOM size on competition in activated carbon adsorption of organic micro-pollutants from treated wastewater, *Water Research*, 65 (2014) 297-306.
- [184] R. Guilloussou, J. Le Roux, R. Mailler, C.S. Pereira-Derome, G. Varrault, A. Bressy, E. Vulliet, C. Morlay, F. Nauleau, V. Rocher, J. Gasperi, Influence of dissolved organic matter on the removal of 12 organic micropollutants from wastewater effluent by powdered activated carbon adsorption, *Water Research*, 172 (2020) 115487.
- [185] M. Zhang, C. Li, M.M. Benjamin, Y. Chang, Fouling and natural organic matter removal in adsorbent/membrane systems for drinking water treatment, *Environmental Science & Technology*, 37 (2003) 1663-1669.
- [186] S. Shao, H. Liang, F. Qu, K. Li, H. Chang, H. Yu, G. Li, Combined influence by humic acid (HA) and powdered activated carbon (PAC) particles on ultrafiltration membrane fouling, *Journal of Membrane Science*, 500 (2016) 99-105.
- [187] S. Shao, L. Cai, K. Li, J. Li, X. Du, G. Li, H. Liang, Deposition of powdered activated carbon (PAC) on ultrafiltration (UF) membrane surface: Influencing factors and mechanisms, *Journal of Membrane Science*, 530 (2017) 104-111.
- [188] S. Lee, J.-W. Lee, S. Kim, P.-K. Park, J.-H. Kim, C.-H. Lee, Removal of 17 β -estradiol by powdered activated carbon—microfiltration hybrid process: The effect of PAC deposition on membrane surface, *Journal of Membrane Science*, 326 (2009) 84-91.
- [189] G. Knopp, F. Yang, P. Cornel, Elimination von Mikroverunreinigungen aus biologisch gereinigtem Kommunalabwasser mittels kombinierter Membran- und Aktivkohleadsorptionsverfahren, *gwf Wasser / Abwasser*, 157 (2016) 46-59.
- [190] L. Paredes, C. Alfonsin, T. Allegue, F. Omil, M. Carballa, Integrating granular activated carbon in the post-treatment of membrane and settler effluents to improve organic micropollutants removal, *Chemical Engineering Journal*, 345 (2018) 79-86.
- [191] S. Gidstedt, A. Betsholtz, P. Falås, M. Cimbritz, Å. Davidsson, F. Micolucci, O. Svahn, A comparison of adsorption of organic micropollutants onto activated carbon following chemically enhanced primary treatment with microsieving, direct membrane filtration and tertiary treatment of municipal wastewater, *Science of the Total Environment*, 811 (2022) 152225.
- [192] M. Tagliavini, A.I. Schäfer, Removal of steroid micropollutants by polymer-based spherical activated carbon (PBSAC) assisted membrane filtration, *Journal of Hazardous Materials*, 353 (2018) 514-521.
- [193] M. Tagliavini, P.G. Weidler, C. Njel, J. Pohl, D. Richter, B. Böhringer, A.I. Schäfer, Polymer-based spherical activated carbon – ultrafiltration (UF-PBSAC) for the adsorption of steroid hormones from water: Material characteristics and process configuration, *Water Research*, 185 (2020) 116249.
- [194] J.K. Holt, H.G. Park, Y. Wang, M. Stadermann, A.B. Artyukhin, C.P. Grigoropoulos, A. Noy, O. Bakajin, Fast mass transport through sub-2-nanometer carbon nanotubes, *Science*, 312 (2006) 1034.

- [195] N. Bui, E.R. Meshot, S. Kim, J. Pena, P.W. Gibson, K.J. Wu, F. Fornasiero, Ultrabreathable and protective membranes with sub-5 nm carbon nanotube pores, *Advanced Materials*, 28 (2016) 5871-5877.
- [196] M.L. Jue, S.F. Buchsbaum, C. Chen, S.J. Park, E.R. Meshot, K.J.J. Wu, F. Fornasiero, Ultra-permeable single-walled carbon nanotube membranes with exceptional performance at scale, *Advanced Science*, 7 (2020) 2001670.
- [197] A.K. Geim, K.S. Novoselov, The rise of graphene, *Nature Materials*, 6 (2007) 183-191.
- [198] T. Barkan, Graphene: the hype versus commercial reality, *Nature Nanotechnology*, 14 (2019) 904-906.
- [199] D. Chen, H. Feng, J. Li, Graphene oxide: Preparation, functionalization, and electrochemical applications, *Chemical Reviews*, 112 (2012) 6027-6053.
- [200] S. Iijima, Helical microtubules of graphitic carbon, *Nature*, 354 (1991) 56-58.
- [201] H.W. Kroto, J.R. Heath, S.C. O'Brien, R.F. Curl, R.E. Smalley, C₆₀: Buckminsterfullerene, *Nature*, 318 (1985) 162-163.
- [202] Y. Saito, T. Yoshikawa, S. Bandow, M. Tomita, T. Hayashi, Interlayer spacings in carbon nanotubes, *Physical Review B*, 48 (1993) 1907-1909.
- [203] G. Bacon, The interlayer spacing of graphite, *Acta Crystallographica*, 4 (1951) 558-561.
- [204] R. Taylor, D.R.M. Walton, The chemistry of fullerenes, *Nature*, 363 (1993) 685.
- [205] P.A. Heiney, J.E. Fischer, A.R. McGhie, W.J. Romanow, A.M. Denenstien, J.P. McCauley Jr, A.B. Smith, D.E. Cox, Orientational ordering transition in solid C₆₀, *Physical Review Letters*, 66 (1991) 2911-2914.
- [206] L. Bulavin, I. Adamenko, Y. Prylutsky, S. Durov, A. Graja, A. Bogucki, P. Scharff, Structure of fullerene C₆₀ in aqueous solution, *Physical Chemistry Chemical Physics*, 2 (2000) 1627-1629.
- [207] K.L. Chen, M. Elimelech, Aggregation and deposition kinetics of fullerene (C₆₀) nanoparticles, *Langmuir*, 22 (2006) 10994-11001.
- [208] F. Banhart, J. Kotakoski, A.V. Krasheninnikov, Structural defects in graphene, *ACS Nano*, 5 (2011) 26-41.
- [209] J.C. Charlier, Defects in carbon nanotubes, *Accounts of Chemical Research*, 35 (2002) 1063-1069.
- [210] W. Liu, G. Speranza, Tuning the oxygen content of reduced graphene oxide and effects on its properties, *ACS Omega*, 6 (2021) 6195-6205.
- [211] G. Ersan, Y. Kaya, O.G. Apul, T. Karanfil, Adsorption of organic contaminants by graphene nanosheets, carbon nanotubes and granular activated carbons under natural organic matter preloading conditions, *Science of the Total Environment*, 565 (2016) 811-817.
- [212] Y. Zhou, O.G. Apul, T. Karanfil, Adsorption of halogenated aliphatic contaminants by graphene nanomaterials, *Water Research*, 79 (2015) 57-67.
- [213] O.G. Apul, Q. Wang, Y. Zhou, T. Karanfil, Adsorption of aromatic organic contaminants by graphene nanosheets: comparison with carbon nanotubes and activated carbon, *Water Research*, 47 (2013) 1648-1654.
- [214] C.-T. Hsieh, H. Teng, Influence of mesopore volume and adsorbate size on adsorption capacities of activated carbons in aqueous solutions, *Carbon*, 38 (2000) 863-869.
- [215] P. Amaral, E. Partlan, M. Li, F. Lapolli, O.T. Mefford, T. Karanfil, D.A. Ladner, Superfine powdered activated carbon (S-PAC) coatings on microfiltration membranes: Effects of milling time on contaminant removal and flux, *Water Research*, 100 (2016) 429-438.
- [216] E. Partlan, K. Davis, Y. Ren, O.G. Apul, O.T. Mefford, T. Karanfil, D.A. Ladner, Effect of bead milling on chemical and physical characteristics of activated carbons pulverized to superfine sizes, *Water Research*, 89 (2016) 161-170.
- [217] N. Cai, P. Larese-Casanova, Sorption of carbamazepine by commercial graphene oxides: A comparative study with granular activated carbon and multiwalled carbon nanotubes, *Journal of Colloid and Interface Science*, 426 (2014) 152-161.
- [218] G. Sun, L. Zheng, Z. Zhan, J. Zhou, X. Liu, L. Li, Actuation triggered exfoliation of graphene oxide at low temperature for electrochemical capacitor applications, *Carbon*, 68 (2014) 748-754.
- [219] E. Papirer, E. Brendle, F. Ozil, H. Balard, Comparison of the surface properties of graphite, carbon black and fullerene samples, measured by inverse gas chromatography, *Carbon*, 37 (1999) 1265-1274.
- [220] M.D. Stoller, S. Park, Y. Zhu, J. An, R.S. Ruoff, Graphene-based ultracapacitors, *Nano Letters*, 8 (2008) 3498-3502.
- [221] Y. Matsui, A. Sakamoto, S. Nakao, T. Taniguchi, T. Matsushita, N. Shirasaki, N. Sakamoto, H. Yurimoto, Isotope microscopy visualization of the adsorption profile of 2-methylisoborneol and geosmin in powdered activated carbon, *Environmental Science & Technology*, 48 (2014) 10897-10903.

- [222] C.-J.M. Chin, L.-C. Shih, H.-J. Tsai, T.-K. Liu, Adsorption of o-xylene and p-xylene from water by SWCNTs, *Carbon*, 45 (2007) 1254-1260.
- [223] S.-u. Rather, R. Zacharia, M.-u.-d. Naik, S.W. Hwang, A.R. Kim, K.S. Nahm, Surface adsorption and micropore filling of the hydrogen in activated MWCNTs, *International Journal of Hydrogen Energy*, 33 (2008) 6710-6718.
- [224] S.F. Buchsbaum, M.L. Jue, A.M. Sawvel, C. Chen, E.R. Meshot, S.J. Park, M. Wood, K.J. Wu, C.L. Bilodeau, F. Aydin, T.A. Pham, E.Y. Lau, F. Fornasiero, Fast permeation of small ions in carbon nanotubes, *Advanced Science*, 8 (2021) 2001802.
- [225] C.J. Corwin, R.S. Summers, Controlling trace organic contaminants with GAC adsorption, *Journal - AWWA*, 104 (2012) E36-E47.
- [226] J.R. Ellerie, O.G. Apul, T. Karanfil, D.A. Ladner, Comparing graphene, carbon nanotubes, and superfine powdered activated carbon as adsorptive coating materials for microfiltration membranes, *Journal of Hazardous Materials*, 261 (2013) 91-98.
- [227] Y. Wang, J. Zhu, H. Huang, H.-H. Cho, Carbon nanotube composite membranes for microfiltration of pharmaceuticals and personal care products: Capabilities and potential mechanisms, *Journal of Membrane Science*, 479 (2015) 165-174.
- [228] Y. Wang, Y. Liu, Y. Yu, H. Huang, Influence of CNT-rGO composite structures on their permeability and selectivity for membrane water treatment, *Journal of Membrane Science*, 551 (2018) 326-332.
- [229] E. Worch, Chapter 5. Adsorption kinetics, in: *Adsorption Technology in Water Treatment: Fundamentals, Processes, and Modeling*, De Gruyter, 2012, pp. 123-168.
- [230] W.J. Weber, E.H. Smith, Simulation and design models for adsorption processes, *Environmental Science & Technology*, 21 (1987) 1040-1050.
- [231] G.E. Boyd, A.W. Adamson, L.S. Myers, The exchange adsorption of ions from aqueous solutions by organic zeolites. II. Kinetics, *Journal of the American Chemical Society*, 69 (1947) 2836-2848.
- [232] T. Furusawa, J.M. Smith, Fluid-particle and intraparticle mass transport rates in slurries, *Industrial & Engineering Chemistry Fundamentals*, 12 (1973) 197-203.
- [233] A.R. Mathews, A.W.J. Weber, Modeling and parameter evaluation for adsorption in slurry reactors, *Chemical Engineering Communications*, 25 (1984) 157-171.
- [234] D.M. Ruthven, *Principles of Adsorption and Adsorption Processes*, Wiley, Hoboken, NJ, USA, 1984.
- [235] F. Wang, W. Sun, W. Pan, N. Xu, Adsorption of sulfamethoxazole and 17 β -estradiol by carbon nanotubes/CoFe₂O₄ composites, *Chemical Engineering Journal*, 274 (2015) 17-29.
- [236] L.A. Al-Khateeb, S. Almotiry, M.A. Salam, Adsorption of pharmaceutical pollutants onto graphene nanoplatelets, *Chemical Engineering Journal*, 248 (2014) 191-199.
- [237] W.J. Weber, J.C. Morris, Kinetics of adsorption on carbon from solution, *Journal of the Sanitary Engineering Division*, 89 (1963) 31-60.
- [238] J. Crank, *The Mathematics of Diffusion*, Clarendon Press, Oxford, England, UK, 1979.
- [239] W.H. Cheung, Y.S. Szeto, G. McKay, Intraparticle diffusion processes during acid dye adsorption onto chitosan, *Bioresource Technology*, 98 (2007) 2897-2904.
- [240] F. Liu, J. Wang, L. Li, Y. Shao, Z. Xu, S. Zheng, Adsorption of Direct Yellow 12 onto ordered mesoporous carbon and activated carbon, *Journal of Chemical and Engineering Data*, 54 (2009) 3043-3050.
- [241] F.-C. Wu, R.-L. Tseng, R.-S. Juang, Initial behavior of intraparticle diffusion model used in the description of adsorption kinetics, *Chemical Engineering Journal*, 153 (2009) 1-8.
- [242] S. Zhang, T. Shao, H.S. Kose, T. Karanfil, Adsorption kinetics of aromatic compounds on carbon nanotubes and activated carbons, *Environmental Toxicology and Chemistry*, 31 (2012) 79-85.
- [243] A.C. Martins, O. Pezoti, A.L. Cazetta, K.C. Bedin, D.A.S. Yamazaki, G.F.G. Bandoch, T. Asefa, J.V. Visentainer, V.C. Almeida, Removal of tetracycline by NaOH-activated carbon produced from macadamia nut shells: Kinetic and equilibrium studies, *Chemical Engineering Journal*, 260 (2015) 291-299.
- [244] M.A.E. de Franco, C.B. de Carvalho, M.M. Bonetto, R.d.P. Soares, L.A. Féris, Removal of amoxicillin from water by adsorption onto activated carbon in batch process and fixed bed column: Kinetics, isotherms, experimental design and breakthrough curves modelling, *Journal of Cleaner Production*, 161 (2017) 947-956.
- [245] B. Xie, J. Qin, S. Wang, X. Li, H. Sun, W. Chen, Adsorption of phenol on commercial activated carbons: Modelling and interpretation, *International Journal of Environmental Research and Public Health*, 17 (2020).

- [246] J. Zhang, M.N. Nguyen, Y. Li, C. Yang, A.I. Schäfer, Steroid hormone micropollutant removal from water with activated carbon fiber-ultrafiltration composite membranes, *Journal of Hazardous Materials*, 391 (2020) 122020.
- [247] C.-H. Wu, Adsorption of reactive dye onto carbon nanotubes: Equilibrium, kinetics and thermodynamics, *Journal of Hazardous Materials*, 144 (2007) 93-100.
- [248] C.-Y. Kuo, C.-H. Wu, J.-Y. Wu, Adsorption of direct dyes from aqueous solutions by carbon nanotubes: Determination of equilibrium, kinetics and thermodynamics parameters, *Journal of Colloid and Interface Science*, 327 (2008) 308-315.
- [249] Y. Yao, F. Xu, M. Chen, Z. Xu, Z. Zhu, Adsorption behavior of methylene blue on carbon nanotubes, *Bioresource Technology*, 101 (2010) 3040-3046.
- [250] T. Liu, Y. Li, Q. Du, J. Sun, Y. Jiao, G. Yang, Z. Wang, Y. Xia, W. Zhang, K. Wang, H. Zhu, D. Wu, Adsorption of methylene blue from aqueous solution by graphene, *Colloids and Surfaces B: Biointerfaces*, 90 (2012) 197-203.
- [251] N. Li, M. Zheng, X. Chang, G. Ji, H. Lu, L. Xue, L. Pan, J. Cao, Preparation of magnetic CoFe₂O₄-functionalized graphene sheets via a facile hydrothermal method and their adsorption properties, *Journal of Solid State Chemistry*, 184 (2011) 953-958.
- [252] S. Zhang, T. Shao, S.S.K. Bekaroglu, T. Karanfil, The impacts of aggregation and surface chemistry of carbon nanotubes on the adsorption of synthetic organic compounds, *Environmental Science & Technology*, 43 (2009) 5719-5725.
- [253] J. Zhao, Z. Wang, Q. Zhao, B. Xing, Adsorption of phenanthrene on multilayer graphene as affected by surfactant and exfoliation, *Environmental Science & Technology*, 48 (2014) 331-339.
- [254] B. Xu, S. Yue, Z. Sui, X. Zhang, S. Hou, G. Cao, Y. Yang, What is the choice for supercapacitors: Graphene or graphene oxide?, *Energy & Environmental Science*, 4 (2011) 2826-2830.
- [255] J. Comer, R. Chen, H. Poblete, A. Vergara-Jaque, J.E. Riviere, Predicting adsorption affinities of small molecules on carbon nanotubes using molecular dynamics simulation, *ACS Nano*, 9 (2015) 11761-11774.
- [256] L. Jiang, Y. Liu, G. Zeng, F. Xiao, X. Hu, X. Hu, H. Wang, T. Li, L. Zhou, X. Tan, Removal of 17 β -estradiol by few-layered graphene oxide nanosheets from aqueous solutions: External influence and adsorption mechanism, *Chemical Engineering Journal*, 284 (2016) 93-102.
- [257] B. Pan, B.S. Xing, Adsorption mechanisms of organic chemicals on carbon nanotubes, *Environmental Science & Technology*, 42 (2008) 9005-9013.
- [258] O.G. Apul, T. Karanfil, Adsorption of synthetic organic contaminants by carbon nanotubes: A critical review, *Water Research*, 68 (2015) 34-55.
- [259] G. Ersan, O.G. Apul, F. Perreault, T. Karanfil, Adsorption of organic contaminants by graphene nanosheets: A review, *Water Research*, 126 (2017) 385-398.
- [260] J.N. Israelachvili, The nature of van der Waals forces, *Contemporary Physics*, 15 (1974) 159-178.
- [261] E.M. Perez, N. Martin, π - π interactions in carbon nanostructures, *Chemical Society Reviews*, 44 (2015) 6425-6433.
- [262] D. Lin, B. Xing, Adsorption of phenolic compounds by carbon nanotubes: Role of aromaticity and substitution of hydroxyl groups, *Environmental Science & Technology*, 42 (2008) 7254-7259.
- [263] W. Chen, L. Duan, L. Wang, D. Zhu, Adsorption of hydroxyl- and amino-substituted aromatics to carbon nanotubes, *Environmental Science & Technology*, 42 (2008) 6862-6868.
- [264] J. Chen, W. Chen, D. Zhu, Adsorption of nonionic aromatic compounds to single-walled carbon nanotubes: Effects of aqueous solution chemistry, *Environmental Science & Technology*, 42 (2008) 7225-7230.
- [265] F. Tournus, S. Latil, M.I. Heggie, J.C. Charlier, π -stacking interaction between carbon nanotubes and organic molecules, *Physical Review B*, 72 (2005).
- [266] S. Ghosh, P.K. Ojha, K. Roy, Exploring QSPR modeling for adsorption of hazardous synthetic organic chemicals (SOCs) by SWCNTs, *Chemosphere*, 228 (2019) 545-555.
- [267] P.D.W. Boyd, M.C. Hodgson, C.E.F. Rickard, A.G. Oliver, L. Chaker, P.J. Brothers, R.D. Bolskar, F.S. Tham, C.A. Reed, Selective supramolecular porphyrin/fullerene interactions, *Journal of the American Chemical Society*, 121 (1999) 10487-10495.
- [268] S. Gotovac, H. Honda, Y. Hattori, K. Takahashi, H. Kanoh, K. Kaneko, Effect of nanoscale curvature of single-walled carbon nanotubes on adsorption of polycyclic aromatic hydrocarbons, *Nano Letters*, 7 (2007) 583-587.

- [269] S. Gotovac, C.M. Yang, Y. Hattori, K. Takahashi, H. Kanoh, K. Kaneko, Adsorption of polyaromatic hydrocarbons on single wall carbon nanotubes of different functionalities and diameters, *Journal of Colloid and Interface Science*, 314 (2007) 18-24.
- [270] J. Chen, H. Liu, W.A. Weimer, M.D. Halls, D.H. Waldeck, G.C. Walker, Noncovalent engineering of carbon nanotube surfaces by rigid, functional conjugated polymers, *Journal of the American Chemical Society*, 124 (2002) 9034-9035.
- [271] A.J. Neel, M.J. Hilton, M.S. Sigman, F.D. Toste, Exploiting non-covalent π interactions for catalyst design, *Nature*, 543 (2017) 637-646.
- [272] M. Nishio, The CH/ π hydrogen bond in chemistry. Conformation, supramolecules, optical resolution and interactions involving carbohydrates, *Physical Chemistry Chemical Physics*, 13 (2011) 13873-13900.
- [273] E. Jimenez-Moreno, G. Jimenez-Oses, A.M. Gomez, A.G. Santana, F. Corzana, A. Bastida, J. Jimenez-Barbero, J.L. Asensio, A thorough experimental study of CH/ π interactions in water: Quantitative structure-stability relationships for carbohydrate/aromatic complexes, *Chemical Science*, 6 (2015) 6076-6085.
- [274] Z.R. Laughrey, S.E. Kiehna, A.J. Riemen, M.L. Waters, Carbohydrate- π interactions: What are they worth?, *Journal of the American Chemical Society*, 130 (2008) 14625-14633.
- [275] M.J. Plevin, D.L. Bryce, J. Boisbouvier, Direct detection of CH/ π interactions in proteins, *Nature Chemistry*, 2 (2010) 466-471.
- [276] P. Borthakur, P.K. Boruah, M.R. Das, N. Kulik, B. Minofar, Adsorption of 17 α -ethynyl estradiol and β -estradiol on graphene oxide surface: An experimental and computational study, *Journal of Molecular Liquids*, 269 (2018) 160-168.
- [277] F. Mouhat, F.-X. Coudert, M.-L. Bocquet, Structure and chemistry of graphene oxide in liquid water from first principles, *Nature Communications*, 11 (2020) 1566.
- [278] B. Lian, S. De Luca, Y. You, S. Alwarappan, M. Yoshimura, V. Sahajwalla, S.C. Smith, G. Leslie, R.K. Joshi, Extraordinary water adsorption characteristics of graphene oxide, *Chemical Science*, 9 (2018) 5106-5111.
- [279] Z. Jin, X. Wang, Y. Sun, Y. Ai, X. Wang, Adsorption of 4-n-Nonylphenol and Bisphenol-A on magnetic reduced graphene oxides: A combined experimental and theoretical studies, *Environmental Science & Technology*, 49 (2015) 9168-9175.
- [280] V.V. Neklyudov, N.R. Khafizov, I.A. Sedov, A.M. Dimiev, New insights into the solubility of graphene oxide in water and alcohols, *Physical Chemistry Chemical Physics*, 19 (2017) 17000-17008.
- [281] N.V. Medhekar, A. Ramasubramaniam, R.S. Ruoff, V.B. Shenoy, Hydrogen bond networks in graphene oxide composite paper: Structure and mechanical properties, *ACS Nano*, 4 (2010) 2300-2306.
- [282] J. Tao, H. Tang, A. Patra, P. Bhattarai, J.P. Perdew, Modeling the physisorption of graphene on metals, *Physical Review B*, 97 (2018).
- [283] F. London, The general theory of molecular forces, *Transactions of the Faraday Society*, 33 (1937) 8b-26.
- [284] A.I. Zhbanov, E.G. Pogorelov, Y.-C. Chang, van der Waals interaction between two crossed carbon nanotubes, *ACS Nano*, 4 (2010) 5937-5945.
- [285] C. Thierfelder, M. Witte, S. Blankenburg, E. Rauls, W.G. Schmidt, Methane adsorption on graphene from first principles including dispersion interaction, *Surface Science*, 605 (2011) 746-749.
- [286] H.Q. Xie, H. Lee, W. Youn, M. Choi, Nanofluids containing multiwalled carbon nanotubes and their enhanced thermal conductivities, *Journal of Applied Physics*, 94 (2003) 4967-4971.
- [287] D. Bouchard, X. Ma, C. Issacson, Colloidal properties of aqueous fullerenes: isoelectric points and aggregation kinetics of C₆₀ and C₆₀ derivatives, *Environmental Science & Technology*, 43 (2009) 6597-6603.
- [288] D. Li, M.B. Muller, S. Gilje, R.B. Kaner, G.G. Wallace, Processable aqueous dispersions of graphene nanosheets, *Nature Nanotechnology*, 3 (2008) 101-105.
- [289] D.D. Perrin, B. Dempsey, E.P. Serjeant, *pKa prediction for organic acids and bases*, Chapman and Hall, London ; New York, 1981.
- [290] K.M. Lewis, R.D. Archer, pKa values of estrone, 17 β -estradiol and 2-methoxyestrone, *Steroids*, 34 (1979) 485-499.
- [291] A. Bhandari, R.Y. Surampalli, C.D. Adams, P. Champagne, S.K. Ong, R.D. Tyagi, T.C. Zhang, *Contaminants of emerging environmental concern*, American Society of Civil Engineers, Reston, Virginia, USA, 2009.
- [292] D.A. Walker, B. Kowalczyk, M.O. de la Cruz, B.A. Grzybowski, Electrostatics at the nanoscale, *Nanoscale*, 3 (2011) 1316-1344.

- [293] V.R. Dugyala, J.S. Muthukuru, E. Mani, M.G. Basavaraj, Role of electrostatic interactions in the adsorption kinetics of nanoparticles at fluid–fluid interfaces, *Physical Chemistry Chemical Physics*, 18 (2016) 5499-5508.
- [294] E.E. Meyer, K.J. Rosenberg, J. Israelachvili, Recent progress in understanding hydrophobic interactions, *PNAS*, 103 (2006) 15739.
- [295] S.H. Donaldson, Jr., A. Royne, K. Kristiansen, M.V. Rapp, S. Das, M.A. Gebbie, D.W. Lee, P. Stock, M. Valtiner, J. Israelachvili, Developing a general interaction potential for hydrophobic and hydrophilic interactions, *Langmuir*, 31 (2015) 2051-2064.
- [296] J. Israelachvili, R. Pashley, The hydrophobic interaction is long range, decaying exponentially with distance, *Nature*, 300 (1982) 341.
- [297] L. Bocquet, E. Charlaix, Nanofluidics, from bulk to interfaces, *Chemical Society Reviews*, 39 (2010) 1073-1095.
- [298] K. Kendall, Adhesion: Molecules and mechanics, *Science*, 263 (1994) 1720-1725.
- [299] P.L. Yap, M.J. Nine, K. Hassan, T.T. Tung, D.N.H. Tran, D. Losic, Graphene-based sorbents for multipollutants removal in water: A review of recent progress, *Advanced Functional Materials*, 31 (2021) 2007356.
- [300] P.W. Atkins, J. De Paula, Chemical equilibrium, in: *Physical Chemistry*, 9th ed., W.H. Freeman, New York, 2010.
- [301] H. Patel, Fixed-bed column adsorption study: A comprehensive review, *Applied Water Science*, 9 (2019) 45.
- [302] M.N. Nguyen, P.B. Trinh, C.J. Burkhardt, A.I. Schäfer, Incorporation of single-walled carbon nanotubes in ultrafiltration support structure for the removal of steroid hormone micropollutants, *Separation and Purification Technology*, 264 (2021) 118405.
- [303] M.N. Nguyen, P.G. Weidler, R. Schwaiger, A.I. Schäfer, Interactions between carbon-based nanoparticles and steroid hormone micropollutants in water, *Journal of Hazardous Materials*, 402 (2020) 122929.
- [304] Y. Shimizu, M. Ateia, C. Yoshimura, Natural organic matter undergoes different molecular sieving by adsorption on activated carbon and carbon nanotubes, *Chemosphere*, 203 (2018) 345-352.
- [305] M.N. Nguyen, R. Hervás-Martínez, A.I. Schäfer, Organic matter interference with steroid hormone removal by single-walled carbon nanotubes - ultrafiltration composite membrane, *Water Research*, 199 (2021) 117148.
- [306] V.K.K. Upadhyayula, S. Deng, M.C. Mitchell, G.B. Smith, Application of carbon nanotube technology for removal of contaminants in drinking water: A review, *Science of the Total Environment*, 408 (2009) 1-13.
- [307] F. Wang, J. Yao, H. Chen, Z. Yi, B. Xing, Sorption of humic acid to functionalized multi-walled carbon nanotubes, *Environmental Pollution*, 180 (2013) 1-6.
- [308] H. Hyung, J.H. Kim, Natural organic matter (NOM) adsorption to multi-walled carbon nanotubes: effect of NOM characteristics and water quality parameters, *Environmental Science & Technology*, 42 (2008) 4416-4421.
- [309] N. Cai, D. Peak, P. Lares-Casanova, Factors influencing natural organic matter sorption onto commercial graphene oxides, *Chemical Engineering Journal*, 273 (2015) 568-579.
- [310] D. Lin, B. Xing, Tannic acid adsorption and its role for stabilizing carbon nanotube suspensions, *Environmental Science & Technology*, 42 (2008) 5917-5923.
- [311] X. Zhang, M. Liu, X. Zhang, F. Deng, C. Zhou, J. Hui, W. Liu, Y. Wei, Interaction of tannic acid with carbon nanotubes: Enhancement of dispersibility and biocompatibility, *Toxicology Research*, 4 (2015) 160-168.
- [312] X.L. Wang, S. Tao, B.S. Xing, Sorption and competition of aromatic compounds and humic acid on multiwalled carbon nanotubes, *Environmental Science & Technology*, 43 (2009) 6214-6219.
- [313] M. Engel, B. Chefetz, Adsorption and desorption of dissolved organic matter by carbon nanotubes: Effects of solution chemistry, *Environmental Pollution*, 213 (2016) 90-98.
- [314] G.S. Ajmani, H.H. Cho, T.E. Abbott Chalew, K.J. Schwab, J.G. Jacangelo, H. Huang, Static and dynamic removal of aquatic natural organic matter by carbon nanotubes, *Water Research*, 59 (2014) 262-270.
- [315] M. Ateia, O.G. Apul, Y. Shimizu, A. Muflihah, C. Yoshimura, T. Karanfil, Elucidating adsorptive fractions of natural organic matter on carbon nanotubes, *Environmental Science & Technology*, 51 (2017) 7101-7110.

- [316] L. Ma, S.R. Yates, Dissolved organic matter and estrogen interactions regulate estrogen removal in the aqueous environment: A review, *Science of the Total Environment*, 640-641 (2018) 529-542.
- [317] P.A. Neale, B.I. Escher, A.I. Schäfer, pH dependence of steroid hormone-organic matter interactions at environmental concentrations, *Science of the Total Environment*, 407 (2009) 1164-1173.
- [318] H. Yamamoto, H.M. Liljestrand, Y. Shimizu, M. Morita, Effects of physical-chemical characteristics on the sorption of selected endocrine disruptors by dissolved organic matter surrogates, *Environmental Science & Technology*, 37 (2003) 2646-2657.
- [319] Y.-L. Yeh, K.-J. Yeh, L.-F. Hsu, W.-C. Yu, M.-H. Lee, T.-C. Chen, Use of fluorescence quenching method to measure sorption constants of phenolic xenoestrogens onto humic fractions from sediment, *Journal of Hazardous Materials*, 277 (2014) 27-33.
- [320] J. Lee, J. Cho, S.H. Kim, S.D. Kim, Influence of 17 β -estradiol binding by dissolved organic matter isolated from wastewater effluent on estrogenic activity, *Ecotoxicology and Environmental Safety*, 74 (2011) 1280-1287.
- [321] S. Zhang, T. Shao, S.S.K. Bekaroglu, T. Karanfil, Adsorption of synthetic organic chemicals by carbon nanotubes: Effects of background solution chemistry, *Water Research*, 44 (2010) 2067-2074.
- [322] B. Martin-Mousset, J.P. Croue, E. Lefebvre, B. Legube, Distribution and characterization of dissolved organic matter of surface waters, *Water Research*, 31 (1997) 541-553.
- [323] G. Aschermann, A. Jeihanipour, J. Shen, G. Mkongo, L. Dramas, J.P. Croue, A. Schäfer, Seasonal variation of organic matter concentration and characteristics in the Maji ya Chai River (Tanzania): Impact on treatability by ultrafiltration, *Water Research*, 101 (2016) 370-381.
- [324] J. Wolters, M. Tagliavini, A.I. Schäfer, Removal of steroid hormone micropollutants by UF-PBSAC composite in presence of organic matter, *Journal of Membrane Science*, 592 (2019) 117315.
- [325] E.M. Thurman, Chapter 10. Aquatic humic substances, in: *Organic geochemistry of natural waters*, Martinus Nijhoff / Dr W. Junk Publishers, Dordrecht, The Netherlands, 1985, pp. 273-362.
- [326] A.I. Schäfer, *Natural organics removal using membranes : Principles, performance and cost*, Technomic Publishing, Lancaster, Pennsylvania, 2001.
- [327] J. Lowe, M.M. Hossain, Application of ultrafiltration membranes for removal of humic acid from drinking water, *Desalination*, 218 (2008) 343-354.
- [328] M.D. Kennedy, H.K. Chun, V.A. Quintanilla Yangali, B.G.J. Heijman, J.C. Schippers, Natural organic matter (NOM) fouling of ultrafiltration membranes: fractionation of NOM in surface water and characterisation by LC-OCD, *Desalination*, 178 (2005) 73-83.
- [329] S.A. Huber, A. Balz, M. Abert, W. Pronk, Characterisation of aquatic humic and non-humic matter with size-exclusion chromatography-organic carbon detection-organic nitrogen detection (LC-OCD-OND), *Water Research*, 45 (2011) 879-885.
- [330] E. Filloux, H. Gallard, J.P. Croue, Identification of effluent organic matter fractions responsible for low-pressure membrane fouling, *Water Research*, 46 (2012) 5531-5540.
- [331] M. Hadidi, J.J. Buckley, A.L. Zydney, Ultrafiltration behavior of bacterial polysaccharides used in vaccines, *Journal of Membrane Science*, 490 (2015) 294-300.
- [332] R. Berenguer, J.P. Marco-Lozar, C. Quijada, D. Cazorla-Amorós, E. Morallón, Comparison among chemical, thermal, and electrochemical regeneration of phenol-saturated activated carbon, *Energy & Fuels*, 24 (2010) 3366-3372.
- [333] O. Zanella, I.C. Tessaro, L.A. Féris, Desorption- and decomposition-based techniques for the regeneration of activated carbon, *Chemical Engineering & Technology*, 37 (2014) 1447-1459.
- [334] Y. Wang, X. Wei, R. Zhang, Y. Wu, M.U. Farid, H. Huang, Comparison of chemical, ultrasonic and thermal regeneration of carbon nanotubes for acetaminophen, ibuprofen, and triclosan adsorption, *RSC Advances*, 7 (2017) 52719-52728.
- [335] L.R. de Carvalho Costa, L. de Moraes Ribeiro, G.E.N. Hidalgo, L.A. Féris, Evaluation of efficiency and capacity of thermal, chemical and ultrasonic regeneration of tetracycline exhausted activated carbon, *Environmental Technology*, 43 (2022) 907-917.
- [336] K.G.P. Nunes, L.W. Sfreddo, M. Rosset, L.A. Féris, Efficiency evaluation of thermal, ultrasound and solvent techniques in activated carbon regeneration, *Environmental Technology*, 42 (2021) 4189-4200.
- [337] E. Worch, Chapter 8. Desorption and reactivation, in: *Adsorption Technology in Water Treatment: Fundamentals, Processes, and Modeling*, De Gruyter, 2012, pp. 253-263.
- [338] C.O. Ania, J.B. Parra, C. Pevida, A. Arenillas, F. Rubiera, J.J. Pis, Pyrolysis of activated carbons exhausted with organic compounds, *Journal of Analytical and Applied Pyrolysis*, 74 (2005) 518-524.

- [339] M. Suzuki, D.M. Mistic, O. Koyama, K. Kawazoe, Study of thermal regeneration of spent activated carbons: Thermogravimetric measurement of various single component organics loaded on activated carbons, *Chemical Engineering Science*, 33 (1978) 271-279.
- [340] Sigma Aldrich, Thermal transitions of homopolymers: Glass transition & melting point, <https://www.sigmaaldrich.com/DE/en/technical-documents/technical-article/materials-science-and-engineering/polymer-synthesis/thermal-transitions-of-homopolymers>, accessed on 15 April 2022.
- [341] H.S. McLaughlin, Regenerate activated carbon using organic solvents, *Chemical Engineering Progress*, 91 (1995) 45–53.
- [342] A. Mittal, D. Kaur, A. Malviya, J. Mittal, V.K. Gupta, Adsorption studies on the removal of coloring agent phenol red from wastewater using waste materials as adsorbents, *Journal of Colloid and Interface Science*, 337 (2009) 345-354.
- [343] S.-H. Kow, M.R. Fahmi, C.Z.A. Abidin, S.-A. Ong, N. Ibrahim, Regeneration of spent activated carbon from industrial application by NaOH solution and hot water, *Desalination and Water Treatment*, 57 (2016) 29137-29142.
- [344] D.O. Cooney, A. Nagerl, A.L. Hines, Solvent regeneration of activated carbon, *Water Research*, 17 (1983) 403-410.
- [345] D. Guo, Q. Shi, B. He, X. Yuan, Different solvents for the regeneration of the exhausted activated carbon used in the treatment of coking wastewater, *Journal of Hazardous Materials*, 186 (2011) 1788-1793.
- [346] D. Chinn, C.J. King, Adsorption of glycols, sugars, and related multiple –OH compounds onto activated carbons. 2. solvent regeneration, *Industrial & Engineering Chemistry Research*, 38 (1999) 3746-3753.
- [347] M.K. Purkait, A. Maiti, S. DasGupta, S. De, Removal of congo red using activated carbon and its regeneration, *Journal of Hazardous Materials*, 145 (2007) 287-295.
- [348] F.M. Machado, C.P. Bergmann, T.H. Fernandes, E.C. Lima, B. Royer, T. Calvete, S.B. Fagan, Adsorption of Reactive Red M-2BE dye from water solutions by multi-walled carbon nanotubes and activated carbon, *Journal of Hazardous Materials*, 192 (2011) 1122-1131.
- [349] X. Cheng, A.T. Kan, M.B. Tomson, Naphthalene adsorption and desorption from aqueous C₆₀ fullerene, *Journal of Chemical and Engineering Data*, 49 (2004) 675-683.
- [350] X.M. Yan, B.Y. Shi, J.J. Lu, C.H. Feng, D.S. Wang, H.X. Tang, Adsorption and desorption of atrazine on carbon nanotubes, *Journal of Colloid and Interface Science*, 321 (2008) 30-38.
- [351] K. Yang, B. Xing, Desorption of polycyclic aromatic hydrocarbons from carbon nanomaterials in water, *Environmental Pollution*, 145 (2007) 529-537.
- [352] S. Sühnhholz, F.-D. Kopinke, B. Weiner, Hydrothermal treatment for regeneration of activated carbon loaded with organic micropollutants, *Science of the Total Environment*, 644 (2018) 854-861.
- [353] G. Berčič, A. Pintar, J. Levec, Desorption of phenol from activated carbon by hot water regeneration. Desorption Isotherms, *Industrial & Engineering Chemistry Research*, 35 (1996) 4619-4625.
- [354] B.M. Aumeier, A.H.Q. Dang, B. Ohs, S. Yüce, M. Wessling, Aqueous-phase temperature swing adsorption for pesticide removal, *Environmental Science & Technology*, 53 (2019) 919-927.
- [355] B.M. Aumeier, H. Graul, A.-K. Müller, C. Lackmann, R. Wünsch, T. Wintgens, H. Hollert, M. Wessling, The hydrothermal solution for self-sustaining drinking water purification at point of use, *Water Research*, 170 (2020) 115338.
- [356] X. Zou, L. Zhang, Z. Wang, Y. Luo, Mechanisms of the antimicrobial activities of graphene materials, *Journal of the American Chemical Society*, 138 (2016) 2064-2077.
- [357] S. Kang, M. Herzberg, D.F. Rodrigues, M. Elimelech, Antibacterial effects of carbon nanotubes: Size does matter!, *Langmuir*, 24 (2008) 6409-6413.
- [358] S. Liu, L. Wei, L. Hao, N. Fang, M.W. Chang, R. Xu, Y. Yang, Y. Chen, Sharper and faster “nano darts” kill more bacteria: A study of antibacterial activity of individually dispersed pristine single-walled carbon nanotube, *ACS Nano*, 3 (2009) 3891-3902.
- [359] C. Yang, J. Mamouni, Y. Tang, L. Yang, Antimicrobial activity of single-walled carbon nanotubes: Length effect, *Langmuir*, 26 (2010) 16013-16019.
- [360] J.K. Stanley, J.G. Laird, A.J. Kennedy, J.A. Steevens, Sublethal effects of multiwalled carbon nanotube exposure in the invertebrate *Daphnia magna*, *Environmental Toxicology and Chemistry*, 35 (2016) 200-204.
- [361] W. Fan, Y. Liu, Z. Xu, X. Wang, X. Li, S. Luo, The mechanism of chronic toxicity to *Daphnia magna* induced by graphene suspended in a water column, *Environmental Science: Nano*, 3 (2016) 1405-1415.

- [362] J.R. Lawrence, M.J. Waiser, G.D.W. Swerhone, J. Roy, V. Tumber, A. Paule, A.P. Hitchcock, J.J. Dynes, D.R. Korber, Effects of fullerene (C₆₀), multi-wall carbon nanotubes (MWCNT), single wall carbon nanotubes (SWCNT) and hydroxyl and carboxyl modified single wall carbon nanotubes on riverine microbial communities, *Environmental Science and Pollution Research*, 23 (2016) 10090-10102.
- [363] L.J. Hazeem, M. Bououdina, E. Dewailly, C. Slomianny, A. Barras, Y. Coffinier, S. Szunerits, R. Boukherroub, Toxicity effect of graphene oxide on growth and photosynthetic pigment of the marine alga *Picochlorum sp.* during different growth stages, *Environmental Science and Pollution Research*, 24 (2017) 4144-4152.
- [364] C. Hu, Q. Wang, H. Zhao, L. Wang, S. Guo, X. Li, Ecotoxicological effects of graphene oxide on the protozoan *Euglena gracilis*, *Chemosphere*, 128 (2015) 184-190.
- [365] M. Mortimer, E.J. Petersen, B.A. Buchholz, E. Orias, P.A. Holden, Bioaccumulation of multiwall carbon nanotubes in *Tetrahymena thermophila* by direct feeding or trophic transfer, *Environmental Science & Technology*, 50 (2016) 8876-8885.
- [366] T.L. Rocha, T. Gomes, V.S. Sousa, N.C. Mestre, M.J. Bebianno, Ecotoxicological impact of engineered nanomaterials in bivalve molluscs: An overview, *Marine Environmental Research*, 111 (2015) 74-88.
- [367] X. Zhu, L. Zhu, Y. Lang, Y. Chen, Oxidative stress and growth inhibition in the freshwater fish *Carassius auratus* induced by chronic exposure to sublethal fullerene aggregates, *Environmental Toxicology and Chemistry*, 27 (2008) 1979-1985.
- [368] C. Pretti, M. Oliva, R.D. Pietro, G. Monni, G. Cevasco, F. Chiellini, C. Pomelli, C. Chiappe, Ecotoxicity of pristine graphene to marine organisms, *Ecotoxicology and Environmental Safety*, 101 (2014) 138-145.
- [369] F. Gottschalk, T. Sonderer, R.W. Scholz, B. Nowack, Modeled environmental concentrations of engineered nanomaterials (TiO₂, ZnO, Ag, CNT, fullerenes) for different regions, *Environmental Science & Technology*, 43 (2009) 9216-9222.
- [370] T.Y. Sun, F. Gottschalk, K. Hungerbühler, B. Nowack, Comprehensive probabilistic modelling of environmental emissions of engineered nanomaterials, *Environmental Pollution*, 185 (2014) 69-76.
- [371] F. von der Kammer, P.L. Ferguson, P.A. Holden, A. Masion, K.R. Rogers, S.J. Klaine, A.A. Koelmans, N. Horne, J.M. Unrine, Analysis of engineered nanomaterials in complex matrices (environment and biota): General considerations and conceptual case studies, *Environmental Toxicology and Chemistry*, 31 (2012) 32-49.
- [372] M. Troester, H.-J. Brauch, T. Hofmann, Vulnerability of drinking water supplies to engineered nanoparticles, *Water Research*, 96 (2016) 255-279.
- [373] E. Emke, J. Sanchís, M. Farré, P.S. Bäuerlein, P. de Voogt, Determination of several fullerenes in sewage water by LC HR-MS using atmospheric pressure photoionisation, *Environmental Science: Nano*, 2 (2015) 167-176.
- [374] M. Farré, S. Pérez, K. Gajda-Schrantz, V. Osorio, L. Kantiani, A. Ginebreda, D. Barceló, First determination of C₆₀ and C₇₀ fullerenes and N-methylfulleropyrrolidine C₆₀ on the suspended material of wastewater effluents by liquid chromatography hybrid quadrupole linear ion trap tandem mass spectrometry, *Journal of Hydrology*, 383 (2010) 44-51.
- [375] A. Astefanei, O. Núñez, M.T. Galceran, Analysis of C₆₀-fullerene derivatives and pristine fullerenes in environmental samples by ultrahigh performance liquid chromatography-atmospheric pressure photoionization-mass spectrometry, *Journal of Chromatography A*, 1365 (2014) 61-71.
- [376] Y. Su, X. Yan, Y. Pu, F. Xiao, D. Wang, M. Yang, Risks of single-walled carbon nanotubes acting as contaminants-carriers: Potential release of phenanthrene in Japanese medaka (*Oryzias latipes*), *Environmental Science & Technology*, 47 (2013) 4704-4710.
- [377] J. Campos-Garcia, D.S.T. Martinez, O.L. Alves, A.F.G. Leonardo, E. Barbieri, Ecotoxicological effects of carbofuran and oxidised multiwalled carbon nanotubes on the freshwater fish Nile tilapia: Nanotubes enhance pesticide ecotoxicity, *Ecotoxicology and Environmental Safety*, 111 (2015) 131-137.
- [378] Z.A. Qiao, B. Guo, A.J. Binder, J. Chen, G.M. Veith, S. Dai, Controlled synthesis of mesoporous carbon nanostructures via a "silica-assisted" strategy, *Nano Letters*, 13 (2013) 207-212.
- [379] X. Li, A. Sotto, J.S. Li, B. Van der Bruggen, Progress and perspectives for synthesis of sustainable antifouling composite membranes containing in situ generated nanoparticles, *Journal of Membrane Science*, 524 (2017) 502-528.
- [380] M.R. Esfahani, S.A. Aktij, Z. Dabaghian, M.D. Firouzjaei, A. Rahimpour, J. Eke, I.C. Escobar, M. Abolhassani, L.F. Greenlee, A.R. Esfahani, A. Sadmani, N. Koutahzadeh, Nanocomposite membranes for

- water separation and purification: Fabrication, modification, and applications, *Separation and Purification Technology*, 213 (2019) 465-499.
- [381] J. Yin, B. Deng, Polymer-matrix nanocomposite membranes for water treatment, *Journal of Membrane Science*, 479 (2015) 256-275.
- [382] R. Pal, Permeation models for mixed matrix membranes, *Journal of Colloid and Interface Science*, 317 (2008) 191-198.
- [383] V.-T. Hoang, S. Kaliaguine, Predictive models for mixed-matrix membrane performance: A review, *Chemical Reviews*, 113 (2013) 4980-5028.
- [384] A. Mollahosseini, A. Rahimpour, M. Jahamshahi, M. Peyravi, M. Khavarpour, The effect of silver nanoparticle size on performance and antibacteriability of polysulfone ultrafiltration membrane, *Desalination*, 306 (2012) 41-50.
- [385] P.F. Andrade, A.F. de Faria, S.R. Oliveira, M.A. Arruda, C. Goncalves Mdo, Improved antibacterial activity of nanofiltration polysulfone membranes modified with silver nanoparticles, *Water Research*, 81 (2015) 333-342.
- [386] X. Li, R. Pang, J. Li, X. Sun, J. Shen, W. Han, L. Wang, In situ formation of Ag nanoparticles in PVDF ultrafiltration membrane to mitigate organic and bacterial fouling, *Desalination*, 324 (2013) 48-56.
- [387] E.M.V. Hoek, A.K. Ghosh, X.F. Huang, M. Liong, J.I. Zink, Physical-chemical properties, separation performance, and fouling resistance of mixed-matrix ultrafiltration membranes, *Desalination*, 283 (2011) 89-99.
- [388] G. Kaminska, J. Bohdziewicz, J.I. Calvo, P. Prádanos, L. Palacio, A. Hernández, Fabrication and characterization of polyethersulfone nanocomposite membranes for the removal of endocrine disrupting micropollutants from wastewater. Mechanisms and performance, *Journal of Membrane Science*, 493 (2015) 66-79.
- [389] Z. Wang, L. Xu, C. Qi, C. Zhao, Fabrication of MWCNTs-polysulfone composite membranes and its application in the removal of bisphenol A, *Materials Research Express*, 5 (2018) 065101.
- [390] A.S. Brady-Estevez, S. Kang, M. Elimelech, A single-walled-carbon-nanotube filter for removal of viral and bacterial pathogens, *Small*, 4 (2008) 481-484.
- [391] Y.-P. An, J. Yang, H.-C. Yang, M.-B. Wu, Z.-K. Xu, Janus membranes with charged carbon nanotube coatings for deemulsification and separation of oil-in-water emulsions, *ACS Applied Materials & Interfaces*, 10 (2018) 9832-9840.
- [392] L. Liu, M. Son, S. Chakraborty, C. Bhattacharjee, H. Choi, Fabrication of ultra-thin polyelectrolyte/carbon nanotube membrane by spray-assisted layer-by-layer technique: characterization and its anti-protein fouling properties for water treatment, *Desalination and Water Treatment*, 51 (2013) 6194-6200.
- [393] A.V. Dudchenko, J. Rolf, K. Russell, W. Duan, D. Jassby, Organic fouling inhibition on electrically conducting carbon nanotube-polyvinyl alcohol composite ultrafiltration membranes, *Journal of Membrane Science*, 468 (2014) 1-10.
- [394] K. Fischer, P. Schulz, I. Atanasov, A. Abdul Latif, I. Thomas, M. Kühnert, A. Prager, J. Griebel, A. Schulze, Synthesis of high crystalline TiO₂ nanoparticles on a polymer membrane to degrade pollutants from water, *Catalysts*, 8 (2018) 376.
- [395] H. Strathmann, *Introduction to membrane science and technology*, Wiley-VCH Verlag & Co., Weinheim, Germany, 2011.
- [396] S.S. Madaeni, S. Zinadini, V. Vatanpour, Preparation of superhydrophobic nanofiltration membrane by embedding multiwalled carbon nanotube and polydimethylsiloxane in pores of microfiltration membrane, *Separation and Purification Technology*, 111 (2013) 98-107.
- [397] S. Pan, J. Li, O. Noonan, X. Fang, G. Wan, C. Yu, L. Wang, Dual-functional ultrafiltration membrane for simultaneous removal of multiple pollutants with high performance, *Environmental Science & Technology*, 51 (2017) 5098-5107.
- [398] Z. Liao, X. Fang, J. Li, X. Li, W. Zhang, X. Sun, J. Shen, W. Han, S. Zhao, L. Wang, Incorporating organic nanospheres into the polyamide layer to prepare thin film composite membrane with enhanced biocidal activity and chlorine resistance, *Separation and Purification Technology*, 207 (2018) 222-230.
- [399] X. Zhang, X. Fang, J. Li, S. Pan, X. Sun, J. Shen, W. Han, L. Wang, S. Zhao, Developing new adsorptive membrane by modification of support layer with iron oxide microspheres for arsenic removal, *Journal of Colloid and Interface Science*, 514 (2018) 760-768.
- [400] J. Xie, Z. Liao, M. Zhang, L. Ni, J. Qi, C. Wang, X. Sun, L. Wang, S. Wang, J. Li, Sequential ultrafiltration-catalysis membrane for excellent removal of multiple pollutants in water, *Environmental Science & Technology*, 55 (2021) 2652-2661.

- [401] Y. Liu, K. Ai, L. Lu, Polydopamine and its derivative materials: Synthesis and promising applications in energy, environmental, and biomedical fields, *Chemical Reviews*, 114 (2014) 5057-5115.
- [402] M. Feins, K.K. Sirkar, Novel internally staged ultrafiltration for protein purification, *Journal of Membrane Science*, 248 (2005) 137-148.
- [403] J. Roslan, S.M. Mustapa Kamal, K.F. Md. Yunos, N. Abdullah, Assessment on multilayer ultrafiltration membrane for fractionation of tilapia by-product protein hydrolysate with angiotensin I-converting enzyme (ACE) inhibitory activity, *Separation and Purification Technology*, 173 (2017) 250-257.
- [404] J. Shen, G. Liu, Y. Han, W. Jin, Artificial channels for confined mass transport at the sub-nanometre scale, *Nature Reviews Materials*, 6 (2021) 294-312.
- [405] J.R. Werber, C.O. Osuji, M. Elimelech, Materials for next-generation desalination and water purification membranes, *Nature Reviews Materials*, 1 (2016) 16018.
- [406] Y. Wu, X. Zhao, Y. Shang, S. Chang, L. Dai, A. Cao, Application-driven carbon nanotube functional materials, *ACS Nano*, 15 (2021) 7946-7974.
- [407] D. Mattia, H. Leese, K.P. Lee, Carbon nanotube membranes: From flow enhancement to permeability, *Journal of Membrane Science*, 475 (2015) 266-272.
- [408] B.J. Hinds, N. Chopra, T. Rantell, R. Andrews, V. Gavalas, L.G. Bachas, Aligned multiwalled carbon nanotube membranes, *Science*, 303 (2004) 62-65.
- [409] E.R. Meshot, S.J. Park, S.F. Buchsbaum, M.L. Jue, T.R. Kuykendall, E. Schaible, L.B. Bayu Aji, S.O. Kucheyev, K.J.J. Wu, F. Fornasiero, High-yield growth kinetics and spatial mapping of single-walled carbon nanotube forests at wafer scale, *Carbon*, 159 (2020) 236-246.
- [410] G.D. Nessim, A.J. Hart, J.S. Kim, D. Acquaviva, J. Oh, C.D. Morgan, M. Seita, J.S. Leib, C.V. Thompson, Tuning of vertically-aligned carbon nanotube diameter and areal density through catalyst pre-treatment, *Nano Letters*, 8 (2008) 3587-3593.
- [411] M. Whitby, L. Cagnon, M. Thanou, N. Quirke, Enhanced fluid flow through nanoscale carbon pipes, *Nano Letters*, 9 (2009) 2802-2802.
- [412] M. Majumder, N. Chopra, B.J. Hinds, Mass transport through carbon nanotube membranes in three different regimes: Ionic diffusion and gas and liquid flow, *ACS Nano*, 5 (2011) 3867-3877.
- [413] W.R. Bowen, J.S. Welfoot, Modelling the performance of membrane nanofiltration—critical assessment and model development, *Chemical Engineering Science*, 57 (2002) 1121-1137.
- [414] M.N. Nguyen, M.L. Jue, S.F. Buchsbaum, S.J. Park, F. Vollnhals, S. Christiansen, F. Fornasiero, A.I. Schäfer, Adsorption of steroid hormone micropollutants in the nanoconfinement of vertically aligned single-walled carbon nanotube membranes, *submitted*, (2022).
- [415] Z. Adamczyk, Molecular–van der Waals interactions, in: *Particles at interfaces: Interactions, deposition, structure*, Elsevier, Academic Press, 2006, pp. 127-169.
- [416] J.N. Israelachvili, Intermolecular, interparticle, and intersurface forces, in: *Intermolecular and surface forces*, 3rd ed., Elsevier, Academic Press, 2011, pp. 205-222.
- [417] J.N. Israelachvili, Repulsive steric forces, total intermolecular pair potentials, and liquid structure, in: *Intermolecular and surface forces*, 3rd ed., Elsevier, Academic Press, 2011, pp. 133-150.
- [418] R.W. Baker, Membrane transport theory, in: *Membrane technology and applications*, 3rd ed., John Wiley & Sons, Chichester, West Sussex, U.K., 2012, pp. 15-96.
- [419] K.-L. Tung, Y.-C. Jean, D. Nanda, K.-R. Lee, W.-S. Hung, C.-H. Lo, J.-Y. Lai, Characterization of multilayer nanofiltration membranes using positron annihilation spectroscopy, *Journal of Membrane Science*, 343 (2009) 147-156.
- [420] F. Fallahianbijan, S. Giglia, C. Carbrello, A.L. Zydney, Quantitative analysis of internal flow distribution and pore interconnectivity within asymmetric virus filtration membranes, *Journal of Membrane Science*, 595 (2020) 117578.
- [421] M. Cieplak, E.D. Smith, M.O. Robbins, Molecular origins of friction: The force on adsorbed layers, *Science*, 265 (1994) 1209.
- [422] A. Imbrogno, A.I. Schäfer, Comparative study of nanofiltration membrane characterization devices of different dimension and configuration (cross flow and dead end), *Journal of Membrane Science*, 585 (2019) 67-80.
- [423] P. Lipp, M. Witte, G. Baldauf, A.A. Povorov, Treatment of reservoir water with a backwashable MF/UF spiral wound membrane, *Desalination*, 179 (2005) 83-94.
- [424] J.C. Mierzwa, I. Hespanhol, M.C.C. da Silva, L.D.B. Rodrigues, C.F. Giorgi, Direct drinking water treatment by spiral-wound ultrafiltration membranes, *Desalination*, 230 (2008) 41-50.

- [425] P.A. Neale, W. Pronk, A.I. Schäfer, Influence of pH on losses of analyte estradiol in sample prefiltration, *Environmental Engineering Science*, 26 (2009) 1157-1161.
- [426] P.A. Neale, A.I. Schäfer, Quantification of solute-solute interactions in steroidal hormone removal by ultrafiltration membranes, *Separation and Purification Technology*, 90 (2012) 31-38.
- [427] A. Imbrogno, J. Biscarat, A.I. Schäfer, Estradiol uptake in a combined magnetic ion exchange - ultrafiltration (MIEX-UF) process during water treatment, *Current Pharmaceutical Design*, 23 (2017) 328-337.
- [428] S.R. Wickramasinghe, S.E. Bower, Z. Chen, A. Mukherjee, S.M. Husson, Relating the pore size distribution of ultrafiltration membranes to dextran rejection, *Journal of Membrane Science*, 340 (2009) 1-8.
- [429] E. Worch, Eine neue Gleichung zur Berechnung von Diffusionskoeffizienten gelöster Stoffe, *Vom Wasser*, 81 (1993) 289-297.
- [430] S.-i. Nakao, Determination of pore size and pore size distribution: 3. Filtration membranes, *Journal of Membrane Science*, 96 (1994) 131-165.
- [431] C. Hansch, A. Leo, D.H. Hoekman, *Exploring QSAR: Hydrophobic, electronic, and steric constants*, American Chemical Society, Washington DC, 1995.
- [432] S.H. Yalkowsky, Y. He, *Handbook of aqueous solubility data*, Taylor & Francis, Andover, England, UK, 2010.
- [433] M.W. Ruchelman, P. Haines, Solubility studies of estradiol in organic solvents using gas-liquid chromatography, *Journal of Chromatographic Science*, 5 (1967) 290-296.
- [434] M.W. Ruchelman, Solubility studies of estrone in organic solvents using gas-liquid chromatography, *Analytical Biochemistry*, 19 (1967) 98-108.
- [435] E.A. Doisy, M.N. Huffman, S.A. Thayer, E.A. Doisy, Solubilities of some estrogens, *Journal of Biological Chemistry*, (1941) 283-285.
- [436] M.W. Ruchelman, Solubility studies of testosterone in organic solvents using gas chromatography, *Journal of Chromatographic Science*, 9 (1971) 235-240.
- [437] L. Sieminska, M. Ferguson, T.W. Zerda, E. Couch, Diffusion of steroids in porous sol-gel glass: Application in slow drug delivery, *Journal of Sol-Gel Science and Technology*, 8 (1997) 1105-1109.
- [438] A.I. Schäfer, A.G. Fane, T.D. Waite, Nanofiltration of natural organic matter: Removal, fouling and the influence of multivalent ions, *Desalination*, 118 (1998) 109-122.
- [439] H. Robles, Tannic acid, in: P. Wexler, *Encyclopedia of Toxicology (Third Edition)*, Academic Press, Oxford, 2014, pp. 474-475.
- [440] A. Crozier, I.B. Jaganath, M.N. Clifford, Phenols, polyphenols and tannins: An overview, in: A. Crozier, M.N. Clifford, H. Ashihara, *Plant Secondary Metabolites: Occurrence, Structure and Role in the Human Diet*, John Wiley & Sons, 2006.
- [441] F.A. Johnson, D.Q.M. Craig, A.D. Mercer, Characterization of the block structure and molecular weight of sodium alginates, *Journal of Pharmacy and Pharmacology*, 49 (1997) 639-643.
- [442] Regulat, Kaskadenfermentation, <https://www.regulat.com/kaskadenfermentation>, accessed on 17 November 2021.
- [443] I.V. Perminova, F.H. Frimmel, A.V. Kudryavtsev, N.A. Kulikova, G. Abbt-Braun, S. Hesse, V.S. Petrosyan, Molecular weight characteristics of humic substances from different environments as determined by size exclusion chromatography and their statistical evaluation, *Environmental Science & Technology*, 37 (2003) 2477-2485.
- [444] H.-S. Shin, J.M. Monsallier, G.R. Choppin, Spectroscopic and chemical characterizations of molecular size fractionated humic acid, *Talanta*, 50 (1999) 641-647.
- [445] T.A. Davis, B. Volesky, A. Mucci, A review of the biochemistry of heavy metal biosorption by brown algae, *Water Research*, 37 (2003) 4311-4330.
- [446] P. Kraal, B. Jansen, K.G.J. Nierop, J.M. Verstraten, Copper complexation by tannic acid in aqueous solution, *Chemosphere*, 65 (2006) 2193-2198.
- [447] P.A. Neale, B.I. Escher, A.I. Schäfer, Quantification of solute-solute interactions using negligible-depletion solid-phase microextraction: Measuring the affinity of estradiol to bulk organic matter, *Environmental Science & Technology*, 42 (2008) 2886-2892.
- [448] L.O. Villacorte, R. Schurer, M.D. Kennedy, G.L. Amy, J.C. Schippers, The fate of transparent exopolymer particles (TEP) in seawater UF-RO system: A pilot plant study in Zeeland, The Netherlands, *Desalination and Water Treatment*, 13 (2010) 109-119.

- [449] International Association for the Properties of Water and Steam, Release on the IAPWS formulation 2008 for the viscosity of ordinary water substance, <http://www.iapws.org/relguide/visc.pdf>, accessed on 31 December 2021.
- [450] S. Mochizuki, A.L. Zydney, Theoretical analysis of pore size distribution effects on membrane transport, *Journal of Membrane Science*, 82 (1993) 211-227.
- [451] J.-D. Jeon, S.J. Kim, S.-Y. Kwak, ¹H nuclear magnetic resonance (NMR) cryoporometry as a tool to determine the pore size distribution of ultrafiltration membranes, *Journal of Membrane Science*, 309 (2008) 233-238.
- [452] M.B. Tanis-Kanbur, R.I. Peinador, X. Hu, J.I. Calvo, J.W. Chew, Membrane characterization via evapoporometry (EP) and liquid-liquid displacement porosimetry (LLDP) techniques, *Journal of Membrane Science*, 586 (2019) 248-258.
- [453] J.I. Calvo, R.I. Peinador, P. Prádanos, L. Palacio, A. Bottino, G. Capannelli, A. Hernández, Liquid-liquid displacement porometry to estimate the molecular weight cut-off of ultrafiltration membranes, *Desalination*, 268 (2011) 174-181.
- [454] M. Sorci, C.C. Woodcock, D.J. Andersen, A.R. Behzad, S. Nunes, J. Plawsky, G. Belfort, "Linking microstructure of membranes and performance", *Journal of Membrane Science*, 594 (2020) 117419.
- [455] S. Shultz, M. Bass, R. Semiat, V. Freger, Modification of polyamide membranes by hydrophobic molecular plugs for improved boron rejection, *Journal of Membrane Science*, 546 (2018) 165-172.
- [456] J.A. Greenwood, M.M. Sandomire, Sample size required for estimating the standard deviation as a per cent of its true value, *Journal of the American Statistical Association*, 45 (1950) 257-260.
- [457] US Environmental Protection Agency, Definition and procedure for the determination of the method detection limit, revision 2, https://www.epa.gov/sites/default/files/2016-12/documents/mdl-procedure_rev2_12-13-2016.pdf, accessed on 10 November 2021.
- [458] J. Taylor, *Introduction to error analysis, the study of uncertainties in physical measurements*, 2 ed., 1997.
- [459] K.S.W. Sing, The use of gas adsorption for the characterization of porous solids, *Colloids and Surfaces*, 38 (1989) 113-124.
- [460] A.V. Neimark, Y. Lin, P.I. Ravikovitch, M. Thommes, Quenched solid density functional theory and pore size analysis of micro-mesoporous carbons, *Carbon*, 47 (2009) 1617-1628.
- [461] T.A. Centeno, F. Stoeckli, The assessment of surface areas in porous carbons by two model-independent techniques, the DR equation and DFT, *Carbon*, 48 (2010) 2478-2486.
- [462] K.L. Parry, A.G. Shard, R.D. Short, R.G. White, J.D. Whittle, A. Wright, ARXPS characterisation of plasma polymerised surface chemical gradients, *Surface and Interface Analysis*, 38 (2006) 1497-1504.
- [463] S. Tanuma, C.J. Powell, D.R. Penn, Calculations of electron inelastic mean free paths. V. Data for 14 organic compounds over the 50–2000 eV range, *Surface and Interface Analysis*, 21 (1994) 165-176.
- [464] J.H. Scofield, Hartree-Slater subshell photoionization cross-sections at 1254 and 1487 eV, *Journal of Electron Spectroscopy and Related Phenomena*, 8 (1976) 129-137.
- [465] M. Rajabi, K. Mahanpoor, O. Moradi, Removal of dye molecules from aqueous solution by carbon nanotubes and carbon nanotube functional groups: critical review, *RSC Advances*, 7 (2017) 47083-47090.
- [466] H. Tang, Y. Zhao, S. Shan, X. Yang, D. Liu, F. Cui, B. Xing, Theoretical insight into the adsorption of aromatic compounds on graphene oxide, *Environmental Science: Nano*, 5 (2018) 2357-2367.
- [467] D.I. Hitchcock, The formal identity of Langmuir's adsorption equation with the law of mass action, *Journal of the American Chemical Society*, 48 (1926) 2870-2870.
- [468] S. Azizian, Kinetic models of sorption: a theoretical analysis, *Journal of Colloid and Interface Science*, 276 (2004) 47-52.
- [469] X. Guo, J. Wang, A general kinetic model for adsorption: Theoretical analysis and modeling, *Journal of Molecular Liquids*, 288 (2019) 111100.
- [470] Y. Liu, L. Shen, From Langmuir kinetics to first- and second-order rate equations for adsorption, *Langmuir*, 24 (2008) 11625-11630.
- [471] S. Lagergren, Zur Theorie der Sogenannten Adsorption Gelöster Stoffe, Kungliga Svenska Vetenskapsakademiens, *Handlingar*, 24 (1898) 1-98.
- [472] Y.S. Ho, G. McKay, Pseudo-second order model for sorption processes, *Process Biochemistry*, 34 (1999) 451-465.
- [473] H. Freundlich, Über die adsorption in lösungen, *Zeitschrift für Physikalische Chemie*, 57 (1907) 385-470.
- [474] K.Y. Foo, B.H. Hameed, Insights into the modeling of adsorption isotherm systems, *Chemical Engineering Journal*, 156 (2010) 2-10.

- [475] I. Langmuir, The adsorption of gases on plane surfaces of glass, mica and platinum, *Journal of the American Chemical Society*, 40 (1918) 1361-1403.
- [476] M. Silva da Rocha, K. Iha, A.C. Faleiros, E.J. Corat, M.E.V. Suárez-Iha, Henry's law as a limit for an isotherm model based on a statistical mechanics approach, *Journal of Colloid and Interface Science*, 208 (1998) 211-215.
- [477] K. Yang, B. Xing, Adsorption of organic compounds by carbon nanomaterials in aqueous phase: Polanyi theory and its application, *Chemical Reviews*, 110 (2010) 5989-6008.
- [478] W. Bunmahotama, T.F. Lin, X. Yang, Prediction of adsorption capacity for pharmaceuticals, personal care products and endocrine disrupting chemicals onto various adsorbent materials, *Chemosphere*, 238 (2019) 124658.
- [479] A.J. Horowitz, K.A. Elrick, M.R. Colberg, The effect of membrane filtration artifacts on dissolved trace element concentrations, *Water Research*, 26 (1992) 753-763.
- [480] D.B. Moore, J. Beck, R.J. Kryscio, An objective assessment of the variability in number of drops per bottle of glaucoma medication, *BMC Ophthalmology*, 17 (2017) 78.
- [481] W. Rudzinski, W. Plazinski, Theoretical description of the kinetics of solute adsorption at heterogeneous solid/solution interfaces, *Applied Surface Science*, 253 (2007) 5827-5840.
- [482] P.V. de Oliveira, I. Zanella, L.O.S. Bulhões, S.B. Fagan, Adsorption of 17 β -estradiol in graphene oxide through the competing methanol co-solvent: Experimental and computational analysis, *Journal of Molecular Liquids*, 321 (2021) 114738.
- [483] L.K. Boateng, J. Heo, J.R.V. Flora, Y.-G. Park, Y. Yoon, Molecular level simulation of the adsorption of bisphenol A and 17 α -ethinyl estradiol onto carbon nanomaterials, *Separation and Purification Technology*, 116 (2013) 471-478.
- [484] C.-J. Shih, S. Lin, R. Sharma, M.S. Strano, D. Blankschtein, Understanding the pH-dependent behavior of graphene oxide aqueous solutions: A comparative experimental and molecular dynamics simulation study, *Langmuir*, 28 (2012) 235-241.
- [485] H. Huang, Y. Mao, Y. Ying, Y. Liu, L. Sun, X. Peng, Salt concentration, pH and pressure controlled separation of small molecules through lamellar graphene oxide membranes, *Chemical Communications*, 49 (2013) 5963-5965.
- [486] Y. Oh, D.L. Armstrong, C. Finnerty, S. Zheng, M. Hu, A. Torrents, B. Mi, Understanding the pH-responsive behavior of graphene oxide membrane in removing ions and organic micropollutants, *Journal of Membrane Science*, 541 (2017) 235-243.
- [487] P.-C. Ma, N.A. Siddiqui, G. Marom, J.-K. Kim, Dispersion and functionalization of carbon nanotubes for polymer-based nanocomposites: A review, *Composites Part A: Applied Science and Manufacturing*, 41 (2010) 1345-1367.
- [488] S. Bai, X. Shen, G. Zhu, A. Yuan, J. Zhang, Z. Ji, D. Qiu, The influence of wrinkling in reduced graphene oxide on their adsorption and catalytic properties, *Carbon*, 60 (2013) 157-168.
- [489] H. Tang, Y. Zhao, S. Shan, X. Yang, D. Liu, F. Cui, B. Xing, Wrinkle- and edge-adsorption of aromatic compounds on graphene oxide as revealed by Atomic Force Microscopy, Molecular Dynamics simulation, and Density Functional Theory, *Environmental Science & Technology*, 52 (2018) 7689-7697.
- [490] J. Wang, B. Chen, B. Xing, Wrinkles and folds of activated graphene nanosheets as fast and efficient adsorptive sites for hydrophobic organic contaminants, *Environmental Science & Technology*, 50 (2016) 3798-3808.
- [491] E.J. Petersen, T.B. Henry, Methodological considerations for testing the ecotoxicity of carbon nanotubes and fullerenes: Review, *Environmental Toxicology and Chemistry*, 31 (2012) 60-72.
- [492] A.R. Petosa, D.P. Jaisi, I.R. Quevedo, M. Elimelech, N. Tufenkji, Aggregation and deposition of engineered nanomaterials in aquatic environments: Role of physicochemical interactions, *Environmental Science & Technology*, 44 (2010) 6532-6549.
- [493] D. Chandler, Interfaces and the driving force of hydrophobic assembly, *Nature*, 437 (2005) 640-647.
- [494] L. Jiang, S. Cao, P.P.-H. Cheung, X. Zheng, C.W.T. Leung, Q. Peng, Z. Shuai, B.Z. Tang, S. Yao, X. Huang, Real-time monitoring of hydrophobic aggregation reveals a critical role of cooperativity in hydrophobic effect, *Nature Communications*, 8 (2017) 15639-15639.
- [495] K.L. Chen, M. Elimelech, Influence of humic acid on the aggregation kinetics of fullerene (C60) nanoparticles in monovalent and divalent electrolyte solutions, *Journal of Colloid and Interface Science*, 309 (2007) 126-134.
- [496] N.B. Saleh, L.D. Pfefferle, M. Elimelech, Aggregation kinetics of multiwalled carbon nanotubes in aquatic systems: Measurements and environmental implications, *Environmental Science & Technology*, 42 (2008) 7963-7969.

- [497] M.M. Gudarzi, Colloidal stability of graphene oxide: Aggregation in two dimensions, *Langmuir*, 32 (2016) 5058-5068.
- [498] Y. Su, G. Yang, K. Lu, E.J. Petersen, L. Mao, Colloidal properties and stability of aqueous suspensions of few-layer graphene: Importance of graphene concentration, *Environmental Pollution*, 220 (2017) 469-477.
- [499] J. Gigault, B. Grassl, G. Lespes, Multi-wall carbon nanotube aqueous dispersion monitoring by using A4F-UV-MALS, *Analytical and Bioanalytical Chemistry*, 401 (2011) 3345-3353.
- [500] S. Ye, J. Feng, The effect of sonication treatment of graphene oxide on the mechanical properties of the assembled films, *RSC Advances*, 6 (2016) 39681-39687.
- [501] H.Q. Xie, L.F. Chen, Adjustable thermal conductivity in carbon nanotube nanofluids, *Physics Letters A*, 373 (2009) 1861-1864.
- [502] L.F. Chen, H.Q. Xie, Surfactant-free nanofluids containing double- and single-walled carbon nanotubes functionalized by a wet-mechanochemical reaction, *Thermochimica Acta*, 497 (2010) 67-71.
- [503] R. Rastogi, R. Kaushal, S.K. Tripathi, A.L. Sharma, I. Kaur, L.M. Bharadwaj, Comparative study of carbon nanotube dispersion using surfactants, *Journal of Colloid and Interface Science*, 328 (2008) 421-428.
- [504] M. Lotya, P.J. King, U. Khan, S. De, J.N. Coleman, High-concentration, surfactant-stabilized graphene dispersions, *ACS Nano*, 4 (2010) 3155-3162.
- [505] S. Deguchi, R.G. Alargova, K. Tsujii, Stable dispersions of fullerenes, C₆₀ and C₇₀, in water. Preparation and characterization, *Langmuir*, 17 (2001) 6013-6017.
- [506] D.R. Dreyer, S. Park, C.W. Bielawski, R.S. Ruoff, The chemistry of graphene oxide, *Chemical Society Reviews*, 39 (2010) 228-240.
- [507] A. Lerf, A. Buchsteiner, J. Pieper, S. Schöttl, I. Dekany, T. Szabo, H.P. Boehm, Hydration behavior and dynamics of water molecules in graphite oxide, *Journal of Physics and Chemistry of Solids*, 67 (2006) 1106-1110.
- [508] D.H. Everett, *Basic principles of colloid science*, Royal Society of Chemistry, London, 1988.
- [509] S.S. Datta, D.R. Strachan, E.J. Mele, A.T.C. Johnson, Surface potentials and layer charge distributions in few-layer graphene films, *Nano Letters*, 9 (2009) 7-11.
- [510] R. Ishikawa, S.D. Findlay, T. Seki, G. Sánchez-Santolino, Y. Kohno, Y. Ikuhara, N. Shibata, Direct electric field imaging of graphene defects, *Nature Communications*, 9 (2018) 3878.
- [511] N. Ghaderi, M. Peressi, First-principle study of hydroxyl functional groups on pristine, defected graphene, and graphene epoxide, *The Journal of Physical Chemistry C*, 114 (2010) 21625-21630.
- [512] B. Grosjean, A. Robert, R. Vuilleumier, M.-L. Bocquet, Spontaneous liquid water dissociation on hybridised boron nitride and graphene atomic layers from ab initio molecular dynamics simulations, *Physical Chemistry Chemical Physics*, 22 (2020) 10710-10716.
- [513] C.W. Yang, K. Miyazawa, T. Fukuma, K. Miyata, I.S. Hwang, Direct comparison between subnanometer hydration structures on hydrophilic and hydrophobic surfaces via three-dimensional scanning force microscopy, *Physical Chemistry Chemical Physics*, 20 (2018) 23522-23527.
- [514] M.R. Uhlig, D. Martin-Jimenez, R. Garcia, Atomic-scale mapping of hydrophobic layers on graphene and few-layer MoS₂ and WSe₂ in water, *Nature Communications*, 10 (2019) 2606.
- [515] J. Zhang, Y. Li, L. Li, W. Li, C. Yang, Dual functional N-doped TiO₂-carbon composite fibers for efficient removal of water pollutants, *ACS Sustainable Chemistry & Engineering*, 6 (2018) 12893-12905.
- [516] Q.-S. Liu, T. Zheng, P. Wang, J.-P. Jiang, N. Li, Adsorption isotherm, kinetic and mechanism studies of some substituted phenols on activated carbon fibers, *Chemical Engineering Journal*, 157 (2010) 348-356.
- [517] G.S. Ajmani, D. Goodwin, K. Marsh, D.H. Fairbrother, K.J. Schwab, J.G. Jacangelo, H. Huang, Modification of low pressure membranes with carbon nanotube layers for fouling control, *Water Research*, 46 (2012) 5645-5654.
- [518] World Health Organization, pH in Drinking-water: Revised background document for development of WHO Guidelines for drinking-water quality (WHO/SDE/WSH/07.01/1), https://www.who.int/water_sanitation_health/dwq/chemicals/ph.pdf, accessed on 6 September 2020.
- [519] A. Aguiar, L. Andrade, L. Grossi, W. Pires, M. Amaral, Acid mine drainage treatment by nanofiltration: A study of membrane fouling, chemical cleaning, and membrane ageing, *Separation and Purification Technology*, 192 (2018) 185-195.
- [520] S.C. Singh, R.A. Khare, Z.V.P. Murthy, Effect of hemicelluloses on pulp characteristics and use of ceramic membranes in the separation of hemicelluloses from highly alkaline industrial process stream, *Cellulose*, 25 (2018) 2577-2588.

- [521] European Parliament, Proposal for a Directive of the European Parliament and of the Council on the quality of water intended for human consumption (recast) 2017/0332/COD, Brussels, 2018.
- [522] X. Jin, J.Y. Hu, S.L. Ong, Influence of dissolved organic matter on estrone removal by NF membranes and the role of their structures, *Water Research*, 41 (2007) 3077-3088.
- [523] M. Engel, B. Chefetz, The missing link between carbon nanotubes, dissolved organic matter and organic pollutants, *Advances in Colloid and Interface Science*, 271 (2019) 101993.
- [524] J.B. Birks, *An introduction to liquid scintillation counting, and solutes and solvents for liquid scintillation counting*, Koch-Light Laboratories, Colnbrook, 1975.
- [525] M. Engel, B. Chefetz, Adsorptive fractionation of dissolved organic matter (DOM) by carbon nanotubes, *Environmental Pollution*, 197 (2015) 287-294.
- [526] W. Chen, L. Duan, D. Zhu, Adsorption of polar and nonpolar organic chemicals to carbon nanotubes, *Environmental Science & Technology*, 41 (2007) 8295-8300.
- [527] C.T. Mant, J.M.R. Parker, R.S. Hodges, Size-exclusion high-performance liquid chromatography of peptides: Requirement for peptide standards to monitor column performance and non-ideal behaviour, *Journal of Chromatography A*, 397 (1987) 99-112.
- [528] J.L. Weishaar, G.R. Aiken, B.A. Bergamaschi, M.S. Fram, R. Fujii, K. Mopper, Evaluation of specific ultraviolet absorbance as an indicator of the chemical composition and reactivity of dissolved organic carbon, *Environmental Science & Technology*, 37 (2003) 4702-4708.
- [529] A. Matilainen, E.T. Gjessing, T. Lahtinen, L. Hed, A. Bhatnagar, M. Sillanpää, An overview of the methods used in the characterisation of natural organic matter (NOM) in relation to drinking water treatment, *Chemosphere*, 83 (2011) 1431-1442.
- [530] J.K. Edzwald, Coagulation in drinking water treatment: Particles, organics and coagulants, *Water Science and Technology*, 27 (1993) 21-35.
- [531] E. Aoustin, A.I. Schäfer, A.G. Fane, T.D. Waite, Ultrafiltration of natural organic matter, *Separation and Purification Technology*, 22-23 (2001) 63-78.
- [532] D. Jermann, W. Pronk, M. Boller, A.I. Schäfer, The role of NOM fouling for the retention of estradiol and ibuprofen during ultrafiltration, *Journal of Membrane Science*, 329 (2009) 75-84.
- [533] H.B. Park, J. Kamcev, L.M. Robeson, M. Elimelech, B.D. Freeman, Maximizing the right stuff: The trade-off between membrane permeability and selectivity, *Science*, 356 (2017).
- [534] L. Bocquet, Nanofluidics coming of age, *Nature Materials*, 19 (2020) 254-256.
- [535] F. Fornasiero, H.G. Park, J.K. Holt, M. Stadermann, C.P. Grigoropoulos, A. Noy, O. Bakajin, Ion exclusion by sub-2-nm carbon nanotube pores, *PNAS*, 105 (2008) 17250-17255.
- [536] F. Fornasiero, J.B. In, S. Kim, H.G. Park, Y. Wang, C.P. Grigoropoulos, A. Noy, O. Bakajin, pH-tunable ion selectivity in carbon nanotube pores, *Langmuir*, 26 (2010) 14848-14853.
- [537] M. Majumder, N. Chopra, B.J. Hinds, Effect of tip functionalization on transport through vertically oriented carbon nanotube membranes, *Journal of the American Chemical Society*, 127 (2005) 9062-9070.
- [538] K. Falk, F. Sedlmeier, L. Joly, R.R. Netz, L. Bocquet, Molecular origin of fast water transport in carbon nanotube membranes: Superlubricity versus curvature dependent friction, *Nano Letters*, 10 (2010) 4067-4073.
- [539] M. Ma, F. Grey, L. Shen, M. Urbakh, S. Wu, J.Z. Liu, Y. Liu, Q. Zheng, Water transport inside carbon nanotubes mediated by phonon-induced oscillating friction, *Nature Nanotechnology*, 10 (2015) 692-695.
- [540] X. Wei, T. Luo, Effects of electrostatic interaction and chirality on the friction coefficient of water flow inside single-walled carbon nanotubes and boron nitride nanotubes, *Journal of Physical Chemistry C*, 122 (2018) 5131-5140.
- [541] N. Kavokine, M.-L. Bocquet, L. Bocquet, Fluctuation-induced quantum friction in nanoscale water flows, *Nature*, 602 (2022) 84-90.
- [542] S. Joseph, N.R. Aluru, Why are carbon nanotubes fast transporters of water?, *Nano Letters*, 8 (2008) 452-458.
- [543] J. Mittal, G. Hummer, Interfacial thermodynamics of confined water near molecularly rough surfaces, *Faraday Discussions*, 146 (2010) 341-352.
- [544] I. Hanasaki, A. Nakatani, Flow structure of water in carbon nanotubes: Poiseuille type or plug-like?, *Journal of Chemical Physics*, 124 (2006) 144708.
- [545] S.K. Kannam, B.D. Todd, J.S. Hansen, P.J. Daivis, How fast does water flow in carbon nanotubes?, *Journal of Chemical Physics*, 138 (2013) 094701.
- [546] D. Di Carlo, D. Irimia, R.G. Tompkins, M. Toner, Continuous inertial focusing, ordering, and separation of particles in microchannels, *PNAS*, 104 (2007) 18892-18897.

- [547] N. Al Quddus, W.A. Moussa, S. Bhattacharjee, Motion of a spherical particle in a cylindrical channel using arbitrary Lagrangian–Eulerian method, *Journal of Colloid and Interface Science*, 317 (2008) 620-630.
- [548] U. Raviv, J. Klein, Fluidity of bound hydration layers, *Science*, 297 (2002) 1540-1543.
- [549] T.-D. Li, J. Gao, R. Szoszkiewicz, U. Landman, E. Riedo, Structured and viscous water in subnanometer gaps, *Physical Review B*, 75 (2007) 115415.
- [550] S. Esconjauregui, R. Xie, M. Fouquet, R. Cartwright, D. Hardeman, J. Yang, J. Robertson, Measurement of area density of vertically aligned carbon nanotube forests by the weight-gain method, *Journal of Applied Physics*, 113 (2013) 144309.
- [551] J. Rabinowitz, C. Cohen, K.L. Shepard, An electrically actuated, carbon-nanotube-based Biomimetic ion pump, *Nano Letters*, 20 (2020) 1148-1153.
- [552] P. Král, M. Shapiro, Nanotube electron drag in flowing liquids, *Physical Review Letters*, 86 (2001) 131-134.
- [553] J.N. Israelachvili, Van der Waals forces between particles and surfaces, in: *Intermolecular and surface forces*, 3rd ed., Elsevier, Academic Press, 2011, pp. 253-289.
- [554] R.F. Rajter, R.H. French, W.Y. Ching, R. Podgornik, V.A. Parsegian, Chirality-dependent properties of carbon nanotubes: Electronic structure, optical dispersion properties, Hamaker coefficients and van der Waals–London dispersion interactions, *RSC Advances*, 3 (2013) 823-842.
- [555] H. Takagishi, T. Masuda, T. Shimoda, R. Maezono, K. Hongo, Method for the calculation of the Hamaker constants of organic materials by the Lifshitz macroscopic approach with Density Functional Theory, *The Journal of Physical Chemistry A*, 123 (2019) 8726-8733.
- [556] D. Ugarte, A. Châtelain, W.A. de Heer, Nanocapillarity and chemistry in carbon nanotubes, *Science*, 274 (1996) 1897-1899.
- [557] A. Imbrogno, A.I. Schäfer, Micropollutants breakthrough curve phenomena in nanofiltration: Impact of operational parameters, *Separation and Purification Technology*, (2021) 118406.
- [558] S. Zhang, T. Hedtke, X. Zhou, M. Elimelech, J.-H. Kim, Environmental applications of engineered materials with nanoconfinement, *ACS ES&T Engineering*, 1 (2021) 706-724.
- [559] X. Chen, J. Li, Superlubricity of carbon nanostructures, *Carbon*, 158 (2020) 1-23.
- [560] Z. Liao, M.N. Nguyen, G. Wan, J. Xie, L. Ni, J. Qi, J. Li, A.I. Schäfer, Low pressure operated ultrafiltration membrane with integration of hollow mesoporous carbon nanospheres for effective removal of micropollutants, *Journal of Hazardous Materials*, 397 (2020) 122779.
- [561] R.E. Beck, J.S. Schultz, Hindered diffusion in microporous membranes with known pore geometry, *Science*, 170 (1970) 1302.
- [562] W.M. Deen, Hindered transport of large molecules in liquid-filled pores, *AIChE Journal*, 33 (1987) 1409-1425.
- [563] W. Hayduk, H. Laudie, Prediction of diffusion coefficients for nonelectrolytes in dilute aqueous solutions, *AIChE Journal*, 20 (1974) 611-615.
- [564] H.-C. Liu, J.R. Fried, Breakthrough of lysozyme through an affinity membrane of cellulose-cibacron blue, *AIChE Journal*, 40 (1994) 40-49.
- [565] C. Laurent, E. Flahaut, A. Peigney, The weight and density of carbon nanotubes versus the number of walls and diameter, *Carbon*, 48 (2010) 2994-2996.
- [566] M.-c. Yang, M.-y. Li, S. Luo, R. Liang, Real-time monitoring of carbon nanotube dispersion using dynamic light scattering and UV-vis spectroscopy, *The International Journal of Advanced Manufacturing Technology*, 82 (2015) 361-367.
- [567] A. Misra, J.R. Raney, A.E. Craig, C. Daraio, Effect of density variation and non-covalent functionalization on the compressive behavior of carbon nanotube arrays, *Nanotechnology*, 22 (2011) 425705.
- [568] H.R. Lohokare, Y.S. Bhole, U.K. Kharul, Effect of support material on ultrafiltration membrane performance, *Journal of Applied Polymer Science*, 99 (2006) 3389-3395.
- [569] L. Bocquet, J.-L. Barrat, Flow boundary conditions from nano- to micro-scales, *Soft Matter*, 3 (2007) 685-693.

Appendices

A. Preparation of calibration solutions

The way that the calibration solutions were prepared can cause bias in the analytical results and affect the discussions. Two measures were applied to prevent this bias, which are: i) performing calibration frequently to building a rich database of independent calibration results, and ii) avoiding serial dilutions from the same stock solution.

The calibration steps that minimise serial dilutions are schematically shown in Figure S1.

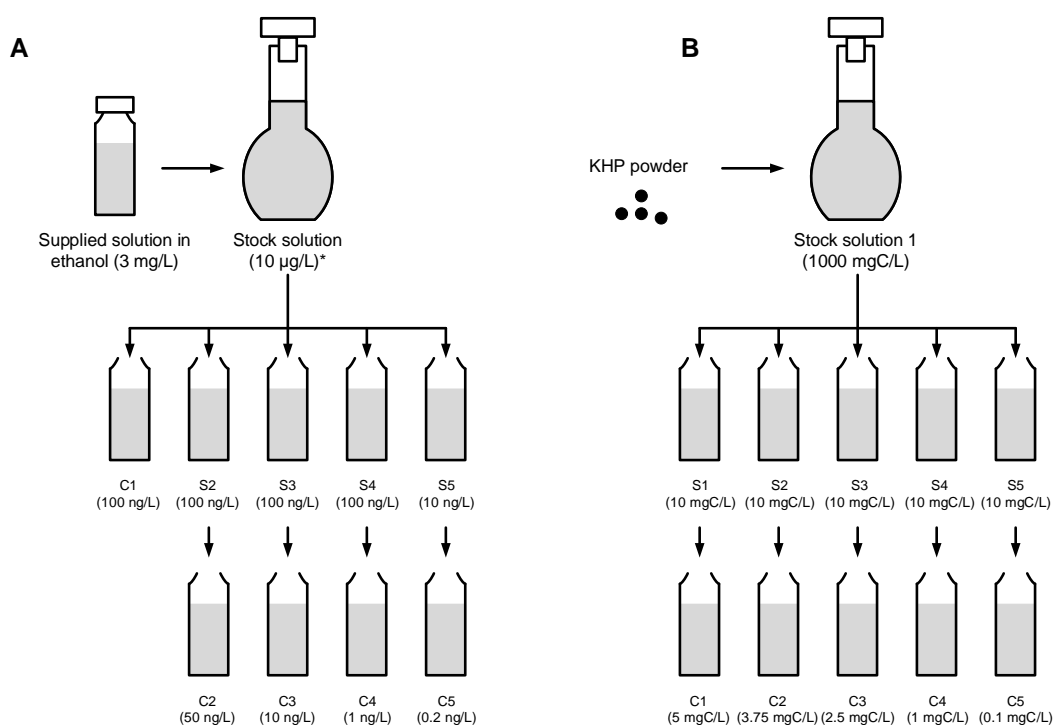


Figure S1: Solution preparation steps for LSC calibration with steroid hormone standards (A) and LC-OCD calibration with potassium hydrogen phthalate (KHP) (B). C1–C5 are the calibration solutions. The star symbol indicates that the step is performed by the responsible for radiotracers.

In LSC calibration, the stock solution (10 µg/L) is prepared (by the responsible for radiotracers) from the radiolabelled standard solution (the hormone concentration is accurately reported by the manufacturer). In LC-OCD calibration, the stock solution (1000 mgC/L) is prepared by mixing an accurate amount of 213 mg of potassium hydrogen phthalate (KHP) in 1 L of Milli-Q water in a volumetric flask. Both the stock solutions for LSC and LC-OCD should have highly accurate concentrations of respective standards.

Separate solutions were diluted from the stock solution, and from these solutions, the correct concentrations were obtained from subsequent dilution. Because this method circumvents dilution in series, any operator's mistake in pipetting and mixing is minimised.

B. Error analysis calculations

The absolute error in flux ΔJ is the same as the relative error in mass change with time, as shown in Eq. (A.1).

$$\Delta J = \frac{1}{2} J \left[\left(\frac{\Delta m}{\Delta t} \right)_{max} - \left(\frac{\Delta m}{\Delta t} \right)_{min} \right] \quad (\text{A.1})$$

Where $\frac{\Delta m}{\Delta t}$ is determined from the slope of mass vs. time within a time range of 120 s.

The error in membrane permeability ΔL_p is determined from Eq. (A.2).

$$\Delta L_p = L_p \sqrt{\left(\frac{\Delta J}{J} \right)^2 + \left(\frac{\Delta P}{P} \right)^2} \quad (\text{A.2})$$

With the assumption that the membrane permeability directly affects the permeate concentration, the error in permeate concentration is the propagation of the analytical error and the permeability error, see Eq. (A.3).

$$\begin{aligned} \Delta c_p &= \sqrt{\Delta c_{anal.}^2 + \Delta c_{prep.}^2 + \Delta c_{fil.}^2} \\ &= \sqrt{\Delta c_{anal.}^2 + c_p^2 \left(\frac{\Delta V_p}{V_p} \right)^2 + c_p^2 \left(\frac{\Delta L_p}{L_p} \right)^2} \end{aligned} \quad (\text{A.3})$$

where $\Delta c_{anal.}$ is the error contributed by the analysis, $\Delta c_{prep.} = c_p \left(\frac{\Delta V_p}{V_p} \right)$ is the error contributed by permeate solution preparation (in LSC, with a analyte volume of 1.00 ± 0.01 mL, $\Delta c_{prep.}$ is 1% of c_p), and $\Delta c_{fil.} = c_p \left(\frac{\Delta L_p}{L_p} \right)$ is the error contributed by the filtration process.

The error in feed concentration is propagated from the analytical error and the feed volume error as shown in Eq. (A.4).

$$\Delta c_f = \sqrt{\Delta c_{anal.}^2 + \Delta c_{prep.}^2} = \sqrt{\Delta c_{anal.}^2 + c_f^2 \left(\frac{\Delta V_f}{V_f} \right)^2} \quad (\text{A.4})$$

where $\Delta c_{prep.} = c_f \left(\frac{\Delta V_f}{V_f} \right)$ is the error contributed by feed solution preparation. With $c_f = 100$ ng/L, $\Delta c_{anal.} = 1$ ng/L, and $\frac{\Delta V_f}{V_f} \sim 1\%$, $\Delta c_f = 1.4$ ng/L.

The absolute error in removal ΔR (in %) is determined from Eq. (A.5).

$$\Delta R = (100 - R) \sqrt{\left(\frac{\Delta c_f}{c_f}\right)^2 + \left(\frac{\Delta c_p}{c_p}\right)^2} \quad (\text{A.5})$$

where Δc_f and Δc_p are the absolute error of the feed and permeate concentrations, respectively.

The retentate concentration error Δc_r can be estimated *via* the same formula used to calculate Δc_p , see Eq. (A.6).

$$\Delta c_r = \sqrt{\Delta c_{anal.}^2 + c_r^2 \left(\frac{\Delta L_P}{L_P}\right)^2} \quad (\text{A.6})$$

The retentate volume error ΔV_r is calculated *via* Eq. (A.7).

$$\Delta V_r = \sqrt{\Delta V_f^2 + \sum \Delta V_{p,i}^2} \quad (\text{A.7})$$

The absolute error in adsorbed mass Δm_{ads} (in ng) in a crossflow filtration is determined from Eq. (A.8).

$$\Delta m_{ads} = \sqrt{\Delta m_f^2 + \Delta m_r^2 + \sum_{i=1}^n \Delta m_{p,i}^2} \quad (\text{A.8})$$

where the absolute mass error Δm_f , Δm_p and Δm_r in ng (referred to as Δm_j) are calculated from the respective volume and concentration errors as shown in Eq. (A.9).

$$\Delta m_i = m_i \sqrt{\left(\frac{\Delta V_j}{V_j}\right)^2 + \left(\frac{\Delta c_j}{c_j}\right)^2} \quad (\text{A.9})$$

C. Static adsorption protocol

Static adsorption experiments were performed to determine how much the CNPs adsorbed steroid hormones. All experiments were conducted with six types of CNPs, which are multi-walled carbon nanotube (MWCNT), single-walled carbon nanotube (SWCNT), graphene grade 1 (GP1), graphene grade 2 (GP2), graphene oxide (GO), and fullerene C₆₀.

To evaluate the adsorption by CNPs of four types of steroid hormones (E1, E2, T and P, described in Section 3.3.4), 0.5–250 mg of CNPs was weighed with an analytical balance (Explorer EX224, Ohaus, USA) and each was transferred into a separate 250 mL conical flask (set A). Then, the conical flask was filled with 50 mL of Milli-Q water and sonicated at a sonic frequency of 35 kHz in an ultrasonic bath (WG300, Endo-Technik WG, Germany) for 1 h to enhance dispersion. Subsequently, background electrolytes and Milli-Q water were added to make up a volume of 125 mL, which inevitably increase the natural aggregation of the CNPs. No organic matter (OM) or

surfactants were added to improve dispersion because they can affect the adsorption performance. The pH of this solution was adjusted to 8.0, unless in the experiments with varying pH where pH was adjusted in the range of 2–12.

In a separate conical flask (set B), 125 mL of hormone solution was prepared separately with background electrolytes and Milli-Q water to obtain twice higher concentration than the initial concentration in static adsorption (100 ng/L, unless indicated otherwise). In experiments with high initial hormone (E2) concentrations of 1–1000 µg/L, radiolabelled E2 (in 10 µg/L stock) were mixed with non-radiolabelled E2 (Sigma-Aldrich, USA) at the required ratio. The solution pH in the set B flask was adjusted to match that of the corresponding set A flask. OM can be added to this flask (20 mgC/L) in the evaluation of interference. From the mixed hormone solution in the set B flask, 0.5 mL was extracted to determine the initial hormone concentration in the absence of CNPs.

At the start of the static adsorption experiment, the hormone solution in the set B conical flasks was added to the CNT suspension in the set A conical flasks in an incubator shaker (Innova 43R, New Brunswick Scientific, USA). Unless indicated otherwise, the hormone concentration in this mixture was 100 ng/L. A maximum of six simultaneous conical flasks were in the shaker at the same time. The shaking speed and temperature were set at 260 rpm and 20 °C, respectively, unless indicated otherwise. At different time intervals (5, 10, 15, 30 and 45 min; 1, 3, 5, 7, 9, 24 and 26 h), a 2.5 mL aliquot of solution in each flask is extracted with a plastic syringe (NORM-JECT 10 mL, HSW, Germany) and immediately filtered to avoid the ongoing interaction with CNPs.

Because of the natural aggregation of CNPs, the MF filters (0.45 µm Teflon and 0.45 µm cellulose acetate, described in Section 3.3.2) can remove CNPs with the exception of C₆₀ that requires UF filters (regenerated cellulose Ultracel 100 kDa, PLHHK, Merck Millipore, USA).

Cellulose acetate filters (used with GO suspensions) adsorbed much steroid hormone and were discarded after each sample extraction. In contrast, the Teflon MF and regenerated cellulose UF filters adsorbed only small amounts of hormone, therefore each membrane was recycled up to 6 times to overcome the time constraints when extracting samples from the multiple flasks in the first hour. In the experiments with varying CNP and E2 concentrations, membrane recycling was done for six simultaneous flasks following an order of increasing E2 concentration. In the experiments with temperatures (with 6 different CNPs), or with 4 different hormones or different pH (except the pH 4–8), membrane recycling was restricted to the specific conical flask, to avoid the effects of the varied solution chemistry. The first 10 drops of each filtration were discarded.

D. Fitting parameters of the adsorption models

The fitting parameters and R^2 values applied to the intra-particle diffusion, first- and second-order kinetic models are shown in Table S1.

Table S1: Adsorption kinetics fitting parameters. Adapted from Nguyen *et al.*³⁰³.

Particle concentration (g/L)	Ads. mass at saturation (ng/g)	First-order			Second-order		IPD R^2	E2 removal (%)
		K_1 (1/h)	q_E (ng/g)	R^2	q_E (ng/g)	R^2		
MWCNT								
0.002	44100	0.60	43500	0.982	47000	0.958	0.705	88.1
0.01	9090	1.59	8970	0.965	9240	0.932	0.062	90.8
0.1	914	13.6	909	0.997	914	0.926	-	91.3
0.2	454	21.4	454	0.999	456	0.940	-	90.7
0.5	175	36.6	176	1.000	176	0.964	-	90.6
1	90.3	62.9	90.5	1.000	90.6	0.989	-	90.7
SWCNT								
0.002	47400	35.6	46400	0.996	46700	0.997	-	96.3
0.01	9820	38.8	9660	0.997	9730	0.998	-	98.3
0.1	960	42.4	958	1.000	961	1.000	-	98.4
0.2	472	43.8	470	0.999	472	1.000	-	98.6
0.5	196	N.D.*	196	0.999	196	0.999	-	97.5
1	94.6	52.6	94.8	1.000	94.9	1.000	-	97.1
GP1								
0.002	42300	16.1	42200	0.999	42400	0.930	-	93.0
0.01	8630	26.0	8460	0.989	8490	0.948	-	92.4
0.1	832	41.7	823	0.998	824	0.971	-	93.8
0.2	438	59.3	438	1.000	438	0.986	-	94.8
0.5	171	57.1	171	1.000	171	0.985	-	94.7
1	84.4	67.0	84.5	1.000	84.6	0.991	-	94.9
GP2								
0.002	30500	46.4	26200	0.993	26300	0.587	-	62.8
0.01	8830	35.9	8200	0.922	8220	0.963	-	88.5
0.1	930	N.D.*	911	0.993	911	1.000	-	93.5
0.2	482	N.D.*	480	0.997	480	1.000	-	96.3
0.5	190	N.D.*	190	0.999	190	1.000	-	96.8
1	98.4	N.D.*	98.6	1.000	98.6	1.000	-	97.1
GO								

0.002	38800	N.D.*	39300	0.997	39300	1.000	-	75.3
0.01	8310	52.8	8340	0.999	8340	0.999	-	80.4
0.1	877	72.6	881	1.000	881	0.993	-	90.7
0.2	460	79.5	461	0.999	461	0.995	-	91.0
0.5	183	84.0	185	0.999	185	0.999	-	92.4
1	93.4	96.7	93.5	0.999	93.5	0.998	-	93.6
C₆₀								
0.002	6180	2.74	5860	0.685	6240	0.679	-	11.8
0.01	622	N.D.*	622	0.446	622	1.000	-	7.26
0.1	194	N.D.*	194	0.261	194	1.000	-	21.3
0.2	237	34.8	237	0.957	238	0.962	-	50.0
0.5	137	32.6	137	0.984	138	0.959	-	70.3
1	67.9	49.5	67.9	0.994	68.0	0.979	-	68.3

* N.D.: not determined (adsorption saturation was reached too quickly).

The fitting parameters and R^2 values applied to the Henry, Freundlich, Langmuir and Polanyi–Mane isotherm models are shown in Table S2. Adapted from Nguyen *et al.*³⁰³.

Table S2: Adsorption isotherm fitting parameters.

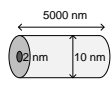
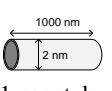
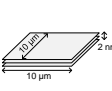
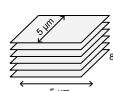
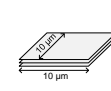
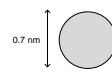
No.	CNP	Henry	Freundlich	Langmuir		Polanyi–Mane		
		R^2	n_F	R^2	q_{max} (mg/g)	R^2	q_{max} (mg/g)	R^2
1	MWCNT	0.998	0.987	1.000	N.D.	N.D.	N.D.	N.D.
2	SWCNT	0.973	0.822	1.000	N.D.	N.D.	N.D.	N.D.
3	GP1	1.000	1.016	1.000	N.D.	N.D.	N.D.	N.D.
4	GP2	0.974	0.36	0.925	6.59	0.991	53.0	0.960
5	GO	0.971	0.56	0.998	2.19	1.000	8.21	0.989
6	C ₆₀	0.872	0.79	1.000	1.78	1.000	3.20	0.943

* N.D.: not determined (Henry isotherm is implied).

E. Surface area and adsorption capacity based on the ideal shapes of CNPs

Hormone adsorption may depend on the structure of individual CNP adsorbents. The structural parameters, surface areas and E2 (MW 272 g/mol, diameter 0.8 nm) adsorption capacities are given in Table S3. Surface heterogeneity and aggregation are not considered, as such the values presented in this table are according to the ideal shapes of CNPs.

Table S3: Structural and adsorption properties of CNPs assuming the ideal shapes (tube-like shape of MW/SWCNTs, flat sheets of GP1, GP2 and GO, and spherical shape of C₆₀). The spaces between nanotube layers (MWCNTs) and stacked sheets (GP1, GP2 and GO) were not accessible. Adapted from Nguyen *et al.*³⁰³.

	MWCNT	SWCNT	GP1	GP2	GO	C ₆₀
Model	 37 nanotube layers	 1 nanotube layer	 3 sheets	 25 sheets	 3 sheets	 0.7 nm
Pore size (nm)	2	2	N.A.	N.A.	N.A.	N.A.
External surface area (nm ²)	$1.6 \cdot 10^5$	$6.3 \cdot 10^3$	$2.0 \cdot 10^8$	$5.0 \cdot 10^7$	$2.0 \cdot 10^8$	1.5
Internal surface area (nm ²)	$3.1 \cdot 10^4$	$5.7 \cdot 10^3$	N.A.	N.A.	N.A.	N.A.
Volume (nm ³)	$3.9 \cdot 10^5$	3150	$2.0 \cdot 10^8$	$2.0 \cdot 10^8$	$2.0 \cdot 10^8$	0.18
Ext. surface area per vol. ratio (nm ⁻¹)	0.4	2.0	1.0	0.3	1.0	8.3
CNP weight (g)	$1.3 \cdot 10^{-14}$	$1.3 \cdot 10^{-17}$	$6.1 \cdot 10^{-13}$	$1.3 \cdot 10^{-12}$	$6.1 \cdot 10^{-13}$	$1.2 \cdot 10^{-21}$
Density (g/cm ³)	33*	4.1	3.1	6.5	3.1	6.7
External surface per mass (m ² /g)	12	490	330	150	330	1250
Total surface per mass (m ² /g)	14	980	330	150	330	1250
E2 ads. capacity (mg/g)	13.2	834	296	35	296	1040

F. 'Pore' characterisation of CNPs

The pore profiles of different CNPs (given as differentiated and cumulative pore volumes vs. pore diameter) are given in Figure S2, which determine the most significant adsorbent pore diameters.

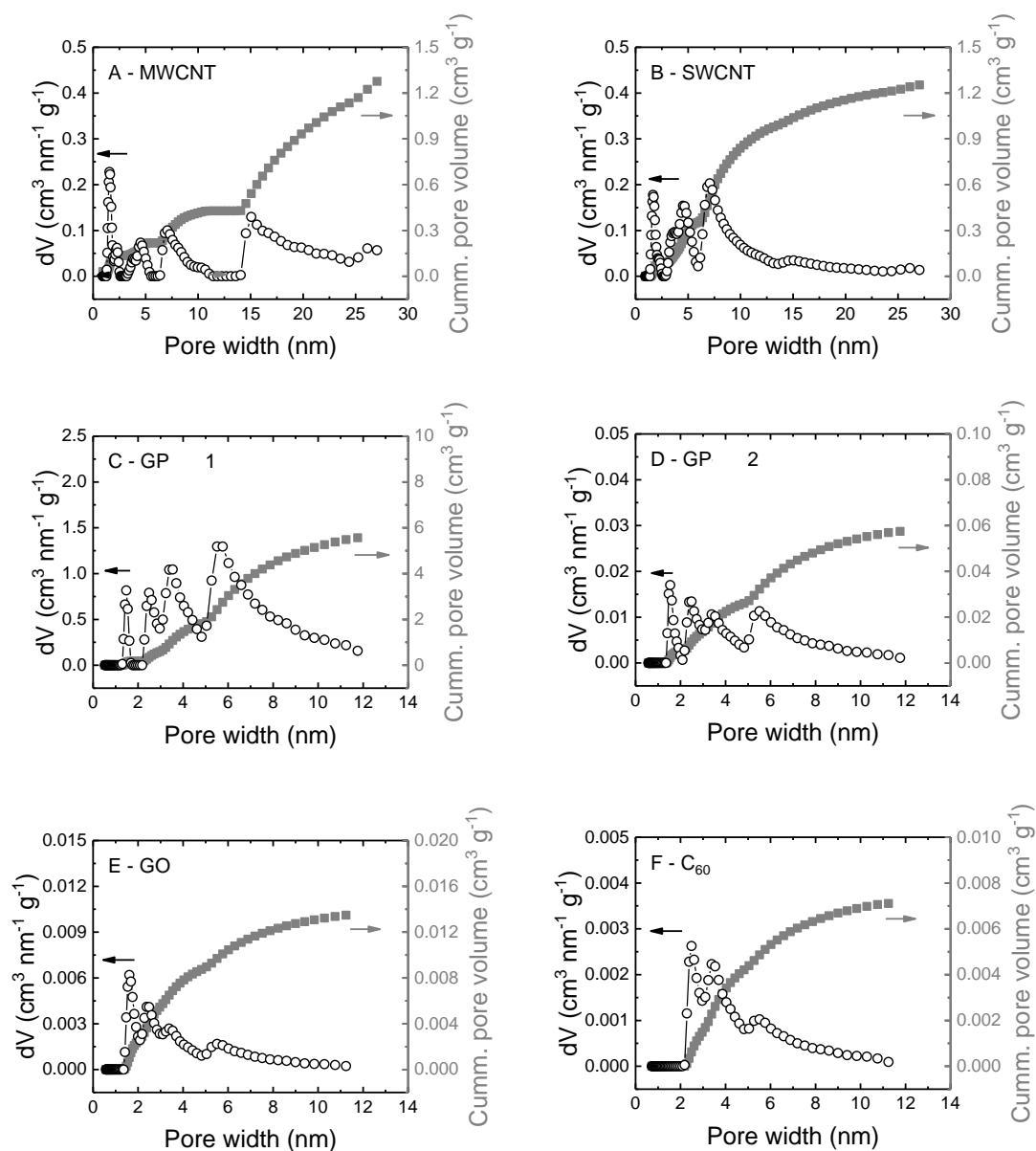


Figure S2: Pore density and cumulative pore volume according to QSDFT model (Argon adsorption / desorption). Reprinted from Nguyen *et al.*³⁰³.

All the CNPs show a trimodal distribution of pores. The smallest pore diameters in MWCNT and SWCNT are <2 nm corresponding to the diameters of the nanotubes. In GP1, GP2 and GO, the smallest diameter of 'pores' is around 1.5 nm, which may correspond to the spaces created by aggregates. The cumulative pore volume follows the order GP1 >> GP2 > GO. The next peaks in C₆₀ has very low pore volume and no pores in the <2 nm region.

G. Filtration protocols

Crossflow filtration with SWCNT–UF membranes

The crossflow filtration protocol used in Chapter 5 is given in Table S4.

Table S4: Protocol of cross-flow filtration with SWCNT–UF. Adapted from Nguyen *et al.* ³⁰².

No.	Step	Conditions	Justification
1	Membrane conditioning	Membrane is gently rinsed with Milli-Q before experiment.	To wash off any kind of additives such as glycerine and Triton-X100.
2	Filtration system cleaning	Without the membrane, set the pump flow rate at 100 mL/min and flush the whole system with Milli-Q water for 30 min.	
4	Membrane compaction	Insert the membrane. Compaction with Milli-Q for 30 min. Set pump flow rate at 30 mL/min. The pressure is adjusted to 4 bar by hand with the needle valve.	
5	Pure water flux (before filtration)	Pure water flux is measured with Milli-Q water at 1 bar for 15 min with the pump flow rate of 30 mL/min.	To determine the pure water permeability of the membrane and make sure the membrane has no defects.
6	Filtration test	Feed volume of 250 mL was used for the experiments with 10 kDa membranes. 500 mL was needed for experiments with 100 kDa membranes, except with 4 bar pressure where 750 mL was required. Change the feed tube from Milli-Q solution to hormone feed solution for experiment. Flow rate is set 30 mL/min. Samples are collected in separate vials during the following periods: once 5 min, once 10 min, once 15 min and five times 30 min.	The system's dead volume and the permeate dead volume are 25.8 and 0.42 mL, respectively. Therefore, the first permeate sample was diluted with residue water in the system; the hormone concentration in this sample is not accurate.
7	Pure water flux (after filtration)	Flushing is operated for 5 min with feed flow rate 30 mL/min and pressure 1 bar. The flush water is discarded and not recirculated to the bottle. Pure water flux is similar to step 5.	Flushing is done to remove contaminants in the system.
9	Membrane removal and storage	The membrane is removed from the system and stored in a plastic petri-dish containing a moist tissue. The petri-dish is then placed in the fridge at 4 °C.	
10	Flushing the system (without membrane)	Flushing was operated for 2 min with pump flow rate 30 mL/min. After that, use a syringe to purge the switching valve with air to remove residue water.	

In Chapter 6, the protocol is slightly modified in Step 6. The modifications are:

- The feed volume is 250 mL.
- Samples were collected in separate vials based on permeate volume. For 3–10 kDa membranes: once 1 mL, twice 2 mL, then five times 5 mL. For 30–100 kDa membranes: once 1 mL, once 4 mL, twice 10 mL, then five times 25 mL.

Dead-end filtration with VaCNT–MF membranes

The dead-end filtration protocol used with the VaCNT–MF membranes is given in Table S5.

Table S5: Protocol of dead-end filtration with VaCNT–MF. Reprinted from Nguyen *et al.* ⁴¹⁴.

No.	Step	Conditions	Justification
1	Membrane conditioning	VaCNT membrane is rinsed with Milli-Q water. MF membrane is submerged in 50/50 ethanol/water (v./v.) for 15 min, and then rinsed thoroughly with Milli-Q water.	To permeate the membrane and wash off additives
2	System flushing	Without the membrane, set the pump rotation to 10 rpm and flush the whole system with Milli-Q water for 15 min.	
3	System drying	Use a syringe and flush the system with air until no water residues come out of the tubing.	To remove water residues especially in the membrane cell outlet and switching valve.
4	Pure water permeability test (before hormone filtration)	Mount the membranes (VaCNT membrane on top of an MF) with a torque of 2 N.m (via a torque wrench). The water chiller is set at 23 °C. Pump flow rate is set at 0.1 mL/min (equivalent flux is 30 L/m ² .h). It then takes around 30–60 minutes until the permeate flux is stable. Filtration continues for at least 15 min at constant permeate flux to determine the permeability.	To determine the pure water permeability and make sure the membrane has no defects (if the membrane is broken or has pinholes, the pressure will be below 0.2 bar).
5	Filtration test with steroid hormone	Feed volume is 250 mL. Disconnect the inlet to the membrane cell and replace the water inside the tubing with feed solution. Turn off the pump and reconnect the inlet to the membrane cell. The water chiller is set at 23 °C. Operate the filtration at experimental fluxes*. Sample collection was based on permeate volumes. Samples 1–5: 1 mL each Samples 6–9: 5 mL each Samples 10 onwards: 20 mL each In all experiments, the filtration system was operated overnight.	Therefore, the purging with 50 mL of feed solution is necessary to minimize water residue in the system (dead volume ~20 mL). The first and second permeate samples (each 1 mL) might contains residue water from the membrane cell. The hormone concentrations in these samples may not be accurate.
6	Pure water permeability test (after filtration)	Change the feed to Milli-Q then follow the same procedure described in step 4.	

7	Membrane removal and storage	The membrane coupons are removed, dried in air for 1 h and stored in a plastic petri-dish.	
8	System flushing	The system is flushed with 1 M NaOH solutions for 15 min, then with warm deionized water (~40 °C) for 15 min, and finally with Milli-Q water for 15 min. Pump flow rate was set at 30 mL/min in all the steps.	NaOH and warm water flushing removes residual organic matter and prevent bacterial growth in the system.

* In the experiment with the lowest flux (6–7 L/m².h, or 0.02 mL/min), the needle valve was partially open, letting only ~30% of feed solution to pass through the membrane. The other 60% was recycled into the feed bottle.

H. Determination of the SWCNT–UF area in contact with water and solution

Radial diffusion can affect the area of the SWCNT layer in SWCNT–UF that is exposed to of water and solute (hormone) as illustrated in Figure S3. The membrane coupon that holds the SWCNTs has an area of 4.9 cm², while the active filtration area is 2 cm² determined by the feed-side polyether-ether-ketone seal ⁴²². SWCNTs outside this 2 cm² area may not be reached effectively for adsorption, and hence only the particles in the 2 cm² are considered in adsorbed mass calculations.

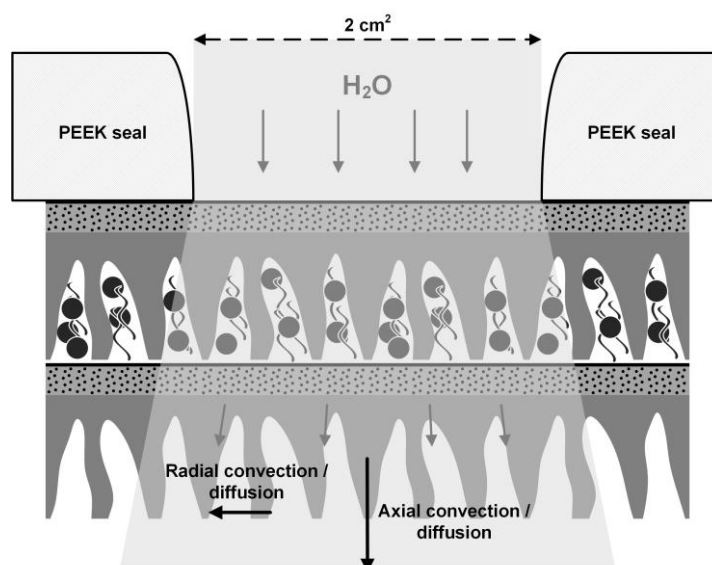


Figure S3: Schematic of water and solute flow through stacked membranes (*e.g.* SWCNT–UF) influenced by axial and radial convection / diffusion. The speed of radial transfer processes relative to the axial ones determines the adsorption area of SWCNTs. Adapted from Nguyen *et al.* ³⁰².

The effective area for filtration and adsorption is determined by the convection of hormones in the UF support structure. With sufficiently fast axial convective flow over a short distance (*i.e.* sub-millimetre membrane thickness, 230–280 μm), the radial movement of hormones (due to

diffusion) might not be relevant. To confirm this, the diffusion time is compared with the residence time in the membrane.

The pore sizes of the dense layer are 5.4 nm and 18.2 nm for 10 kDa and 100 kDa membranes, respectively. The effective diffusivity D_{eff} (m²/s) in these pores can be estimated from Beck and Schultz's empirical correlation (Eq. (A.10))⁵⁶¹. An alternative empirical equation proposed by Deen *et al.*⁵⁶² yields a similar D_{eff} value.

$$\frac{D_{eff}}{D_0} = \left(1 - \frac{d_{water}}{d_p}\right)^4 \quad (A.10)$$

where d_{water} and d_p (nm) are the diameters of water molecule (0.3 nm) and the membrane pore, respectively, and $D_0 = 2.45 \cdot 10^{-9}$ m²/s is the water diffusivity in the bulk⁵⁶³. D_{eff} for water diffusion in 10 kDa and 100 kDa membranes are $1.9 \cdot 10^{-9}$ and $2.3 \cdot 10^{-10}$ m²/s, respectively. In the support layers, $d_p \gg d_{E2}$, and $D_{eff} \approx D_0 = 2.45 \cdot 10^{-9}$ m²/s. The diffusion time in radial direction t_r is calculated with Eq. (A.11)⁵⁶⁴.

$$t_D = \frac{d_p^2}{D_{eff}} \quad (A.11)$$

In the dense layer ($d_p = 5.4\text{--}18.2$ nm), t_D is very short ($10^{-7} - 10^{-8}$ s). In the support layer that contributes majorly to the membrane thickness, r_p can reach 0.25 mm (as shown in the SEM images), and as a result t_r is long (100 s). This t_D value is 2–4 orders of magnitude higher than the residence time in SWCNT–UF (up to several seconds), indicating that radial diffusion of water is much slower than convection.

In summary, because radial diffusion is negligible compared to axial convection, it is assumed that the membrane and SWCNT area for filtration and adsorption is always 2 cm². A methylene blue dye test shows that the dye stained an area of 2 cm² of the top and bottom membranes³⁰².

I. Maximum loading of SWCNTs in SWCNT–UF

The maximum amount of SWCNTs that the UF support structure can hold is calculated as described in Table S6.

Table S6: Calculations of the maximum SWCNT loading. Adapted from Nguyen *et al.*³⁰².

Parameter (units)	Value	Type of value	Comments
True density of SWCNTs (g/cm ³)	1.0–1.8	Reported	True density is the density of particles that make up the material. True density had been reported as a function of the no. of nanotube walls ⁵⁶⁵ .
Bulk density of SWCNTs in water / air (g/cm ³)	0.1–0.3	Reported	Bulk density is the ratio between the mass and volume of the material in the medium (water or air). The bulk density is reported

			in several publications to be 0.1–0.3 g/cm ³ 321, 566, 567.
Porosity of UF support fibers	0.4–0.6	Reported	Value is taken from a report on the properties of non-woven UF supports ⁵⁶⁸ , which are similar to those used in this work.
Thickness of the SWCNT layer per g/m ² loading (μm)	13	Calculated	Calculated by dividing the loading (1 g/m ²) by the bulk density (0.15 g/cm ³) and the porosity of UF support (0.5).
Thickness of the UF support (μm)	> 150	Determined from SEM characterization	Estimated from the cross-section micrographs of the UF membranes. It is assumed that SWCNTs did not penetrate the middle microporous layer.
Maximum loading of SWCNT in theory (g/m ²)	~11.5	Calculated	Calculated by dividing the thickness of the UF support (150 μm) by the thickness of the SWCNT layer per g/m ² loading (13 μm).

J. Maximum E2 adsorbed mass with SWCNT–UF

To determine the maximum adsorbed amount of E2 that SWCNT layer can offer, the theoretical E2 adsorption capacity and maximum treated volume of 100 ng/L hormone by the SWCNT layer are calculated (Table S7) based on the following assumptions:

- E2 with surface area of 0.5 nm² form a full monolayer coverage on the SWCNT external surface (400 m²/g).
- E2 does not access the internal surface of SWCNT because the area of tube entrance (10 nm² per SWCNT) is much smaller than the total external area (8,000 nm² per SWCNT).

Table S7: Calculations of the adsorption capacity and maximum treated volume. Adapted from Nguyen *et al.*³⁰².

Loading (g/m ²)	0.1	0.5	1	2	4
SWCNT external surface area per m ² of membrane area assuming a specific SWCNT external surface of 400 m ² /g (m ² /m ²)	40	200	400	800	1600
SWCNT surface area in the 2 cm ² membrane coupon (m ²)	0.008	0.04	0.08	0.16	0.32
External surface area of SWCNTs in the 2 cm ² membrane coupon per 1 g/m ² loading (m ²)			0.08		
Cross-sectional surface area of each E2 molecule (nm ²) – <i>Note: this surface area is also relevant to E1, T and P.</i>			0.5		
Maximum no. of E2 molecules occupying SWCNT surface in the 2 cm ² membrane coupon (· 10 ¹⁶)	1.6	8.0	16	32	64

Maximum no. of mol of E2 occupying SWCNT surface in the 2 cm ² membrane coupon ($\cdot 10^{-8}$ mol)	2.7	14	27	54	110
No. of mol of E2 in a litre of 100 ng/L E2 solution (mol)	(All loadings) $3.7 \cdot 10^{-10}$				
Theoretical volume of 100 ng/L E2 needed with 2 cm ² SWCNT-UF to achieve the adsorption capacity (L)	73	370	730	150	300
Mass of E2 (272 g/mol) occupying 1 cm ² of SWCNT-UF membrane ($\mu\text{g}/\text{cm}^2$)	3.6	18	36	72	144
Estimated E2 adsorption capacity (mg/g)	(All loadings) 360				

K. Characterisation of organic matter with LC-OCD

Table S8 shows the fraction concentrations from LC-OCD of nine OM types. The concentration of the OM solutions is uniform at 5 mgC/L, measured with the TOC analyser. An issue of LC-OCD is that hydrophobic fractions (HOC) can be adsorbed to the capillaries and SEC column. LC-OCD system. The HOC is calculated as the difference between the bypass DOC and eluate DOC, while the OM loss caused by the capillaries is estimated by subtracting the bypassed DOC from the expected concentration (5 mgC/L).

Table S8: Fraction concentrations as dissolved organic carbon (DOC) from LC-OCD (Bio. = biopolymer, HS = humic substances, BB = building blocks, LMW = low molecular weight compounds, HOC = hydrophobic organic carbon). The percentages of OM by the LC-OCD and average molecular weights (MWs) of the HS fraction are also given. Adapted from Nguyen *et al.* ³⁰⁵.

No.	OM type	DOC from bypass (mgC/L)	DOC from SEC (mgC/L)	DOC in specific fractions (mgC/L)					Estimated percentage of adsorbed DOC (%)	Average MW of HS (g/mol)
				Bio	HS	BB	LMW	HOC		
1	HA	4.2	3.6	0	1.5	0.8	1.3	0.5	13	790
2	AUS	4.2	4.2	0	2.8	0.6	0.8	0	0	540
3	GLU	4.2	4.2	0	0	0.3	3.9	0	0	N.D.
4	TA	0.5	0.4	0	0	0.1	0.3	0.1	~90	N.D.
5	TANN	1.8	0.7	0.1	0.3	0.1	0.2	1.1	~80	520
6	ALG	4.1	4.1	3.9	0	0	0.2	0	0	N.D.
7	TEA	2.5	2.2	0	0.4	1.2	0.6	0.3	~50	380
8	FP	4.4	4.4	0	0.2*	0.6	3.6	0	0	830
9	WF	2.7	1.4	1.2		0	0.2	1.3	~70	N.D.

* A small peak is observed in the HS region, but this peak may not correspond to HS because the corresponding fraction was not UV-active (absorbance is equal to zero according to UVD)

The retention of phenol-rich compounds and WF by the LC-OCD capillaries are high: 40% for TEA and WF, 55% for TANN and especially 90% for TA. The percentage of organic carbon adsorbed by both the capillaries and SEC column were around 80% for TANN, 70 for WF, 90% for TA and 50% for TEA. These are a major source of error in calculations. A small percentage of adsorbed mass percentage of HA was found, which serves as a small additional source of error in OM removal and mass loss calculations. For the other OM types (AUS, FP, ALG and FP), no adsorption by the LC-OCD system was observed.

L. Reproducibility of OM analysis with LC-OCD

To determine whether the OCD results were reproducible for different OM types, each OM type was analysed twice at different times (2 months to a year), and the corresponding chromatograms are overlapped in Figure S4. The WF and FP solutions were prepared by dilution from the original solutions (described in Section 3.3.4), whereas the solutions of other OM types were prepared fresh by dissolving the powders. A significant difference in peak positions between the two repeats indicates that sample analysis is not reproducible.

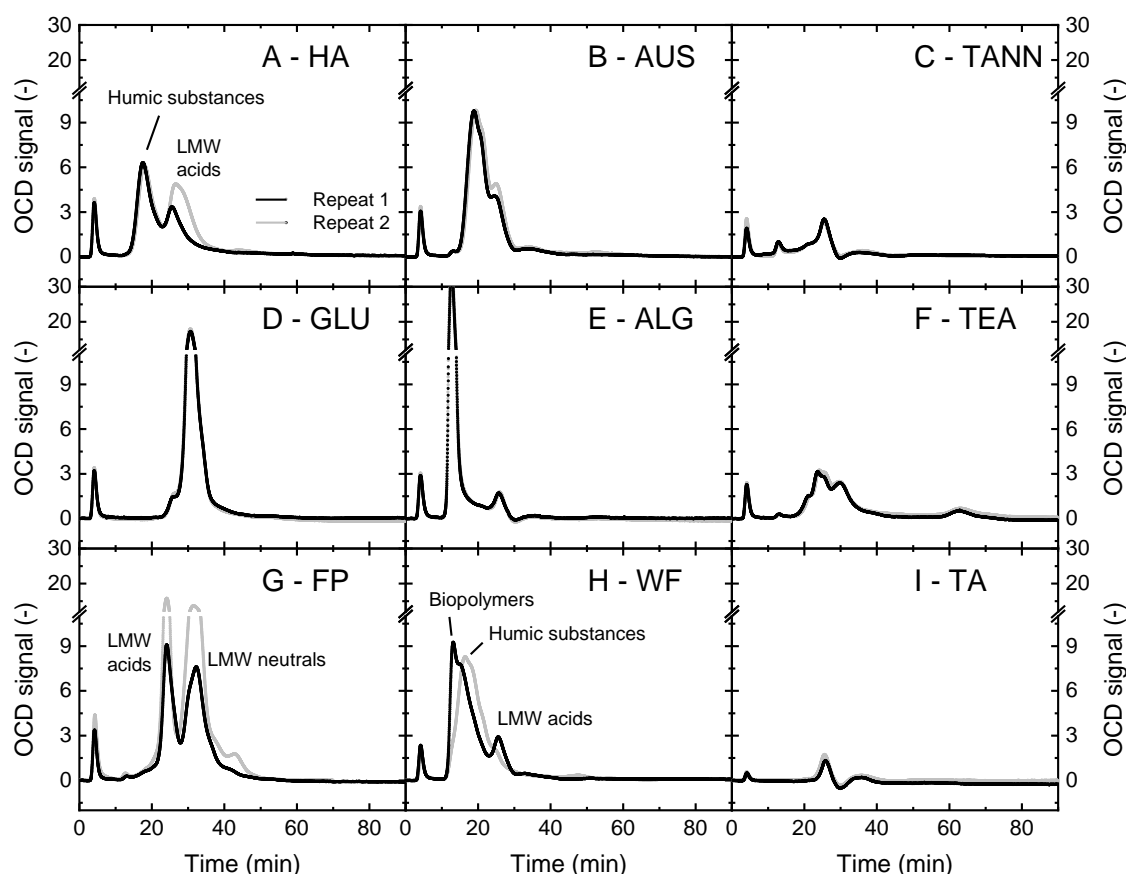


Figure S4: OCD signal vs. time for different OM types at a uniform concentration of 5 mgC/L. Each OM type was analysed twice at different times (a fresh stock solution was prepared for each repeat). LMW: Low molecular-weight.

The following points are drawn from observing Figure S4:

- The OCD results between the two repeats with AUS, TANN, GLU, ALG, TEA, and TA are similar. The heights of the three peaks with FP vary between the two repeats and may be attributed to the variation in the individual calibrations.
- With HA, the peaks corresponding to humic substances are superimposed in the two repeats, but the trails of low molecular-weight (LMW) acids varied, which is likely attributed to artifacts caused by pH adjustment.
- With WF, the composition of biopolymers is lower and that of humic substances is higher in Repeat 2 compared with Repeat 1. This is because the biopolymers in the raw solution degraded over time, and hence the analysis of WF does not yield reproducible results.

M. UV–Vis absorbance of nine OM types

The UV and visible light absorbance of nine OM types is given in Figure S5 at different wavelength between 250 and 700 nm. The absorbance in UV range gives information about the aromaticity of the OM, and whether the OM can be analysed by UV–Vis spectroscopy.

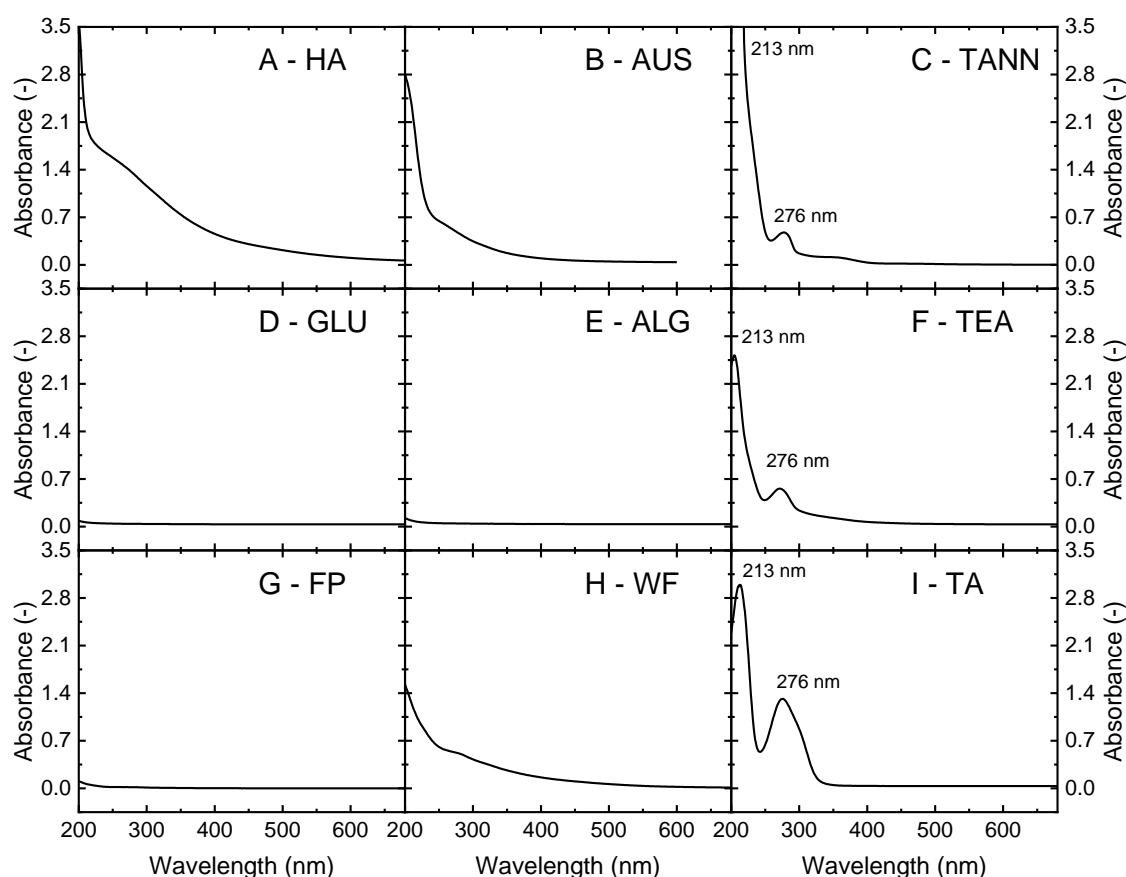


Figure S5: Absorbance vs. UV–Vis wavelength for different OM types (20 mgC/L). Adapted from Nguyen *et al.*³⁰⁵.

The absorbance of GLU, ALG and FP is very little in the entire wavelength range of 250–700 nm. It is implied that these OM types lack aromatic rings. TEA, AUS, WF, TANN, TA and HA are UV-active because of the transitions in response to UV light caused by aromatic rings. For the phenol-rich TEA, TA and TANN, a characteristic peak at 276 nm is observed.

The concentration of TA can be determined with UV–Vis spectroscopy at 213 nm, which is the wavelength that results in the highest absorbance.

N. Flow enhancement in VaCNT membranes

With the VaCNT membranes, the flux of water was much faster than the values calculated according to the Hagen–Poiseuille equation, see Eq. (3.16). To illustrate this flow enhancement, the EF calculated with Eq. (3.17) and slip length b calculated with Eq. (3.14) are given in Figure S6.

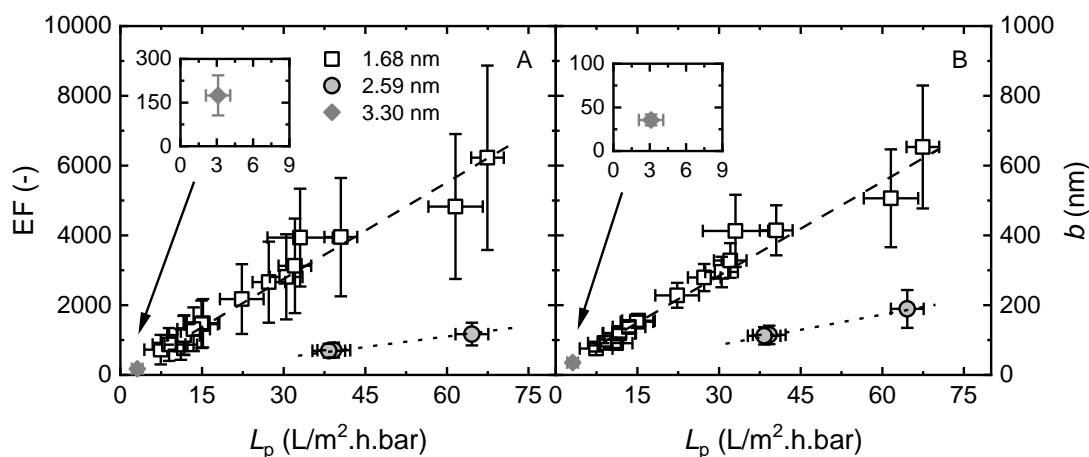


Figure S6: Enhancement factor (EF, A) and slip length b (B) as functions of pure water permeability L_p , for various VaCNT membranes with average pore diameters 1.7, 2.6 and 3.3 nm, respectively. The respective number of data points are 16, 3 and 1. Reprinted from Nguyen *et al.*⁴¹⁴, copyright 2022 American Chemical Society.

The pure water permeability of the 1.7 nm pore diameter membranes was between 8 and 65 $L/m^2.h.bar$, which falls in the permeability ranges of NF and dense UF membranes (see Table 1.3). However, the slip lengths are 85–8000, and the EFs are 3–4 orders of magnitude. Similar EFs and slip lengths were reported by Holt *et al.*¹⁹⁴.

The permeability of the 2.6 nm pore diameter membranes was in the same range as the 1.68 nm ones, but although the EF and slip length of the 2.6 nm membranes were lower. The 3.3 nm pore diameter membrane has the lowest permeability (3 $L/m^2.h.bar$), slip length (30 nm) and lowest EF (150).

All the membranes have very high slip length compared with the pore radius (*i.e.* $b \gg \frac{d_p}{2}$), and the EFs were 2–4 orders of magnitude. The imperfect plug flow condition can be assumed in all

these experiments. To achieve the hypothetical perfect plug flow, the slip length needs to be ∞ and hence the EF is ∞ ⁵⁶⁹. It is also noted that the plug flow condition is only applied for the flowing water inside the VaCNT membrane and not the steroid hormones that may interact strongly with the pore wall.

O. Pressure issues in VaCNT membranes

The experiment to investigate the pressure increase is described in Section 7.2.5. The experimental results at a controlled temperature of 23.0 ± 0.2 °C are given in Figure S5.

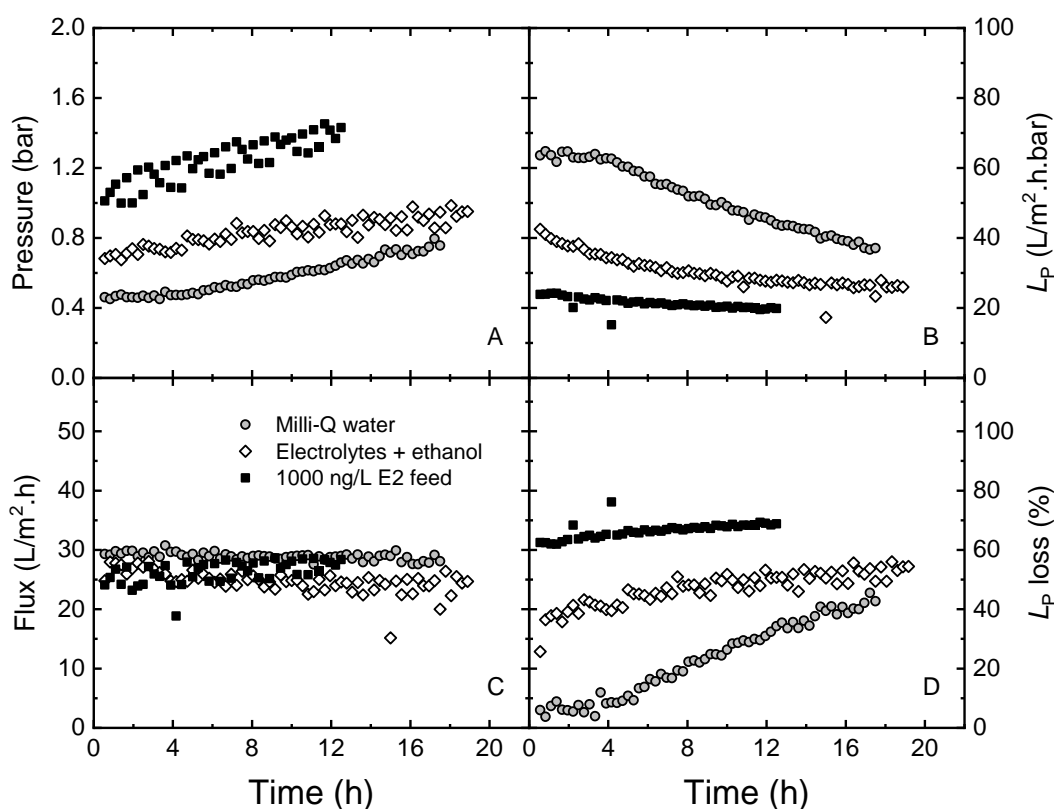


Figure S7: Change in pressure (A), membrane permeability L_P (B), flux (C), and L_P loss (percentage of L_P decrease from the initial pure water L_P) (D) in the filtration with Milli-Q water, simulated water matrix (1 mM NaHCO₃, 10 mM NaCl and 30 mg/L ethanol), and subsequent E2 solution (1000 ng/L E2, 1 mM NaHCO₃, 10 mM NaCl and 300 mg/L ethanol). The membrane pore diameter was 2.6 nm. Adapted from Nguyen *et al.*⁴¹⁴, copyright 2022 American Chemical Society.

In the first 4 h of filtration with Milli-Q water, the pressure and permeability were constant at 0.45 bar and 62 L/m².h.bar, respectively. However, in the next 16 h of the filtration with Milli-Q water, the pressure increased from 0.45 to 0.8 bar, which causes a loss of permeability loss of 42%. It is likely that the membrane was compressed. Pore blocking by contaminants was avoided (although it is still possible) because the feed container and tubing had been thoroughly cleaned with calcium hypochlorite, acid, and base solutions prior to this experiment.

In the subsequent experiments with simulated background (with electrolytes and ethanol) and 1000 ng/L E2 solution, the pressure increased from 0.7 to 1.0 and from 1.0 to 1.5 bar, respectively. These pressure increases correspond to permeability losses of 60% and 70% from the initial pure water permeability. There is no evidence that ethanol and electrolytes intensified the permeability loss.

To determine if the permeability loss is seen with the smaller pore diameter membrane (1.7 nm), a shorter filtration experiment (5 h) with only Milli-Q water was performed with this membrane. The pressure and permeability data are given for both the 2.6 and 1.7 nm pore diameter membranes in Figure S8.

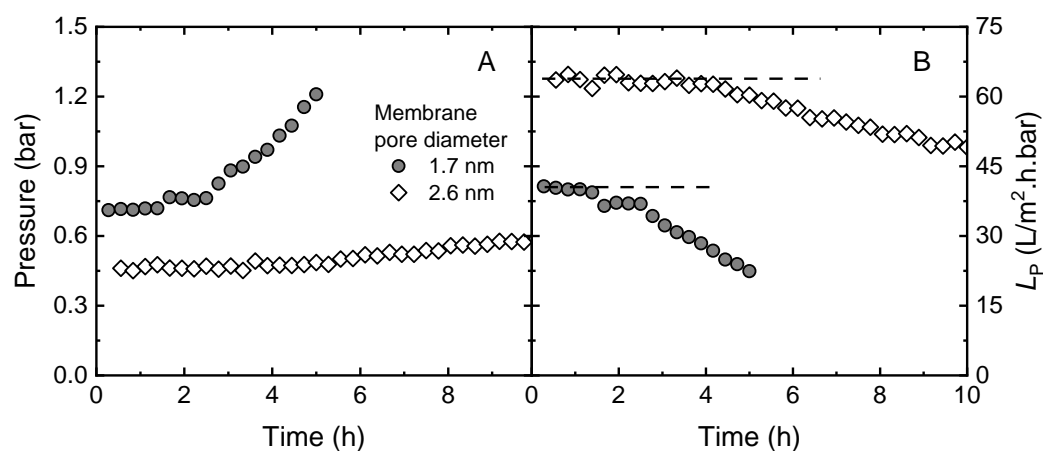


Figure S8: Change in pressure (A) and membrane permeability L_P (B) in the filtration with Milli-Q water. Two membrane pore diameters are compared (1.7 and 2.6 nm). The horizontal dashed lines in B indicate the initial permeabilities of the membranes. The flux was set constant at 30 L/m².h. Reprinted from Nguyen *et al.*⁴¹⁴, copyright 2022 American Chemical Society.

The VaCNT 1.7 nm membrane suffers from a similar permeability loss as the VaCNT 2.6 nm membrane. In the first 2 h, the permeability of the 1.7 nm pore diameter membrane was stable at around 40 L/m².h.bar. In the next 3 h, the permeability decreased in from 40 to 20 L/m².h.bar, corresponding to an increase in pressure by 2 times. It appears that the permeability loss is a common issue and can be expected with all VaCNT 1.7 and 2.6 nm membranes. The 3.3 nm pore diameter membranes may suffer from the same permeability drop but this was not observed in the only performed experiment.

Abbreviations

17 α -E2	17 α -estradiol
AC	Activated carbon
ACM	Adsorptive composite membrane
ACS	American Chemical Society
ALG	Alginate
AUS	Australian natural organic matter
BB	Building block
BET	Brunauer–Emmett–Teller
BMBF	Federal Ministry of Education and Research
BPA	Bis-phenol A
BW	Baden–Württemberg
CA	Cellulose acetate (membrane)
CAS	Chemical Abstracts Service (CAS number)
CNP	Carbon-based nanoparticle
CNP–UF	Carbon-based nanoparticle – ultrafiltration composite membrane
DAAD	German Academic Exchange Service
DB	Double blank (membrane)
DFT	Density functional theory
DLS	Dynamic light scattering
DLVO	Derjaguin–Landau–Verwey–Overbeek
E1	Estrone
E2	17 β -estradiol
E3	Estriol

EDC	Endocrine disrupting chemicals
EE2	17 α -ethinylestradiol
EF	(Flow) enhancement factor
ELS	Electrophoretic light scattering
EU	European Union
FP	Fermentation products
FWHM	Full-width-at-half-maximum
GAC	Granular activated carbon
GLU	Glucose
GO	Graphene oxide
GP	Graphene
GP1 / GP2	Graphene grade 1 (2–3 monolayers) / grade 2 (~30 monolayers)
GTSW	Green Technologies for Sustainable Water
HA	Humic acid
HIM	Helium ion microscopy
HMCN	Hollow mesoporous carbon nanosphere
HMCN–UF	Hollow mesoporous carbon nanosphere – ultrafiltration composite membrane
HOC	Hydrophobic organic carbon
HPLC	High-performance liquid chromatography
HS	Humic substance
IAM	Institute for Applied Materials
IAMT	Institute for Advanced Membrane Technology
IET	Institute of Environmental Technology (Vietnam)
IFG	Institute of Functional Interfaces
IMT	Institute of Microstructure Technology
IMVT	Institute for Micro Process Engineering
INE	Institute for Nuclear Waste Disposal

IPD	Intra-particle diffusion
KOMS-BW	Competence Center for Trace Substances – Baden–Württemberg
KHP	Potassium hydrogen phthalate
KIT	Karlsruhe Institute of Technology
LC-OCD	Liquid chromatography – organic carbon detection
LDL-BW	State Office for Geoinformation and Rural Development – Baden–Württemberg
LLNL	Lawrence Livermore National Laboratory
LMW	Low molecular weight
LOD	Detection limit
LOQ	Limit of quantification
LSC	Liquid scintillation counting
MF	Microfiltration
MMM	Mixed-matrix membrane
MW	Molecular weight
MWCNT	Multi-walled carbon nanotube
MWCO	Molecular weight cut-off
NDMA	N-Nitrosodimethylamine
NF	Nanofiltration
NMI	Natural Science and Medical Institute
NMR	Nuclear magnetic resonance
NOM	Natural organic matter
OCD	Organic carbon detection / detector
OM	Organic matter
OND	Organic nitrogen detection / detector
P	Progesterone
PAC	Powdered activated carbon
PBSAC	Polymer-based spherical activated carbon

PDA	Polydopamine
PES	Polyethersulfone (membrane)
PNEC	Predicted no-effect concentration
PTFE	Polytetrafluoroethylene (membrane)
PVDF	Polyvinylidene fluoride (membrane)
QSDFT	Quenched-solid density functional theory
RC	Regenerated cellulose (membrane)
RO	Reverse osmosis
SB	Single blank (membrane)
SEM	Scanning electron microscopy
SH	Steroid hormone
SSA	Specific surface area
SUVA	Specific ultraviolet absorbance
SWCNT	Single-walled carbon nanotube
SWCNT–UF	Single-walled carbon nanotube – ultrafiltration composite membrane
T	Testosterone
TA	Tannic acid
TANN	Tannin
TEM	Transmission electron microscopy
TOC	Total organic carbon
UF	Ultrafiltration
UNICEF	United Nations International Children's Emergency Fund
UV–Vis	Ultraviolet–visible (spectroscopy)
UVD	Ultraviolet detection / detector
VaCNT	Vertically aligned carbon nanotube
VaCNT–MF	Vertically aligned carbon nanotube membrane on a microfiltration support
VAST	Vietnam Academy of Science and Technology

Abbreviations

WF	Worm farm extract
WHO	World Health Organisation
WWTP	Wastewater treatment plant
XPS	X-ray photoelectron microscopy

List of Symbols

α	Membrane tortuosity (-)
A_m	Membrane area (cm ² or m ²)
b	Slip length (nm)
b_L	Langmuir equilibrium constant (L/ng)
C	Correction factor of intra-particle diffusion model (ng/g)
c_0	Initial concentration in static adsorption and filtration (ng/L or mgC/L)
c_{blank}	Measured concentration of the blank sample (ng/L or mgC/L)
c_E	Concentration at equilibrium (ng/L or mgC/L)
c_f	Feed concentration (ng/L or mgC/L)
c_n	Concentration at nth extraction in static adsorption (ng/L or mgC/L)
c_p	Permeate concentration (ng/L or mgC/L)
c_r	Retentate concentration (ng/L or mgC/L)
$c(t)$	Concentration at time t in static adsorption (ng/L or mgC/L)
d	Membrane pore diameter (nm)
d_{OM}	Hydrodynamic diameter of a certain organic matter molecule (nm)
d_p or d_{SH}	Hydrodynamic diameter of the hormone (nm)
d_{PM}	Polanyi–Mane isotherm model constant (nm)
δ_m	Membrane separation layer thickness (m)
ε	Membrane porosity (-)
EF	(Flow) enhancement factor (-)
ε_{VaCNT}	VaCNT membrane porosity (-)
H	Hamaker constant for the pair-wise hormone and CNT wall interaction (J)
H_{CNT}	Hamaker constant for the CNT–CNT pair interaction (J)

H_{SH}	Hamaker constant for the hormone–hormone pair interaction (J)
H_{water}	Hamaker constant for the water–water pair interaction (J)
J or J_{exp}	Flux (L/m ² .h)
J_0	Pure water flux (L/m ² .h)
K_1	First-order kinetic rate constant (1/h)
K_2	Second-order kinetic rate constant (g/ng.h)
K_a	Acid dissociation constant (-)
K_d	Intraparticle diffusion constant (g/ng.h ^{0.5})
K_F	Freundlich isotherm constant (g/ng.h ^{0.5})
K_{FD}	Film diffusion constant (1/h)
K_H	Henry isotherm constant (L/g)
K_{OW}	Octanol–water partition coefficient (-)
L	Membrane thickness (μm)
L_p or $L_{p,exp}$	Membrane permeability (L/m ² .h.bar)
$L_{p,HP}$	Membrane permeability determined w/ Hagen–Poiseuille equation (L/m ² .h.bar)
M	Molecular weight (g/mol)
m_{ads}	Adsorbed mass (ng or mgC)
$m_{adsorbent}$	Mass of adsorbent (g)
m_p	Permeate mass (ng or mgC)
N	Number of repeats (-)
n_F	Freundlich isotherm constant (-)
n_{CNT}	Number of carbon nanotubes (-)
μ	Dynamic viscosity of the solvent / water (kg/m.s or Pa.s)
ΔP	Pressure difference / applied pressure (bar)
ρ_{wat}	Water density (g/cm ³)
$q_{ads,A}$	Specific adsorbed mass per membrane area (ng/m ² or mgC/cm ²)

$q_{ads,s}$	Specific adsorbed mass per adsorbent mass (ng/g)
q_E	Specific adsorbed mass at equilibrium (ng/g)
q_{max}	Adsorption capacity (ng/g)
R	Removal (%)
σ_{blank}	Standard deviation of the blank sample concentration (ng/L or mgC/L)
$SUVA_{254}$	Specific ultraviolet absorbance at 254 nm wavelength (L/mg.m)
t	Time (s)
t_R	Residence time (s)
V_0	Initial volume (static adsorption) (L)
V_e	Extracted volume (static adsorption) (L)
v_{water}	Flow velocity of water (m/s)
z	Distance between the centre of the hormone molecule and the CNT wall (nm)
Z_{PM}	Polanyi–Mane isotherm constant ($J^{1/d}$)

In Appendices B and H

Δ	Operator referring to the absolute error of a parameter
$\Delta c_{anal.}$	Error in concentration from analytical instrument (ng/L or mgC/L)
$\Delta c_{prep.}$	Error in concentration from sample preparation (ng/L or mgC/L)
$\Delta c_{fil.}$	Error in concentration from the filtration operation (ng/L or mgC/L)
Δc_j	General term for the error in concentration (ng/L or mgC/L)
D_0	Water diffusivity in the bulk (m^2/s)
D_{eff}	Water diffusivity in the (VaCNT) membrane pore
D_{water}	Hydrodynamic diameter of a water molecule (nm)
Δm_j	General term for the error in mass (ng or mgC)
t_D	Diffusion time (s)
ΔV_j	General term for the error in volume (L)

List of Figures

Figure 1.1:	Population share without access to an improved water source in 2020. The database was published by WHO/UNICEF (JMP_2021_WLD) in 2022 ⁷). The map was created by M.N.	2
Figure 1.2:	Summary of steps in conventional wastewater and drinking water treatment facilities. Micropollutants can penetrate through all these steps and occur in the drinking water. The investigation in this dissertation fits in the tertiary treatment step of wastewater treatment.	3
Figure 1.3:	Simplistic view of the biotransformation of steroid hormones in the body; each arrow represents a biotransformation pathway. The four hormones E1, E2, T and P are the removal targets of this research project. Adapted from Chatuphonprasert <i>et al.</i> ³⁴	4
Figure 1.4:	Map of WWTPs with micropollutant removal technologies (granular / powdered activated carbon (GAC/PAC) adsorption, and ozonation) in Baden–Württemberg (BW), including those in construction or planned. Data were taken from the BW websites ^{87, 88} in March 2022. The map was created by M.N.	8
Figure 1.5:	Schematic view of the ozonation process.	9
Figure 1.6:	Schematic of different adsorption system designs based on the adsorbent size: large (GAC, several millimetres), medium (PAC and PBSAC, several to a few hundred micrometres), and small (<i>e.g.</i> CNPs, a few nanometres to sub-micrometres). The adsorptive composite membranes are the research targets of this dissertation.	10
Figure 1.7:	Schematic of the dissertation structure.	14
Figure 2.1:	Schematic of three hybrid system designs: feed-side adsorption (Design 1), integrated adsorption–filtration (Design 2) and permeate-side adsorption (Design 3). Concentrate flow is not available in Design 2 and optional in Designs 1 and 3. In Design 2, PAC is injected into the filtration module. Adapted from Stoquart <i>et al.</i> ¹¹⁹	18
Figure 2.2:	Schematic of the deposition of PAC on the UF or MF membrane in the presence of OM.	19
Figure 2.3:	The concept of permeate side deposition of adsorbents (polymer-based spherical activated carbon) described by Tagliavini <i>et al.</i> ^{192, 193}	20
Figure 2.4:	Main types of carbon-based nanoparticles (MW-/SWCNTs, graphenes, and C ₆₀) ^{197, 200, 201} and the VaCNT membrane ¹⁹⁴	22
Figure 2.5:	Schematic of adsorbate mass transfer mechanisms (in activated carbons as an example). Ext.: external, Int.: internal.	24

Figure 2.6:	Directional interactions between parts of the CNP (black) and hormone E2 (grey), including π - π stacking, X-H / π interaction (X = C, O), and O...H hydrogen bonding.	27
Figure 2.7:	Non-directional interactions at atomic level (London dispersion), and ionic / molecular level (electrostatic interaction and hydrophobic effect). The symbol -ve indicates the local negative charge of the ion or molecule.	28
Figure 2.8:	Five technical considerations (in grey spheres) with ACMs. The chapters (CH) in this dissertation are indicated where the relevant determining factors (in the rectangular boxes) are evaluated.	29
Figure 2.9:	Permeate E2 concentration (A) and specific adsorbed mass (B) determined with SWCNT-UF composite membranes at two SWCNT loadings (0.1 and 2 g/m ²). 100 ng/L feed E2, 1 mM NaHCO ₃ , 10 mM NaCl, pH 8.1 \pm 0.2, 23.0 \pm 1.6 °C. Data taken from Nguyen <i>et al.</i> ³⁰²	30
Figure 2.10:	Adsorbed mass of steroid hormone (E2) vs. residence time in static adsorption obtained with MW- and SWCNT (0.01 g/L). Grey box indicates the hydraulic residence time range relevant in an ACM (~1 min). Data taken from Nguyen <i>et al.</i> ³⁰³	31
Figure 2.11.	OM (TA) interference mechanisms relevant to hormone (E2) adsorption by adsorbents (SWCNTs). Models of idealised molecules were constructed in Chem3D 19.0, PerkinElmer, USA. SWCNTs are viewed from the top. Reprinted from Nguyen <i>et al.</i> ³⁰⁵	32
Figure 2.12.	Schematic of the shielding of organic matter by UF membrane in an advanced composite membrane set-up. Adapted from the graphical abstract of Nguyen <i>et al.</i> 2021 ³⁰⁵	34
Figure 2.13:	Schematic of common composite membrane configurations where particles or nanoparticles (grey spheres) are incorporated.	37
Figure 2.14:	Schematic of the dual membrane composite concept. Reprinted from Nguyen <i>et al.</i> ³⁰²	40
Figure 2.15:	Schematic of the transfer of steroid hormone (E2) molecules through a VaCNT membrane (A) and active / dense layer of an UF or NF membrane (B), and the forces acting on the molecules (F_H : hydrodynamic drag, F_F : friction, F_A : adhesive, F_R : repulsive). The pore and hormone diameters are roughly to scale. Adapted from Nguyen <i>et al.</i> ⁴¹⁴	42
Figure 3.1:	Photograph (A) and schematic (B) of the micro-crossflow filtration system.	45
Figure 3.2:	Photographs of the incubator shaker.	46
Figure 3.3:	Apparatuses for SWCNT incorporation into the UF support: vacuum filtration device for 10–100 kDa UF (A) and stirred cell for 3–5 kDa UF (B).	49
Figure 3.4:	Schematic of VaCNT membrane fabrication. Adapted from Bui <i>et al.</i> ¹⁹⁵	50
Figure 3.5:	A – Photograph of the Tri-Carb 2250 TR/AB instrument (the Tri-Carb 4910 TR looks similar and is not shown). B – Calibration curves with steroid hormone standards (E1, E2, T and P) are given in log scale. The positions of the LOD	

	and LOQ for E2 calibration are highlighted (determined <i>via</i> Method 3 in Section 3.6.2).	54
Figure 3.6:	A – Photograph of the TOC analyser. B – Calibration curve with KHP standards is given in log scale. The positions of the LOD and LOQ are highlighted (determined <i>via</i> Method 3 in Section 3.6.2).	54
Figure 3.7:	A – Schematic of VaCNT membrane fabrication. B – An example LC-OCD chromatogram of a soil extract with peak annotations (Australian natural OM). C – Calibration curve with KHP standards is given log scale. The positions of the LOD and LOQ are highlighted (determined <i>via</i> Method 3 in Section 3.6.2).	55
Figure 3.8:	A – Photograph of the UV-Vis spectroscopy instrument. B – Calibration curve with TA standards and LOD (determined <i>via</i> Method 1 in Section 3.6.2).	57
Figure 3.9:	Calibration of steroid hormones (A) and organic matter (B). The dotted lines indicate the regressions of the calibration.....	63
Figure 3.10:	Organic carbon signal as function of elution time between 15 and 30 min at concentrations of 0.005–0.05 mgC/L. Results from only one repeat per concentration is illustrated.	63
Figure 3.11:	Illustration of the relationships between measured and calculated parameters in a typical filtration experiment with CNP–UF membranes.	66
Figure 4.1:	Permeate E2 concentration (A) and adsorbed mass (B) after recycling the membranes up to 6 times. Total filtered volume 7.5 mL, 100 ng/L E2, 1 mM NaCO ₃ , 10 mM NaCl, pH 8.2 ± 0.1. Permeate volume is roughly determined from the number of drops. Adapted from Nguyen <i>et al.</i> ³⁰³	75
Figure 4.2:	Permeate E2 concentration and adsorbed mass by the membrane filters with different feed concentrations. Adsorbed mass was calculated for a rough value of filtered volume of 1.25 mL. 1 mM NaCO ₃ , 10 mM NaCl, pH 8. Adapted from Nguyen <i>et al.</i> ³⁰³	76
Figure 4.3:	Permeate E2 concentration (A) and adsorbed mass (B) at pH 8, 11 and 12 with different feed concentrations. Adsorbed mass was calculated for a rough value of filtered volume of 1.25 mL. 1 mM NaCO ₃ , 10 mM NaCl. Adapted from Nguyen <i>et al.</i> ³⁰³	77
Figure 4.4:	E2 adsorbed mass a function of time with varied CNP doses. Data are fitted with the first-order kinetics model. Conditions: 100 ng/L E2, 1 mM NaHCO ₃ , 10 mM NaCl, 20.0 ± 0.5 °C, pH 8.0 ± 0.1. Adapted from Nguyen <i>et al.</i> ³⁰³	79
Figure 4.5:	A and B – Specific adsorbed mass of E2 q_E vs. E2 concentration at equilibrium c_E . Henry model was applied for MW-/SWCNT, GP1 and GO (dashed lines). Langmuir model was applied for GP2 and C ₆₀ (solid curves). Inset of B shows the GP2 and C ₆₀ data in linear scale. Conditions: 0.1 g/L CNP, 1 mM NaHCO ₃ , 10 mM NaCl, 20.0 ± 0.5 °C, pH 8.0 ± 0.1. Adapted from Nguyen <i>et al.</i> ³⁰³	80
Figure 4.6:	Relative hormone concentration c/c_0 (A) and specific adsorbed mass at equilibrium q_E (B) of four hormones. Conditions: 0.1 g/L CNPs, 100 ng/L	

	hormone (E1, E2, T and P), 1 mM NaHCO ₃ , 10 mM NaCl, 20.0 ± 0.5 °C, pH 8.0 ± 0.1. Adapted from Nguyen <i>et al.</i> ³⁰³	82
Figure 4.7:	Specific adsorbed mass of E2 at equilibrium (q_E) vs. temperature. Conditions: 0.1 g/L CNP, 100 ng/L E2, 1 mM NaHCO ₃ , 10 mM NaCl, pH 8.0 ± 0.1. Adapted from Nguyen <i>et al.</i> ³⁰³	83
Figure 4.8:	A and B – E2 adsorbed mass at equilibrium q_E as a function of pH (100 ng/L E2, 1 mM NaHCO ₃ , 10 mM NaCl, 20.0 ± 0.5 °C, pH 2–12). Vertical line indicates the pKa of E2 ²⁸⁹ . Adapted from Nguyen <i>et al.</i> ³⁰³	84
Figure 4.9:	HIM micrographs of MWCNT (A), SWCNT (B), GP1 (C), GP2 (D), GO (E) and C ₆₀ (F). The TEM grid on which the CNPs were deposited can be seen in the background. Reprinted from Nguyen <i>et al.</i> ³⁰³	87
Figure 4.10:	Aggregate size of CNPs vs. time where the suspensions were prepared <i>via</i> three methods indicated in Section 3.7.4. Adapted from Nguyen <i>et al.</i> ³⁰³	89
Figure 4.11:	Geometries of MW-/SWCNT, graphene, GO and C ₆₀ molecules and aggregates. Different adsorption sites are illustrated with E2 molecules. Only the size of C ₆₀ is to scale with the size of E2. Adapted from Nguyen <i>et al.</i> ³⁰³	90
Figure 4.12:	Zeta potential as function of pH. Colloids are expected to be stable if the magnitude of zeta potential exceeded 30 mV (grey region) according to Everett ⁵⁰⁸ . Reprinted from Nguyen <i>et al.</i> ³⁰³	92
Figure 4.13:	Mechanisms of steroid hormone adsorption by CNPs based on the proximity (CNP–hormone distance follows the order A > B > C). CNP aggregates are represented as SWCNT segments as an example. Adapted from Nguyen <i>et al.</i> ³⁰³	93
Figure 5.1:	High-resolution micrograph of SWCNT deposits on a support structure of an UF support structure (loading 2 g/m ²), showing SWCNTs as individual rod-like structures (with diameters of around 2–3 nm), and in aggregate form. Reprinted from Nguyen <i>et al.</i> ³⁰²	99
Figure 5.2:	Pure water permeability L_p of the single blank (SB), double blank (DB), and SWCNT–UF membranes at different SWCNT loadings. Adapted from Nguyen <i>et al.</i> ³⁰²	101
Figure 5.3:	A, C and E – Respective surfaces of the support layer of RC 10 kDa, RC 100 kDa and PES 100 kDa; B, D and F – Respective surfaces of the support layer of SWCNT–RC10, –RC100 and –PES100 at 2 g/m ² (the inset in B shows the coating of SWCNTs); G – Cross-section of SWCNT–RC100 at 2 g/m ² ; H – Surface of SWCNT–PES100 at 4 g/m ² that shows overloading. Adapted from Nguyen <i>et al.</i> ³⁰²	103
Figure 5.4:	E2 breakthrough of SB, DB, and SWCNT–UF at different loadings. 100 ng/L E2, 1 mM NaHCO ₃ , 10 mM NaCl, 24 ± 2 °C, pH 8.2 ± 0.1, pressure 1 bar. Volume scale is different between 10 kDa and 100 kDa membranes. Reprinted from Nguyen <i>et al.</i> ³⁰²	104

- Figure 5.5: E2 breakthrough of SB and DB of PES 100 kDa, and SWCNT–PES100 at different loadings. 100 ng/L E2, 1 mM NaHCO₃, 10 mM NaCl, 24 ± 2 °C, pH 8.2 ± 0.1, pressure 1 bar. Adapted (extracted) from Nguyen *et al.* ³⁰²..... 105
- Figure 5.6: E2 removal R_{E2} and specific adsorbed mass by SWCNTs $q_{ads,s}$ at a permeate volume of 25 mL for 10 kDa and 180 mL for 100 kDa membranes. Adsorbed mass for SWCNT–PES100 was not determined because of the strong adsorption by the blank membranes. 100 ng/L E2, 1 mM NaHCO₃, 10 mM NaCl, 24 ± 2 °C, pH 8.2 ± 0.1, pressure 1 bar. Adapted (extracted) from Nguyen *et al.* ³⁰². 106
- Figure 5.7: Flux and residence time in SWCNT–UF vs. pressure (100 ng/L E2, 2 g/m² loading, 1 mM NaHCO₃, 10 mM NaCl, 24 ± 2 °C, pH 8.2 ± 0.1). Adapted from Nguyen *et al.* ³⁰² 107
- Figure 5.8: E2 removal R_{E2} (A and B) and adsorbed mass corrected by the treated volume m_{ads} / V_p (C and D) after three hours vs. pressure and residence time. Adsorbed mass with SWCNT–PES100 was not determined because of the strong adsorption by the blank membranes. 100 ng/L E2, 2 g/m² loading, 1 mM NaHCO₃, 10 mM NaCl, 24 ± 2 °C, pH 8.2 ± 0.1. Adapted from Nguyen *et al.* ³⁰² 108
- Figure 5.9: E2 removal R_{E2} (A and B) and specific adsorbed mass $q_{ads,A}$ (C and D) by SWCNT–UF membranes at the same treated volumes (indicated in the legend) vs. pressure and residence time t_R . Adsorbed mass for SWCNT–PES100 was not determined because of the strong adsorption by the blank membranes. 100 ng/L E2, 2 g/m² loading, 1 mM NaHCO₃, 10 mM NaCl, 24 ± 2 °C, pH 8.2 ± 0.1. Adapted from Nguyen *et al.* ³⁰² 109
- Figure 5.10: E2 removal R_{E2} and specific adsorbed mass $q_{ads,A}$ by SWCNT–RC10 at 25 mL vs. pH. Vertical line indicates the pKa of E2 according to Perrin ²⁸⁹. 100 ng/L E2, 2 g/m² loading, 1 mM NaHCO₃, 10 mM NaCl, 24 ± 2 °C, pressure 1 bar. Adapted from Nguyen *et al.* ³⁰² 110
- Figure 5.11: Hormone removal R_H and specific adsorbed mass $q_{ads,A}$ at 25 mL by SWCNT–RC10. 100 ng/L hormone, 2 g/m² loading, 1 mM NaHCO₃, 10 mM NaCl, 24 ± 2 °C, pH 8.2 ± 0.1, pressure 1 bar. Adapted from Nguyen *et al.* ³⁰² 111
- Figure 6.1: Measured E2 concentration in the presence of OM as a function of OM concentration. The horizontal solid line indicates the E2 concentration without OM. The vertical dashed line indicates the maximum OM concentration where interference is low (< 10%). Adapted from Nguyen *et al.* ³⁰⁵ 117
- Figure 6.2: E2 adsorbed mass at equilibrium $q_{ads,s}$ (A) and kinetic rate constant k_{E2} (B) vs. OM type. 100 ng/L E2, 10 mgC/L OM, 0.1 g/L SWCNTs, 1 mM NaHCO₃, 10 mM NaCl, 20 ± 1 °C, pH 8.1 ± 0.2. Adapted from Nguyen *et al.* ³⁰⁵ 118
- Figure 6.3: Relative permeate E2 concentration c/c_0 vs. permeate volume V_p (A and B) with SWCNT–UF 100 kDa. Dotted curves are the guides for the eye. 100 ng/L E2, 10 mgC/L OM, pressure 1 bar, 1 mM NaHCO₃, 10 mM NaCl, 24 ± 2 °C, pH 8.1 ± 0.2. Adapted from Nguyen *et al.* ³⁰⁵ 119

Figure 6.4:	E2 removal R_{E2} (A), E2 adsorbed mass $q_{ads,A}$ (B), OM removal R_{OM} (C) and OM mass loss (D) with SWCNT–UF 100 kDa vs. OM type. The dotted horizontal lines indicate R_{E2} and $q_{ads,A}$ without OM. *TA was quantified from the UV absorbance (213 nm). 100 ng/L E2, 10 mgC/L OM, 1 mM NaHCO ₃ , 10 mM NaCl, 24 ± 2 °C, pH 8.1 ± 0.2. Adapted from Nguyen <i>et al.</i> ³⁰⁵120
Figure 6.5:	Raw organic carbon (OCD) signal (without normalization) of the nine OM types at 5 mgC/L (By: bypass, Bio: biopolymers, HS: humic substances, BB: building blocks, LMW: low molecular-weight substances). Adapted from Nguyen <i>et al.</i> ³⁰⁵122
Figure 6.6:	Specific ultraviolet absorbance (SUVA ₂₅₄) of the nine OM types. Reprinted from Nguyen <i>et al.</i> 2021 ³⁰⁵123
Figure 6.7:	Hormone removal R_H (A), adsorbed mass of hormone $q_{ads,A}$ (B), TA removal R_{TA} (C) and TA mass loss with SWCNT–UF 100 kDa. 100 ng/L hormone, 10 mgC/L TA, 1 mM NaHCO ₃ , 10 mM NaCl, 24 ± 2 °C, pH 8.1 ± 0.2. Adapted from Nguyen <i>et al.</i> 2021 ³⁰⁵125
Figure 6.8:	E2 removal R_{E2} (A and B), E2 adsorbed mass $q_{ads,A}$ (C and D), TA removal R_{TA} (E and F) and TA mass loss (G and H) with SWCNT–UF 10 kDa vs. flux and residence time, respectively. 100 ng/L E2, 10 mgC/L, 1 mM NaHCO ₃ , 10 mM NaCl, 24 ± 2 °C, pH 8.1 ± 0.2. Adapted from Nguyen <i>et al.</i> ³⁰⁵126
Figure 6.9:	E2 removal R_{E2} (A), E2 adsorbed mass $q_{ads,A}$ (B), TA / HA removal R_{OM} (C) and TA / HA mass loss (D) vs. UF MWCO. Permeate volume 30 mL for 1–10 kDa membranes, and 150 mL for 30–100 kDa membranes, 100 ng/L E2, 1 mM NaHCO ₃ , 10 mM NaCl, 24 ± 2 °C, pH 8.1 ± 0.2. Adapted from Nguyen <i>et al.</i> ³⁰⁵128
Figure 7.1:	Schematic of the forces acting on a hormone molecule inside a VaCNT membrane pore: adhesive, repulsive, hydrodynamic drag, and friction forces. The hormone diameter (0.8 nm), gap thickness (0.3 nm) and pore diameter (2 nm) are approximately to scale. The magnitudes of the forces are not to scale.131
Figure 7.2:	Schematic of the filtration system; when pressure control valve (item 7) is closed, the system is operated in dead-end mode.134
Figure 7.3:	Potential reasons for the pressure increase in the filtration experiments: internal pore blocking (A), external pore blocking (B), and membrane deformation (C). Membrane thickness, pore size, and the sizes of ethanol, hormone and contaminant are not to scale.135
Figure 7.4:	Specific E2 adsorbed mass $q_{ads,s}$ vs. time for four types of CNPs and VaCNT membrane at the same concentration of 0.01 g/L (A), and E2 adsorbed mass per adsorbent surface area $m_{ads,s} / S$ between SWCNT and VaCNT membrane (B). 100 ng/L E2, 1 mM NaHCO ₃ , 10 mM NaCl, 20 °C, pH 8. Reprinted from Nguyen <i>et al.</i> ⁴¹⁴ , copyright 2022 American Chemical Society.137
Figure 7.5:	Relative E2 concentration c/c_0 vs. permeate volume V_p (A), and specific adsorbed mass $q_{ads,A}$ of VaCNT and UF membrane at 65 mL, and NF270 membrane at 18 mL (B; star symbol indicates the lower permeate volume).

- Dashed line in A indicates the maximum permeate concentration due to retention by NF⁵⁵⁷. In VaCNT–MF and MF experiments: CNT pore diameter 1.7 nm, flux 57 ± 3 L/m².h, 100 ng/L E2, 1 mM NaHCO₃, 10 mM NaCl, pH 8.2 ± 0.1 , 23.0 ± 0.2 °C. Reprinted from Nguyen *et al.*⁴¹⁴, copyright 2022 American Chemical Society. SWCNT–UF data are taken from Nguyen *et al.*³⁰². 138
- Figure 7.6: Relative E2 concentration c/c_0 (A) and specific adsorbed mass $q_{ads,A}$ (B) vs. permeate volume V_p with varying flux. The dashed line and grey box in B indicate the adsorbed mass by MF and error bar at 100 mL. CNT pore diameter 1.7 nm, 100 ng/L E2, 1 mM NaHCO₃, 10 mM NaCl, pH 8.2 ± 0.1 , 23.0 ± 0.2 °C. Reprinted from Nguyen *et al.*⁴¹⁴, copyright 2022 American Chemical Society. 139
- Figure 7.7: Specific E2 adsorbed mass $q_{ads,A}$ of VaCNT–MF and MF vs. flux (A), and $q_{ads,A}$ of VaCNT membrane vs. hydrodynamic drag force F_H and flow velocity (B) at 65 mL permeate volume. The dashed lines are guides for the eye. CNT pore diameter 1.7 nm, 100 ng/L E2, 1 mM NaHCO₃, 10 mM NaCl, pH 8.2 ± 0.1 , 23.0 ± 0.2 °C. Reprinted from Nguyen *et al.*⁴¹⁴, copyright 2022 American Chemical Society. 140
- Figure 7.8: Specific hormone adsorbed mass $q_{ads,A}$ vs. adhesive force F_A . The dashed curve is a guide for the eye. CNT pore diameter 1.7 nm, flux 27 ± 3 L/m².h, 100 ng/L E2, 1 mM NaHCO₃, 10 mM NaCl, pH 8.2 ± 0.1 , 23.0 ± 0.5 °C. Reprinted from Nguyen *et al.*⁴¹⁴, copyright 2022 American Chemical Society. 141
- Figure 7.9: Specific E2 adsorbed mass $q_{ads,A}$ and relative membrane resistance R/R_{HP} vs. pore diameter. Flux 27 ± 3 L/m².h, permeate volume 100 mL, 100 ng/L E2, 1 mM NaHCO₃, 10 mM NaCl, pH 8.2 ± 0.1 , 23.0 ± 0.5 °C. Reprinted from Nguyen *et al.*⁴¹⁴, copyright 2022 American Chemical Society. 142
- Figure 8.1: Adsorption of steroid hormone molecules by CNPs. From left to right: MWCNT, SWCNT / VaCNT membrane pore, graphene, and fullerene (C₆₀) aggregates. 145
- Figure 8.2: Steroid hormone removal with the SWCNT–UF membrane. 146
- Figure 8.3: Interference of OM and shielding of UF with the SWCNT–UF membrane. Adapted from the graphical abstract of Nguyen *et al.*³⁰⁵. 147
- Figure 8.4: Transfer of hormone through the nanopores of a VaCNT membrane. Reprinted from the graphical abstract of Nguyen *et al.*⁴¹⁴, copyright 2022 American Chemical Society. 148
- Figure 8.5: Schematics of steroid hormone transport through the adsorbent layer of VaCNT membrane (A), SWCNT–UF (B) and an untested carbonaceous membrane in which adsorption may be effective (C). 150

List of Tables

Table 1.1:	Maximum concentrations of steroid hormone micropollutants (E1, E2, E3 and EE2) in wastewater effluents and surface water ^{43, 44, 47-58} . Abbreviations: WE: wastewater effluent, SW: surface water, N.A.: not available, N.D.: not detected (below detection limit).	5
Table 1.2:	Notable laws (in italics) and guidelines / recommendations on the monitoring and treatment of EDCs and steroid hormones.	7
Table 1.3:	Characteristics of different types of membranes (MF, UF, NF and RO) ¹²⁹⁻¹³⁶ . N.D.: Not determined.	11
Table 2.1:	Comparison between ACMs and hybrid membrane processes (that combine adsorption and filtration).	21
Table 3.1:	List of carbon-based nanoparticles. N.A.: not available.	47
Table 3.2:	Characteristics of commercial UF and MF membranes (generously provided by Merck Millipore, USA) used in filtration experiments.	48
Table 3.3:	Physiochemical properties of the four steroid hormone types ^{289-291, 429, 431-437} ...	51
Table 3.4:	OM types. Bio: biopolymers, HS: humic substances, BB: building blocks, LMW: low molecular-weight acids and neutrals, HOC: hydrophobic organic carbon). N.D.: not determined. Liquid chromatography – organic carbon detection (LC-OCD) separates the OM into fractions and determines the composition.	52
Table 3.5:	Error sources, and a list of methods to notice and tackle the errors.	61
Table 3.6:	Detection limits (LOD) and limits of quantifications (LOQ) of analytical instrument determined with the three methods. The detection limits for LSC are ~2 times higher than previously reported with a smaller set of data ¹¹² . N.A.: not available, because the raw data of signal and noise are not accessible.	64
Table 4.1:	Overview of the static adsorption experiment design and conditions. For each investigated parameter, experiments with all the six CNPs were performed.	72
Table 4.2:	Surface area, pore characteristics and adsorption capacities (experimental and theoretical) of CNPs. PBSAC is also included for comparison ¹¹² . N.D.: not determined. Adapted from Nguyen <i>et al.</i> ³⁰³	86
Table 4.3:	Percentages of carbon and oxygen, and their respective electronic states at the CNP surface. Reprinted from Nguyen <i>et al.</i> ³⁰³	91
Table 5.1:	Overview of the filtration experiment design and conditions.	100
Table 6.1:	Overview of the filtration experiment design and conditions. The loading of SWCNTs in all SWCNT–UF membranes is 2 g/m ² and the OM concentration was fixed at 10 mgC/L. The solution pH in all experiments is 8.1 ± 0.2.	116

Table 7.1:	List of VaCNT membranes. Adapted from Nguyen <i>et al.</i> ⁴¹⁴ , copyright 2022 American Chemical Society.	133
------------	---	-----